University of Milano-Bicocca
School of Medicine and School of Science

PhD program in
Translational and Molecular Medicine – DIMET
XXIX Cycle

Nanoparticles for the treatment of Alzheimer's disease

Dr. Simona MANCINI
Matr. 717615

Tutor: Prof. Massimo MASSERINI
Coordinator: Prof. Andrea BIONDI

ACADEMIC YEAR 2015/2016

TABLE OF CONTENTS

CHAPTER 1

General introduction

1.1 ALZHEIMER'S DISEASE

1.1.1 Overview of the pathology

Alzheimer's disease (AD) is the most common form of dementia in the elderly (> 65 years of age), accounting for up to 75% of all dementia cases. It is largely diffuse and its prevalence is estimated at 36 million cases worldwide (Wimo et al., 2011; Huang and Mucke, 2012). Due to the increase of lifespan, especially in developing countries, prevalence of AD is expected to rise reaching 65.7 million cases in 2030 and 115.4 million patients by 2050.

AD is a neurodegenerative disease characterized by an irreversible deterioration of cognition, behavior and emotion. Although AD shows a phenotypical heterogeneity between individuals, there are many common symptoms. Short-term memory loss is the major symptom in the early stage of the disease (Salmon, 2012). Progressive deterioration occurs with the advancement of the pathology and leads to difficulties with language, executive functions, perception (agnosia), or execution of movements (apraxia) (Weintraub et al., 2012). Apathy can be observed at this stage, and remains the most persistent neuropsychiatric symptom throughout the course of the disease (Rea et al., 2014). In an advanced stage of the pathology, memory problems worsen, and long-term memory, which was previously intact, becomes impaired, leading to the inability of patients to recognize familial place or faces (Weintraub et al., 2012). In the final stage of AD, language and other cognitive skills fail and complete loss of autonomy occurs (Weintraub et al., 2012). Death usually occurs within 10 years from the onset of the first signs of the disease and it is typically not due to the disease itself, but to external factors, mostly septicemia from pneumonia (Weintraub

et al., 2012).

From the histological point of view, AD is characterized by senile plaques and neurofibrillary tangles (NFT) (Figure 1).

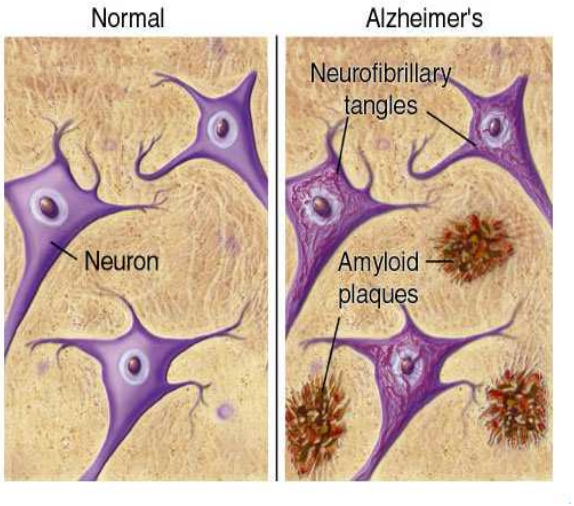

Figure 1. AD histological hallmarks: senile plaques and neurofibrillary tangles (from www.ahaf.org).

Senile plaques are extracellular deposits consisting of a dense core formed by the aggregation of different proteins, including filaments of β-amyloid peptide (Aβ), proteoglycans and apolipoprotein E, surrounded by dystrophic neuritic processes, microglia and astrocytes (Tuppo and Arias, 2005). They are characterized by a β-sheet conformation that enable them to bind to some histochemical dyes, such as Congo Red and Thioflavin. Senile plaques are not specific for AD. In fact, they can be found in small amounts in the hippocampus, amygdala and other limbic structures of healthy individuals over 60 years of age (Xekardaki et al., 2015). However, the discovery of these

structures in large amount and with a topographic distribution including not only the limbic cortex but also the associative ones constitutes the only reliable marker for the diagnosis of AD. Aβ protein deposits, in addition to be present in the brain parenchyma, are also commonly observed (90% of AD cases) in in the media and adventitia of small and mid-sized arteries (and, less frequently, veins) of the cerebral cortex and the leptomeninges, a feature known as Cerebral Amyloid Angiopathy (CAA) (Rensink et al., 2003).

NFT, the other histological hallmark of AD, are aggregates of tau protein in hyperphosphorylated form, which are found in the cytoplasm of neurons, especially of the pyramidal neurons of the hippocampus and cortex (Serrano-Pozo et al., 2011). Physiologically, the tau protein is abundant in neurons, where it binds to microtubules stabilizing their structure. The hyperphosphorylation of the protein causes its separation from such structures and its aggregation in an insoluble form, with consequent destruction of microtubules and impairment of neuronal functions. NFT are a less specific marker than senile plaques. They, in fact, can be found in the absence of amyloid plaques in a wide range of neurological diseases called tauopathies, such as frontotemporal dementia and Pick's disease (Delacourte, 1999). Moreover, 10-15% of AD cases show a large amount of senile plaques in the absence, or almost, of intracellular deposits.

The analysis of the deposition of senile plaques and NFT shows that they first appear in the transentorhinal and entorhinal regions of the temporal lobe (Braak and Braak, 1991). The degenerative process then spreads into the hippocampus and finally reaches the cortex. This three-

step progression (transentorhinal, limbic and cortical) correlates with the clinical picture (Figure 2) and the macroscopic features of AD.

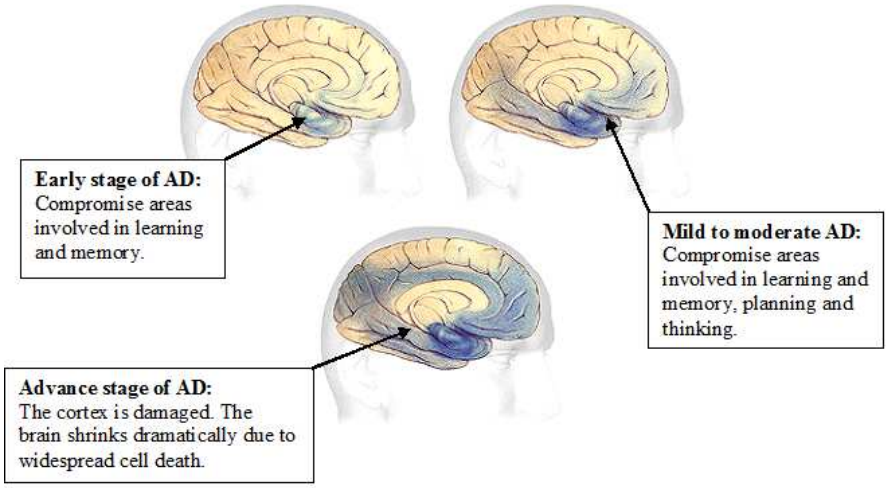

Figure 2. Brain regions affected by AD (from www.alzorg.org).

In fact, the formation of intracellular aggregates and senile plaques leads to neuronal and synaptic degeneration and, consequently, to extensive cerebral atrophy, visible as enlargement of the *sulci*, flattening of the *gyri* and dilatation of lateral ventricles (Figure 3). This causes a decrease in brain weight and volume, especially those areas that are significantly affected by the presence of histological markers (entorhinal cortex, hippocampus and neocortex).

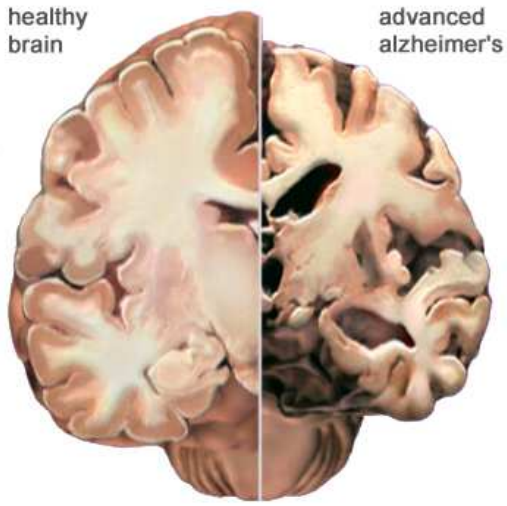

Figure 3. Representation of a healthy (left) and AD (right) brain (from www.alzorg.org).

1.1.2 Etiology of AD

Despite remarkable improvements in understanding the pathogenesis of AD have been made over the last several decades, the exact mechanisms underlying the neuropathological changes in AD remain unclear. AD is a multifactorial disease and contributing to disease onset and progression are many factors, including cognitive reserve, medical and social support, genetics, environmental and cerebrovascular pathologic conditions (Storandt et al., 2012). Age is the strongest risk factor, suggesting that aging-related biological processes may be implicated in the pathogenesis of the disease. It has also been speculated that late-onset AD, which represents about 90% of all AD cases, is the result of unknown environmental factors acting on a predisposing genetic background (Borenstein et al., 2006). Several indpendent

hypothesis have been proposed, among which the amyloid cascade one has been so far the best accepted and most studied (Barage and Sonawane, 2015). According to this hypothesis, the alterated Aβ peptide metabolism, due to either its increased production or decresead clearance, and subsequent aggregation are the primary events driving AD pathogenesis. High levels of Aβ consequently lead to a series of downstream pathological events, including hyperphosphorylation of tau with consequent NFT formation, inflammation, oxidative stress, excitotoxicity, loss of synaptic connections and cell death, which cause the clinical manifestations of AD (Hardy and Higgins, 1992; Dickson, 1997; Selkoe, 1999).

Aβ peptide is a 4 KDa peptide derived from the proteolytic cleavage of the amyloid precursor protein (APP) (Selkoe, 2006). It is composed of 37-43 amino acids, 28 of which are located at the extracellular N-terminal of APP. The remaining amino acids are located in the trans-membrane domain of APP (Verdile et al., 2004) and confer to the peptide hydrophobic properties that induce its aggregation (Harrington, 2012). APP is an integral membrane protein expressed in many tissues and concentrated in the synapses of neurons. Its primary function is not yet known, though it has been implicated as a regulator of synapse formation, neural plasticity and iron export. APP can be proteolytically processed in two different pathways: the non amyloidogenic and the amyloidogenic pathway (Figure 4). In the non amyloidogenic pathway, APP is cleaved by the α-secretase and γ-secretase. The α-secretase cleavage occurs within the Aβ region between Lys16 and Leu17, precluding Aβ peptide formation. The α-secretase cleavage leads to the formation of a soluble N-terminal fragment (sAPPα) that is secreted

extracellularly and is thought to be involved in neuronal plasticity and survival. The resulting C-terminal fragment (α-CTF or C83) remains anchored to the membrane and undergoes to a second cleavage by the γ-secretase complex. This second cleavage produces the APP intracellular domain (AICD) and the non amyloidogenic fragment p3, which biological role is not yet clear (Selkoe, 1994). On the contrary, in the amyloidogenic pathway, APP is cleaved through β-secretase and γ-secretase. The β-secretase cleaves APP, releasing the ectodomain of APP as a soluble fragment (sAPPβ). sAPPβ differs from sAPPα by lacking the Aβ1-16 region at the carboxyl terminus and for this reason it loses the neuroprotective properties associated to sAPPα. The resulting C-terminal fragment (βCTF or C99) remains associated to the membrane and undergoes to γ-secretase cleavage. This leads to the formation of two fragments: the AICD and the Aβ peptide.

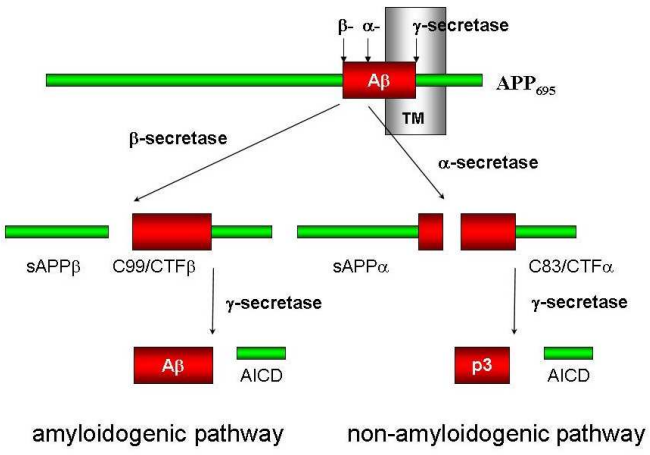

Figure 4. APP processing by secretases.

The existence of different γ-secretase cutting sites leads to the generation of Aβ peptides of different length, which exhibit distinct physical properties and, in particular, show an aggregating behavior that changes in accordance to the length (Lu et al., 2009). The two most common variants are Aβ40 and Aβ42. Both type of peptides could be found in amyloid plaques, but Aβ42, being more hydrophobic, shows a higher aggregation propensity than Aβ40 and is considered the primary toxic peptide that begin the cascade of amyloid deposition. Several genetic and environmental factors have been associated with protein misfolding and aggregation, such as mutations, changes in metal ions, pathological chaperone proteins, pH or oxidative stress and an increase in the concentration of the misfolding protein (Soto, 2003). Many of these alterations are associated with aging, consistent with the late onset of neurodegenerative diseases (Mrak et al., 1997). Kinetic studies have shown that aggregation of Aβ peptides follows a seeding/nucleation mechanism (Bartolini et al., 2007). The key event of this mechanism is the transition of the protein from an α-helix secondary structure to a β-sheet one. This conversion triggers the aggregation of Aβ to form soluble oligomers that act as nucleation centers for the subsequent formation of protofilaments and mature fibrils, which precipitate in the brain parenchyma (Figure 5).

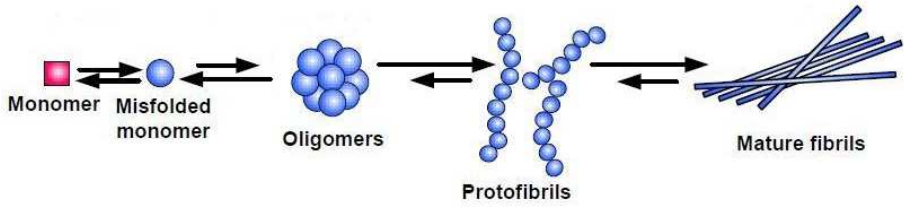

Figure 5. Representation of the pathway leading to protein misfolding and aggregation (Kumar and Walter, 2011).

Genetics, histopathology, cell biology and animal models have supported the amyloid cascade hypothesis. The identification of Aβ peptide as the major constituent of senile plaques (Glenner and Wong, 1984a; Glenner and Wong, 1984b), the association of AD with Down's syndrome (which results from trisomy 21, on which APP gene locus is present), the demonstration of Aβ toxicity on cultured neuronal cells and the generation of animal models developing Aβ plaques and exhibiting memory deficits, all established the importance of Aβ in AD pathogenesis (Glenner and Wong, 1984b; Radde et al., 2008). Moreover, many human biomarker studies, have shown that the accumulation of Aβ precede other AD-related changes (increased CSF tau, brain atrophy, clinical dementia) by decades (Bateman et al., 2012). However, genetic studies of the rare cases of familial AD (about 10%) have provided the strongest evidence supporting the amyloid hypothesis. In fact, mutations in the gene encoding for APP and the genes for presenilins 1 and 2 (PSEN1 and PSEN2) account for all the cases of familial AD and are all related to Aβ production/aggregation (Van Broeck et al., 2007). Mutations in APP are localized at or near the cleavage sites that give rise to Aβ, although some mutations are mapped in the middle of the Aβ peptide and are thought to increase fibrillization. Mutations in PSEN1 and PSEN2, unlike those in APP, are distributed throughout the molecule and alter the cleavage site of γ-secretase, of which presenilins are part (Migliore and Coppedè, 2009). In addition to deterministic mutations, the ε4 allele of APOE gene was found to markedly decrease brain clearance of Aβ, increasing the risk of

developing sporadic and familial late-onset (over 65 years) AD (Castellano et al., 2011).

Although the amyloid cascade hypothesis is the best described and it has been supported by a large volume of data, recently there is growing realization that the role of Aβ in AD pathogenesis may be more limited than previously thought. The presence of Aβ plaques in normal individuals and repeated disappointments with Aβ-centered therapeutic clinical trials are more consistent with the view that Aβ is one of the factors, and not the only factor, that causes AD. This new concept is likely to give a more accurate, albeit complex, picture of AD pathogenesis and promote comprehensive and effective therapeutic strategies against AD (Sorrentino et al., 2014).

1.1.3 Current diagnosis and treatment

Currently, a definitive diagnosis of AD becomes possible only after the patient's death, when the presence of histological hallmarks can be revealed after pathological examination (Jellinger, 1998). Current diagnostic practices, using patient history and cognitive testing, such as the Mini-Mental State Examination, have limited sensitivity and specificity and can be used only to screen patients for "probable" AD. By the time signs and symptoms are sufficient for clinical diagnosis, brain pathology is often quite advanced, limiting benefits of treatment. New techniques have been developed in recent years allowing more definitive diagnosis while the patient is still alive (Fraller, 2013). The deposition of β-amyloid protein within cortical regions of the brain is a pathologic hallmark of AD that is believed to precede clinical symptoms by several years (Pike et al., 2007). This feature of the

disease makes *in vivo* imaging of β-amyloid in the brain of particular interest for the identification of individuals at risk for AD and in the early stages of the pathology (Nordberg, 2007; Forsberg et al., 2008). The most used marker for optimal cortical Aβ burden detection is Pittsburgh Compound B (PIB), used in conjunction with positron emission tomography (PET) (Klunk et al., 2004). PIB binding requires an extended Aβ pleated sheet structure found in Aβ fibrils and plaques in order to bind with high affinity, so it does not bind to oligomeric forms of Aβ nor to nonfibrillar plaques until they reach some critical size. A number of high-resolution MRI-based methods for visualizing the structure of the whole brain, as well as specific brain regions, have been also developed in recent years and adapted for the study of Alzheimer disease (Teipel et al., 2008). Atrophy of the hippocampus, the most widely accepted marker for earlystage Alzheimer disease, is readily detectable by high-resolution MRI. In addition, hippocampal volume loss is predictive of conversion to Alzheimer disease, with an accuracy rate of approximately 80% (Wang et al., 2006). Measurements of various other brain regions and structures have been proposed as biomarkers for Alzheimer disease. However, these measurements, including volumetric analysis of the entorhinal cortex and calculation of cortical thickness, generally have the same drawbacks as hippocampal volumetric assessment, that is to be time- and labor-intensive. Regarding biomarkers in biological fluids, the concentrations of several proteins in cerebrospinal fluid (CSF) have been associated with increased risk and conversion to AD. Chief among these proteins are Aβ42, total tau protein, and phosphorylated tau protein. In the case of Aβ42, the correlation between protein concentration and AD is

negative, that is, increased risk for disease is associated with a lower concentration of Aβ42 in CSF (Fjell et al., 2010). Presumably, the sequestration of the protein inside amyloid plaques, located throughout the cortex, subsequently decrease the amount of Aβ arriving in the CSF after its clearance. The opposite is true for the relationships between AD and tau proteins, which are positively correlated with risk (Hampel et al., 2010). Although decreased CSF Aβ42 levels are typically observed in patients several years before clinical symptoms and cognitive decline, increased concentrations of total and phosphorylated tau in CSF occur later in the course of disease and are more closely aligned with the onset of disease symptoms. Some evidence suggests that CSF levels of total and phosphorylated tau protein, as well as ratios of Aβ42 to other Aβ isomers and to tau protein, can be used to discriminate between Alzheimer disease and other forms of dementia (Bibl et al., 2007). However, although advanced neuroimaging techniques and assessment of protein concentrations in CSF are accurate diagnostic tools, these technologies are not widely available. In contrast, the development of a blood-based biomarker or biomarker panel test would provide a screening method that could be performed in nearly any clinical setting, resulting in increased access to proper care for patients with AD. Recent studies using panels of blood biomarkers have been promising, but none of these studies has been cross-validated in independent samples of subjects yet, leaving the ideal biomarker enabling early detection of AD to be still identified.

Regarding AD treatment, despite the high incidence of AD and all scientific efforts, actually no cure exists. All available treatments are only symptomatic and aim at modulating disease-associated

neurotransmitter alterations. Since a decrease in the levels of acetylcholine (ACh) by degeneration of the basal nucleus was shown in AD and since ACh appears to play an important role in memory and cognition, increasing cholinergic transmission was one of the first therapeutic targets. Among different strategies employed, blocking ACh elimination from the synaptic space obtained by the inhibition of acetylcholinesterase proved to be the most satisfactory in increasing the cholinergic tone (Giacobini, 2000). Four acetylcholinesterase inhibitors (AChE-I) have been approved by FDA: tacrine, donepezil, galantamine and rivastigmine. Tacrine was the first drug of this class to be approved, but today its use has been largely replaced by other AChE-Is due to their more favorable therapeutic profiles, greater convenience and absence of liver toxicity. In addition to cholinergic transmission, the excitatory neurotransmitter glutamate plays a role in the pathophysiology of AD (Hynd et al., 2004). It is believed that an increase in extracellular glutamate induces excessive activation of NMDA receptors resulting in the accumulation of intracellular Ca^{2+}, which triggers a cascade of events culminating in neuronal death. Currently, the only available drug targeting cognitive symptoms via a putative glutamatergic mechanism is memantine hydrochloride. Memantine is the first drug approved by the FDA for the treatment of moderate to severe AD, which confers significant benefit on cognition, global outcomes and behavior when administered alone or in combination with donezepil (Rogawski and Wenk, 2003). Memantine is a low-affinity noncompetitive NMDA (N-methyl-D-aspartate) receptor antagonist that blocks pathologic neural toxicity associated with prolonged glutamate release without interfering with the normal

physiological actions of glutamate required for learning and memory functions (Evans et al., 2004). In recent years, new pharmacological approaches have been developed in order to target inflammation, oxidative stress, Aβ peptide or tau protein (Bonda et al., 2010). Of interest are anti-Aβ therapies, which aim to reduce Aβ levels in the brain parenchyma with three different strategies: block Aβ aggregation, modulate secretase enzymes and increase Aβ clearance. Anti-Aβ aggregation agents may be able to interfere with Aβ aggregation at an early stage of the pathology, by competing with monomers or oligomers or disrupting the β-sheet folding of Aβ. Metal chelators, like desferrioxamine, ethylenediaminetetracetic acid and clioquinol (Sampson et al., 2008) can disrupt interaction of Aβ with redox metal (i.e. iron, copper or zinc) in the brain, thereby preventing aggregation (Greenough et al., 2013). However, their use as therapeutic agents is hindered by their inability to cross the blood brain barrier (BBB). Secretase enzyme modulators targeting β- and γ-secretase cleaving enzymes have been design to reduce Aβ production. Many γ-secretase inhibitors have been designed and tested in clinical trials, but all failed due to adverse effects originating from the involvement of the enzyme in a lot of cellular pathways (Mikulca et al., 2014). On the contrary, inhibition of β-secretase seems to be the most promising strategy, since genetic ablation of the BACE1 gene in mice did not induce evident problems (Luo et al., 2001). Currently, the only secretase inhibitor in clinical trials is Verubecestat, a BACE inhibitor, which successfully passed safety profile phase I studies and was shown to reduce in a dose-dependent manner the level of Aβ in the CSF in over 90% of patients (Mikulca et al., 2014). Verubecestat is now being tested in phase III

clinical trials in people with prodromal AD (Panza et al., 2016). Since active and passive immunotherapy to lower amyloid was first conceptualized (Schenk et al., 1999; Bard et al., 2000), antibody trials have taken the lead among putative disease-modifying therapeutics for AD. Immunotherapies are designed to use the body's immune system to eliminate the deposition of existing Aβ senile plaques. Passive immunization is currently the most widely developed approach in clinical trials. The advantage of this approach is that it involves administration of a known amount of a specific antibody and, in the case of side effects, rapid clearance of the antibody can be effected. On the other hand,the therapy calls for repeated infusions of antibodies over time, proper selection of antigen targets, blood-brain barrier penetration and development of an immune response to injected antibodies (Lannfelt et al., 2014; Panza et al., 2014). Despite the excellent pre-clinical premises, all clinical trials with anti-Aβ antibodies have failed. No trial in AD patients have resulted in unequivocal improvement, with the addition of the demonstration of significant adverse effects, the most dangerous of which were vasogenic edema and intracerebral microhemorrhages detected by magnetic resonance imaging (MRI) as amyloid-related imaging abnormalities (ARIA) (Wisniewski and Goni, 2014). After the recent failure of Solanezumab, the only anti-Aβ antobody still in clinical trial is Aducanumab, a human monoclonal antibody. In patients with prodromal or mild AD, one year of monthly intravenous infusions of aducanumab reduced brain Aβ in a dose- and time-dependent manner, together with a slowing of clinical decline. Although some cases of ARIA were reported, Aducanumab is

undergoing phase III clinical trial, where its efficacy on AD symptoms and its safety will be more deeply evaluated (Sevigny et al., 2016).

As already mentioned above, the failure of all Aβ-centered therapeutic strategies has recently lead to consider a more wide and complex picture of AD, in which AD pathogenesis and progression result from the interplay between Ab and the other involved factors. This new concept is likely to promote the development of more effective therapeutic strategies against the pathology.

1.2 NANOMEDICINE

1.2.1 Nanoparticles for biomedical applications

The term nanotechnology refers to a scientific area involved in the manipulation of atoms and molecules leading to the production of materials and tunable devices with the size in the order of billionth of meters and that show peculiar properties (surface area to volume ratio, electrical, chemical, optical properties) (Moghimi et al., 2005; Holmes, 2013).

Nanomedicine is the application of nanotechnology to healthcare, mainly in the field of diagnosis, drug delivery and tissue regeneration. Among different devices, nanoparticles (NPs) technology is gaining increasing interest and is emerging as a powerful strategy for the treatment of several pathologies.

NPs are colloidal objects sized between 1 and 100 nm (Youns et al., 2011) that work as a whole unit in terms of properties. The reason why NPs are attractive form medical purposes is mainly linked to the possibility to multifunctionalize their surface, attaching one or more targeting ligands to accomplish several functions (i.e. biological barrier crossing, targeting of specific molecules/pathways). The large surface-area-to-volume ratio of NPs allows attaching multiple copies of a ligand, dramatically increasing their binding affinity via multivalent interactions (Montet et al., 2006). Moreover, NPs can be loaded with drugs or contrast agents and the encapsulation improves the solubility, pharmacokinetics and pharmacodynamic profiles of compounds, enhances their stability by reducing their degradation in the systemic circulation and increases their concentration at the diseased tissue through active targeting, reducing toxic side effects in normal tissues

(Biswas and Torchilin, 2014).What makes NPs even more attractive for medical applications is the possibility to be administered by a variety of routes (including oral, inhalational, and parenteral) (Petkar et al., 2011) and the possibility of modulating NPs composition in order to confer them specific features (Figure 6).

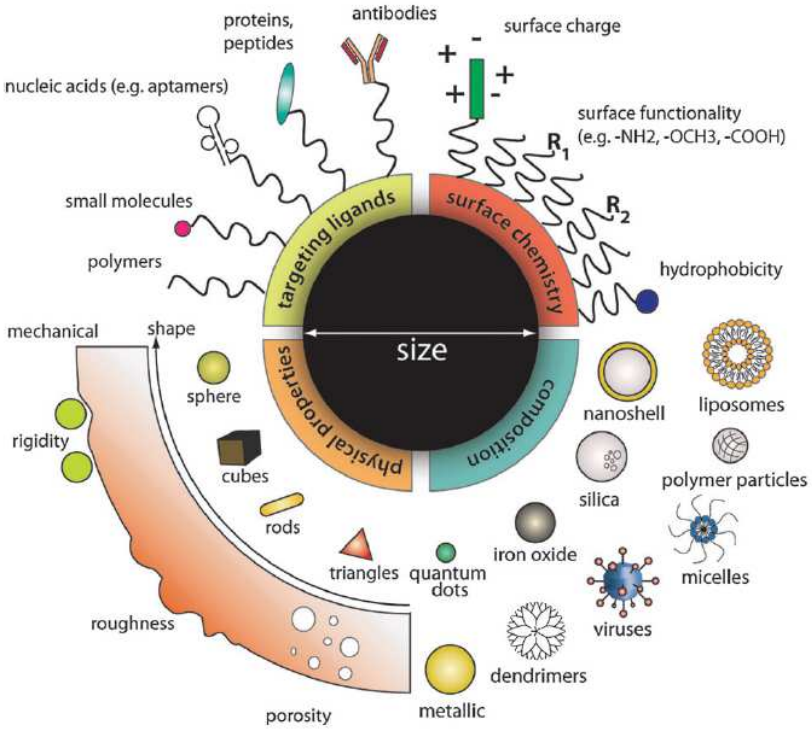

Figure 6. Nanoparticles can be modularly assembled from different materials composition with different physical and chemical properties and functionalized with a myriad of ligands for biological targeting. Such flexibility in design freedom enables researchers to tailor nanoparticle for specific applications as contrast agents, drug delivery vehicles and therapeutics (Chou et al., 2011).

Biocompatibility and biodegradability can be reach using natural or synthetic polymers or lipids to made NPs. Regarding the ability to overcome biological barriers, it depends on parameters such as NP shape, size, composition, surface charge and surface functionalization

(Blanco et al., 2015). NPs size is critical for avoiding a rapid clearance. Renal filtration is responsible for the elimination of NPs with a diameter below 5 nm. On the contrary, reticuloendothelial system (RES), liver and spleen account for the clearance of particles larger than 200 nm. Therefore, 100 nm NPs have a prolonged circulation time. In addition, the shape and the surface charge influence NPs fate. It has been demonstrated that neutral or negatively charged NPs have longer circulation half-lives compared to positively charged NPs because the latter have a higher affinity for serum proteins, thus promoting the elimination by RES. Instead, NPs shape conditions their margination to vessel walls, which is essential for NPs interaction with receptor express on the endothelium (Blanco et al., 2015). Blood flow dynamic simulations demonstrate that discoidal NPs are more prone to marginate to the vascular wall compared to spherical NPs (Gentile et al., 2008; Vahidkhah and Bagchi, 2015). Finally, NPs circulation lifetime is strongly affected by serum proteins absorption on their surface and by the formation of the so-called protein corona. The protein corona assembly, and in particular the binding of opsonins (IgG, complement components and fibrinogen) to the NPs surface, causes NPs sequestration by RES, mainly located in liver and spleen, thus reducing their half-lives in the bloodstream. The composition of the protein corona depends on the route of administration and is strongly affected by the surface properties of NPs (Masserini, 2013; Blanco et al., 2015). The most common method to avoid the rapid clearance of NPs is to coat their surface with polyethylene glycol (PEG), a hydrophilic surfactant that forms a tight association with water molecules, reducing opsonization and the consequent NPs elimination. For this reason,

PEGyaltion of NPs strongly increases their circulation time (Blanco et al., 2015). Alternative strategies to PEG are represented by the coating of NPs surface with cellular membranes purified by leukocytes (Parodi et al., 2013) or with membranes isolated from red blood cells (Hu et al., 2011), both resulting in increased NPs retention in the bloodstream (Blanco et al., 2015).

Research on NPs technology has progressed through three generation of nanovectors (Figure 7).

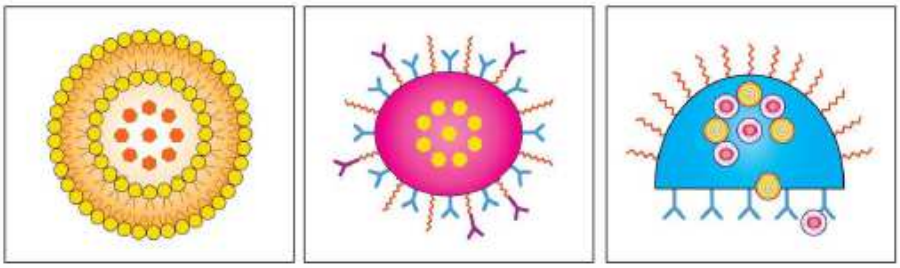

Figure 7. Schematic representation of first-generation (left panel), second-generation (middle panel) and third-generation (right panel) nanovectors (Godin et al., 2010).

The first generation of nanovectors consists of simple colloidal particles loaded with a therapeutic compound. They exploit passive mechanisms to deliver the drug to the target site. An example is given by doxorubicin-loaded liposomes (FDA-approved and used in clinic for cancer therapy), which take advantage of the enhanced permeability and retention (EPR) properties of tumors to reach the lesion (Godin et al., 2010). The surface modification of first-generation nanovectors with PEG avoids immune system recognition and degradation.

Second-generation nanovectors are engineered with ligands or antibodies to allow an active targeting through the binding to specific

receptors. The payload release can also be modulated by pH- or enzyme-sensitive polymers, as well as by external stimuli (for instance the application of a magnetic field). Finally, third-generation nanoparticles are complex structures aiming to sequential overcoming of biological barriers and time-controlled release of multiple payloads (Godin 2010).

1.2.2 Liposomes

Currently several kinds of nanoparticles with different phsyco-chemical properties have been tested for biomedical applications (Figure 8).
Among all different types of NPs, liposomes have been the first ones to be investigated (Budai and Szogyi, 2001). They are made up of one or more phospholipid bilayers, called lamellae, composed of amphiphilic lipids, delimiting an internal aqueous core (Hillaireau and Couvreur, 2009). According to their size and the number of bilayers, liposomes can be classified in multilamellar vesicles (MLV), that can reach a size of several μm and made of many concentric lipid bilayers, large unilamellar vesicles (LUV) made up of a single lamella and bigger than 100 nm, and small unilamellar vesicles (SUV) composed of a single bilayer and with a size up to 100 nm (Masserini, 2013).

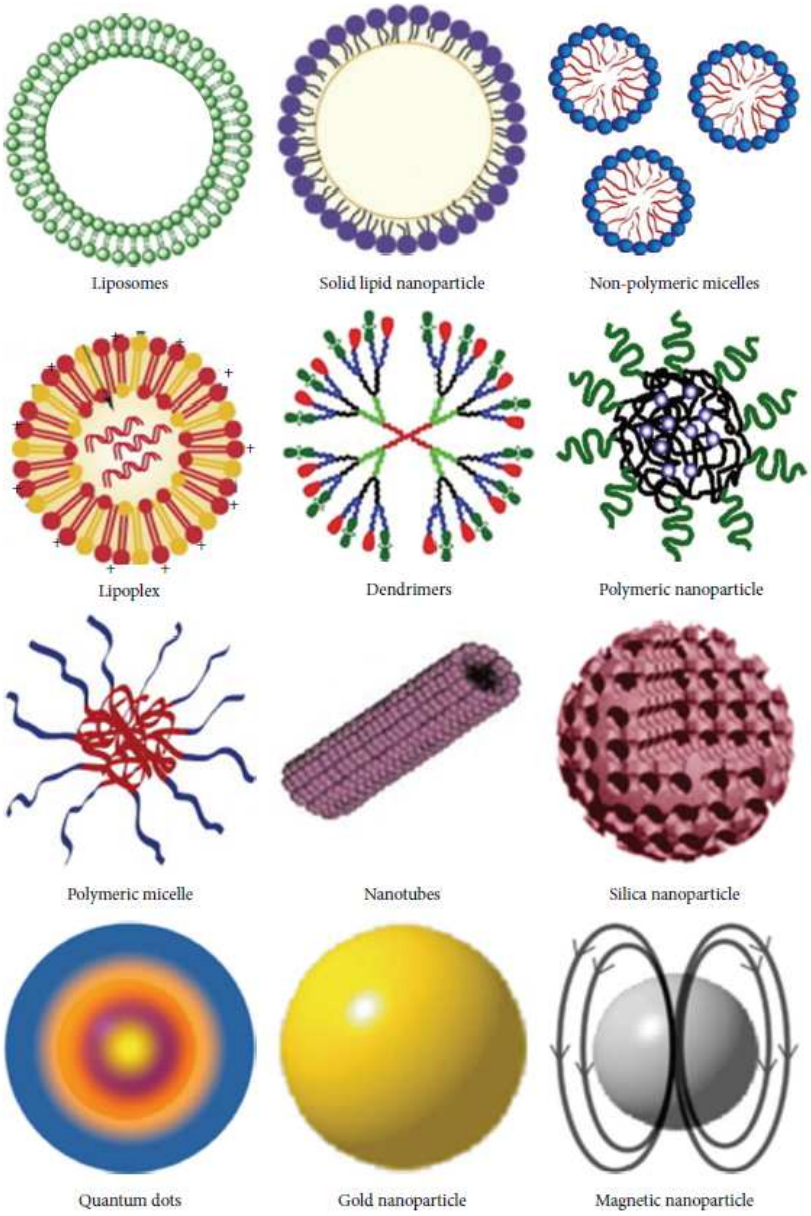

Figure 8. Different types of nanoparticles (NPs). Graphical representation of the most commonly used NPs for biomedical applications. NPs are typically by a size measuring not more than 100 nm. The size of quantum dots is usually less than 10 nm (Masserini, 2013).

There are many different methods for the preparation of liposomes. The choice of the appropriate method depends on several factors: 1) the physicochemical characteristics of the liposome components and those of the drug to be entrapped; 2) the toxicity and the concentration of the loaded substance; 3) additional processes involved in application/delivery of liposomes; 4) optimum size, polydispersity and shelf-life of the liposomes for the intended application and 5) batch-to-batch reproducibility and possibility of large-scale production and good manufacturing practice-relevant issues (Wagner and Vorauer-Uhl 2011). They can be prepared using handshaking, re-hydration and reverse-phase evaporation methods, followed by sonication, freeze/thawing cycles or extrusion to downsize the particles produced (Wagner and Vorauer-Uhl 2011).

Liposome research started in the 1960s and has progressed from conventional vesicles ("first-generation liposomes") to "second-generation liposomes", in which modulation of lipid composition, size and charge of the vesicle and addition of surface coatings and ligands has been investigated in order to improve efficacy, reduce RES clearance and minimize toxicity (Bozzuto and Molinari, 2015; Sercombe et al., 2015). Nowadays, liposomes are extensively used as carriers for numerous molecules in cosmetic, food, farming and pharmaceutical industries (Akbarzadeh et al., 2013). In particular, liposomes are attractive tools in biomedical applications thanks to their biocompatibility, non-immunogenicity, non-toxicity, biodegradability and high physical stability. In fact, liposomes are usually composed of physiological lipids, mainly sphingomyelin, phosphatididylcholine, glycerophospholipids and cholesterol, frequently included in liposome

formulations in order to decrease bilayer permeability and increase liposome stability *in vivo* (Masserini, 2013).

Liposomes are used to improve the pharmacokinetics and protect drugs from the environment. As for others NPs, encapsulation in liposomes protects drugs against degradation and enhances their circulation half-lives. Moreover, the surface of liposomes can be easily functionalized in order to obtain a site specific targeting of the payload, thus reducing side effects (Sanvicens and Marco, 2008). Besides the more general 'nanocarrier advantages', liposomes have an additional benefit: thanks to their amphiphilic nature, liposomes can be load with both hydrophilic, entrapped in the aqueous core, or lipophilic compounds, dissolved in the lipid bilayer, without modification of the encapsulated molecules. This makes the liposomal approach attractive for the delivery of biologicals like peptides, proteins and especially RNA or DNA variants (Bozzuto and Molinari, 2015).

1.2.3 Clinically approved NP-based pharmaceuticals

A summary published in 2013 counted exactly 100 products, described as nanopharmaceuticals, that are clinically approved and on the market, including medical devices, such as implants or surgical instruments, and imaging and diagnostic agents (Etheridge et al., 2013). So far, 43 products have been approved as nanodrugs, comprising lipid-, polymer- and protein-based NPs, reported in Figure 9 (Weissig et al., 2014).

PRODUCT	COMPOSITION	INDICATION	APPROVED
Lipid-based Nanoparticles			
Abelcet	Lipid complex formulation of amphotericin B	Invasive fungal infections	1995
Doxil/Caelyx	PEGylated liposomal formulation of doxorubicin	Various cancers	1995
DaunoXome	Liposomal preparation of daunorubicin	HIV-related Kaposi's sarcoma	1996
AmBisome	Lipsomal preparation of amphotericin B	Fungal and protozoal infections	1997
Inflexal V	Liposomal influenza vaccine	Influenza	1997
DepoCyt	Liposomal formulation of cytarabine	Lymphomatous meningitis	1999
Visudyne	Liposomal formulation of verteporfin	Wet age-related macular degeneration	2000
Myocet	Liposomal formulation of doxorubicin	Metastatic breast cancer	2000
DepoDur	Liposomal formulation of morphine sulfate	Relief of postsurgical pain	2004
Mepact	Liposomal formulation of mifamurtide	Non-metastasizing resecatable osteosarcoma	2009
Marqibo	Liposomal formulation of vincristine	Acute lymphoid leukemia	2012
Polymer-based Nanoparticles			
Adagen	PEGylated adenosine deaminase enzyme	Severe combined immunodeficiency disease	1990
Oncaspar	PEGylated formulation of L-asparaginase	Acute lymphoblastic leukemia	1994
Copaxone	Polymer composed of L-glutamic acid, L-alanine, L-lysine and L-tyrosine	Multiple sclerosis	1996
Renagel	Polyamine (polymer loaded with amine groups)	Chronic kidenty disease	2000
PegIntron	PEGylated interferon alfa-2b	Hepatitis C	2001
Eligard	Leuprolide acetate and PLGH polymer formulation	Advanced prostate cancer	2002
Neulasta	Conjugate of PEG and filgrastim	Chemotherapy-induced neutropenia	2002
Pegasys	PEGylated interferon alfa-2a	Hepatitis C	2002
Somavert	PEGylated human growth hormone receptor anatgonist	Acromegaly	2003
Macugen	PEG-anti-VFGF aptamer	Neovascular age-related macular degeneration	2004
Mircera	Chemically synthetised ESA, methoxy PEG-epoetin beta	Symptomatic anemia associated with chronic kidney disease	2007
Cimzia	PEGylated Fab fragment of a humanized anti-TNF-alpha antibody	Crohn's disease, rheumatoid arthritis	2008
Protein-based Nanoparticles			
Abraxane	Albumin-bound paclitaxel (*nab*-paclitazel)	Breast cancer	2005

Figure 9. FDA-approved agents utilizing NPs.

The largest share of approved nanodrugs is intended for tumour therapy, but overall a wide range of applications is covered, including infectious diseases, pain treatment, diagnostic use, vaccines, autoimmune diseases and immunosuppression required for organ transplants.

It takes about 10 years for a product to pass from its discovery to its approval as a commercial drug. For nanopharmaceuticals this process took, and takes, even longer for new exploited principles to be

specifically examined.

Due to their biocompatibility and biodegradability, liposomes, in the form of Doxil, were the first drug-delivery system approved for clinical purposes by FDA in 1995 (Barenholz, 2012). In the following years, additional liposome products were approved for the market, achieving familiar status with global health authorities due to the number of precedent products to guide regulatory decision-making.

However, the majority of lipid-based therapeutics and, in general, NPs approved is based on first-generation nanovectors. The next phases of development in nanomedicine are likely to take advantage of combined applications in the form of both multimodal treatments, utilizing nanomedicine in combination with current treatments, and theranostic platforms, single nanomedicine applications with multiple modes of action. Second generation nanovectors are currently at various stages of clinical and pre-clinical studies. These NPs functionalized for the active targeting struggle to reach the clinic and, subsequently, the market mostly due to problems in large scale good manufacturing production, costs and product evaluation. Multifunctionalized NPs are, indeed, more complex to produce on large scale because they require multiple synthesis steps and formulation processes, thus increasing the cost of production. They also required more accurate *in vitro* and *in vivo* preclinical studies, thus lengthening the time necessary for the developmental process (Bozzuto and Molinari, 2015; Sercombe et al., 2015). Moreover, physicochemical modifications in a nanoformulation system, such as the use of synthetic coatings and ligands, makes further evaluations to understand the interaction of the NPs with biological tissues and cells necessary (Sawant and Torchilin, 2012; Narang et al.,

2013; Tinkle et al., 2014). This may account for the fact that almost all the products in development are pursuing a nanoparticle-based technology where success has already been established such as lipid-, polymer- and protein-based NPs, nanocrystals and micellar systems (Weissig and Guzman-Villanueva, 2015).

Finally, clinical trials of NPs are generally more complex than conventional formulations, as a number of control groups are required to account for different aspects of the drug delivery system.

1.2.4 Nanotoxicity

Even if the use of engineered NPs represents one of the main hopes for innovative pharmacological strategies, how they behave inside the body is still a major question that needs to be resolved (Teli et al., 2010; Khanna et al., 2015). The first aspect to be considered is the material by which NPs are constituted. Beyond biodegradability that determines NPs retention in the body, the greater chemical reactivity of some nanomaterials, as in the case NPs made of metals, can result in increased production of reactive oxygen species (ROS), including free radicals (Nel et al., 2006), resulting in oxidative stress, inflammation and consequent damage to proteins and membranes, chromosomal fragmentation, DNA strand breakages, point mutations, oxidative DNA adducts and alterations in gene expression (Singh et al., 2009).

The unique properties such as small size, relatively high surface-to-volume ratio, quantum dot effect and reactivity of NPs are also a cause of concern for their possible impact on human health that is not known (Petrinca et al., 2009). Particle size and surface area are considered important factors that contribute directly and significantly to toxicity of

NPs, with smaller sized NPs exhibiting higher toxic effects due to increased surface area (Oberdörster et al., 2005). In addition, some NPs seem to be able to translocate from their site of deposition to distant sites such as the blood and the brain.

Apart from size, structure and shape of NPs also contribute to nanotoxicity (Grabinski et al., 2007). Moreover, when assessing the possible neurotoxicity of NPs, also the surface and its functionalization needs to be taken into consideration because it dictates the adsorption of ions and biomolecules, thus influencing biological processes and inducing toxicity of otherwise safe particles (Rivet et al., 2012; Li et al., 2015).

It should be pointed out that different types of NPs, showing promising features for *in vivo* applications at the beginning, were successively discarded after having demonstrated their toxicity when utilized *in vivo*. This is the case, for instance, of quantum dots and carbon nanotubes that proved to be toxic *in vivo* (Win-Shwe and Fujimaki, 2011), and for this reason, their prospective use in medicine will be likely limited to *in vitro* diagnostics.

A better understanding of the mechanisms involved in nanotoxicity may provide clues for circumventing the toxicological effects of NPs and may help to improve NPs design in the field of nanomedicine.

1.3 NANOMEDICINE FOR THE TREATMENT OF ALZHEIMER'S DISEASE

Maria Gregori, Massimo Masserini, Simona Mancini

Nanomedicine (London, England), 2015; 10(7):1203-18

Abstract

Alzheimer's disease affects more than 35 million people worldwide and this number is presumed to double by the year 2050. Currently, there is no efficient therapy for this disorder but a promising approach is represented by nanotechnology, easily multifunctionalizable devices with size in the order of billionth of meter. This review provides a concise survey on the nano-based strategies for Alzheimer's disease treatment, aiming at carrying drugs across the blood–brain barrier, in particular to target the metabolism of β-amyloid peptide, a pivotal player in this pathology.

1.3.1 Introduction

Alzheimer's disease (AD) is the most common neurodegenerative disorder in the elderly. According to a recent report, it currently affects about 36 million people worldwide, and that number is expected to rise to over 115 million by 2050 (Gaugler et al., 2013). AD is clinically characterized by a progressive decline in cognition and histologically by the presence in the brain of intracellular neurofibrillary tangles and extracellular amyloid plaques (Ittner and Götz, 2011). Neurofibrillary tangles are consisting of intraneuronal paired helical filaments of a microtubule-associated protein (Tau), hyper-phosphorylated at multiple sites. Amyloid plaques are extracellular aggregates whose

main component is a peptide called amyloid β (Aβ) (40–42 amino acids in length) generated by the sequential cleavage of the amyloid precursor protein (APP) by BACE1 (β-secretase) and γ-secretase (Murphy and LeVine, 2010). Aβ spontaneously and progressively undergoes aggregation, forming oligomers and fibrils and ending with the deposition *in vivo* of senile plaques. Aβ oligomers ranging in size from two to 12 subunits are now considered the main responsible for the synaptic damage and memory deficit in AD (Haass and Selkoe, 2007). During the past two decades, one of the primary goals in medical research was to better understand the molecular mechanisms involved in AD onset for the development of safe and effective pharmacological treatments. However, successful treatment strategies for AD have so far been limited. The current available treatments of AD are only symptomatic in nature, mainly trying to counterbalance the neurotransmitter disturbance associated to the disease (Yiannopoulou and Papageorgiou, 2013). However, established treatments provide only transitory symptomatic relief, temporarily improving cognitive function, but do not slow the long-term progression of the disorder (Bullock and Dengiz, 2005). Moreover, the treatment of AD is particularly complicated due to the presence of the blood–brain barrier (BBB), a physical and biochemical barrier which protects the brain from potential hazardous substances in the blood flow and which prevents the passage, thus the activity, of 98% of potential neuropharmaceuticals (Wolburg et al., 2009). Therefore, there is an urgent need to develop strategies to improve the efficacy, the transport across the BBB, the bioavailability and simultaneously to limit the adverse effects of pharmaceutical compounds for the treatment of AD.

Moreover, it would be desirable that the advancement in the elucidation of AD aetiology would bring new therapeutic molecules able to block definitively the progression of the disorder.

Nanoparticles (NPs), submicron-sized (3–200-nm) particles, devices or systems made using a variety of materials including polymers, lipids, viruses and organometallic compounds, represent promising candidates in this regard and may provide a possible contribution to the treatment of AD, carrying drug molecules by encapsulation or covalently linked on their surface. Table 1 shows different NPs proposed for the treatment of AD and considered in the present investigation. NP-mediated drug delivery offers unique advantages over free drug administration, such as: increased drug concentration at the diseased tissue through active targeting, reducing toxic side effects in normal tissues; improve the solubility, pharmacokinetics and pharmacodynamic profiles of the drugs; improve drug stability by reducing its degradation in the systemic circulation (Biswas and Torchilin, 2014).

The current state-of-the-art of nanotechnology-based drugs intended for AD diagnosis and therapy has been already discussed elsewhere (Brambilla et al., 2011; Sahni et al., 2011). The purpose of this article is to focus on NPs devoted to AD therapy and properly functionalized to cross the BBB and to target Aβ, as a widely recognized pivotal molecule in the etiology of the disease. It should be pointed out that the current nanomedicine approaches for AD therapy are still limited to preclinical studies. In fact, although several clinical trials investigate the suitability of NPs for CNS drug delivery (Service, 2010), none of them is concerning AD.

Type	Size	Drugs	Refs.
Polymeric NP 	40-240 nm	Curcumin Neuroprotective peptide Rivastigmine Estradiol S14G-humanin Anti Aβ antibody Fibriblast Growth Factor Aβ-targeting peptide Iron chelator Selegiline Aβ 1-15 ROCKII-siRNA	(Mathew et al., 2012; Cheng wt al., 2013) (Liu et al., 2013) (Wilson et al., 2008) (Mittal et al., 2011) (Yu et al., 2014) (Jaruszewski et al., 2012; Le Droumaguet et al., 2012) (Zhang et al., 2014b) (Zhang et al., 2014a) (Liu et al., 2009) (Baysal et al., 2013) (Puras et al., 2011) (Liu et al., 2013)
Liposomes 	100-150 nm	Curcumin or curcumin derivatives Phosphatidic Acid Cardiolipin XO4 Glycofused benzopyrane Anti Aβ antibody ZnAc, EDTA, His Epigallocatechin-3-gallate	(Mourtas et al., 2011; Re et al., 2011; Sancini et al., 2013; Mourtas et al., 2014; Taylor et al., 2011) (Gobbi et al., 2010; Ahyayauch et al., 2012; Salvati et al., 2013; Balducci et al., 2014; Bana et al., 2014) (Gobbi et al., 2010; Ahyayauch et al., 2012) (Tanifum et al., 2012) (Airoldi et al., 2014) (Canovi et al., 2011) (Mufamadi et al., 2012) (Smith et al., 2010)
Solid lipid NP 	250-350 nm	Piperine	(Yusuf et al., 2013)
Chitosan NP 	15-200 nm	Tacrine Aβ fragment	(Elmizadeh et al., 2013) (Songjiang and Lixiang, 2009)
Magnetite μP 	5μm	Tacrine	(Wilson et al., 2009)
Albumin NP 	150-250 nm	Tacrine	(Luppi et al., 2011)
Gold NP 	10 nm	Aβ-binding peptide	(Kogan et al., 2006; Prades et al., 2012)
Exosomes 	40-100 nm	BACE1-siRNA	(Alvarez-Erviti et al., 2011)

Table 1. Nanoparticles proposed for the treatment of Alzheimer's disease and cited in the present review.

1.3.2 The BBB

The main component of the BBB is specialized brain microvascular endothelial cells that regulate the flow of substances into and out of the brain. In addition, the BBB is composed by the capillary basement

membrane, astrocyte end-feet and pericytes. It is well known that all the components of the BBB are essential for its physiological function and stability (Wolburg et al., 2009). The access of molecules to the brain is difficult because paracellular diffusion is very limited at the BBB, due to the presence of 'tight junctions' between the endothelial cells. Therefore, molecules in the circulation may gain access to the brain only across endothelial cells by three main mechanisms: lipid-mediated free diffusion; carrier- or receptor-mediated transport; absorptive-mediated transport (Begley, 2004). Figure 10 shows a simplified scheme of the passage of substances across the BBB. For these reasons, transport of drug across the BBB is very limited and precludes the treatment of many brain disorders.

.

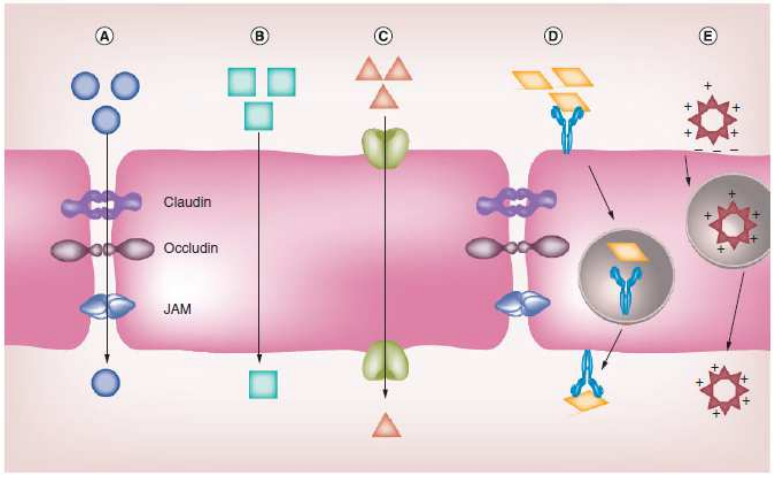

Figure 10. Graphical representation of the main routes for molecular traffic across the blood–brain barrier.**A**, Paracellular aqueous passage possible by opening the tight junctions (occludin, claudin and JAM);**B**, transcellular lipophilic pathway; **C**, carrier-mediated transport; **D**, receptor-mediated transcytosis and **E**, adsorptive-mediated transcytosis.
JAM: Junctional adhesion molecule.

Strategies proposed to enhance drug delivery to CNS are described in

Table 2. It is worth noting that various clinical investigations detected functional alterations of the BBB in AD, in particular an increase in the permeability compared with healthy controls and an alteration in the Aβ transport activity. Furthermore, it is reported that Aβ is able to induce monocytes infiltration through the BBB (Weiss et al., 2009). Despite the increased permeability, crossing the BBB remains a key obstacle in the use of pharmaceuticals for the treatment of this pathology (Pardridge, 2005).

Strategy	Advantages	Drawbacks
Osmotic opening of the BBB by hypertonic solutions.	Delivery of a variety of agents in a wide range of sizes.	The permeability effect is largely reversed within 10 min. Neurons may be damaged from blood components entering the brain.
BBB disruption by focused ultrasound.	Non invasive method.	Cost of the system. Risks of overheating the skull. Blood components entering the brain.
Intrathecal /intracerebroventricular administration.	Smaller dose can be used, potentially minimizing systemic toxicity. Longer drug half-life.	Difficult dose calculation. Slow rate of drug distribution. Possible increase in intracranial pressure. Possible CNS infections.
Intranasal administration.	Large surface area available for drug absorption. Rapid achievement of target drug levels. Avoidance of first-pass metabolism.	Clearance by mucus layer and cilia. Poor drug amount delivered.
Use of brain targeted nanoparticles (NP) as drug carriers.	Properly functionalized NP can exploit the existing physiological mechanisms of transport through the BBB. Possibility of controlled drug release. NP available in a wide range of size and composition to transport a large variety of drugs. Possibility of diagnosis and therapy at the same time (theranostics). Non invasive method.	Only a small part of the administered dose will reach the brain. Clearance by reticuloendothelial system. Systemic side effects.

Table 2. Strategies for drug delivery to the CNS.

1.3.3 NPs for AD treatment

1.3.3.1 BBB crossing

NPs have been proposed as intriguing tools potentially able to solve the unmet problem of enhancing transports of drugs from the blood to brain, in particular by the functionalization of their surface with BBB targeting agents. Liposomes, solid lipid NPs (SLN), polymeric NPs and gold NPs are the most studied NPs for brain drug delivery, due to their common features of biocompatibility, stability, biodegradability, nontoxicity, limited antigenicity and suitability for surface functionalization. Moreover, they can incorporate both hydrophobic and hydrophilic drugs and a controlled drug release can be achieved. Liposomes are spherical vesicles (20 nm–500 μm of size) in which an aqueous inner volume is enclosed by a membrane bilayer usually composed of naturally occurring phospholipids and cholesterol (Antimisiaris et al., 2007). SLN are nanospheres (50–1000 nm of size) composed by lipids that are solid at physiological temperature, stabilized by physiologically compatible emulsifiers. SLN are very stable NPs that can be produced easily on a large scale (Gastaldi et al., 2014). Polymeric NPs are nanosized carriers (1–1000 nm), made of natural or synthetic polymers (Patel et al., 2012). Gold NPs (1–150 nm of size) are the most stable metal NPs with unique optical, electronic and magnetic properties exhibited at nanoscale level. Interestingly, gold NPs have been shown to reach the brain and accumulate in neurons even in the absence of any specific functionalization, with a mechanism that is still to be understood (Sousa et al., 2010).

NPs suitable for BBB crossing should carry specific features. For example, they should have long half-life in circulation since, following

their entrance in the blood, they are rapidly cleared by the reticuloendothelial system and mainly sequestered in liver and spleen. A great advance in this area was the finding that surface stabilization of NPs with nonionic surfactants or polymeric macromolecules can prolong half-life up to 24 h in mice and rats and 45 h in humans (Moghimi and Szebeni, 2003). Concerning the size, it is suggested that NPs for brain drug delivery should be kept below 200 nm diameter to allow their diffusion within the brain, because it is estimated that in human brain tissue the extracellular spaces have only some pores larger than 200 nm and that more than one-quarter of all pores are ≥100 nm (Masserini, 2013).

The most common approach to enhance the passage of NPs from the bloodstream to the brain is to exploit the existing physiological mechanisms of transport, for example, receptor-mediated endocytosis and adsorptive-mediated endocytosis, even if it is not completely understood whether these mechanisms are altered in AD. Moreover, we have also to remind that alterations of microvascular permeability and disruption of the BBB, reported in the brains of AD subjects (Weiss, 2009), could lead to an increased permeability of the barrier.

To enhance the BBB passage of AD drugs-loaded NPs by using receptor or adsorptive-mediated endocytosis, NP surface multifunctionalization with proper ligands is critical. Different coupling reactions have been reported to link to NP peptides or antibodies (Abs) able to bind specific receptors on BBB cells surfaces (Figure 11). Peptides or Abs could be linked to NPs by a covalent bond between a thiol present on the peptide or on Abs (already present or generated by thiolation on its primary amines) and a maleimide group present on NP

surface (Re et al., 2011a). In particular cases, such as that of gold NPs, the thiol group may form a stable S-Au bond with the NP core (Prades et al., 2012). Immunoliposomes can be prepared also by activating free carboxyl group on the NP surface with ethylcarbodiimide and N-hydroxysuccinimide and then by covalently conjugating Abs through displacement of N-hydroxysuccinimide groups by antibody amines (Mathew et al., 2012). However, it is possible to functionalize NPs by means of a non-covalent bond, by taking advantage of the high affinity between biotin and streptavidin (Figure 11).

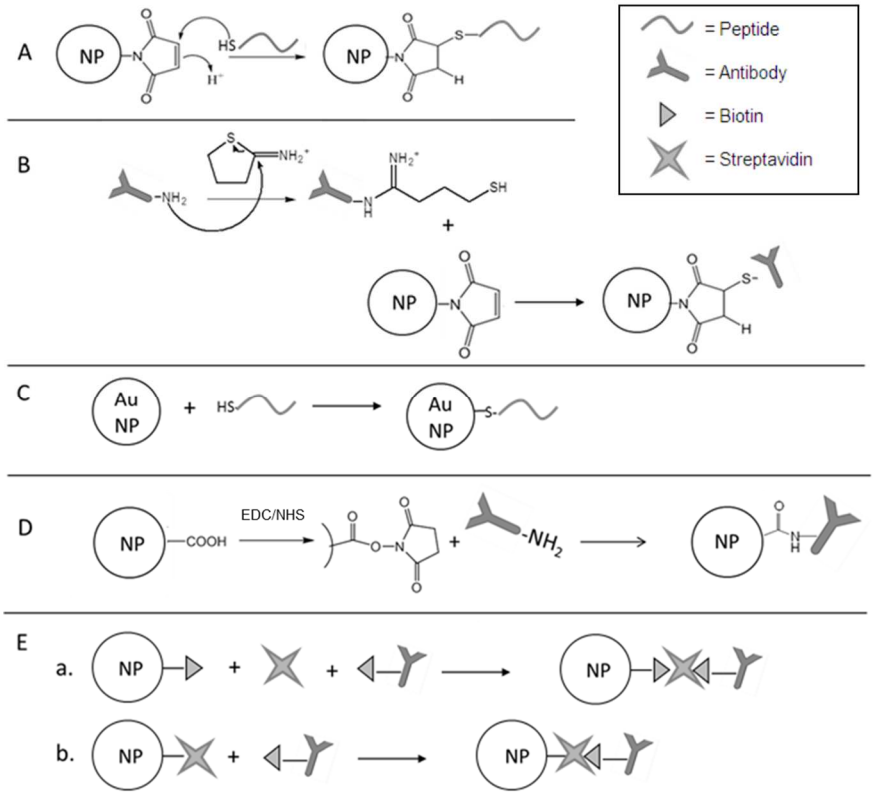

Figure 11. Strategies for the surface decoration of nanoparticles with antibodies or peptides. **A**, Conjugationof thiol-containing peptide to maleimide-functionalized NPs. **B**, Thiolation of antibody using Traut's reagent and successive conjugation to maleimide-functionalized NPs. **C**, Reaction between thiol-containing peptide and Au NPs. **D**, Conjugation of antibody to COOH-functionalized NPs activated by

ethylcarbodiimide/N-hydroxysuccinimide treatment. **E**, Biotin-streptavidin conjugation strategy: (i) conjugation of biotinylated-antibody to biotinylated-NPs via streptavidin bridge; (ii) conjugation of biotinylated-antibody to streptavidin-functionalized NPs.
EDC: 1-ethyl-3-(3-dimethylaminopropyl) carbodiimide; NHS: N-hydroxysuccinimide; NP: Nanoparticle.

A widely investigated surface decoration is with ligands triggering receptor-mediated endocytosis. In particular, three receptors on the BBB have received more attention as targets mediating NP interaction: transferrin receptor (TfR), low-density lipoprotein receptor (LDLr) and lactoferrin receptor (LacR) (Krol, 2012). The main drawback is that all three receptors are not exclusively expressed on the BBB, thus high amounts of NPs engineered to target these molecules will arrive massively to other organs before reaching the brain. Ligands for TfR range from peptides selected from a phage display library (Liu et al., 2013) to anti-TfR Abs (Salvati et al., 2013; Mourtas et al., 2014). It is interesting to note that, concerning anti-TfR Abs, Salvati et al. showed the superior efficacy of covalent coupling to liposomes of RI7217, an anti-TfR Abs, versus biotin/streptavidin ligation in overcoming a human BBB cellular model (Salvati et al., 2013). Ligands for LDLr are ApoE (physiological ligand of the receptor) or peptides derived from it. Re et al. showed that the functionalization with the monomeric fragment 141–150 of human ApoE peptide (mApoE), or its tandem dimer, enhances the permeability *in vitro* across a BBB model and *in vivo* in healthy mice (Re et al., 2011a; Bana et al., 2014). Finally, lactoferrin, the endogenous ligand for LacR was used by Yu et al. to increase the brain delivery properties of PEG-polylactide-co-glycolide (PEG-PLGA) polymersomes in mice (Yu et al., 2012).

Utilizing the strategy of TfR targeting, Liu et al. synthesized poly(ethylene glycol)-poly(lactic acid) block copolymer (PEG-PLA) NPs functionalized with a peptide (CGHKAKGPRK), called B6, selected from phage display and showing high affinity to TfR. Functionalization of PEG-PLA NPs with B6 peptide enhances their brain accumulation *in vivo* in BALB/c nude mice compared with NPs (Figure 12) (Liu et al., 2013).

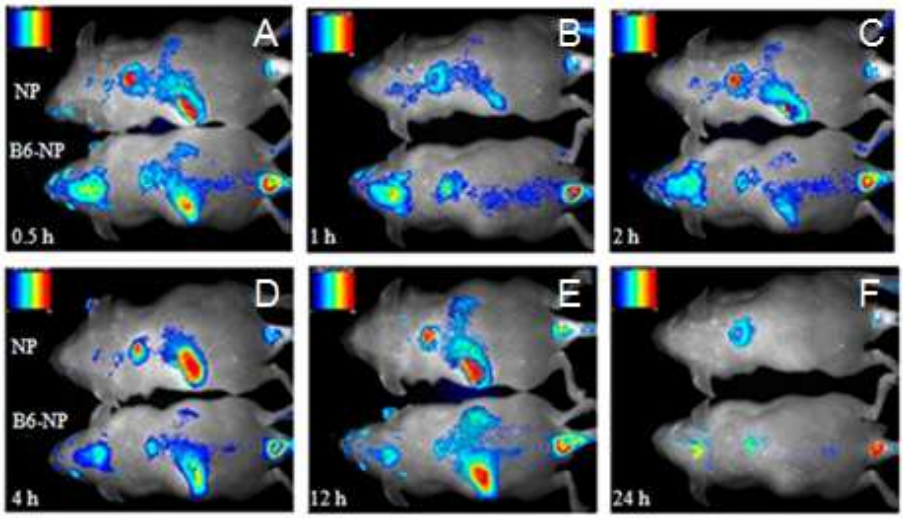

Figure 12. Functionalization of PEG-PLA nanoparticles with B6 peptide enhances their brain accumulation *in vivo* compared with nanoparticles. Distribution and retention of NPs or B6-NPs in BALB/c nude mice wasassessed by an *in vivo* fluorescence imaging system 0.5 h (**A**), 1h (**B**), 2h (**C**), 4h (**D**), 12h (**E**) and 24h (**F**) after tail vein intravenous administration. Near-infrared dyeDiR (1 mg/kg) was used as probe.
NP: Nanoparticle.
Reproduced with permission from Liu et al., 2013 © AmericanChemical Society (2013).

Injection into the tail vein of AD mouse models of B6-NPs encapsulating a neuroprotective agent showed excellent amelioration in learning impairment, cholinergic disruption and loss of hippocampal

neurons even at low drug dose (0.02 μg/day). In contrast, the free agent solution at concentrations up to 0.08 μg/day failed to produce any significant enhancement (Liu et al., 2013). This could result from a slowdown of the agent degradation after encapsulation in NPs, together with the ability of NPs to cross the BBB. Recently, Mourtas et al. prepared multifunctional liposomes decorated with OX26, an anti-TfR Abs and incorporating a curcumin derivative, proposed as AD drug candidate, which displayed significantly increased uptake by a BBB cellular model made with immortalized human brain capillary endothelial cells (hCMEC/D3) (Mourtas et al., 2014).

The approach involving LDLr ligands has been considered by Re et al., showing that the permeability of curcumin across a rat brain endothelial cell line monolayer was increased after its entrapment in mApoE-functionalized liposomes (Re et al., 2011a). Another approach indirectly exploiting ApoE, involves the coating of NPs with polysorbate 80 (P-80). In fact, according to several reports, after injection into the blood stream, apolipoproteins are adsorbed onto the surface of P-80-coated NPs (Kreuter et al., 2002). Then, the coated NPs mimic natural LDL and interact with their receptor on brain capillary endothelial cells, being endocytosed. This approach has been used also to increase the concentration of drugs intended for AD therapy in the brain. P-80 coated poly(n-butylcyanoacrylate) NPs enhanced the brain concentration of embedded rivastigmine about fourfold compared with the free drug, both intravenously injected in healthy rats (Figure 13) (Wilson et al., 2008).

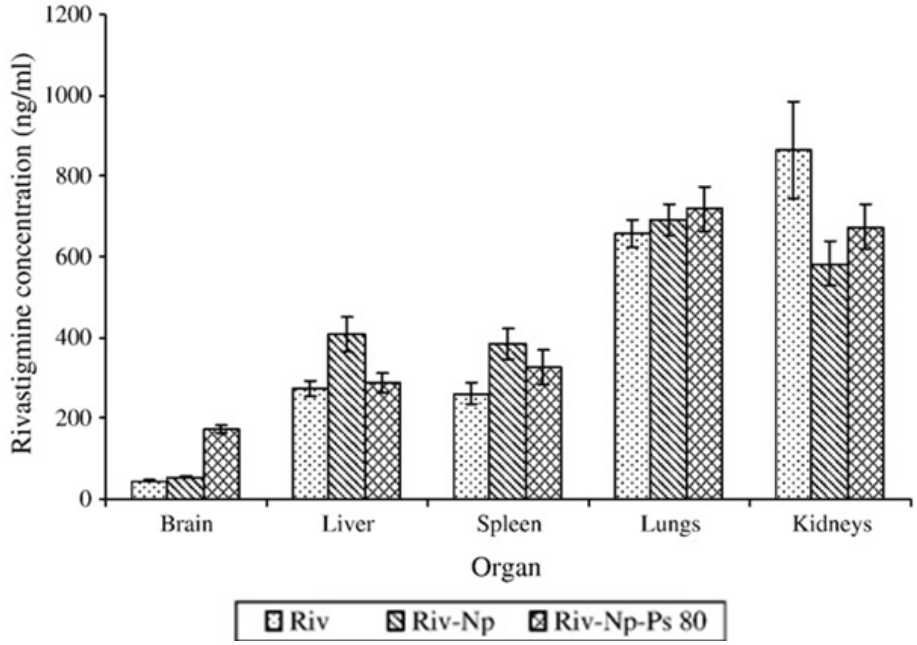

Figure 13. Coating of poly(n-butylcyanoacrylate) nanoparticles with polysorbate 80 enhances the brain accumulation of incorporated rivastigmine compared with free rivastigmine and rivastigmine incorporatedin uncoated nanoparticles. Rivastigmine concentrations (ng/ml) in different organs after intravenous injection of different rivastigmine formulations (1 mg/kg) was determined by HPLC.
NP: Nanoparticle; Riv: Rivastigmine solution; Riv–Np: Rivastigmine bound to Np; Riv–Np-Ps80: Rivastigmine bound to Np coated with 1% polysorbate 80.
Reproduced with permission fromWilson et al., 2008© Elsevier.

Orally administered P-80 coated PLGA estradiol-loaded NPs resulted in significantly higher brain levels of the hormone after 24h (1.969 ± 0.197 ng/g tissue) as compared with uncoated ones (1.105 ± 0.136 ng/g tissue) in a rat AD model (Mittal et al., 2011). One of the few examples where SLN have been proposed as drug carriers for AD therapy is reported by Yusuf et al., using P-80 coating to impart brain specific targeting to SLN containing piperine, the main alkaloid of black pepper, which has been shown to possess antioxidant activity (Chonpathompikunlert et al., 2010). These NPs showed promising

therapeutic effects in an experimentally induced AD model suggesting their ability to cross BBB (Yusuf et al., 2013).

Utilizing the strategy of LacR, Yu et al. proposed polymersomes composed by PEG-PLGA, conjugated with lactoferrin, and carrying S14G-humanin, a neuroprotective peptide. These NPs protected rats treated with Aβ from learning and memory impairment in a dose-dependent response, while S14G-humanin solution did not (Yu et al., 2014).

Several research groups supported the approach of promoting BBB endocytosis by conjugation of positively charged ligands to NP surface, exploiting the so-called adsorptive-mediated endocytosis triggered by electrostatic interactions of the ligand with the negatively charged endothelial cell surface. Sancini et al. functionalized nanoliposomes displaying high affinity for Aβ made of sphingomyelin and cholesterol with a modified cell-penetrating TAT-peptide to enhance BBB passage. The results showed an increase in the permeability across a BBB model made with hCMEC/D3 cells after the functionalization with TAT peptide (Sancini et al., 2013).

Some groups proposed NPs composed by or coated with a biocompatible and biodegradable polymer, chitosan, which enhances positive charge density on the NP surface at physiological pH. Jaruszewski et al. demonstrated that surface-adsorbed chitosan promotes the transcytosis of PLGA NPs functionalized with an anti-Aβ Abs (IgG4.1) across the BBB in a polarized canine kidney cell monolayer (Jaruszewski et al., 2012). Chitosan NPs loaded with tacrine, the first cholinesterase inhibitor approved for the treatment of AD, have been prepared by the group of Elmizadeh (Elmizadeh et al., 2013) but

not further tested. An *in vivo* demonstration of the suitability of chitosan NPs to enhance BBB crossing has been reported by Songjiang et al., showing an increased brain uptake of NPs loaded with Aβ fragment compared with the free fragment in mice (Songjiang and Lixiang, 2009). Current studies show that, in general, chitosan is a relatively nontoxic, and biocompatible material (Keana and Thanou, 2010), but the variety of existing forms, differing in size and degree of deacetylation, exponentially increases the number of biocompatibility studies needed to ensure a safe use of this material.

An original delivery system to the brain is based on the use of magnetic NPs, which could be focused within the brain region by using an externally applied magnet. Wilson et al. used magnetite chitosan microparticles, which were intravenously injected in healthy rats, to deliver the drug tacrine to the brain, by keeping a magnet at the target region. This system increased more than fivefold the concentration of tacrine in the brain in comparison with the free drug (Wilson et al., 2009).

As already mentioned, in search of alternative routes, the nasal one has been taken into account. Several compounds, such as cyclodextrins, phosphatidylcholines and fusidic acid derivatives, have been investigated as nasal absorption enhancers (Türker et al., 2004). Luppi et al. prepared albumin NPs carrying cyclodextrin and tacrine. This nanodevice produced lower drug permeation than tacrine itself in *ex vivo* permeation studies across sheep nasal mucosa, but good adhesion to nasal mucosa *in vitro* (Luppi et al., 2011). For the same purpose, Zhang et al. prepared PEG-PLGA NPs entrapping fibroblast growth factor, intended as drug for AD treatment, and decorated with Solanum

tuberosum lectin, which selectively binds to N-acetylglucosamine on the nasal epithelial membrane. The brain content of growth factor increased almost twice (1.79-folds) following intranasal administration of targeted NPs compared with intravenous administration of the same dose of free drug. Moreover, spatial learning and memory of AD rats were improved (Zhang et al., 2014).

1.3.3.2 NPs to target Aβ

For the treatment of brain disorders, the overcoming of the BBB is not the only requisite. A successful therapeutic strategy should be addressed to specifically involved regions in order to avoid adverse effects and to allow higher drug accumulation only where it is needed. Moreover, drug diffusion throughout the brain parenchyma reduces the therapeutic effect due to the minor amount of substance reaching the target. Therefore, the development of strategies specifically directed to the pathological sites into the brain parenchyma, in other words, where amyloid plaques are forming, is very important. As already mentioned, NPs with appropriate surface modifications can be advantageous candidates for brain disorders treatment because they can be functionalized to head toward specific molecular targets.

Given the pivotal role played by Aβ in AD, strategies directly or indirectly targeting the peptide are actively sought after. These may include either modulation of Aβ production, by targeting enzymes responsible for APP amyloidogenic cleavage, or peptide binding by specific ligands. Moreover, direct interaction with Aβ may interfere with its aggregation/disaggregation features (Figure 14). In fact, neo-formed Aβ monomers undergo spontaneous aggregation to form

oligomers and fibrils. Since oligomer formation is thought to be the main toxic event in AD, leading to neuronal dysfunction and death, Aβ ligands may interfere at an early stage of the pathology, by disrupting oligomers or preventing their formation.

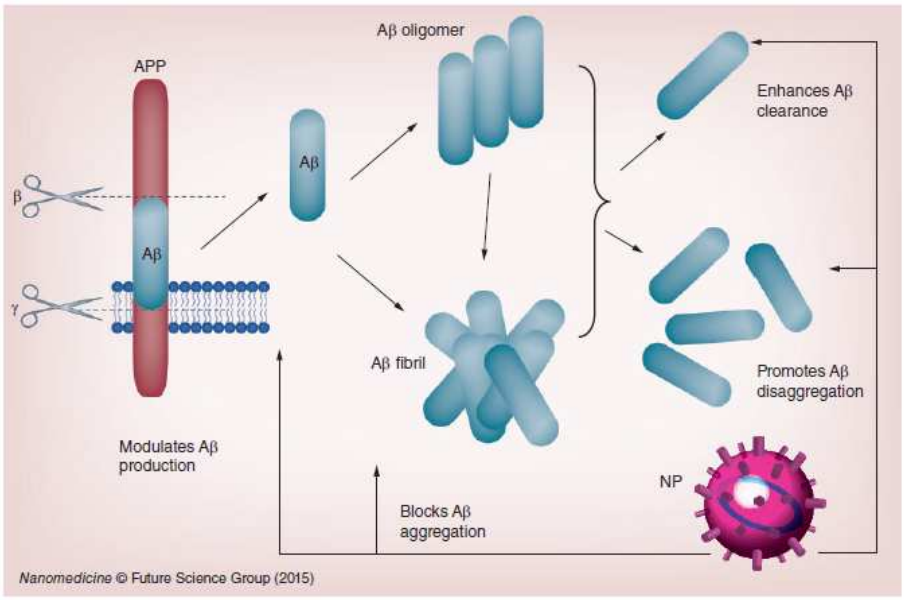

Figure 14. Strategies employed to reduce amyloid β levels in brain parenchyma through nanoparticles. In the amyloidogenic pathway, the amyloid precursor protein is cleaved subsequentially by β- and γ-secretases releasing β-amyloid peptide. Then, Aβ monomers undergo aggregation processes leading to the formation of oligomers and fibrils. Properly functionalized NPs can influence Aβ production or clearance. Moreover, properly functionalized NPs may affect Aβ aggregation features, blocking its aggregation or disgregating its assemblies.
Aβ: Amyloid β; APP: Amyloid precursor protein; NP: Nanoparticle.

Aβ-binding molecules have been conjugated to NPs both for diagnostic (the development of plaque-staining probes) and therapeutic purposes (the transport of drugs to the sites of lesion). Among different NPs, liposomes and PEG-PLA NPs have been the most used for their reported lack of toxicity, low immunogenicity and full biodegradability

(Antimisiaris et al., 2007; Xiao et al., 2010). Liposomes decorated with curcumin derivatives showed a very high affinity (1–5 nM) for Aβ fibrils *in vitro* (Mourtas et al., 2011). The observation that Aβ can interact with GM1 ganglioside (Matsuzaki, 2007) led to investigate whether other lipids may bind Aβ, and eventually to the synthesis of liposomes carrying phospatidic acid (PA) or cardiolipin (CL), binding Aβ with great affinity (22–60 nM) (Gobbi et al., 2010). Molecular dynamics simulations confirmed that the presence of negatively charged PA or CL is pivotal to facilitate the interaction of liposomes with positively charged amino acids of Aβ peptide. However, since Aβ carries also negatively charged a.a, residues, low proportions (5%) of these lipids in the bilayer are advantageous to decrease mutual repulsion (Ahyayauch et al., 2012). Another ligand used to functionalize NPs was XO4, a Chrysamine G derivative and β-sheet binder. Liposomes decorated with XO4 can target parenchyma plaques and amyloid associated with cerebral amyloid angiopathy, not only *in vitro* but even when intravenously injected in animal AD models (Tanifum et al., 2012). Moreover, Zhang et al. recently used a new Aβ-targeting peptide, QSH, screened using a mirror-image phage display selection and using $A\beta_{1–42}$ as the target. QSH-conjugated PEG-PLA NPs bound Aβ in the sub-micromolar range and stained $A\beta_{1–42}$ deposits in the brains of both AD model mice and humans (Zhang et al., 2014). Recently, also a tricyclic benzopyrane-glycofused structure was exploited as Aβ peptide ligand and linked to liposomes. NMR experiments revealed the ability of the liposomes to efficiently interact with Aβ (Airoldi et al., 2014). However, despite the availability of many ligands, it should be said that those displaying the greatest affinity

for Aβ are anti-Aβ monoclonal Abs. Both liposomes and poly(alkyl cyanoacrylate) NP surface decorated with anti-Aβ Abs bind the peptide with a KD as low as 0.5 nM and their affinity increases as a function of Ab surface density (Canovi et al., 2011; Le Droumaguetet al., 2012).
An original information has been provided by Brambilla et al., who demonstrated that PEGylation of polymeric NPs, besides to prolong their half-life in the circulation, favours interaction with the peptide both in solution and in serum (Brambilla et al., 2012).

1.3.3.2.1 Targeting Aβ aggregation

Concerning the possible effect on Aβ aggregation paradigm, curcumin, previously used for its antioxidant and anti-inflammatory activity, has been widely tested associated to NPs for this purpose. In fact, this naturally occurring phytochemical was reported to inhibit amyloid $A\beta_{1-42}$ oligomer formation and peptide-induced cell toxicity at micromolar concentrations *in vitro* (Yang et al., 2005). However, because of its low water solubility, it has often been included in NPs in order to increase its bioavailability. Cheng et al. have recently showed the lack of effect of curcumin-loaded PEG-PLA NPs on brain amyloid plaques in an *in vivo* model of AD: after oral administration of NPs to Tg2576 mice, plaque density was not affected, although the treatment resulted in significant improvements in working and cue memory (Cheng et al., 2013).
A strategy used to increase the binding affinity of curcumin for Aβ peptide has been its attachment onto the surface of NPs by the conjugation with a phospholipid. Lipid-curcumin liposomes actually showed a stronger inhibition of Aβ aggregation than curcumin-loaded

liposomes *in vitro*, but *in vivo* experiments are still lacking (Taylor et al., 2011).

Currently under development are also curcumin analogues with similar biological activity to curcumin itself, but with improved pharmacokinetics, water solubility and stability. Liposomes, covalently conjugated to an alkyne derivative of curcumin by using click-chemistry reaction, showed good ability to inhibit Aβ aggregation *in vitro*. These liposomes are supposed to be more effective as aggregation inhibitors because the curcumin-derivative molecules protrude completely from the liposome surface rather than entering the liposome bilayer as the lipid-curcumin conjugates and so they are more amenable to the interaction with Aβ species (Taylor et al., 2011).

As for liposomes functionalized with the tricyclic benzopyrane-glycofused structure, mentioned above, they were found to inhibit the formation of Aβ fibrils *in vitro*, even though their activity against aggregation was much lower than that demonstrated by liposomes decorated with curcumin (Airoldi et al., 2014).

Other molecules known to prevent aggregation are metal chelators, which are able to disrupt the interaction of Aβ with redox metal (i.e., iron, copper or zinc). However, their use as therapeutic agents is hindered by their inability to cross the BBB and for this reason they have been included in NPs. Nanoliposomes functionalized with zinc acetate, histidine residues or EDTA displayed the ability to disaggregate and resolubilize $CuA\beta_{1–42}$ and $ZnA\beta_{1–42}$ aggregates *in vitro* and to protect PC12 neuronal cells from toxicity induced by Aβ aggregates (Mufamadi et al., 2012). Similarly, nanoparticle-chelator conjugates, developed by Liu et al. by reaction between properly

functionalized polystyrene NPs and the iron chelator, 2-methyl-N-(2'-aminoethyl)-3-hydroxyl-4-pyridinone, protected human cortical neurons from Aβ-induced toxicity by inhibiting Aβ aggregation (Liu et al., 2009).

Concerning liposomes embedding acidic lipids (PA, CL), although binding Aβ with high affinity (Gobbi et al., 2010), they demonstrated poor anti-aggregation properties (Taylor et al., 2011). Nevertheless, both inhibition of fibrillation and increased disaggregation of Aβ assemblies *in vitro* was found, when liposomes embedding PA were further functionalized with mApoE (PA-mApoE) (Bana et al., 2014). This suggests the existence of a synergic action of PA and mApoE likely arising from their interaction with different amino acids residues on Aβ. Molecular dynamics simulation studies suggested that PA phosphate group, negatively charged, can interact with positively charged residues on Aβ peptide, while mApoE, positively charged, is likely to interact with negatively charged ones (Bana et al., 2014). Perhaps, other ligands that, taken individually, do not destabilize β-amyloid aggregates could give rise to a similar mechanism when combined.

Amazing results have been recently obtained *in vivo* with PA-mApoE double functionalized liposomes in two mouse AD models (APP/PS1 or APP23). In fact, the intraperitoneal injection of PA-mApoE in transgenic mice, three-times a week for 3 weeks, resulted in an improvement of their impaired memory, together with a significant reduction in the number of amyloid plaques, assessed both histologically and by PET (Figure 15).

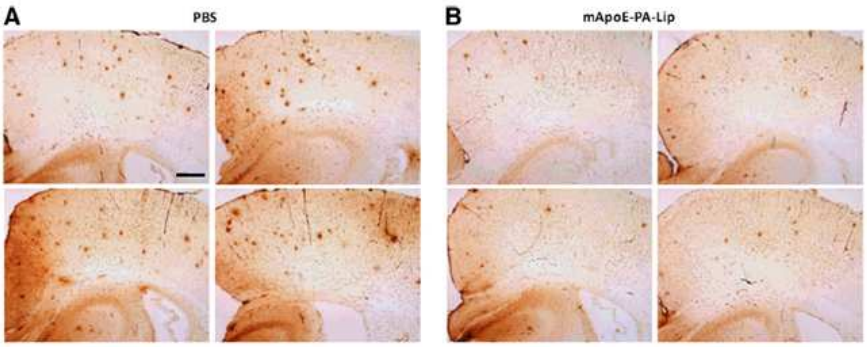

Figure 15. The treatment with liposomes functionalized with phospatidic acid and mApoE significantly reduced plaque load in the brain of APP/PS1 and APP23 Tg mice. Immunohistochemistry with anti-Aβ 6E10 monoclonal antibody of representative cortical and hippocampal brain sections of APP/PS1 Tg mice treated with (**A**) PBS or (**B**) mAPOE-PA-Lip at the end of the treatment.(Scale bar = 250 μm).
Aβ: Amyloid β; mAPOE-PA-Lip: Liposomes functionalized with phospatidic acid and mApoE; PA: Phospatidic acid.

Noteworthy, at the end of the treatment also the total amount of brain Aβ was considerably decreased, in particular its oligomeric forms, considered to be the most toxic Aβ species, responsible for neuronal dysfunction and death (Balducci et al., 2014).

Another drug, whose destabilizing properties on Aβ assemblies have recently emerged, is Selegiline, a selective MAO-B inhibitor, known to have beneficial effects in brain regions rich in dopamine receptors. Baysal et al. investigated inhibitory effects of Selegiline-loaded PLGA-PEG NPs and found out that these NPs are able to inhibit Aβ aggregation in a concentration and incubation time-dependent manner (Baysal et al., 2013).

Also gold NPs conjugated with an Aβ-binding peptide, coupled with the use of weak microwave fields, have been used to locally and remotely heat up and dissolve amyloid deposits *in vitro* (Figure 16) (Kogan et al., 2006). The rationale of this approach is based on affecting the equilibrium between soluble monomers and aggregates. The energy provided by irradiation may reverse this equilibrium and re-dissolve the precipitates. Irradiation as a mean of remotely heating biological tissues mediated by inorganic NPs has been extensively explored (Alexiou et al., 2000) and results of the study (Kogan et al., 2006) suggest it could be also be used as a molecular surgery to safely remove toxic and clogging aggregates.

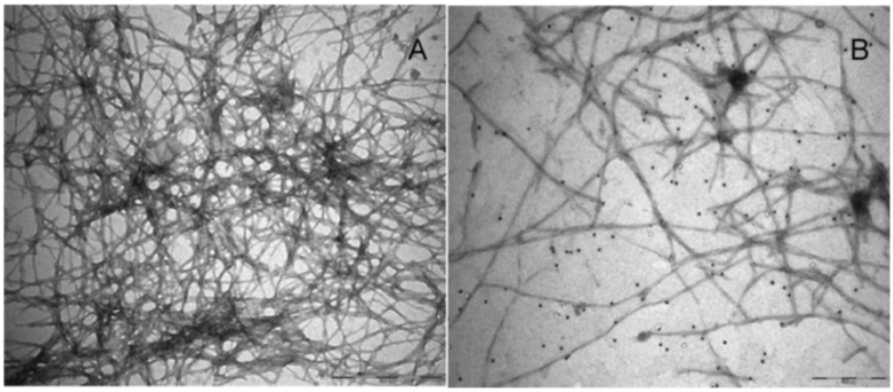

Figure 16. Gold nanoparticles conjugated with anamyloid β-binding peptide and coupled with the use of weak microwave fields are able to dissolve amyloid deposits *in vitro*. Electron microscopy of (**A**) control amyloid β $(Aβ)_{1–42}$ alone incubated for 48 h and irradiated for 8 h (bar is 500 nm) and (**B**) gold nanoparticles conjugated with an Aβ-binding peptide + $Aβ_{1–42}$ grown for 48 h after 10 min of irradiation (bar is 200 nm).
Reproduced with permission fromKogan et al., 2006 © American Chemical Society (2006).

1.3.3.2.2 Targeting Aβ clearance

Another approach to reduce the cerebral levels of Aβ, increasing its

clearance, is immunotherapy. Immunotherapies are designed to use the body's immune system to eliminate the deposition of existing Aβ senile plaques. Active immunization requires the introduction of an antigen that mimics Aβ, so that Abs targeting the antigen are produced and bind Aβ facilitating its clearance from the CNS, while the passive immunization method involves the parenteral administration of a specific antibody or pooled nonspecific Abs, thus requiring less contribution from the patient's immune response. However, even though immunization against Aβ showed promising results in preclinical animal models, its translation to humans has faced severe adverse effects, such as T-cell mediated meningo-encephalopathy, vasogenic oedema or intracerebral microhemorrhages (Delrieu et al., 2012).

The use of NPs could have many advantages compared with classical immunotherapy. For instance, NPs do not necessarily require additional adjuvants and can release the antigen gradually, reducing the number of immunizations needed. Finally, NPs can stabilize encapsulated vaccine antigens and deliver them to specific targets thanks to surface modifications. Regarding AD therapy, currently, NPs have been exploited only for active immunization in order to allow BBB permeation of fragments of Aβ. For example, chitosan NPs were loaded with an Aβ fragment (IF-A) and their immunogenicity was tested in mice. The IF-A-NPs elicited favorable titers of antiamyloid Abs in plasma and in the brain of treated animals, acting as a nano-vaccine (Songjiang and Lixiang, 2009). In another study, the first 15 amino acids of the $A\beta_{1–42}$ peptide ($A\beta_{1–15}$), were encapsulated in PLGA microparticles. After immunization by subcutaneous or intranasal

route, Balb/c mice displayed Abs levels elicited against full Aβ, comparable to the ones induced by the potent Freund's complete adjuvant, with the advantage of the lack of its toxicity (Figure 17) (Puras et al., 2011).

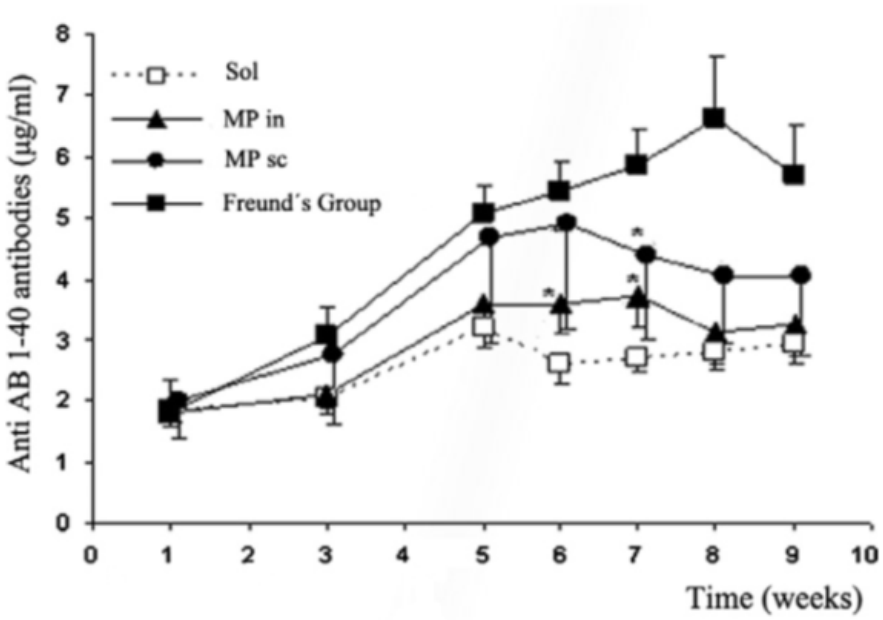

Figure 17. $A\beta_{1–15}$-loaded polylactide-co-glycolide microparticles elicit antibodies levels comparable to the ones induced by Freund's complete adjuvant. Serum anti-$A\beta_{1–40}$ antibody levels were determined by ELISA in immunized mice. Values given are mean ± standard deviation for ten mice per group. Differences between Sol and the groups immunized with PLGA microparticles loaded with $A\beta_{1–15}$ (MP in. or MP sc.) reached statistical significance at weeks 6 and 7(*$p < 0.05$).
Aβ: Amyloid β; in.: Intranasal; MP: Microparticles; sc.: Subcutaneous; Sol: Solution group; PLGA: Polylactide-co-glycolide.

These results indicate that immunotherapy with Aβ-loaded NPs could be a promising approach for the future development of a safe vaccine against AD.

1.3.3.2.3 Targeting Aβ production

As for modulation of Aβ production, β- and γ-secretase, involved in the amyloidogenic processing of APP, are the main pharmacological targets. As a first consideration, it should be taken into account that targeting secreatases could affect also physiological pathways, as those relevant for differentiation and development in which γ-secretase is involved (Evinet al., 2006). From this point of view, the inhibition of β-secretase seems to be the most promising approach, since deletion of this enzyme in mice did not cause noticeable problems (Luo et al., 2001). siRNA have been widely used to hinder directly or indirectly Aβ production, even though they rose problems of specific targeting and immunogenicity when used *in vivo*. To overcome these problems, efficient delivery technologies have been sought for and NPs have been used for their ability to deliver RNA to specific tissues or cell types, while protecting it from degradation. Alvarez-Erviti et al. loaded siRNA against BACE1 into exosomes, naturally occurring NPs with a diameter of 40–100 nm. Exosomes were prepared from immature murine dendritic cells engineered to express a fusion protein between the exosomal membrane protein Lamp2b and the neuron-targeting peptide RVG (rabies viral glycoprotein). By this strategy RVG was protruding from the membrane, mediating specific delivery to neuronal cells. These NPs were then administered both *in vitro*, in Neuro2A cells, and *in vivo*, in normal C57BL/6 mice, and delivery efficiency and knockdown extent were evaluated. Results showed a dose-dependent knockdown *in vitro* and a strong decrease of BACE1 mRNA (60%) and protein (62%) expression, together with a reduction in the total $A\beta_{1–42}$ levels (55%), *in vivo* (Alvarez-Erviti et al., 2011). Another example of

Aβ-production modulation by siRNA has been reported by Liu et al., who utilized NPs made of PEG-PEI co-polymer to mediate the delivery of ROCK-II-siRNA into C17.2 neural stem cells *in vitro*. ROCK-II is a Rho-associated serine/threonine kinase involved in AD, since its knockdown results in a decrease of amyloid-β production (Herskowitz et al., 2011). The results indicated that PEG–PEI/ROCK-II-siRNA complexes effectively suppressed ROCK-II mRNA expression, making it a promising candidate for the treatment of AD (Liu et al., 2013).

A different strategy to modulate Aβ production is the upregulation of α-secretase, the enzyme involved in the non-amyloidogenic processing of APP. An attempt to pursue this route came from Smith et al., who used lipid-based NPs functionalized with epigallocatechin-3-gallate (EGCG) to increase α-secretase activity (Smith et al., 2010). EGCG is a green tea polyphenol known for its antioxidant properties and recently shown to promote non-amyloidogenic processing of APP by upregulating α-secretase, thus preventing brain Aβ plaque formation. Specifically, EGCG indirectly (via PI3K/Akt pathway) enhances the phosphorylation of the enzyme substrate, APP, favoring substrate-mediated enzyme activation (Fernandez et al., 2010). However, despite these properties, EGCG use in clinic has been problematic, primarily as a result of poor bioavailability and inefficient delivery to the CNS, attributed to its extensive gastrointestinal degradation, poor membrane permeability and transporter-mediated intestinal efflux (Kanwar et al., 2012). However, EGCG-NPs demonstrated to be able to double the oral availability of EGCG in rats but also to promote α-secretase activity in a neuronal cell model of AD by up to 91% (Smith et al., 2010).

1.3.4 Potential neurotoxicity of NPs

While there is a growing interest on the application of NPs in biomedical field, little is known about their potential hazard for human health, in particular their possible toxic effects on CNS. Most of the data in the literature demonstrated that size, size distribution, purity, shape, crystal structure, composition, surface coating, surface charge and surface reactivity result in a different distribution, accumulation and transport of NPs to different organs, as well as across the BBB (Win-Shwe and Fujimaki, 2011). Thus, it is difficult to find general rules about brain toxicity of NPs.

It has to be noted that most neurotoxicity studies performed so far focused on metal and carbon-based NPs. Significant evidences both *in vitro* and *in vivo* indicate that these systems produce toxicity and may be associated with neurodegeneration (Karmakar et al., 2014). Thus, the benefits of NPs must be weighed against their potential toxic effects.

Polymeric NPs have been repeatedly used as biodegradable polymers because of their reported safety, good biodegradability and low immunogenicity. As for example, Hu et al. showed that PEG-PLA NPs did not present toxic effects on immortalized mouse brain endothelial cells, confirming the good *in vitro* safety of this system. However, its long-term *in vivo* brain toxicity and immunogenicity should be further investigated (Hu et al., 2009).

Concerning gold NPs, it is reported that this systems are able to cross the BBB and accumulate in the neural tissue with no evidence of toxicity in mice at least after short periods (8 days) (Lasagna-Reeves et al., 2010). Guerrero et al. showed that intraperitoneal administration in Sprague-Dawley rats of gold NPs (1.86 mg of gold/kg) conjugated with

an amphipathic peptide, increasing the *in vivo* penetration of these particles to the rat brain, had no effect on BBB integrity (Guerrero et al., 2010). Koch et al. demonstrated that gold-NPs exposure (2.84 μg/ml) for 24 h did not alter viability or induce cytotoxicity *in vitro* in murine microglial cells and human neuroblastoma cells (Koch et al., 2014). More deeply, Hutter et al. studied the interactions of gold NPs of different morphologies (spherical, rod and urchin) and coatings (PEG or cetyl trimethylammonium bromide) with microglia and neurons. Activation of microglia can affect brain functionality. Thus, studying the response of microglia to NPs is of considerable importance in the development of nanotherapeutics. *In vitro* experiments showed that microglia cells internalized all gold NPs (<109 NPs/ml) without cytotoxicity. *In vivo*, after intranasal administration in transgenic mice, rod and urchin NPs caused transient microglial activation (Hutter et al., 2010).

An important issue to be investigated is the activation of complement system (CS) triggered by NPs. Neurons and glial cells in the brain are capable of producing the full range of complement components, not only as a response to injury or infection, but also at a constant level in order to maintain normal brain functioning (Lettiero et al., 2012). Concerning AD brain, some works showed that CS is strongly activated in senile plaques (Itagaki et al., 1994), and that the classical pathway components are upregulated in the cortex (Yasojima et al., 1999). Therefore, it is critical that NPs delivered to the brain do not induce additional complement activation.

Donev et al. indicated that poly(acrylic acid)-polystyrene NPs and PEG-b-poly(propylene oxide)-b-PEG NPs did not compromise

neurogenesis and neurodevelopment in cultured human neural progenitor cells, and did not activate CS (Donev et al., 2011). Concerning liposomes, several studies provide evidences that liposomes could activate CS through two routes: naturally occurring Abs with high affinity for phospholipid headgroups or cholesterol binding to these vesicles (Alving, 1984) or the positively charged molecule C1q interacts directly with anionic phospholipids, such as CL, phosphatidic acid, phosphatidylserine and phosphatidylinositol, in the absence of specific Abs (Bradley et al., 1999). In addition, *in vitro* studies in rat serum have further demonstrated a key role for vesicle size in complement activation. Indeed, larger liposomes (200 nm or above) appeared to be stronger complement activators than their smaller counterpart of identical lipid composition and equivalent total surface area (Devine et al., 1994). Hypersensitivity reactions caused by liposomal and micellar drugs have also been reported from time to time and reviewed elsewhere (Szebeni et al., 2011). Since all these data concern the CS activation in blood, further studies on liposomal biocompatibility should be conducted in CNS to provide further insights on the risks associated with these promising targeting systems.

1.3.5 Conclusion & future perspective

Over the last decade, the potential use of NPs for AD therapy has been widely explored and relevant strategies have emerged to cross the BBB and manipulate the production, aggregation and clearance of Aβ, a putative main player in AD. However, many issues remain to be considered before nanotechnologies can be counted among AD remedies. For instance, the brain delivery of drugs obtained with drug-

loaded NPs is currently quantitatively limited in comparison with the free drug, thus future emphasis should be addressed to the development of systems transporting pharmacologically relevant amounts of AD drugs into the brain. Another issue to be considered is the safety of developed nano-devices. As already mentioned, in fact, toxicity of NPs has not yet been fully understood, hence studies on this subject are mandatory. In the meanwhile, a complete understanding of the molecular and pathogenic events of AD could suggest new strategies for specific targeting of diseased brain areas, limiting adverse effects to bystanding healthy cells.

It is desirable that these improvements could be reached working on already existing nano-devices rather than developing new ones. This would shorten the path to an effective therapy for AD.

1.4 *IN VITRO* AND *IN VIVO* MODELS FOR DRUG DESIGN AND TESTING

1.4.1 *In vitro* models of the BBB

A significant number of potential drugs for the treatment of CNS disorders fail because of their inability to penetrate through the BBB. Therefore, in order to evaluate the BBB permeability properties of drug targeting the CNS *in vitro* models of the BBB have been developed (Wilhelm et al., 2014). Although *in vivo* experiments represent the most accurate way to measure the ability of a drug to reach the brain, these experiments pose ethical and cost problems that make them poorly suitable for medium or high throughput screening. Conversely, reduced costs and greater reproducibility together with simplicity and versatility of working conditions make *in vitro* models useful tools that fulfil the most important criteria required in early stage of drug discovery (Reichel, 2006).

The most widely used *in vitro* models are based on the culture of rodent or other non-human mammalian cells. However, interspecies differences of tight junction proteins, transporters, enzymes and specific receptors on endothelial cells must be considered because they might influence BBB permeability. For this reason, considerable effort has been made to establish human cerebral endothelial cell lines. One of the best characterized and most widely used human cerebral endothelial cell lines is the hCMEC/D3 that phenocopies the normal human BBB, in terms of polarized secretion and transport, architectural organization and protein expression (Weksler et al., 2005). Since its development, about 150 studies on different aspects of cerebral endothelial biology and pharmacology have been published (Weksler

et al., 2013). Therefore, this cell line represents a widely validated model of the human BBB that can be easily grown and is suitable for drug screening.

In testing potential drugs for CNS disease, it is also important to consider that available BBB models mimic only healthy conditions without taking into account the BBB alterations associated with neurodegenerative diseases. In AD for example, several findings suggest the existence of alterations at the BBB level, which may affect drug performance *in vivo*: overexpression of RAGE (receptor for advanced glycation end-products), that transports Aβ, into the brain from the blood (Bell, 2012); downregulation of LRP1 (low-density lipoprotein-related protein-1) and P-glycoprotein (Pgp), that transport Aβ from the brain to the blood (Bell, 2012; van Assema et al., 2012); overexpression of claudin-5, a TJ protein sealing brain endothelium at cell-cell junctions, suggesting reduced paracellular BBB permeability in AD patients (Romanitan et al., 2010).

Therefore, no truthful model for drug screening exists. However, a careful choice of the *in vitro* model, depending on the scope of the experiments, can make different BBB models very useful tools in drug delivery studies.

The simplest models are based on a vertical distribution system, called tranwell system, in which cerebral endothelial cells are seeded on the porous filter of an insert in order to separate two different compartments: an upper one representing the blood (blood side) and a lower one representing the brain (brain side) (Figure 18). The pores of the membrane allow exchange of solutes between the apical and basolateral compartments and, depending on the pore size, even cellular

trafficking can be investigated.

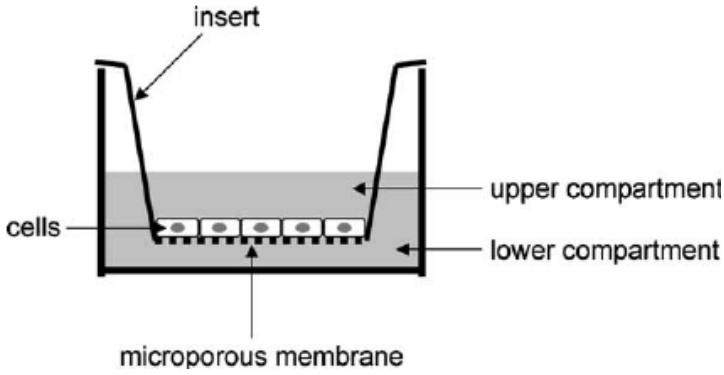

Figure 18. Graphical rapresentation of a transwell system.

The major advantage of this monoculture models is their simplicity, which allows for relative high throughput screenings at moderate costs (Berezowski et al., 2004). The major disadvantage of the model is that the effects of other cellular components of the neurovascular unit (astrocytes, pericytes and neurons) is neglected. Nevertheless, this may be sufficient for many applications investigating the BBB permeability of potential drug candidates.

However, as cell culture techniques have advanced in the last decade, more-sophisticated models that better reflect *in vivo* anatomy of the neurovascular unit have begun to emerge. These models are based on cerebral endothelial cells cultured in the presence of pericytes, astrocytes, and/or neurons in different arrangements. The major disadvantages of these type of models are to be relatively expensive and time-consuming.

Since shear stress induced by blood flow has been demonstrated to significantly influence endothelial properties including barrier

properties as well (Cucullo et al., 2011; Naik and Cucullo, 2012), dynamic BBB models have been developed. These models try to mimic the *in vivo* blood flow by culturing endothelial cells in hollow fibers and circulating culture media creating a tunable shear stress. Despite the numerous advantages of this system, it is not suitable for rapid, high throughput studies and the establishment of the model requires specific technical skills. Furthermore, initially a large number of cells are needed to load the capillaries and the optically monitoring of cell morphology is not possible.

Last generation of BBB *in vitro* models are represented by microfluidic models (van der Helm et al., 2016), which allow considerable downsizing of BBB models with the advantage of lower required cell number. In these models, cells of the neurovascular unit are also cultured on porous membranes but the membrane is placed at the interface of two microchannels, which allows flow of the culture medium. Again high costs and the lack of standardization are the main disadvantages of this method.

1.4.2 Animal models of AD

Despite their low cost and simplicity, *in vitro* models cannot resemble the complicated physiological environment of a whole organism. Although cell-based assays can provide some information, cultured cells do not mimic physiological conditions and complex interactions among different cell types and tissues, which are crucial in the evolution of the most of disorders. For this reason, animal studies remain dominant in the current paradigm for drug development, though time-consuming, costly and ethically problematic.

Animal models aiming at studying human diseases emerged in the 1800s and experienced a major boost during the last decades. In general, animal models of human disease can be classified into spontaneous models, presumed to develop their condition without experimental manipulation, pharmacological models, in which anatomical structures or essential pathways involved in the pathology are altered in order to lead to the condition, and transgenic models, based on one or several inserted human genes relevant to the disease.

All types of animal models aim at replicating the symptoms and the lesions of AD have been produced in order to better understand the mechanisms leading to AD pathogenesis and progression and to test compounds for its treatment. However at the moment no animal model recapitulates all aspects of human AD, reflecting the limitations of using a non-human *in vivo* system to model a human condition that takes decades to develop and mainly involves higher cognitive functions (Van Dam and De Deyn, 2011).

Early-stage animal testing for AD research is typically performed in rodents, followed by drug safety testing and certain efficacy evaluations in larger mammals, such as rabbits and dogs. Recently, alternative small-animal models are emerging, enabling a more cost-effective and rapid screening of compounds. These new models are characterized by small size, high fecundity and simpler experimental tractability and use both vertebrates (zebrafish, *Danio rerio*) and invertebrates (fruit fly, *Drosophila melanogaster*, and nematode, *Caenorhabditis elegans*) (Langley, 2014). However, by far the dominant animal models for AD research have been transgenic (Tg) mice, mostly based on amyloid hypothesis of AD causation (Elder et al., 2010; Howlett, 2011).

Modelling of AD in transgenic mouse models became reality in the mid-1990s with the development of the PDAPP model (Games et al., 1995), followed in subsequent years by the Tg2576 (Hsiao et al., 1996) and APP23 (Sturchler-Pierrat et al., 1997) mouse models, currently the most widely used amyloidosis models in AD-related research. These first transgenic models overexpress the gene encoding for the human APP carrying mutations that increased the production of Aβ peptide. In particular, both the Tg2576 and APP23 model express human APP with the Swedish mutation driven by the hamster PrP and murine Thy-1 promoter, respectively. These mice show striking histological similarities to features of AD at 12-15 months, with deposition of amyloid plaques in the cortex and hippocampus. Cognitive deficits are also observed, before plaques deposition in the brain parenchyma, at around 6-11 months, depending from the model (Dodart et al., 1999; Van Dam et al., 2003; Van Dam et al., 2005) and persist at later stages of the pathology.

The discovery of familial AD mutations in the presenilin genes, which influence APP processing, opened the path for PS1 and PS2 transgenic mouse models and double-cross APP/PS models (McGowan et al., 2006). In particular, double-cross APP/PS mice show an early onset if compared to Tg2576 and APP23 and a more severe pathology, thereby supporting the modifying role of PSEN. Among them, APP/PS1, overexpressing the Swedish mutation of APP together with PS1 deleted in exon 9 (Jankowsky et al., 2004), are characterized by early amyloid deposition, detectable at 5 months of age, followed by cognitive deficits, that appear at 9 months of age. Astrocytosis develops in parallel with plaque deposition, with severe gliosis starting around six

months, especially in the proximity of plaques. In addition, deficits in synaptic plasticity have been observed. The major limitations of the above-mentioned models are the lack of Neurofibrillary Tangles (NFT) formation and the absence of extensive neuronal death, characteristics that are both found in the human pathology. The lack of NFT was partially counterbalanced with the development of several (mutated) tau models and the crossing of tau and amyloidosis models. This triple mice, produced by the group of La Ferla (Oddo et al., 2003a; Oddo et al., 2003b) featured enhanced amyloid deposition prior to NFT pathology with a temporal and spatial profile equivalent to AD (McGowan et al., 2006) accompanied by tau phosphorylation, NFT-like formation and overt neuronal loss (Götz et al., 2004; Pérez et al., 2005). In addition, they show early-stage synaptic dysfunction and induction of inflammatory processes (Oddo et al., 2003a; Oddo et al., 2003b; Janelsins et al., 2005).

The generation of transgenic rodent research models that develop some of the pathological hallmarks of AD has given a sizable boost to drug discovery efforts and has also raised many intriguing questions about the underlying disease process. However, one should never neglect the potential dangers of uncritical extrapolating from mouse to humans.

1.5 PREMISES FOR THE PRESENT WORK

1.5.1 mApoE-PA-LIP

In the context of AD, liposomes composed of sphingomyelin (Sm) and cholesterol (Chol) and functionalized with phosphatidic acid (PA) and with a modified peptide derived from the receptor-binding domain of Apolipoprotein E (mApoE) were designed (mApoE-PA-LIP) in order to cross the BBB and target Aβ.

Liposomes composed of a matrix of Sm and Chol in equimolar ratio have been repeatedly utilized *in vivo* for therapeutic purposes, displaying good circulation times in blood, biocompatibility, resistance to hydrolysis, low ion permeability (Webb et al., 1995; Thomas et al., 2006). Moreover, Sm/Chol bilayers are known to form raft-like or liquid-ordered domains that are representative of a native cellular membrane where Aβ accumulates (Choucair et al., 2007) and the presence of cholesterol was shown to strengthen the Aβ-membrane interaction (Qiu et al., 2009). In fact, the involvement of membrane lipids in AD had been extensively studied and a number of investigations reported their ability to interact with the peptide (Matsuzaki, 2007; Taylor and Hooper, 2007). Within this frame, preliminary immunostaining studies identified anionic phospholipids, such as PA, as suitable Aβ ligands. Molecular dynamics simulations confirmed that the presence of negatively charged phospholipids is pivotal to facilitate the interaction of liposomes with positively charged amino acids of Aβ peptide. However, since Aβ carries also negatively charged amino acids, residues, low proportions (5%) of these lipids in the bilayer are advantageous to decrease mutual repulsion (Ahyayauch et al., 2012). For this reason, and to avoid complement activation, PA

was integrated in the liposome bilayer at the concentration of 5 mol%. PA conferred liposomes a very high affinity for Aβ in all its aggregation forms, mostly oligomers and fibrils, as indicated by ultracentrifugation and Surface Plasmon Resonance (SPR) experiments. This high binding affinity was likely due to the occurrence of multivalent interactions, which also made the binding between liposomes and Aβ pseudo-irreversible, with a very low dissociation rate constant (Gobbi et al., 2010).

Subsequently, in the searching for a strategy to cross the BBB, the attention was focused on the low-density lipoprotein receptor (LDLr)-mediated pathway (Cerletti et al., 2000; Markoutsa et al., 2011). LDLr is present on capillary endothelial cells of several species and its expression is upregulated in the BBB with respect to other endothelia (Dehouck et al., 1994). Moreover, nanoparticles interacting with the LDLr *via* a specific apolipoprotein E (ApoE) amino acid sequence (corresponding to the binding domain of the ApoE, aa. 141-150) were shown to be transported across the BBB by transcytosis, bypassing the lysosomal degradation (Dehouck et al., 1997). To exploit the LDL-r pathway, the sequence corresponding to residues 141-150 of human ApoE peptide, modified with the attachment of the CWG sequence, CWG-LRKLRKRLLR, was attached at high density (1.25 mol%) as a monomer to Sm/Chol liposomes. As chemical linkage between the peptide and the NPs, the thiol-maleimide covalent coupling was chosen because of its ability to confer NPs the best performance in terms of permeability across an *in vitro* model of the BBB (Salvati et al., 2013). To allow the functionalization 2.5 mol% of 1,2-stearoyl-sn-glycero-3-phosphoethanolamine-N-[maleimide(polyethylene glycol)-2000)],

mal-PEG-PE, was added to the liposome composition. Functionalization with mApoE peptide increased the uptake of plain NPs by endothelial cells and enhanced the transport of a drug payload through the BBB *in vitro* (Re et al., 2011a).

Joining the Aβ binding ability of PA with the ability of mApoE to cross the BBB, mApoE-PA-LIP were developed. Experiments with dually radiolabelled liposomes showed that bifunctionalization enhanced the passage of radioactivity across the BBB *in vitro* of 5-fold higher with respect to PA-LIP (Bana et al., 2014). Moreover, liposomes containing PA and decorated with the mApoE displayed the most efficient targeting of hCMEC/D3 cells. The competition experiments, showing a decreased mApoE-PA-LIP uptake in presence of free mApoE peptide, suggest the involvement of saturable system in their cellular internalization, most likely a receptor-mediated pathway (Pinzón-Daza et al., 2012), as already reported for other synthetic peptides mimetic of human ApoE (Datta et al., 2010). This speculation is supported by the experiments devoted to assess the intracellular distribution of mApoE-PA-LIP, which showed that the uptake of these liposomes is presumably mediated by endocytosis (Garcia-Garcia et al., 2005; Re et al., 2011b). Regarding the Aβ binding ability, SPR showed that bifunctionalized liposomes mantained the ability to strongly bind Aβ (K_d = 0.6 μM) (Bana et al., 2014). Since Aβ aggregation process is central in AD pathogenesis and progression, the ability of mApoE-PA-LIP to affect Aβ aggregation/disaggregation features was also evaluated *in vitro* through Thioflavin-T and SDS-PAGE/WB assays. mApoE-PA-LIP inhibited peptide aggregation (70% inhibition after 72 h) and triggered the disaggregation of preformed Aβ aggregates (60% decrease

after 120 h incubation) (Bana et al., 2014). The fact that mono-functionalized liposomes (PA-LIP or mApoE-LIP) were not able to do the same suggest the existence of a synergic action of PA and mApoE. The synergic action could arise from their interaction with different amino acids residues on Aβ aggregates. In fact, Molecular Dynamics Simulation studies (Ahyayauch et al., 2012) suggest that PA phosphate group, negatively charged, can interact with positively charged residues on Aβ peptide, while mApoE, positively charged (Datta et al., 2000), is likely to interact with negatively charged residues, present on Aβ peptide at physiological pH (Martineau et al., 2010). As for toxicity, biocompatibility studies were carried out *in vitro* on different cells types (endothelial and differentiated neuroblastoma cells) and showed that mApoE-PA-LIP did not affect the cell viability, BBB monolayer integrity, nitric oxide production and did not induce endoplasmic reticulum stress (Bana et al., 2014). Finally, before the *in vivo* proof of concept, a preliminary biodistribution study was carried out in Balb/c mice. Results showed a higher brain accumulation of radioactivity after peripheral administration of dually-radiolabeled mApoE-PA-LIP, with respect to PA-LIP, suggesting that bifunctionalization is crucial to enhance BBB crossing also *in vivo*. The ratio between the two radiotracers, comparable in the blood and in the brain, suggested that mApoE-PA-LIP could reach the brain in an intact form (Bana et al., 2014).

Taken all together, these results suggest that mApoE-PA-LIP are valuable nanodevices with a potential applicability *in vivo* for the treatment of AD.

1.5.2 PINPs

In parallel with the development of mApoE-PA-LIP, liposomes functionalized with a fusion peptide (RI-OR2-TAT), made by a retro-inverted peptide (RI-OR2) attached to the HIV cell-penetrating sequence (TAT), were also designed for AD therapy.

OR2 peptide (RGKLVFFGR-NH_2) was designed as a potential Aβ aggregation inhibitor using Aβ hydrophobic residues 16-20 (KLVFF), part of the binding region responsible for Aβ self-association and consequent aggregation (Tjernberg et al., 1996). It was already demonstrated that modified synthetic peptides based on the sequence of Aβ central region were able to prevent its conversion to β-sheet-rich aggregated structures (Ghanta et al., 1996; Soto et al., 1998; Findeis et al., 1999; Gordon et al., 2001; Kokkoni et al., 2006). However, these reported inhibitors were designed to block the formation of the late aggregates rather than the most toxic early aggregates of Aβ and therefore, they were only able to partially reverse the toxicity of Aβ aggregates. To aid solubility and, at the same time, to prevent it from self-aggregating and so acting as a "seed" to promote Aβ aggregation, an additional cationic Arg was added at its N- and C-termini using a Gly as a spacer. An amide group was also added at the C-terminus to render the peptide less charged.

As assessed by Th-T assay and electron microscopy, OR2 was able to completely prevent Aβ fibril formation and was also shown to be a potent inhibitor of Aβ oligomerization, as shown by size exclusion chromatography and oligomer specific ELISA (Austen et al., 2008). This latter effect was probably due to the binding of the monomeric Aβ molecule and correlated with the ability of the peptide to protect human

neuroblastoma SHSY5Y cells from Aβ-induced toxicity (Austen et al., 2008). However, peptides are short-lived molecules *in vivo* and to convert them into useful drugs it is usually necessary to transform them into peptidomimetics. Many previous studies, with a variety of different peptide ligands, showed that retro-inverso peptides can maintain a topology, a potency, and a selectivity similar to those of their native "parent" molecules, but displaying a much improved bioavailability profile, following oral or intravenous administration, because of their greatly enhanced stability to proteolysis (Chorev and Goodman, 1993; Chorev and Goodman, 1995). In fact, in a retro-inverso peptide, all of the natural L-amino acids are replaced with the D-enantiomer and the peptide bonds are also reversed, conferring proteolysis resistance. For these reasons, a "retro-inverso" version of OR2 was designed (RI-OR2). Unlike OR2, RI-OR2 was highly stable to proteolysis and completely resisted breakdown in human plasma and brain extracts. In SPR experiments, RI-OR2 was shown to bind to both Aβ monomers and fibrils and maintained the OR2 ability to inhibit Aβ oligomer and fibril formation as well as to reverse Aβ toxicity toward SH-SY5Y neuroblastoma cells (Taylor et al., 2010).

As a final step in the design of the fusion peptide to be linked on the surface of PINPs liposomes, a retro-inverted version of the HIV protein transduction domain 'TAT' (Green and Loewenstein, 1988) was attached to RI-OR2 in order to target the peptide, called RI-OR2-TAT, to the brain and make it a suitable drug candidate for AD. RI-OR2-TAT displayed similar properties to RI-OR2 as an inhibitor of Aβ aggregation and Aβ-induced toxicity *in vitro* and showed an increased binding affinity to Aβ, probably due to the presence of several

positively charged amino-acid residues on the TAT portion (Parthsarathy et al., 2013). The retro-inverted TAT sequence was effective as a transit peptide, as demonstrated by the rapid entry of the fluorescent peptide into cultured SHSY-5Y cells. Following its peripheral injection, a fluorescein-labelled version of RI-OR2-TAT was also found to cross the blood brain barrier and bind to the amyloid plaques and activated microglial cells present in the cerebral cortex of 17-months-old APP/PS1 transgenic mice (Parthsarathy et al., 2013). The interaction with amyloid plaques was in accordance with the relatively high binding affinity between RI-OR2-TAT and Aβ fibrils, as assessed by SPR. The finding that RI-OR2-TAT accumulates inside activated microglial cells was also expected, because they actively take up amyloid by phagocytosis and are involved in the clearance of Aβ (Paresce et al., 1997). In order to determine effects on brain pathology, RI-OR2-TAT was injected peripherally into APP/PS1 mice every day for 21 days, at 100 nmol/kg. This dose was chosen because it is similar to that used in a previous study with another peptide drug (McClean et al., 2011). The treatment resulted in a marked and highly significant reduction in amyloid plaque load, in the numbers of activated microglial cells and in the amount of oxidative damage. RI-OR2-TAT also reduced the level of Aβ oligomers in the cerebral cortex of the APP/PS1 mice. The inhibition of amyloid plaque load as well as the reduction of oxidative stress were speculated to be a consequence of RI-OR2-TAT ability to reduce microglial cell number, resulting in fewer activated microglial cells congregating around the amyloid cores of senile plaques and releasing less free radicals and cytokines involved in chronic inflammation and oxidation reactions (Holscher, 1998).

However, the inhibition of oxidative damage could also be linked directly with the effects of RI-OR2-TAT on Aβ aggregation. Reactive oxygen species (ROS) have been shown to be generated during the early stages of Aβ aggregation, via an interaction between Aβ and redox-active metal ions, and an early-stage aggregation inhibitor would be expected to block this source of ROS formation (Tabner et al., 2005). Aβ oligomers have also been reported to induce calcium ion influx into cells and, subsequently, oxidative damage, through their ability to form ion-permeable 'pores' in cell membranes (Kagan and Thundimadathil, 2010). The reduction of microglial cell load and oxidative stress seen following treatment with RI-OR2-TAT could, therefore, be a 'downstream' consequence of the ability of this inhibitor to reduce Aβ oligomer and/or amyloid fibril formation. The peripheral administration of RI-OR2-TAT had also a marked effect on stimulation of neurogenesis. Inhibition of nerve stem cell proliferation could be a downstream consequence of Aβ aggregation (Monje et al., 2003; Cunningham and Skelly, 2011). Thus, RI-OR2-TAT could rescue brain stem cells from the damaging pro-inflammatory effects of Aβ.

Together, the obtained results identify RI-OR2-TAT as a potential disease-modifying treatment for AD.

1.6 SCOPE OF THE THESIS

A consistent body of evidence establishes a central role of Aβ in the pathogenesis of AD. This peptide, released from cells, progressively aggregates and accumulates, depositing as extracellular plaques detectable *post mortem* in AD brains and causing a downstream series of pathological events that finally lead to neuronal degeneration, cognitive dysfunction and memory loss, main clinical features of the disease. Focusing on brain Aβ as the target, the aim of the present work was the design and testing of nanoliposomes functionalized to cross the BBB and to interact with Aβ. Two different liposome preparations were object of the present work: i) mApoE-PA-LIP, liposomes bifunctionalized with mApoE, a peptide derived from the apolipoprotein-E receptor-binding domain for BBB targeting, and with PA, phosphatidic acid, for Aβ binding; ii) PINPs, liposomes functionalized with RI-OR2-TAT, a retro-inverted fusion peptide made by a combination of the Aβ aggregation inhibitor, RI-OR2, and the HIV 'TAT' cell penetrating peptide.

Based on previous observations obtained *in vitro*, in Chapter 2 the therapeutic efficacy of mApoE-PA-LIP was investigated in Tg AD mouse models, considering the effects of the treatment on memory impairment and amyloid pathology.

In Chapter 3 the mechanism of action of mApoE-PA-LIP was explored and their ability to draw out Aβ from the brain (sink effect), previously postulated, was evaluated using a transwell cellular model of the BBB.

The possibility to prevent or delay AD progression by a long-term treatment with mApoE-PA-LIP was analyzed in Chapter 4. Besides the effects on memory impairment and amyloid pathology, the influence on the onset of anatomical abnormalities linked to AD, the modification of molecular pathways involved in Aβ production and clearance and the toxicity of the treatment were considered.

Regarding PINPs, in Chapter 5 their effects on Aβ aggregation and toxicity as well as their ability to cross the BBB were assessed *in vitro*. Moreover, their efficiency in entering the brain of healthy mice and in affecting cognitive deficit in AD Tg mice was investigated.

References

Ahyayauch H, Raab M, Busto JV, Andraka N, Arrondo JL, Masserini M, Tvaroska I, Goni FM (2012) Binding of β-amyloid (1–42) peptide to negatively charged phospholipid membranes in the liquid-ordered state: modeling and experimental studies. Biophys. J. 103(3):453-63.

Airoldi C, Mourtas S, Cardona F, Zona C, Sironi E, D'Orazio G, Markoutsa E, Nicotra F, Antimisiaris SG, La Ferla B (2014) Nanoliposomes presenting on surface a cis-glycofused benzopyran compound display binding affinity and aggregation inhibition ability towards Amyloid β1–42 peptide. Eur. J. Med. Chem. 85:43-50.

Akbarzadeh A, Rezaei-Sadabady R, Davaran S, Joo SW, Zarghami N, Hanifehpour Y, Samiei M, Kouhi M and Nejati-Koshki K (2013) Liposome: classification, preparation, and applications. Nanoscale Res Lett. 8(1): 102.

Alexiou C, Arnold W, Klein RJ, Parak FG, Hulin P, Bergemann C, Erhardt W, Wagenpfeil S, Lübbe AS (2000) Locoregional cancer treatment with magnetic drug targeting. Cancer Res. 60(23):6641-8.

Alvarez-Erviti L, Seow Y, Yin H, Betts C, Lakhal S, Wood MJ (2011) Delivery of siRNA to the mouse brain by systemic injection of targeted exosomes. Nat. Biotechnol. 29(4):341-5.

Alving CR (1984) Natural antibodies against phospholipids and liposomes in human. Biochem. Soc. Trans. 12(2):342-4.

Antimisiaris SG, Kallinteri P, Fatouros DG (2007) Liposomes and drug delivery. In: Pharmaceutical Manufacturing Handbook:

Production and Processes. Gad SC (Ed.). John Wiley & Sons, Inc., NJ, USA, Chapter 13.

Austen BM, Paleologou KE, Ali SA, Qureshi MM, Allsop D, El-Agnaf OM (2008) Designing peptide inhibitors for oligomerization and toxicity of Alzheimer's beta-amyloid peptide. Biochemistry 47(7):1984-92.

Balducci C, Mancini S, Minniti S, La Vitola P, Zotti M, Sancini G, Mauri M, Cagnotto A, Colombo L, Fiordaliso F, Grigoli E, Salmona M, Snellman A, Haaparanta-Solin M, Forloni G, Masserini M, Re F (2014) Multifunctional liposomes reduce brain β-amyloid burden and ameliorate memory impairment in Alzheimer's disease mouse models. J. Neurosci. 34(42):14022-31.

Bana L, Minniti S, Salvati E, Sesana S, Zambelli V, Cagnotto A, Orlando A, Cazzaniga E, Zwart R, Scheper W, Masserini M, Re F (2014) Liposomes bifunctionalized with phosphatidic acid and an ApoE-derived peptide affect Aβ aggregation features and cross the blood-brain barrier: Implications for therapy of Alzheimer disease. Nanomedicine 10(7):1583-90.

Barage SH, Sonawane KD (2015) Amyloid cascade hypothesis: Pathogenesis and therapeutic strategies in Alzheimer's disease. Neuropeptides 52:1-18.

Bard F, Cannon C, Barbour R, Burke RL, Games D, Grajeda H, Guido T, Hu K, Huang J, Johnson-Wood K, Khan K, Kholodenko D, Lee M, Lieberburg I, Motter R, Nguyen M, Soriano F, Vasquez N, Weiss K, Welch B, Seubert P, Schenk D, Yednock T (2000) Peripherally administered antibodies against amyloid beta-

peptide enter the central nervous system and reduce pathology in a mouse model of Alzheimer disease. Nat. Med. 6(8):916-9.

Barenholz Y (2012) Doxil® – the first FDA-approved nano-drug: lessons learned. J. Control Release 160:117–134.

Bartolini M, Bertucci C, Bolognesi ML, Cavalli A, Melchiorre C, Andrisano V (2007) Insight into the kinetic of amyloid beta (1-42) peptide self-aggregation: elucidation of inhibitors' mechanism of action. Chembiochem. 8(17):2152-61.

Bateman RJ, Xiong C, Benzinger TL, Fagan AM, Goate A, Fox NC, Marcus DS, Cairns NJ, Xie X, Blazey TM, Holtzman DM, Santacruz A, Buckles V, Oliver A, Moulder K, Aisen PS, Ghetti B, Klunk WE, McDade E, Martins RN, Masters CL, Mayeux R, Ringman JM, Rossor MN, Schofield PR, Sperling RA, Salloway S, Morris JC, Dominantly Inherited Alzheimer Network (2012) Clinical and biomarker changes in dominantly inherited Alzheimer's disease. N. Engl. J. Med. 367(9):795-804.

Baysal I, Yabanoglu-Ciftci S, Tunc-Sarisozen Y, Ulubayram K, Ucar G (2013) Interaction of selegiline-loaded PLGA-b-PEG nanoparticles with beta-amyloid fibrils. J. Neural. Transm. 120(6):903-10.

Begley DJ (2004) Delivery of therapeutic agents to the central nervous system: the problems and the possibilities. Pharmacol. Ther. 104(1):29-45.

Bell RD (2012) The imbalance of vascular molecules in Alzheimer's disease. J Alzheimer Dis 32(3):699-709.

Berezowski V, Landry C, Lundquist S, Dehouck L, Cecchelli R, Dehouck MP, Fenart L (2004) Transport screening of drug

cocktails through an in vitro blood-brain barrier: is it a good strategy for increasing the throughput of the discovery pipeline? Pharm. Res. 21, 756−60.

Bibl M, Mollenhauer B, Lewczuk P, Esselmann H, Wolf S, Trenkwalder C, Otto M, Stiens G, Rüther E, Kornhuber J, Wiltfang J (2007) Validation of amyloid-beta peptides in CSF diagnosis of neurodegenerative dementias. Mol. Psychiatry 12(7):671-80.

Biswas S, Torchilin VP (2014) Nanopreparations for organelle-specific delivery in cancer. Adv. Drug. Deliv. Rev. 66:26-41.

Blanco E, Shen H, Ferrari M (2015) Principles of nanoparticle design for overcoming biological barriers to drug delivery. Nat. Biotechnol. 33:941-51.

Bonda DJ, Lee HP, Lee HG, Friedlich AL, Perry G, Zhu X, Smith MA (2010) Novel therapeutics for Alzheimer's disease: an update. Curr. Opin. Drug Discov. Devel. 13(2):235-46.

Borenstein AR, Copenhaver CI, Mortimer JA (2006) Early-life risk factors for Alzheimer disease.Alzheimer Dis. Assoc. Disord. 20(1):63-72.

Bozzuto G, Molinari A (2015) Liposomes as nanomedical devices. Int. J. Nanomed. 10:975–99.

Braak H, Braak E (1991) Neuropathological stageing of Alzheimer-related changes. Acta Neuropathol. 82(4):239-59.

Bradley AJ, Maurer-Spurej E, Brooks DE, Devine DV (1999) Unusual electrostatic effects on binding to C1q to anionic liposomes: role of anionic phospholipid domains and their line tension. Biochemistry 38(25):8112-23.

Brambilla D, Le Droumaguet B, Nicolas J, Hashemi SH, Wu LP, Moghimi SM, Couvreur P, Andrieux K (2011) Nanotechnologies for Alzheimer's disease: diagnosis, therapy, and safety issues. Nanomedicine 7(5):521-40.

Brambilla D, Verpillot R, Le Droumaguet B, Nicolas J, Taverna M, Kóňa J, Lettiero B, Hashemi SH, De Kimpe L, Canovi M, Gobbi M, Nicolas V, Scheper W, Moghimi SM, Tvaroška I, Couvreur P, Andrieux K (2012) PEGylated nanoparticles bind to and alter amyloid-beta peptide conformation: toward engineering of functional nanomedicines for Alzheimer's disease. ACS Nano 6(7):5897-908.

Budai M, Szogyi M (2001) Liposomes as drug carrier systems. Preparation, classification and therapeutical advantages of liposomes. Acta Pharm. Hung. 71(1):114-8.

Bullock R, Dengiz A (2005) Cognitive performance in patients with Alzheimer's disease receiving cholinesterase inhibitors for up to 5 years. Int. J. Clin. Pract. 59(7):817-22.

Canovi M, Markoutsa E, Lazar AN, Pampalakis G, Clemente C, Re F, Sesana S, Masserini M, Salmona M, Duyckaerts C, Flores O, Gobbi M, Antimisiaris SG (2011) The binding affinity of anti-Aβ1–42 MAb-decorated nanoliposomes to Aβ1–42 peptides in vitro and to amyloid deposits in post-mortem tissue. Biomaterials 32(23):5489-97.

Castellano JM, Kim J, Stewart FR, Jiang H, DeMattos RB, Patterson BW, Fagan AM, Morris JC, Mawuenyega KG, Cruchaga C, Goate AM, Bales KR, Paul SM, Bateman RJ, Holtzman DM (2011) Human apoE isoforms differentially regulate brain

amyloid-β peptide clearance. Sci. Transl. Med. 3(89):89ra57.

Cerletti A, Drewe J, Fricker G, Eberle AN, Huwyler J (2000) Endocytosis and transcytosis of an immunoliposome-based brain drug delivery system. J. Drug. Target 8:435-46.

Cheng KK, Yeung CF, Ho SW, Chow SF, Chow AH, Baum L (2013) Highly stabilized curcumin nanoparticles tested in an in vitro blood–brain barrier model and in Alzheimer's disease Tg2576 mice. AAPS J. 15(2):324-36.

Chonpathompikunlert P, Wattanathorn J, Muchimapura S (2010) Piperine, the main alkaloid of Thai black pepper, protects against neurodegeneration and cognitive impairment in animal model of cognitive deficit like condition of Alzheimer's disease. Food Chem. Toxicol. 48(3):798-802.

Chorev M, Goodman M (1993) A dozen years of retro-inverso peptido mimetics. Acc. Chem. Res. 26:266-73.

Chorev M, Goodman M (1995) Recent developments in retro peptides and proteins: An ongoing topochemical exploration. Trends Biotechnol. 13:438-45.

Chou LY, Ming K, Chan WC (2011) Strategies for the intracellular delivery of nanoparticles. Chem Soc Rev. 40(1):233-45.

Choucair A, Chakrapani M, Chakravarthy B, Katsaras J, Johnston LJ (2007) Preferential accumulation of Abeta(1-42) on gel phase domains of lipid bilayers: an AFM and fluorescence study. Biochim Biophys Acta 1768(1):146e54.

Cucullo L, Hossain M, Puvenna V, Marchi N, Janigro D (2011) The role of shear stress in Blood-Brain Barrier endothelial physiology. BMC Neurosci. 12:40.

Cunningham C, Skelly DT (2011) Non-steroidal anti-inflammatory drugs and cognitive function: are prostaglandins at the heart of cognitive impairment in dementia and delirium? J Neuroimmune Pharmacol 7:60-73.

Datta G, Chaddha M, Garber DW, Chung BH, Tytler EM, Dashti N, Bradley WA, Gianturco SH, Anantharamaiah GM (2000) The receptor binding domain of apolipoprotein E, linked to a model class A amphipathic helix, enhances internalization and degradation of LDL by fibroblasts. Biochemistry 39(1):213-20.

Datta G, Chaddha M, Handattu SP, Palgunachari MN, Nayyar G, Garber DW, Gupta H, White CR, Anantharamaiah GM (2010) ApoE mimetic peptide reduces plasma lipid hydroperoxide content with a concomitant increase in HDL paraoxonase activity. Adv. Exp. Med. Biol. 660:1-4.

Dehouck B, Dehouck MP, Fruchart JC, Cecchelli R (1994) Upregulation of the low-density lipoprotein receptor at the blood-brain barrier: intercommunications between brain capillary endothelial cells and astrocytes. J. Cell. Biol. 126:465-73.

Dehouck B, Fenart L, Dehouck MP, Pierce A, Torpier G, Cecchelli R (1997) A new function for the LDL receptor: transcytosis of LDL across the blood-brain barrier. J. Cell. Biol. 138:877-89.

Delacourte A (1999) Biochemical and molecular characterization of neurofibrillary degeneration in frontotemporal dementias. Dement. Geriatr. Cogn. Disord. 10 Suppl 1:75-9.

Delrieu J, Ousset PJ, Caillaud C, Vellas B (2012) Clinical Trials in Alzheimer's disease: immunotherapy approaches. J. Neurochem. 120:186-93.

Devine DV, Wong K, Serrano K, Chonn A, Cullis PR (1994) Liposome–complement interactions in rat serum: implications for liposome survival studies. Biochim. Biophys. Acta 1191(1):43-51.

Dickson DW (1997) The pathogenesis of senile plaques. J. Neuropathol. Exp. Neurol. 56:321-39.

Dodart, J. C., H. Meziane, Mathis C, Bales KR, Paul SM, Ungerer A (1999) Behavioral disturbances in transgenic mice overexpressing the V717F beta-amyloid precursor protein. Behav. Neurosci. 113(5): 982-90.

Donev R, Koseva N, Petrov P, Kowalczuk A, Thome J (2011) Characterisation of different nanoparticles with a potential use for drug delivery in neuropsychiatric disorders. World J. Biol. Psychiatry 12(Suppl. 1):44-51.

Elder GA, Gama Sosa MA, De Gasperi R (2010) Transgenic mouse models of Alzheimer's disease. Mt Sinai J Med. 77(1):69-81.

Elmizadeh H, Khanmohammadi M, Ghasemi K, Hassanzadeh G, Nassiri-Asl M, Garmarudi AB (2013) Preparation and optimization of chitosan nanoparticles and magnetic chitosan nanoparticles as delivery systems using Box-Behnken statistical design. J. Pharm. Biomed. Anal. 80:141-6.

Etheridge ML, Campbell SA, Erdman AG, Haynes CL, Wolf SM, McCullough J (2013) The big picture on nanomedicine: the state of investigational and approved nanomedicine products. Nanomedicine. 9(1):1-14.

Evans JG, Wilcock G, Birks J (2004) Evidence-based pharmacotherapy of Alzheimer's disease. Int. J. Neuropsychopharmacol. 7(3):351-

69.

Evin G, Sernee MF, Masters CL (2006) Inhibition of gamma-secretase as a therapeutic intervention for Alzheimer's disease: prospects, limitations and strategies. CNS Drugs 20(5):351-72.

Fernandez JW, Rezai-Zadeh K, Obregon D, Tan J (2010) EGCG functions through estrogen receptor-mediated activation of ADAM10 in the promotion of non-amyloidogenic processing of APP. FEBS Lett. 584(19):4259-67.

Findeis MA, Musso GM, Arico-Muendel CC, Benjamin HW, Hundal AM, Lee JJ, Chin J, Kelley M, Wakefield J, Hayward NJ, Molineaux SM (1999) Modified-peptide inhibitors of amyloid β-peptide polymerization. Biochemistry 38:6791-800.

Fjell AM, Walhovd KB, Fennema-Notestine C, McEvoy LK, Hagler DJ, Holland D, Brewer JB, Dale AM; Alzheimer's Disease Neuroimaging Initiative (2010) CSF biomarkers in prediction of cerebral and clinical change in mild cognitive impairment and Alzheimer's disease. J. Neurosci. 30(6):2088-101.

Forsberg A, Engler H, Almkvist O, Blomquist G, Hagman G, Wall A, Ringheim A, Långström B, Nordberg A (2008) PET imaging of amyloid deposition in patients with mild cognitive impairment. Neurobiol. Aging 29(10):1456-65.

Fraller DB (2013) State of the science: use of biomarkers and imaging in diagnosis and management of Alzheimer disease. J. Neurosci. Nurs. 45(2):63-70.

Ghanta J, Shen CL, Kiessling LL, Murphy RM (1996) A strategy for designing inhibitors of β-amyloid toxicity. J. Biol. Chem. 271:29525-8.

Games D, Adams D, Alessandrini R, Barbour R, Borthelette P, Blackwell C, Carr T, Clemens J, Donaldson T, Gillespie F, Guido T, Hagopian S, Johnson-Wood K, Khan K, Lee M, Leibowitz P, Lieberburg I, Little S, Masliahparallel E, McConlogue L, Montoya-Zavala M, Muckestar L, Paganini L, Penniman E, Power M, Schenk D, Seubert P, Snyder B, Soriano F, Tan H, Vitale J, Wadsworth S, Wolozin B, Zhao J (1995) Alzheimer-type neuropathology in transgenic mice overexpressing V717F beta-amyloid precursor protein. Nature 373(6514): 523-7.

Garcia-Garcia E, Andrieux K, Gil S, Kim HR, Le Doan T, Desmaële D, d'Angelo J, Taran F, Georgin D, Couvreur P (2005) A methodology to study intracellular distribution of nanoparticles in brain endothelial cells. Int J Pharm. 298(2):310-4.

Gastaldi L, Battaglia L, Peira E, Chirio D, Muntoni E, Solazzi I, Gallarate M, Dosio F (2014) Solid lipid nanoparticles as vehicles of drugs to the brain: current state of the art. Eur. J. Pharm. Biopharm. 87:433-44.

Gaugler J, James B, Johnson T, Scholz K, Weuve J (2013) Alzheimer's disease facts and figures 2013. Alzheimer 's disease Association on line source. www.alz.org/downloads/facts_figures_2013.pdf

Gentile F, Chiappini C, Fine D, Bhavane RC, Peluccio MS, Cheng MM, Liu X, Ferrari M, Decuzzi P (2008) The effect of shape on the margination dynamics of non-neutrally buoyant particles in two-dimensional shear flows. J. Biomech. 41:2312-8.

Giacobini E (2000) Cholinesterase inhibitors stabilize Alzheimer's disease. Ann. NY Acad. Sci. 920:321-7.

Glenner GG, Wong CW (1984a) Alzheimer's disease: initial report of

the purification and characterization of a novel cerebrovascular amyloid protein. Biochem. Biophys. Res. Commun. 120(3):885-90.

Glenner GG, Wong CW (1984b) Alzheimer's disease and Down's syndrome: sharing of a unique cerebrovascular amyloid fibril protein. Biochem Biophys. Res. Commun. 122(3):1131-5.

Gobbi M, Re F, Canovi M, Beeg M, Gregori M, Sesana S, Sonnino S, Brogioli D, Musicanti C, Gasco P, Salmona M, Masserini ME (2010) Lipid-based nanoparticles with high binding affinity for amyloid-beta1–42 peptide. Biomaterials 31(25):6519-29.

Godin B, Driessen WH, Proneth B, Lee SY, Srinivasan S, Rumbaut R, Arap W, Pasqualini R, Ferrari M, Decuzzi P (2010) An integrated approach for the rational design of nanovectors for biomedical imaging and therapy. Adv. Genet. 69:31-64.

Gordon DJ, Sciarretta KL, Meredith SC (2001) Inhibition of β-amyloid(40) fibrillogenesis and disassembly of β-amyloid(40) fibrils by short β-amyloid congeners containing N-methyl amino acids at alternate residues. Biochemistry 40:8237-45.

Götz J, Schild A, Hoerndli F, Pennanen L (2004) Amyloid-induced neurofibrillary tangle formation in Alzheimer's disease: insight from transgenic mouse and tissue-culture models. Int J Dev Neurosci. 22(7):453-65.

Grabinski C, Hussain S, Lafdi K, Braydich-Stolle L, Schlager J (2007) Effect of particle dimension on biocompatibility of carbon nanomaterials. Carbon 45, 2828-35.

Green M, Loewenstein PM (1988) Autonomous functional domains of chemically synthesized human immunodeficiency virus tat trans-

activator protein. Cell 55: 1179-88.

Greenough MA, Camakaris J, Bush AI (2013) Metal dyshomeostasis and oxidative stress in Alzheimer's disease. Neurochem. Int. 62(5):540-55.

Guerrero S, Araya E, Fiedler JL, Arias JI, Adura C, Albericio F, Giralt E, Arias JL, Fernández MS, Kogan MJ (2010) Improving the brain delivery of gold nanoparticles by conjugation with an amphipathic peptide. Nanomedicine 5(6):897-913.

Haass C, Selkoe DJ (2007) Soluble protein oligomers in neurodegeneration: lessons from the Alzheimer’s amyloid beta-peptide. Nat. Rev. Mol. Cell. Biol. 8(2):101-12.

Hampel H, Blennow K, Shaw LM, Hoessler YC, Zetterberg H, Trojanowski JQ (2010) Total and phosphorylated tau protein as biological markers of Alzheimer disease. Exp. Gerontol. 45(1):30-40.

Hardy JA, Higgins GA (1992) Alzheimer's disease: the amyloid cascade hypothesis. Science 256:184-5.

Harrington CR (2012) The molecular pathology of Alzheimer's disease. Neuroimaging Clin. N. Am. 22(1):11-22, vii.

Herskowitz JH, Seyfried NT, Gearing M, Kahn RA, Peng J, Levey AI, Lah JJ (2011) Rho kinase II phosphorylation of the lipoprotein receptor LR11/SORLA alters amyloid-beta production. J. Biol. Chem. 286(8):6117-27.

Hillaireau H, Couvreur P (2009) Nanocarriers' entry into the cell: relevance to drug delivery. Cell. Mol. Life Sci. 66:2873-96.

Holmes D (2013) The next big things are tiny. Lancet Neurol. 12:31-2.

Holscher C (1998) Possible causes of Alzheimer’s disease: amyloid

fragments, free radicals, and calcium homeostasis. Neurobiol Dis 5:129-41.

Howlett DR (2011) APP transgenic mice and their application to drug discovery. Histol. Histopathol. 26:1611–32.

Hsiao K, Chapman P, Nilsen S, Eckman C, Harigaya Y, Younkin S, Yang F, Cole G (1996) Correlative memory deficits, Abeta elevation, and amyloid plaques in transgenic mice. Science 274(5284): 99-102.

Hu CM, Zhang L, Aryal S, Cheung C, Fang RH, Zhang L (2011) Erythrocyte membrane-camouflaged polymeric nanoparticles as a biomimetic delivery platform. Proc. Natl. Acad. Sci. U S A. 108:10980-5.

Hu K, Li J, Shen Y, Lu W, Gao X, Zhang Q, Jiang X (2009) Lactoferrin-conjugated PEG-PLA nanoparticles with improved brain delivery: in vitro and in vivo evaluations. J. Control. Release 134(1):55-61.

Huang Y, Mucke L (2012) Alzheimer mechanisms and therapeutic strategies. Cell 148(6):1204-22.

Hutter E, Boridy S, Labrecque S, Lalancette-Hébert M, Kriz J, Winnik FM, Maysinger D (2010) Microglial response to gold nanoparticles. ACS Nano 4(5):2595-606.

Hynd MR, Scott HL, Dodd PR (2004) Glutamate-mediated excitotoxicity and neurodegeneration in Alzheimer's disease. Neurochem. Int. 45(5):583-95.

Itagaki S, Akiyama H, Saito H, McGeer PL (1994) Ultrastructural localization of complement membrane attack complex (MAC)-like immunoreactivity in brains of patients with Alzheimer’s

disease. Brain Res. 645(1–2):78-84.

Ittner LM, Götz J (2011) Amyloid-β and tau-a toxic pas de deux in Alzheimer's disease. Nat. Rev. Neurosci. 12(2):65-72.

Janelsins MC, Mastrangelo MA, Oddo S, LaFerla FM, Federoff HJ, Bowers WJ (2005) Early correlation of microglial activation with enhanced tumor necrosis factor-alpha and monocyte chemoattractant protein-1 expression specifically within the entorhinal cortex of triple transgenic Alzheimer's disease mice. J Neuroinflammation 2:23.

Jankowsky JL, Fadale DJ, Anderson J, Xu GM, Gonzales V, Jenkins NA, Copeland NG, Lee MK, Younkin LH, Wagner SL, Younkin SG, Borchelt DR (2004) Mutant presenilins specifically elevate the levels of the 42 residue beta-amyloid peptide in vivo: evidence for augmentation of a 42-specific gamma secretase. Hum Mol Genet. 13(2):159-70.

Jaruszewski KM, Ramakrishnan S, Poduslo JF, Kandimalla KK (2012) Chitosan enhances the stability and targeting of immuno-nanovehicles to cerebro-vascular deposits of Alzheimer's disease amyloid protein. Nanomedicine 8(2):250-60.

Jellinger KA (1998) The neuropathological diagnosis of Alzheimer disease. J. Neural. Transm. Suppl. 53:97-111.

Kagan BL, Thundimadathil J (2010) Amyloid peptide pores and the β-sheet conformation. Adv. Exp. Med. Biol. 677:150-67.

Kanwar J, Taskeen M, Mohammad I, Huo C, Chan TH, Dou QP (2012) Recent advances on tea polyphenols. Front. Biosci. (Elite Ed.) 4:111-31.

Karmakar A, Zhang Q, Zhang Y (2014) Neurotoxicity of nanoscale

materials. Yao Wu Shi Pin Fen Xi 22(1):147-60.

Keana T, Thanou M (2010) Biodegradation, biodistribution and toxicity of chitosan. Adv. Drug Deliv. Rev. 62(1):3-11.

Khanna P, Ong C, Bay BH, Baeg GH (2015) Nanotoxicity: An Interplay of Oxidative Stress, Inflammation and Cell Death. Nanomaterials 5, 1163-80.

Klunk WE, Engler H, Nordberg A, Wang Y, Blomqvist G, Holt DP, Bergström M, Savitcheva I, Huang GF, Estrada S, Ausén B, Debnath ML, Barletta J, Price JC, Sandell J, Lopresti BJ, Wall A, Koivisto P, Antoni G, Mathis CA, Långström B (2004) Imaging brain amyloid in Alzheimer's disease with Pittsburgh Compound-B. Ann. Neurol. 55(3):306-19.

Koch F, Möller AM, Frenz M, Pieles U, Kuehni-Boghenbor K, Mevissen M (2014) An in vitro toxicity evaluation of gold-, PLLA- and PCL-coated silica nanoparticles in neuronal cells for nanoparticle-assisted laser-tissue soldering. Toxicol. In vitro 28(5):990-8.

Kogan MJ, Bastus NG, Amigo R, Grillo-Bosch D, Araya E, Turiel A, Labarta A, Giralt E, Puntes VF (2006) Nanoparticle-mediated local and remote manipulation of protein aggregation. Nano Lett. 6(1):110-5.

Kokkoni N, Stott K, Amijee H, Mason JM, Doig AJ (2006) N-Methylated peptide inhibitors of β-amyloid aggregation and toxicity. Optimization of the inhibitor structure. Biochemistry 45:9906-18.

Kreuter J, Shamenkov D, Petrov V (2002) Apolipoprotein-mediated transport of nanoparticle-bound drugs across the blood-brain

barrier. J. Drug Target 10(4):317-25.

Krol S (2012) Challenges in drug delivery to the brain: nature is against us. J. Control. Release 164(2):145-55.

Kumar S, Walter J (2011) Phosphorylation of amyloid beta (Aβ) peptides - a trigger for formation of toxic aggregates in Alzheimer's disease. Aging (Albany NY) 3(8):803-12.

Langley GR (2014) Considering a new paradigm for Alzheimer's disease research. Drug discovery today 19(8):1114-24.

Lannfelt L, Relkin NR, Siemers ER (2014) Amyloid-ss-directed immunotherapy for Alzheimer's disease. J. Intern. Med. 275(3):284-95.

Lasagna-Reeves C, Gonzalez-Romero D, Barria MA, Olmedo I, Clos A, Sadagopa Ramanujam VM, Urayama A, Vergara L, Kogan MJ, Soto C (2010) Bioaccumulation and toxicity of gold nanoparticles after repeated administration in mice. Biochem. Biophys. Res. Commun. 393(4):649-55.

Le Droumaguet B, Nicolas J, Brambilla D, Mura S, Maksimenko A, De Kimpe L, Salvati E, Zona C, Airoldi C, Canovi M, Gobbi M, Magali N, La Ferla B, Nicotra F, Scheper W, Flores O, Masserini M, Andrieux K, Couvreur P (2012) Versatile and efficient targeting using a single nanoparticulate platform: application to cancer and Alzheimer's disease. ACS Nano 6(7):5866-79.

Lettiero B, Andersen AJ, Hunter AC, Moghimi SM (2012) Complement system and the brain: selected pathologies and avenues toward engineering of neurological nanomedicines. J. Control. Release 161(2):283-9.

Li X, Liu W, Sun L, Aifantis KE, Yu B, Fan Y, Feng Q, Cui F, Watari

F (2015) Effects of physicochemical properties of nanomaterials on their toxicity. J. Biomed. Mater Res A. 103(7):2499-507.

Liu G, Men P, Kudo W, Perry G, Smith MA (2009) Nanoparticle-chelator conjugates as inhibitors of amyloid-beta aggregation and neurotoxicity: a novel therapeutic approach for Alzheimer disease. Neurosci. Lett. 455(3):187-90.

Liu Y, Liu Z, Wang Y, Liang YR, Wen X, Hu J, Yang X, Liu J, Xiao S, Cheng D (2013) Investigation of the performance of PEG-PEI/ROCK-II-siRNA complexes for Alzheimer's disease in vitro. Brain Res. 1490:43-51.

Liu Z, Gao X, Kang T, Jiang M, Miao D, Gu G, Hu Q, Song Q, Yao L, Tu Y, Chen H, Jiang X, Chen J (2013) B6 Peptide-Modified PEG-PLA nanoparticles for enhanced brain delivery of neuroprotective peptide. Bioconjug. Chem. 24(6):997-1007.

Lu Y, Derreumaux P, Guo Z, Mousseau N, Wei G (2009) Thermodynamics and dynamics of amyloid peptide oligomerization are sequence dependent. Proteins 75(4):954-63.

Luo Y, Bolon B, Kahn S, Bennett BD, Babu-Khan S, Denis P, Fan W, Kha H, Zhang J, Gong Y, Martin L, Louis JC, Yan Q, Richards WG, Citron M, Vassar R (2001) Mice deficient in BACE1, the Alzheimer's beta-secretase, have normal phenotype and abolished beta-amyloid generation. Nat. Naurosci. 4(3):231-2.

Luppi B, Bigucci F, Corace G, Delucca A, Cerchiara T, Sorrenti M, Catenacci L, Di Pietra AM, Zecchi V (2011) Albumin nanoparticles carrying cyclodextrins for nasal delivery of the anti-Alzheimer drug tacrine. Eur. J. Pharm. Sci. 44(4):559-65.

Markoutsa E, Pampalakis G, Niarakis A, Romero IA, Weksler B,

Couraud PO, Antimisiaris SG (2011) Uptake and permeability studies of BBB-targeting immunoliposomes using the hCMEC/D3 cell line. Eur J Pharm Biopharm. 77(2):265-74.

Martineau E, de Guzman JM, Rodionova L, Kong X, Mayer PM, Aman AM (2010) Investigation of the noncovalent interactions between anti-amyloid agents and amyloid beta peptides by ESI-MS. J. Am. Soc. Mass. Spectrom. 21(9):1506-14.

Masserini M (2013) Nanoparticles for brain drug delivery. ISRN Biochemistry. Article ID 238428.

Mathew A, Fukuda T, Nagaoka Y, Hasumura T, Morimoto H, Yoshida Y, Maekawa T, Venugopal K, Kumar DS (2012) Curcumin loaded-PLGA nanoparticles conjugated with Tet-1 peptide for potential use in Alzheimer's Disease. PLoS ONE 7(3):e32616.

Matsuzaki K (2007) Physicochemical interactions of amyloid beta-peptide with lipid bilayers. Biochim. Biophys. Acta 1768(8):1935-42.

McClean P, Parthsarathy V, Faivre E, Holscher C (2011) The diabetes drug liraglutide prevents degenerative processes in a mouse model of Alzheimer's disease. J Neurosci 31:6587-94.

McGowan E, Eriksen J, Hutton M (2006) A decade of modeling Alzheimer's disease in transgenic mice. Trends Genet. 22(5):281-9.

Migliore L, Coppedè F (2009) Genetics, environmental factors and the emerging role of epigenetics in neurodegenerative diseases. Mutat. Res. 667(1-2):82-97.

Mikulca JA, Nguyen V, Gajdosik DA, Teklu SG, Giunta EA, Lessa EA, Tran CH, Terak EC, Raffa RB (2014) Potential novel targets for

Alzheimer pharmacotherapy: II. Update on secretase inhibitors and related approaches. J. Clin. Pharm. Ther. 39(1):25-37.

Mittal G, Carswell H, Brett R, Currie S, Kumar MN (2011) Development and evaluation of polymer nanoparticles for oral delivery of estradiol to rat brain in a model of Alzheimer's pathology. J. Control. Release 150(2):220-8.

Moghimi SM, Szebeni J (2003) Stealth liposomes and long circulating nanoparticles: critical issues in pharmacokinetics, opsonization and protein-binding properties. Prog. Lipid Res. 42(6):463-78.

Moghimi SM, Hunter AC, Murray JC (2005) Nanomedicine: current status and future prospects. FASEB J. 19:311-30.

Monje ML, Toda H, Palmer TD (2003) Inflammatory blockade restores adult hippocampal neurogenesis. Science 302:1760-5.

Montet X, Funovics M, Montet-Abou K, Weissleder R, Josephson L (2006) Multivalent effects of RGD peptides obtained by nanoparticle display. J. Med. Chem. 49(20):6087-93.

Mourtas S, Canovi M, Zona C, Aurilia D, Niarakis A, La Ferla B, Salmona M, Nicotra F, Gobbi M, Antimisiaris SG (2011) Curcumin-decorated nanoliposomes with very high affinity for amyloid-β1–42 peptide. Biomaterials 32(6):1635-45.

Mourtas S, Lazar AN, Markoutsa E, Duyckaerts C, Antimisiaris SG (2014) Multifunctional nanoliposomes with curcumine lipid derivative and brain targeting functionality with potential applications for Alzheimer disease. Eur. J. Med. Chem. 80:175-83.

Mrak RE, Griffin ST, Graham DI (1997) Aging-associated changes in human brain. J. Neuropathol. Exp. Neurol. 56(12):1269-75.

Mufamadi MS, Choonara YE, Kumar P, Modi G, Naidoo D, Ndesendo VM, du Toit LC, Iyuke SE, Pillay V (2012) Surface-engineered nanoliposomes by chelating ligands for modulating the neurotoxicity associated with β-amyloid aggregates of Alzheimer's disease. Pharm. Res. 29(11):3075-89.

Murphy MP, LeVine H 3rd (2010) Alzheimer's disease and the amyloid-beta peptide. J. Alzheimers Dis. 19(1):311-23.

Naik P, Cucullo L (2012) In vitro blood-brain barrier models: current and perspective technologies. J. Pharm. Sci. 101;1337−54.

Narang AS, Chang RK, Hussain MA (2013) Pharmaceutical development and regulatory considerations for nanoparticles and nanoparticulate drug delivery systems. J. Pharm. Sci. 102, 3867-82.

Nel A, Xia T, Mädler L, Li N (2006) Toxic potential of materials at the nanolevel. Science 311(5761):622-7.

Nordberg A (2007) Amyloid imaging in Alzheimer disease. Curr. Opin. Neurol. 20(4):398- 402.

Oberdörster G, Oberdörster E, Oberdörster J (2005) Nanotoxicology: An emerging discipline evolving from studies of ultrafine particles. Environ. Health Perspect. 113, 823-39.

Oddo S, Caccamo A, Shepherd JD, Murphy MP, Golde TE, Kayed R, Metherate R, Mattson MP, Akbari Y, LaFerla FM (2003a) Triple-transgenic model of Alzheimer's disease with plaques and tangles: intracellular Abeta and synaptic dysfunction. Neuron 39(3):409-21.

Oddo S, Caccamo A, Kitazawa M, Tseng BP, LaFerla FM (2003b) Amyloid deposition precedes tangle formation in a triple

transgenic model of Alzheimer's disease. Neurobiol Aging.24(8):1063-70.

Panza F, Solfrizzi V, Imbimbo BP, Tortelli R, Santamato A, Logroscino G (2014) Amyloid-based immunotherapy for Alzheimer's disease in the time of prevention trials: the way forward. Expert Rev. Clin. Immunol. 10(3):405–19.

Panza F, Seripa D, Solfrizzi V, Imbimbo BP, Lozupone M, Leo A, Sardone R, Gagliardi G, Lofano L, Creanza BC, Bisceglia P, Daniele A, Bellomo A, Greco A, Logroscino G (2016) Emerging drugs to reduce abnormal β-amyloid protein in Alzheimer's disease patients. Expert Opin. Emerg. Drugs. 21(4):377-91.

Pardridge WM (2005) The blood–brain barrier: bottleneck in brain drug development. NeuroRx 2(1):3-14.

Paresce D, Chung H, Maxfield F (1997) Slow degradation of aggregates of the Alzheimer's disease amyloid b-protein by microglial cells. J Biol Chem 114:29390-7.

Parodi A, Quattrocchi N, van de Ven AL, Chiappini C, Evangelopoulos M, Martinez JO, Brown BS, Khaled SZ, Yazdi IK, Enzo MV, Isenhart L, Ferrari M, Tasciotti E (2013) Synthetic nanoparticles functionalized with biomimetic leukocyte membranes possess cell-like functions. Nat. Nanotechnol. 8:61-8.

Parthsarathy V, McClean PL, Hölscher C, Taylor M, Tinker C, Jones G, Kolosov O, Salvati E, Gregori M, Masserini M, Allsop D (2013) A novel retro-inverso peptide inhibitor reduces amyloid deposition, oxidation and inflammation and stimulates neurogenesis in the APPswe/PS1ΔE9 mouse model of Alzheimer's disease. PLoS One 8(1):e54769.

Patel T, Zhou J, Piepmeier JM, Saltzman WM (2012) Polymeric nanoparticles for drug delivery to the central nervous system. Adv. Drug Deliv. Rev. 64(7):701-5.

Pérez M, Ribe E, Rubio A, Lim F, Morán MA, Ramos PG, Ferrer I, Isla MT, Avila J (2005) Characterization of a double (amyloid precursor protein-tau) transgenic: tau phosphorylation and aggregation. Neuroscience 130(2):339-47.

Petkar KC, Chavhan SS, Agatonovik-Kustrin S, Sawant KK (2011) Nanostructured materials in drug and gene delivery: a review of the state of the art. Crit. Rev. Ther. Drug Carrier Syst. 28(2):101-64.

Petrinca AR, Pietroiusti A, Argentin G, Cicchetti R, Donia D, Gabrieli R, Vignoli I, Magrini A, Divizia M (2009) The birth of nanobiotechnologies: new nanomaterials, potential uses, toxic effects and implications for public health. Ig Sanita Pubbl. 2009 Mar-Apr;65(2):169-88.

Pike KE, Savage G, Villemagne VL, Ng S, Moss SA, Maruff P, Mathis CA, Klunk WE, Masters CL, Rowe CC (2007) Beta-amyloid imaging and memory in non-demented individuals: evidence for preclinical Alzheimer's disease. Brain 130(Pt 11):2837-44.

Pinzón-Daza M1, Garzón R, Couraud P, Romero Ia, Weksler B, Ghigo D, Bosia A, Riganti C (2012) The association of statins plus LDL receptor-targeted liposome-encapsulated doxorubicin increases in vitro drug delivery across blood-brain barrier cells. Br. J. Pharmacol. 167(7):1431-47.

Prades R, Guerrero S, Araya E, Molina C, Salas E, Zurita E, Selva J, Egea G, López-Iglesias C, Teixidó M, Kogan MJ, Giralt E (2012)

Delivery of gold nanoparticles to the brain by conjugation with a peptide that recognizes the transferrin receptor. Biomaterials 33(29):7194-205.

Puras G, Salvador A, Igartua M, Hernández RM, Pedraz JL (2011) Encapsulation of Aβ(1–15) in PLGA microparticles enhances serum antibody response in mice immunized by subcutaneous and intranasal routes. Eur. J. Pharm. Sci. 44(3):200-6.

Qiu L, Lewis A, Como J, Vaughn MW, Huang J, Somerharju P, Virtanen J, Cheng KH (2009) Cholesterol modulates the interaction of beta-amyloid peptide with lipid bilayers. Biophys J. 96(10):4299-307.

Radde R, Duma C, Goedert M, Jucker M (2008) The value of incomplete mouse models of Alzheimer's disease. Eur. J. Nucl. Med. Mol. Imaging. 35 Suppl 1:S70-4.

Re F, Cambianica I, Zona C, Sesana S, Gregori M, Rigolio R, La Ferla B, Nicotra F, Forloni G, Cagnotto A, Salmona M, Masserini M, Sancini G (2011a) Functionalization of liposomes with ApoE-derived peptides at different density affects cellular uptake and drug transport across a blood–brain barrier model. Nanomedicine 7(5):551-9.

Re F, Cambianica I, Sesana S, Salvati E, Cagnotto A, Salmona M, Couraud PO, Moghimi SM, Masserini M, Sancini G (2011b) Functionalization with ApoE-derived peptides enhances the interaction with brain capillary endothelial cells of nanoliposomes binding amyloid-beta peptide. J Biotechnol. 156(4):341-6.

Rea R, Carotenuto A, Fasanaro AM, Traini E, Amenta F (2014) Apathy

in Alzheimer's disease: any effective treatment? ScientificWorld Journal Article ID:421385.

Reichel A (2006) The role of blood-brain barrier studies in the pharmaceutical industry. Curr. Drug Metab. 7:183−203.

Rensink AA, De Waal RM, Kremer B, Verbeek MM (2003) Pathogenesis of cerebral amyloid angiopathy. Brain Res Rev 43:207-23.

Rivet CJ, Yuan Y, Borca-Tasciuc DA, Gilbert RJ (2012) Altering iron oxide nanoparticle surface properties induce cortical neuron cytotoxicity. Chem. Res Toxicol. 25(1):153-61.

Rogawski MA, Wenk GL (2003) The neuropharmacological basis for the use of memantine in the treatment of Alzheimer's disease. J. CNS Drug Rev. 9(3):275-308.

Romanitan MO, Popescu BO, Spulber S, Băjenaru O, Popescu LM, Winblad B, Bogdanovic N (2010) Altered expression of claudin family proteins in Alzheimer's disease and vascular dementia brains. J Cell Mol Med 14;1088–100.

Sahni JK, Doggui S, Ali J, Baboota S, Dao L, Ramassamy C (2011) Neurotherapeutic applications of nanoparticles in Alzheimer’s disease. J. Control. Release 152(2):208-31.

Salmon DP (2012) Neuropsychological features of mild cognitive impairment and preclinical Alzheimer's disease. Curr. Top. Behav. Neurosci. 10:187-212.

Salvati E, Re F, Sesana S, Cambianica I, Sancini G, Masserini M, Gregori M (2013) Liposomes functionalized to overcome the blood-brain barrier and to target amyloid-β peptide: the chemical design affects the permeability across an in vitro model. Int. J.

Nanomedicine 8:1749-58.

Sampson E, Jenagaratnam L, McShane R (2008) Metal protein attenuating compounds for the treatment of Alzheimer's disease. Cochrane Database Syst. Rev. (1):CD005380.

Sancini G, Gregori M, Salvati E, Cambianica I, Re F, Ornaghi F, Canovi M, Fracasso C, Cagnotto A, Colombo M, Zona C, Gobbi M, Salmona M, La Ferla B, Nicotra F, Masserini M (2013) Functionalization with TAT-peptide enhances blood–brain barrier crossing in vitro of nanoliposomes carrying a curcumin-derivative to bind Amyloid-b peptide. J. Nanomed. Nanotechol. 4(3):171-8.

Sanvicens N, Marco MP (2008) Multifunctional nanoparticles--properties and prospects for their use in human medicine. Trends Biotechnol. 26:425-33.

Sawant RR, Torchilin VP (2012) Challenges in development of targeted liposomal therapeutics. AAPS J. 14, 303-15.

Schenk D, Barbour R, Dunn W, Gordon G, Grajeda H, Guido T, Hu K, Huang J, Johnson-Wood K, Khan K, Kholodenko D, Lee M, Liao Z, Lieberburg I, Motter R, Mutter L, Soriano F, Shopp G, Vasquez N, Vandevert C, Walker S, Wogulis M, Yednock T, Games D, Seubert P (1999) Immunization with amyloid-beta attenuates Alzheimer-disease-like pathology in the PDAPP mouse. Nature 400(6740):173-7.

Selkoe DJ (1994) Cell biology of the amyloid beta-protein precursor and the mechanism of Alzheimer's disease. Annu. Rev. Cell. Biol. 10:373-403.

Selkoe DJ (1999) Translating cell biology into therapeutic advances in

Alzheimer's disease. Nature 399:A23-31.

Selkoe DJ (2006) Amyloid beta-peptide is produced by cultured cells during normal metabolism: a reprise. J. Alzheimers Dis. 9(3 Suppl):163-8.

Sercombe L, Veerati T, Moheimani F, Wu SY, Sood AK, Hua S (2015) Advances and Challenges of Liposome Assisted Drug Delivery. Front. Pharmacol. 6:286.

Serrano-Pozo A, Frosch MP, Masliah E, Hyman BT (2011) Neuropathological alterations in Alzheimer disease. Cold Spring Harb. Perspect. Med. 1(1):a006189.

Service RF. Nanotechnology (2010) Nanoparticle Trojan horses gallop from the lab into the clinic. Science 330(6002):314-5.

Sevigny J, Chiao P, Bussière T, Weinreb PH, Williams L, Maier M, Dunstan R, Salloway S, Chen T, Ling Y, O'Gorman J, Qian F, Arastu M, Li M, Chollate S, Brennan MS, Quintero-Monzon O, Scannevin RH, Arnold HM, Engber T, Rhodes K, Ferrero J, Hang Y, Mikulskis A, Grimm J, Hock C, Nitsch RM, Sandrock A (2016) The antibody aducanumab reduces Aβ plaques in Alzheimer's disease. Nature 537(7618):50-6.

Singh N, Manshian B, Jenkins GJ, Griffiths SM, Williams PM, Maffeis TG, Wright CJ, Doak SH (2009) NanoGenotoxicology: the DNA damaging potential of engineered nanomaterials. Biomaterials 30(23-24):3891-914.

Smith A, Giunta B, Bickford PC, Fountain M, Tan J, Shytle RD (2010) Nanolipidic particles improve the bioavailability and alpha-secretase inducing ability of epigallocatechin-3-gallate (EGCG) for the treatment of Alzheimer’s disease. Int. J. Pharm. 389(1–

2):207-12.

Songjiang Z, Lixiang W (2009) Amyloid-beta associated with chitosan nano-carrier has favorable immunogenicity and permeates the BBB. AAPS PharmSciTech. 10(3):900-5.

Sorrentino P, Iuliano A, Polverino A, Jacini F, Sorrentino G (2014) The dark sides of amyloid in Alzheimer's disease pathogenesis. FEBS Lett. 588(5):641-52.

Soto C, Sigurdsson EM, Morelli L, Kumar RA, Castano EM, Frangione B (1998) β-Sheet breaker peptides inhibit fibrillogenesis in a rat brain model of amyloidosis: implications for Alzheimer's therapy. Nat. Med. 4:822-6.

Soto C (2003) Unfolding the role of protein misfolding in neurodegenerative diseases. Nat. Rev. Neurosci. 4(1):49-60.

Sousa F, Mandal S, Garrovo C, Astolfo A, Bonifacio A, Latawiec D, Menk RH, Arfelli F, Huewel S, Legname G, Galla HJ, Krol S (2010) Functionalized gold nanoparticles: a detailed in vivo multimodal microscopic brain distribution study. Nanoscale 2(12):2826-34.

Storandt M, Head D, Fagan AM, Holtzman DM, Morris JC (2012) Toward a multifactorial model of Alzheimer disease.Neurobiol. Aging. 33(10):2262-71.

Sturchler-Pierrat C, Abramowski D, Duke M, Wiederhold KH, Mistl C, Rothacher S, Ledermann B, Bürki K, Frey P, Paganetti PA, Waridel C, Calhoun ME, Jucker M, Probst A, Staufenbiel M, Sommer B (1997) Two amyloid precursor protein transgenic mouse models with Alzheimer disease-like pathology. Proc. Natl. Acad. Sci. U S A 94(24):13287-92.

Szebeni J, Muggia F, Gabizon A, Barenholz Y (2011) Activation of complement by therapeutic liposomes and other lipid excipient-based therapeutic products: prediction and prevention. Adv. Drug Deliv. Rev. 63(12):1020-30.

Tabner BJ, El-Agnaf OM, Turnbull S, German MJ, Paleologou KE, Hayashi Y, Cooper LJ, Fullwood NJ, Allsop D (2005) Hydrogen peroxide is generated during the very early stages of aggregation of the amyloid peptides implicated in Alzheimer disease and familial British dementia. J Biol Chem. 280(43):35789-92.

Tanifum EA, Dasgupta I, Srivastava M, Bhavane RC, Sun L, Berridge J, Pourgarzham H, Kamath R, Espinosa G, Cook SC, Eriksen JL, Annapragada A (2012) Intravenous delivery of targeted liposomes to amyloid-β pathology in APP/PSEN1 transgenic mice. PLoS ONE 7(10):e48515.

Taylor DR, Hooper NM (2007) Role of lipid rafts in the processing of the pathogenic prion and Alzheimer's amyloid-beta proteins. Semin. Cell. Dev. Biol. 18 (5):638e48.

Taylor M, Moore S, Mayes J, Parkin E, Beeg M, Canovi M, Gobbi M, Mann DM, Allsop D (2010) Development of a proteolytically stable retro-inverso peptide inhibitor of beta-amyloid oligomerization as a potential novel treatment for Alzheimer's disease. Biochemistry 49(15):3261-72.

Taylor M, Moore S, Mourtas S, Niarakis A, Re F, Zona C, La Ferla B, Nicotra F, Masserini M, Antimisiaris SG, Gregori M, Allsop D (2011) Effect of curcumin-associated and lipid ligand-functionalized nanoliposomes on aggregation of the Alzheimer's Aβ peptide. Nanomedicine 7(5):541-50.

Teipel SJ, Meindl T, Grinberg L, Heinsen H, Hampel H (2008) Novel MRI techniques in the assessment of dementia. Eur. J. Nucl. Med. Mol. Imaging 35 suppl 1:S58-S69.

Teli MK, Mutalik S, Rajanikant GK (2010) Nanotechnology and nanomedicine: going small means aiming big. Curr. Pharm. Des. 16, 1882-92.

Thomas DA, Sarris AH, Cortes J, Faderl S, O'Brien S, Giles FJ, Garcia-Manero G, Rodriguez MA, Cabanillas F, Kantarjian H (2006) Phase II study of sphingosomal vincristine in patients with recurrent or refractory adult acute lymphocytic leukemia. Cancer 106(7):1641.

Tinkle S, McNeil SE, Mühlebach S, Bawa R, Borchard G, Barenholz YC, Tamarkin L, Desai N (2014) Nanomedicines: addressing the scientific and regulatory gap. Ann. N.Y. Acad. Sci. 1313, 35–56.

Tjernberg LO, Naslund J, Lindqvist F, Johansson J, Karlstrom AR, Thyberg J, Terenius L, Nordstedt C (1996) Arrest of β-amyloid fibril formation by a pentapeptide ligand. J. Biol. Chem. 271:8545-8.

Tuppo EE, Arias HR (2005) The role of inflammation in Alzheimer's disease. Int. J. Biochem. Cell. Biol. 37(2):289-305.

Türker S, Onur E, Ozer Y (2004) Nasal route and drug delivery systems. Pharm. World Sci. 26(3):137-42.

Vahidkhah K, Bagchi P (2015) Microparticle shape effects on margination, near-wall dynamics and adhesion in a three-dimensional simulation of red blood cell suspension. Soft Matter. 11:2097-109.

van Assema DM, Lubberink M, Rizzu P, van Swieten JC, Schuit RC,

Eriksson J, Scheltens P, Koepp M, Lammertsma AA, van Berckel BN (2012) Blood-brain barrier P-glycoprotein function in healthy subjects and Alzheimer's disease patients: effect of polymorphisms in the ABCB1 gene.EJNMMI Res. 2(1):57.

Van Broeck B, Van Broeckhoven C, Kumar-Singh S (2007) Current insights into molecular mechanisms of Alzheimer disease and their implications for therapeutic approaches. Neurodegener. Dis. 4(5):349-65.

Van Dam D, D'Hooge R, Staufenbiel M, Van Ginneken C, Van Meir F, De Deyn PP (2003) Age-dependent cognitive decline in the APP23 model precedes amyloid deposition. Eur J Neurosci. 17(2):388-96.

Van Dam D, Vloeberghs E, Abramowski D, Staufenbiel M, De Deyn PP (2005) APP23 mice as a model of Alzheimer's disease: an example of a transgenic approach to modeling a CNS disorder. CNS Spectr. 10(3):207-22.

Van Dam D, De Deyn PP (2011) Animal models in the drug discovery pipeline for Alzheimer's disease. Br J Pharmacol. 164(4):1285-300.

van der Helm MW, van der Meer AD, Eijkel JC, van den Berg A, Segerink LI (2016) Microfluidic organ-on-chip technology for blood-brain barrier research. Tissue Barriers 4(1):e1142493.

Verdile G, Fuller S, Atwood CS, Laws SM, Gandy SE, Martins RN (2004) The role of beta amyloid in Alzheimer's disease: still a cause of everything or the only one who got caught? Pharmacol. Res. 50(4):397-409.

Wagner A, Vorauer-Uhl K (2011) Liposome technology for industrial

purposes. J. Drug Deliv. Article ID:591325.

Wang PN, Lirng JF, Lin KN, Chang FC, Liu HC (2006) Prediction of Alzheimer disease in mild cognitive impairment: a prospective study in Taiwan. Neurobiol. Aging 27(12):1797-806.

Webb MS, Harasym TO, Masin D, Bally MB, Mayer LD (1995) Sphingomyelincholesterol liposomes significantly enhance the pharmacokinetic and therapeutic properties of vincristine in murine and human tumour models. Br J Cancer 72(4):896e904.

Weintraub S, Wicklund AH, Salmon DP (2012) The neuropsychological profile of Alzheimer disease.Cold Spring Harb. Perspect Med. 2(4):a006171.

Weiss N, Miller F, Cazaubon S, Couraud P-O (2009) The blood-brain barrier in brain homeostasis and neurological diseases. Biochim. Biophys. Acta 1788(4):842-57.

Weissig V, Pettinger TK, Murdock N (2014) Nanopharmaceuticals (part 1): products on the market. Int. J. Nanomedicine 9:4357-73.

Weissig V, Guzman-Villanueva D (2015) Nanopharmaceuticals (part 2): products in the pipeline. Int. J. Nanomedicine. 10:1245-57.

Weksler BB, Subileau EA, Perriere N, Charneau P, Holloway K, Leveque M, Tricoire-Leignel H, Nicotra A, Bourdoulous S, Turowski P, Male DK, Roux F, Greenwood J, Romero IA, Couraud PO (2005) Blood-brain barrier-specific properties of a human adult brain endothelial cell line. FASEB J. 19:1872-4.

Weksler B, Romero IA, Couraud PO (2013) The hCMEC/D3cell line as a model of the human blood brain barrier. Fluids BarriersCNS 10(1):16. Wilhelm I, Krizbai IA (2014) In vitro models of the blood-brain barrier for the study of drug delivery to the brain. Mol

Pharm. 11(7):1949-63.

Wilson B, Samanta MK, Santhi K, Kumar KP, Paramakrishnan N, Suresh B (2008) Poly(n-butylcyanoacrylate) nanoparticles coated with polysorbate 80 for the targeted delivery of rivastigmine into the brain to treat Alzheimer's disease. Brain Res. 1200:159-68.

Wilson B, Samanta MK, Santhi K, Sampath Kumar KP, Ramasamy M, Suresh B (2009) Significant delivery of tacrine into the brain using magnetic chitosan microparticles for treating Alzheimer's disease. J. Neurosci. Methods 177(2):427-33.

Wimo A, Jönsson L, Gustavsson A, McDaid D, Ersek K, Georges J, Gulácsi L, Karpati K, Kenigsberg P, Valtonen H (2011) The economic impact of dementia in Europe in 2008-cost estimates from the Eurocode project. Int. J. Geriatr. Psychiatry 26(8):825-32.

Win-Shwe TT, Fujimaki H (2011) Nanoparticles and neurotoxicity. Int. J. Mol. Sci. 12(9):6267-80.

Wisniewski T, Goni F (2014) Immunotherapy for Alzheimer's disease. Biochem. Pharmacol. 88(4):499–507.

Wolburg H, Noell S, Mack A, Wolburg-Buchholz K, Fallier-Becker P (2009) Brain endothelial cells and the glio-vascular complex. Cell Tissue Res. 335(1):75-96.

Xekardaki A, Kövari E, Gold G, Papadimitropoulou A, Giacobini E, Herrmann F, Giannakopoulos P, Bouras C (2015) Neuropathological changes in aging brain. Adv. Exp. Med. Biol. 821:11-7.

Xiao RZ, Zeng ZW, Zhou GL, Wang JJ, Li FZ, Wang AM (2010) Recent advances in PEG–PLA block copolymer nanoparticles.

Int. J. Nanomedicine 5:1057-65.

Yang F, Lim GP, Begum AN, Ubeda OJ, Simmons MR, Ambegaokar SS, Chen PP, Kayed R, Glabe CG, Frautschy SA, Cole GM (2005) Curcumin inhibits formation of amyloid beta oligomers and fibrils, binds plaques, and reduces amyloid in vivo. J. Biol. Chem. 280(7):5892-901.

Yasojima K, Schwab C, McGeer EG, McGeer PL (1999) Upregulated production and activation of the complement system in Alzheimer's disease brain. Am. J. Pathol. 154(3):927-36.

Yiannopoulou KG, Papageorgiou SG (2013) Current and future treatments for Alzheimer's disease. Ther. Adv. Neurol. Disord. 6(1):19-33.

Youns M, Hoheisel JD, Efferth T (2011) Therapeutic and diagnostic applications of nanoparticles. Curr. Drug Targets 12(3):357–65.

Yu Y, Jiang X, Gong S, Feng L, Zhong Y, Pang Z (2014) The proton permeability of self-assembled polymersomes and their neuroprotection by enhancing a neuroprotective peptide across the blood–brain barrier after modification with lactoferrin. Nanoscale 6(6):3250-8.

Yu Y, Pang Z, Lu W, Yin Q, Gao H, Jiang X (2012) Self-assembled polymersomes conjugated with lactoferrin as novel drug carrier for brain delivery. Pharm. Res. 29(1):83-96.

Yusuf M, Khan M, Khan RA, Ahmed B (2013) Preparation, characterization, in vivo and biochemical evaluation of brain targeted Piperine solid lipid nanoparticles in an experimentally induced Alzheimer's disease model. J. Drug Target 21(3):300-11.

Zhang C, Wan X, Zheng X, Shao X, Liu Q, Zhang Q, Qian Y (2014b)

Dual-functional nanoparticles targeting amyloid plaques in the brains of Alzheimer’s disease mice. Biomaterials 35(1):456-65.

Zhang C, Chen J, Feng C, Shao X, Liu Q, Zhang Q, Pang Z, Jiang X (2014a) Intranasal nanoparticles of basic fibroblast growth factor for brain delivery to treat Alzheimer’s disease. Int. J. Pharm. 461(1-2):192-202.

CHAPTER 2

Multifunctional liposomes reduce brain β-Amyloid burden and ameliorate memory impairment in Alzheimer's disease mouse models

Claudia Balducci, Simona Mancini, Stefania Minniti, Pietro La Vitola, Margherita Zotti, Giulio Sancini, Mario Mauri, Alfredo Cagnotto, Laura Colombo, Fabio Fiordaliso, Emanuele Grigoli, Mario Salmona, Anniina Snellman, Merja Haaparanta-Solin, Gianluigi Forloni, Massimo Masserini, Francesca Re

The Journal of Neuroscience, 2014; 34(42):14022-31

Abstract

Alzheimer's disease is characterized by the accumulation and deposition of plaques of β-amyloid (Aβ) peptide in the brain. Given its pivotal role, new therapies targeting Aβ are in demand. We rationally designed liposomes targeting the brain and promoting the disaggregation of Aβ assemblies and evaluated their efficiency in reducing the Aβ burden in Alzheimer's disease mouse models.

Liposomes were bifunctionalized with a peptide derived from the apolipoprotein-E receptor-binding domain for blood-brain barrier targeting and with phosphatidic acid for Aβ binding. Bifunctionalized liposomes display the unique ability to hinder the formation of, and disaggregate, Aβ assemblies *in vitro* (EM experiments). Administration of bifunctionalized liposomes to APP/presenilin 1 transgenic mice (aged 10 months) for 3 weeks (three injections per week) decreased total brain-insoluble $A\beta_{1-42}$ (-33%), assessed by ELISA, and the number and total area of plaques (-34%) detected histologically. Also, brain Aβ oligomers were reduced (-70.5%), as assessed by SDS-PAGE. Plaque reduction was confirmed in APP23 transgenic mice (aged 15 months) either histologically or by PET imaging with [^{11}C]Pittsburgh compound B (PIB). The reduction of brain Aβ was associated with its increase in liver (+18%) and spleen (+20%). Notably, the novel-object recognition test showed that the treatment ameliorated mouse impaired memory. Finally, liposomes reached the brain in an intact form, as determined by confocal microscopy experiments with fluorescently labeled liposomes.

These data suggest that bifunctionalized liposomes destabilize brain Aβ aggregates and promote peptide removal across the blood– brain barrier

and its peripheral clearance. This all-in-one multitask therapeutic device can be considered as a candidate for the treatment of Alzheimer’s disease.

2.1 INTRODUCTION

Alzheimer's disease (AD), the most common form of dementia afflicting ~36 million people worldwide, is a neurodegenerative disease characterized by synaptic dysfunction, memory loss, and neuronal cell death (Selkoe et al., 2012). It is mainly diffused in its sporadic form, although in a minor population, it is of the familial type, which is caused by mutations in the amyloid precursor protein (APP) or presenilin 1 (PS1) or 2 (PS2) genes (Bertram and Tanzi, 2012). AD brains are characterized by extracellular plaques, mainly composed of β-amyloid (Aβ), a 40–42 aa ($A\beta_{1-40}$; $A\beta_{1-42}$) proteolytic fragment of the membrane-associated APP (Verbeek et al., 1997). Aβ undergoes an aggregation process leading to the formation of small, soluble oligomeric species and large, insoluble fibrillar species (Bruggink et al., 2012) and ending with the deposition of plaques. Elevated levels of Aβ and its neurotoxic aggregates, oligomers in particular, in the brain are believed to be associated with perturbations of synaptic function and neural network activity, leading to cognitive deficits and neurodegeneration (Palop and Mucke, 2010).

Based on this knowledge, different Aβ-directed therapeutic strategies attempting to reduce brain Aβ burden are currently under investigation, including possibly drawing the Aβ excess out of the brain by peripheral administration of Aβ-binding agents: the so-called "sink effect" (Matsuoka et al., 2003; Biscaro et al., 2009; Sutcliffe et al., 2011). Nanotechnological devices, and in particular nanoparticles, have been suggested as potential tools for the therapy of CNS diseases (Re et al., 2012). Liposomes (LIPs), the best-known nanoparticles (Chang and Yeh, 2012), are currently used in the clinic as drug vehicles. However,

the possibility of multifunctionalization may confer on them the ability to perform multiple tasks at the same time. Following this view, within the present investigation, we have designed multifunctional LIPs for AD therapy.

The objectives for their construction were to confer on them the abilities to (1) cross the blood-brain barrier (BBB), (2) hinder the formation of and enhance the disruption of brain Aβ aggregates into smaller soluble assemblies, and (3) enhance their clearance from the brain. To reach this goal, relying on previous observations obtained *in vitro*, we have bifunctionalized LIPs composed of sphingomyelin (Sm) and cholesterol (Chol) with phosphatidic acid (PA) with the task of binding Aβ (Gobbi et al., 2010) and with a peptide (mApoE) derived from the receptor-binding domain of apolipoprotein E, with the task of targeting and crossing the BBB (Re et al., 2010, 2011; Bana et al., 2013). The present study reports the therapeutic effectiveness of bifunctionalized LIPs (mApoE-PA-LIP) in transgenic (Tg) AD mouse models, demonstrating their effects on both the reduction of amyloid burden and memory improvement.

2.2 MATERIALS AND METHODS

Preparation and characterization of LIPs

Bifunctionalized LIPs (mApoE-PA-LIP) were prepared as described previously (Re et al., 2010; Bana et al., 2013) by an extrusion procedure using polycarbonate filters (100 nm pore size diameter) and were composed of a matrix of bovine brain Sm and Chol at 1:1 molar ratio, mixed with 5% molar of dimyristoyl-PA and further surface functionalized with 1.25% molar of mApoE peptide. mApoE peptide, carrying the amino acid sequence CWG-LRKLRKRLLR corresponding to residues 141–150 of human ApoE, modified with the addition of a tryptophan, glycine, and cysteine residue at the C-terminal, was synthesized and purified as described previously (Re et al., 2010, 2011). As controls, monofunctionalized LIPs with PA (PA–LIP) or mApoE (mApoE–LIP) were also prepared as described previously (Gobbi et al., 2010; Re et al., 2011).

For pharmacokinetic and biodistribution experiments, LIPs contained $6X10^5$ dpm of either [^{14}C]PA or [^{3}H]Sm (~0.001-0.002 molar percentage of total lipids) added as tracers to follow lipid distribution by radioactivity counting.

For confocal microscopy experiments, fluorescent LIPs were used carrying BODIPY-FL C12-sphingomyelin in the lipid bilayer and Rhodamine B encapsulated in the aqueous core. BODIPY-FL C12-sphingomyelin (Invitrogen) was added to the lipid mixture during the preparation of LIPs, and the lipid film was rehydrated with a solution of 20 mM Rhodamine B (Sigma-Aldrich) and submitted to six cycles of freezing and thawing before being extruded. To remove any unencapsulated material, LIPs were subjected to three cycles of

diafiltration through 30,000 molecular weight (MW) cutoff membranes.

LIP size and ζ-potential were characterized as described previously (Re et al., 2010; Bana et al., 2013) and were stable for at least 5 d, as reported (Bana et al., 2013). However, LIPs for animal treatment were freshly prepared on the same day of each injection.

Electron microscopy

Electron microscopy (EM) was used to characterize bifunctionalized LIPs and to investigate their ability to either hinder the formation of fibrils or disrupt preformed $A\beta_{1-42}$ aggregates. To verify the shape and size, 400 μM mApoE-PA-LIP in PBS were dropped onto nickel Formvar–carbon-coated 300 mesh EM grids (Electron Microscopy Science) for 3 min, successively stained for 5 min with a saturated solution of uranyl acetate, washed to eliminate excess uranyl acetate, and allowed to air dry. To study the ability of LIPs to hinder the formation of or to disaggregate preformed fibrils of $A\beta 1_{-42}$, the following procedure was used: in the former case, a solution of 25 μM $A\beta_{1-42}$ was incubated alone or in the presence of a 1 mM solution of LIPs for 5 d at 37°C in PBS, and, in the latter case, after peptide aggregation, fibril suspension was incubated for 5 d with 1 mM LIP solution. At the end of the incubation in either case, all samples were diluted to a final concentration of 5 μM $A\beta_{1-42}$ and dropped onto nickel Formvar-carbon grids. EM analyses was done with a Libra 120 transmission electron microscope operating at 120 kV equipped with a Proscan Slow Scan CCD camera (Carl Zeiss SMT).

Pharmacokinetic and biodistribution experiments

Six- to 8-week-old BALB/c mice weighting 22-25 g were used for these studies. One hundred microliters of 40 mM (total lipid concentration) PA-LIP or mApoE-PA-LIP, containing 130μg of PA and $6X10^5$ dpm of [^{14}C]PA and [^{3}H]Sm (in 1:1 ratio), were administered by three intraperitoneal injections (48 h apart). Mice were killed 24 h after the last injection (three mice per experimental group). Blood, liver, spleen, kidneys, lungs, and brain were collected and solubilized by digestion as described previously (Wan et al., 2007). Radioactivity was measured by a Packard Tricarb 2200CA liquid scintillation counter (PerkinElmer Life and Analytical Sciences).

Animals

Forty APPswe/PS1Δe9 (APP/PS1) 10-month-old Tg male mice [B6C3-Tg(APPswe,PSEN1dE9)85Dbo/Mmjax mice; The Jackson Laboratory], mean weight of 33–34 g, and 20 non-Tg (WT) age-matched littermates were used. For some confirmatory positron emission tomography (PET) experiments, three APPswe single Tg (APP23) mice, 15 months old (Novartis Pharma), and three non-Tg (WT) C57/6N mice, 18 months old, were used. All animals were specific pathogen free (SPF) and were housed in an SPF facility in groups of four in standard mouse cages containing sawdust with food (2018S Harlan diet) and water *ad libitum*, under conventional laboratory conditions (room temperature, 20 ± 2°C; humidity, 60%) and a 12 h light/dark cycle (7:00 A.M. to 7:00 P.M.). No environmental enrichment was used because it notably improves AD pathology in mouse models of AD (Lazarov et al., 2005; Valero et al., 2011). Mice

were all drug and behavioral test naive, and the experiments were all conducted during the light cycle. All procedures involving animals and their care were conducted according to European Union (EEC Council Directive 86/609, OJ L 358,1; December 12, 1987) and Italian (Decreto legislativo 116, Gazzetta Ufficiale s40, February 18, 1992) laws and policies and in accordance with the United States Department of Agriculture Animal Welfare Act and the National Institutes of Health policy on Human Care and Use of Laboratory Animals. They were reviewed and approved by the Mario Negri Institute Animal Care and Use Committee, which includes ad hoc members for ethical issues (1/04-D).

Animal treatment

All animals (Tg or WT) were intraperitoneally injected with mApoE–PA–LIP (100 μl, 73.5 mg of total lipids/kg) or with PBS as a vehicle (100 μl) once every other day for 3 weeks. The weight of the animals was recorded before each treatment. Two experimental groups were treated with mApoE–PA–LIP (APP/PS1 and WT mice, n=10 for each), two control groups were treated with PBS (APP/PS1 and WT, n=19 for each), and two more Tg groups received monofunctionalized PA-LIP or mApoE-LIP (n=10 for each). To minimize the effect of subjective bias, animals were allocated to treatment by an operator not involved in the study, and animal groups were named with numbers. Drug treatments were performed in a blind manner by naming them with alphabetic letters. Mice were treated always at the same time of the day (9:00–10:00 A.M.) in a specific room inside the animal facility,

following a randomized order. Each single mouse was our experimental unit.

Blood and tissue collection

Animals were deeply anesthetized with an overdose of ketamine/medetomidine (1.5 and 1.0 mg/kg, respectively), and the blood was collected from the heart for plasma separation. Afterward, liver, spleen, and brain were dissected and weighed. One brain hemisphere was fixed and processed for immunohistochemistry; the other hemisphere, liver, spleen, and plasma were snap frozen in dry ice and stored at -80°C (Cramer et al., 2012) until Aβ dosage by ELISA.

Brain immunohistochemistry

APP/PS1 plaque deposition was examined using the 6E10 monoclonal anti-Aβ antibody (Covance), microglia with anti-ionized calcium binding adaptor molecule 1 (Iba1; DBA), and astrocytes with anti-glial fibrillary acidic protein (GFAP; Millipore) antibodies. Brain coronal cryostat sections (30 μm; three slices per mouse) were incubated for 1 h at room temperature with blocking solutions [6E10: 10% normal goat serum (NGS); Iba1: 0.3% Triton X-100 plus 10% NGS; GFAP: 0.4% Triton X-100 plus3%NGS] and then overnight at 4°C with the primary antibodies (6E10, 1:500; Iba1, 1:1000; GFAP, 1:3500). After incubation with the anti-mouse biotinylated secondary antibody (1:200; 1 h at room temperature; Vector Laboratories) immunostaining was developed using the avidin– biotin kit (Vector Laboratories) and diaminobenzidine (Sigma). Tissue analysis and image acquisition were done using an Olympus image analyzer and the Cell-R software.

Plaques were quantified by an operator blind to genotype and treatment using Fiji software, through the application of a homemade macro. Plaque deposition was also examined on APP23 mice using either the 6E10 monoclonal anti-Aβ antibody as described above or Thioflavin-S as described previously (Snellman et al., 2013).

Aβ plaque imaging by PET in APP23 mice

APP23 mice were used for PET experiments because it has been shown that the probe does not sufficiently bind to the plaques in the APP/PS1 mouse brain (Snellman et al., 2013). [^{11}C]Pittsburgh compound B (PIB) was synthesized as published previously (Snellman et al., 2013). Mean specific radioactivity of the batches was 536 ± 112 GBq/μmol at the end of synthesis. [^{11}C]PIB (injected dose, 10.4 ± 0.7 MBq) was administered via the tail vain. PET/computed tomography (CT) scans were performed with Inveon Multimodality PET/CT device (Siemens), and dynamic 60 min scans (timeframes, 30X10, 15X60, 4X300, and 2X600 s) in 3-D list mode were initiated simultaneously with the injection. Images were reconstructed with a 2-D filtered backprojection algorithm. Animals were first imaged during the week before treatment (scan 1 at 15 and 18 months of age), then during the week after the treatment (scan 2 at 16 and 19 months of age), and finally 3 months after the treatment (scan 3 at 19 and 22 months of age). From the dynamic PET images, time-radioactivity curves for brain, frontal cortex, and cerebellum were obtained from regions of interest manually drawn to the CT image and projected to the PET image. Bound-to-free ratios (B/F40–60) for the frontal cortex were determined from the late

phase (40–60 min) of the time-radioactivity curves as described recently using cerebellum as a reference region (Snellman et al., 2013).

Novel-object recognition test

The novel-object recognition (NOR) test is a memory test that relies on spontaneous animal behavior without the need of stressful elements, such as food or water deprivation or electric footshock (Antunes and Biala, 2012). In the NOR test, mice are introduced into an arena containing two identical objects that they can explore freely. Twenty-four hours later, mice are reintroduced into the arena containing two different objects, one of which was presented previously (familiar) and a new completely different one (novel). At the end of treatment, mice were tested in an open-square gray arena (40 X 40 cm), 30 cm high, with the floor divided into 25 squares by black lines, placed in a specific room dedicated to behavioral analysis and separated from the operator's room. The following objects were used: a black plastic cylinder (4 X 5 cm), a glass vial with a white cup (3 X 6 cm), and a metal cube (3X5 cm). The task started with a habituation trial during which the animals were placed in the empty arena for 5 min, and their movements were recorded as the number of line crossings, which provide an indication of both WT and Tg mice motor activity. Mice were tested following a predefined scheme (five mice for each treatment group and the remaining mice by following the same scheme) so to precisely maintain the 24 h of retest for each mouse. The next day, mice were again placed in the same arena containing two identical objects (familiarization phase). Exploration was recorded in a 10 min trial by an investigator blinded to the genotype and treatment. Sniffing, touching, and

stretching the head toward the object at a distance of no more than 2 cm were scored as object investigation. Twenty-four hours later (test phase), mice were again placed in the arena containing two objects, one of the objects presented during the familiarization phase (familiar object) and a new different one (novel object), and the time spent exploring the two objects was recorded for 10 min. Results were expressed as percentage time of investigation on objects per 10 min or as discrimination index (DI), i.e., (seconds spent on novel – seconds spent on familiar)/(total time spent on objects). Animals with no memory impairment spent a longer time investigating the novel object, giving a higher DI.

Aβ quantification in animal organs

Mouse brains were treated as described previously (Steinerman et al., 2008) with some modifications. Mouse brain hemispheres were homogenized in a Tris buffer containing 50 mM Tris-HCl, pH 7.4, 150 mM NaCl, 50 mM EDTA, 1% Triton X-100, and 2% protease inhibitor. After centrifugation (15,000 rpm, 21,000 X g, 4°C for 25 min), the supernatant was retained as the Triton-soluble fraction (soluble Aβ). The pellet was homogenized a second time in the presence of 70% formic acid (FA) (10% v/w) and ultracentrifuged (55,000 rpm, 100,000 X g, 4°C, 1 h), and the resulting FA-extracted supernatant was neutralized with 1 M Tris buffer, pH 11, representing the FA-extracted insoluble fraction. Levels of $A\beta_{1–40}$ and $A\beta_{1–42}$ in each fraction were quantified by sandwich ELISA (ELISA kit; IBL).

Liver and spleen were homogenized, and their Aβ levels were quantified as for the brain. Levels of plasma $A\beta_{1–40}$ and $A\beta_{1–42}$ were

quantified by ELISA (Wako Chemicals). Each sample was assayed in triplicate.

Brain Aβ oligomer analysis

Aliquots of the Triton-soluble fractions (soluble Aβ), containing 45μg of total protein, were run on a precast NuPAGE 4–12% bis-Tris gel (Invitrogen), transferred to a nitrocellulose membrane, probed with the 6E10 anti-Aβ antibody (1:1000 dilution), and visualized with enhanced chemiluminescence (ECL) by ImageQuant LAS4000. The protein load was controlled either by Ponceau S staining or β-actin immunoblotting using rabbit anti-β-actin antibody (1:1500 dilution; Invitrogen). The content of soluble Aβ assemblies was quantified by the intensity of the chemiluminescent bands using NIH ImageJ Software and normalized with respect to the β-actin content of the same sample.

Confocal microscopy

To investigate whether mApoE-PA-LIP entered the brain in an intact form, APP/PS1 mice (100 μl, 73.5 mg of total lipids/kg) were intraperitoneally injected with fluorescently labeled mApoE-PA-LIP or with PBS as vehicle (100 μl), once a day for 3 consecutive days. Three hours after the last injection, animals were killed, and the brains were fixed in 4% paraformaldehyde for 24 h, transferred to 30% sucrose until the tissue sank, and frozen at -80°C. Brain coronal cryostat sections (30 μm) were washed three times in PBS, and the nuclei were stained with DAPI (1:500 in PBS) for 10 min and then washed again four times in PBS. The sections were finally mounted with Fluorsave (Calbiochem) and viewed under a laser-scan confocal microscope (Zeiss LSM 710)

using a 20X objective in fluorescence and bright-field combined acquisition mode.

Images were acquired focusing on the hippocampus using a 63X oil-immersion objective, generating a 3-D reconstruction using an appropriate optical sectioning (Z-stack). The images shown have been obtained as the sum of several focal planes with a thickness of 0.63 μm each, giving information related to the entire volume of the analyzed sections. This procedure ensures a "full-volume" data collection. Acquisition parameters were set to select the specific wavelength of the fluorescent LIPs injected, reducing any possible interference from auto-fluorescence, and were maintained constant for all the experiments. In detail, DAPI signals were recorded in the 406-475 nm emission range using a 405 nm laser wavelength, and mApoE-PA-LIP signals were detected in the 493-542 nm emission range using a 488 nm laser wavelength for BODIPY-FL and in the 562-626 nm emission range using a 561 nm laser wavelength for Rhodamine B.

Statistical analysis

Data were expressed as mean ± SEM. For ELISA assay, Western blot and plaque quantification data were analysed by Student's t test. For the NOR test, data were analyzed by a two-way ANOVA. In the presence of a significant interaction between the factors Tg X treatment, the Tukey's post hoc test was applied. $p < 0.05$ was considered significant.

2.3 RESULTS

The physicochemical features of mApoE-PA-LIP are reported in Table 1.

Table 1. Physicochemical features of LIPs used in the present investigation

Liposome	Size (nm)	PDI	ζ potential (mV)
PA–LIP	109 ± 8	0.10	−23.6 ± 4
mApoE–LIP	119 ± 7	0.12	−15.3 ± 3
mApoE–PA–LIP	121 ± 7	0.15	−18.7 ± 4

Table 1. Size, polydispersity index (PDI), and ζ-potential of LIPs were measured by the dynamic light scattering technique and interferometric Doppler velocimetry.

An EM image of the LIP preparation is shown in Figure 1A. EM experiments confirmed their ability to inhibit, *in vitro*, the formation of amyloid aggregates and to disrupt preformed fibrils, as reported previously using other techniques (Bana et al., 2013). In fact, as shown in Figure 1B-D, the meshwork of the amyloid fibrils formed by $A\beta_{1–42}$ was significantly reduced when the peptide aggregation was performed in the presence, or after incubation, of mApoE-PA-LIP with preformed fibrils.

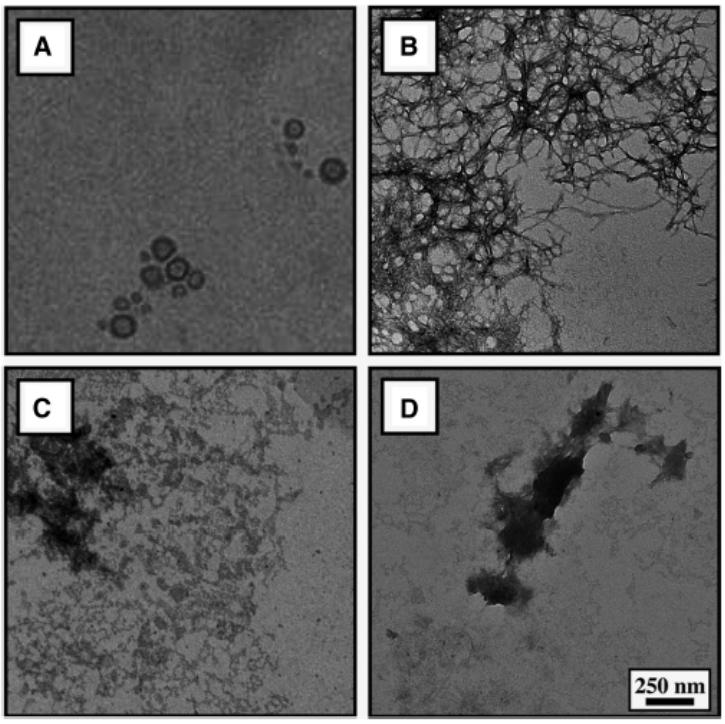

Figure 1. EM characterization of mApoE-PA-LIP and their ability to hinder the formation and disaggregate Aβ assemblies *in vitro*. **A**, Electron micrograph of mApoE-PA-LIP used in the present investigation. **B**, Fibrillary assemblies of 25μM $A\beta_{1-42}$ formed after 5 d incubation at 37°C. **C**, Fibrillary assemblies of 25μM $A\beta_{1-42}$ formed after 5 d incubation with 1 mM mApoE-PA-LIP at 37°C. **D**, Fibrillary assemblies of $A\beta_{1-42}$ obtained as in **B** and then incubated with 1 mM mApoE-PA-LIP.

Pharmacokinetic experiments, reported in Figure 2, were performed by intraperitoneal administration of dually radiolabeled ([^{14}C]PA and [^{3}H]Sm) PA-LIP or mApoE-PA-LIP in BALB/c mice to assess the radioactivity distribution in blood, liver, spleen, kidneys, lungs, and brain. The results show that the amount of radioactivity reaching the brain *in vivo* is higher for mApoE-PA-LIP than for monofunctionalized PA-LIP. Furthermore, the data show that the ratio between ^{14}C and ^{3}H detected in the brain is comparable with the ratio between the two isotopes (~1:1) of the mApoE-PA-LIP injected.

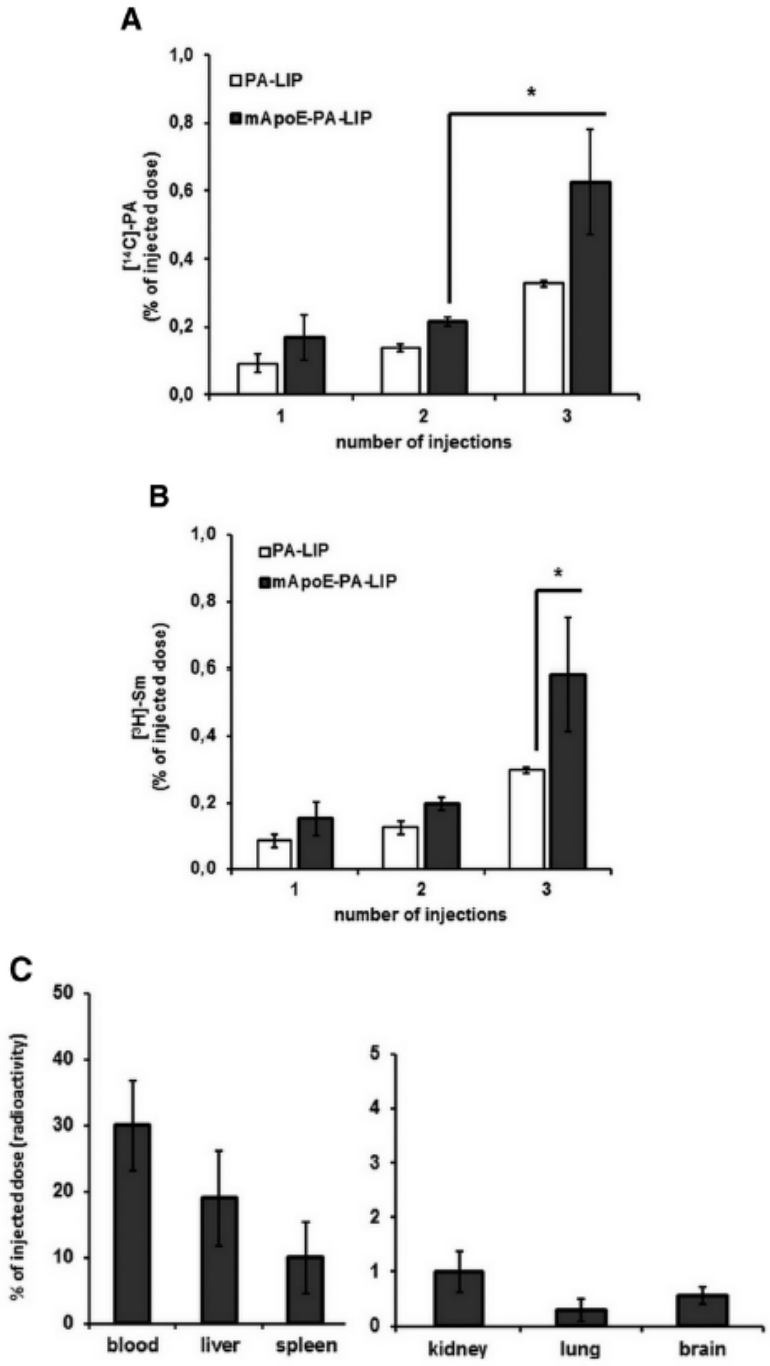

Figure 2. The additional functionalization with mApoE of radiolabeled PA-LIP administered to healthy mice increases the amount of brain-associated radioactivity. Dually radiolabeled ([^{3}H]Sm and [^{14}C]PA) mApoE-PA-LIP or PA-LIP (100µl, 73.5

mg of total lipids/kg) were administered intraperitoneally to BALB/c mice (n = 3; 6-8 weeks old), three injections (1 injection every 48 h). Mice were killed 3 h after the injections, blood, liver, spleen, kidneys, lungs, and brain were collected, and radioactivity was measured. **A**, Amount of [^{14}C]PA (expressed as percentage of injected dose) in mouse brain after one, two, or three injections of PA-LIP or mApoE-PA-LIP. **B**, Amount of [^{3}H]Sm (expressed as percentage of injected dose) in mouse brain after one, two, or three injections of PA-LIP or mApoE-PA-LIP. **C**, [^{14}C]PA biodistribution (expressed as radioactivity percentage of injected dose) in blood, liver, spleen, kidney, lung, and brain. Student's *t* test , **p* < 0.05.

APP/PS1 Tg mice were treated with either bifunctionalized mApoE-PA-LIP or monofunctionalized LIP (PA-LIP or mApoE-LIP) or with PBS, as vehicle, for 3 weeks and submitted to an NOR test. Figure 3 shows that, although PBS-treated APP/PS1 mice were unable to discriminate between the familiar and the novel object (percentage time of investigation per 10 min: familiar, 47.2 ± 2.2; novel, 52.8 ± 2.2; DI, 0.02 ± 0.04; n = 19), after treatment, only mice receiving mApoE–PA–LIP significantly recovered their long-term recognition memory (percentage time of investigation per 10 min: familiar, 36.2 ± 5.1; novel, 63.8 ± 5.1; DI, 0.28 ± 0.1; n = 10), close to the values of PBS-treated WT mice (percentage time of investigation per 10 min: familiar, 37.0 ± 2.4; novel, 63.0 ± 2.4; DI, 0.28 ± 0.04; n = 19). One-way ANOVA for the DI found a significant effect of treatment ($F(5,72) = 3.5$, $p = 0.006$). Interestingly, in contrast to bifunctionalized LIPs, only a slight, albeit nonstatistically, significant memory improvement was observed after treatment with monofunctionalized LIP (percentage time of investigation per 10 min: PA–LIP, familiar, 41.3 ± 4.2; novel, 59.0 ± 4.2; DI, 0.18 ± 0.08; n = 10; mApoE-LIP, familiar, 43.7 ± 2.8; novel, 56.3 ± 2.8; DI, 0.13 ± 0.06; n = 10).

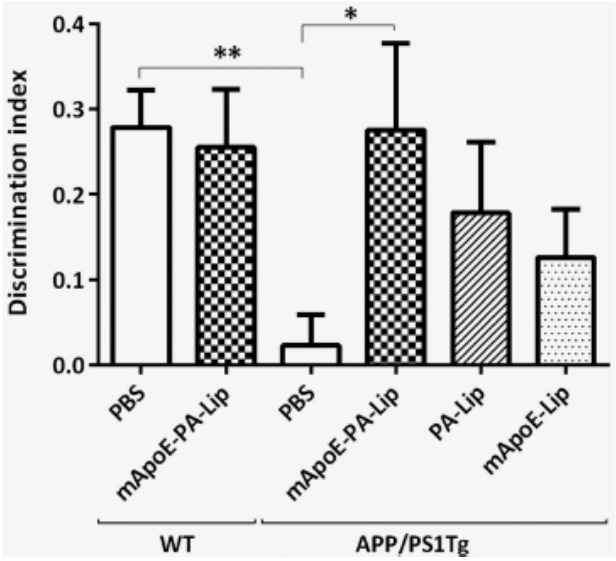

Figure 3. Treatment with bifunctionalized mApoE-PA-LIP significantly restores long-term recognition memory in APP/PS1 Tg mice. APP/PS1 Tg or WT mice were treated with mApoE-PA-LIP, PA-LIP, mApoE- LIP, or vehicle, and, at the end of treatment, their memory was tested with the NOR test. Histograms are mean ± SEM of the corresponding DI. One-way ANOVA found a significant effect of treatment ($F_{(5,72)} = 3.5$, p = 0.006). Tukey's *post hoc* test, $*p < 0.05$,$**p < 0.01$.

In addition, we demonstrated that mApoE–PA–LIP treatment had no negative effect on the memory of WT mice (percentage time of investigation per 10 min: familiar, 37.3 ± 3.4; novel, 62.7 ± 3.4; DI, 0.25 ± 0.07; n = 10) and did not affect mouse weight and motor activity (data not shown).

At the end of behavioral investigation by the NOR test, APP/PS1 mice were killed, and half of the brain was postfixed and subsequently immunostained for plaque quantification. As expected at the age investigated (Balducci and Forloni, 2011), APP/PS1 mice treated with PBS displayed important deposits of plaques that were significantly reduced in APP/PS1 mice treated with mApoE–PA–LIP. As shown in

Figure 4, we found that mApoE–PA–LIP reduced the number and total area of brain Aβ plaques by ~ 34% in both the cortex and the hippocampus. Student's t test for the two treatment groups, mApoE–PA–LIP (n = 10) versus PBS (n = 10), found a significant reduction in the number of plaques ($t(17) = -3.0$, $p = 0.008$) and in the total plaque area ($t(17) = -2.5$, $p = 0.02$). The treatment of APP/PS1 Tg mice with PA–LIP or mApoE–LIP, which did not significantly recover from memory impairment, did not reduce brain plaques either (data not shown).

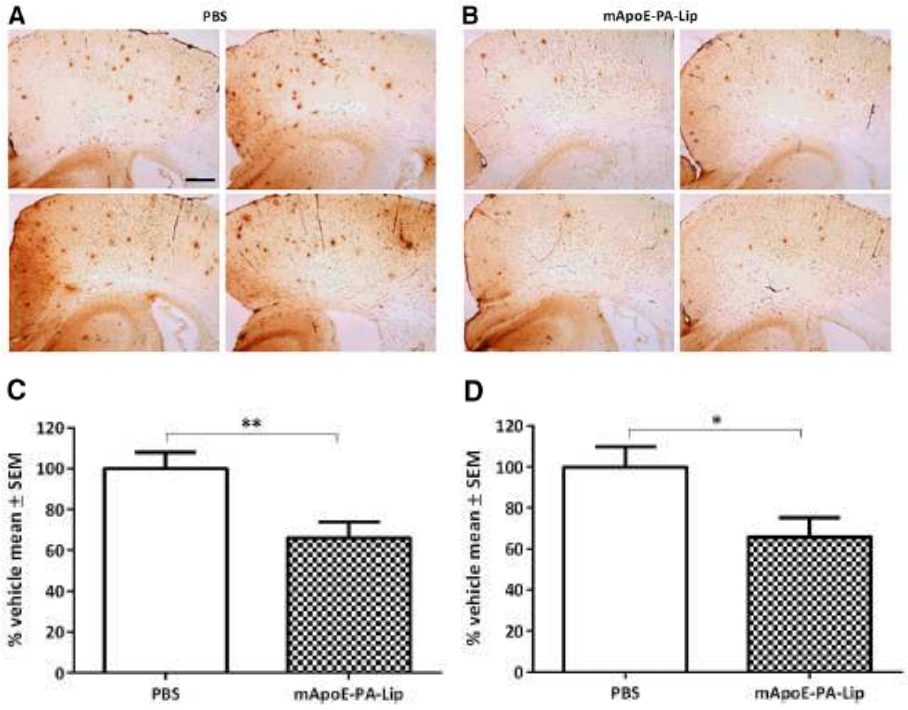

Figure 4. mApoE-PA-LIP treatment significantly reduced Aβ plaque load in the brain of APP/PS1 Tg mice. APP/PS1 Tg mice were treated with mApoE-PA-LIP or vehicle, and, at the end of treatment, the brain Aβ burden was analyzed by immunohistochemistry. **A**, Representative cortical and hippocampal brain sections of mice treated with PBS. **B**, Representative cortical and hippocampal brain sections of mice treated with mApoE-PA-LIP. Brain sections were stained with the anti-Aβ6E10 monoclonal antibody. **C**, Histograms report the percentage reduction (mean ± SEM) of the total number of plaques in mApoE-PA-LIP-treated mice. **D**, Histograms report

the percentage reduction (mean ± SEM) of the total plaque area in mApoE-PA-LIP-treated mice. Student's *t* test, **p* < 0.05, ***p* < 0.01. Scale bar, 250 μm.

The plaque reduction induced by mApoE–PA–LIP treatment on APP/PS1 mice was also confirmed on APP23 mice by either Thioflavin-S or 6E10 anti-Aβ staining on brain sections (Figure 5). The effect of decreasing the plaque load was also followed on APP23 mice by PET using [^{11}C]PIB (Snellman et al., 2013) as the plaque-detecting probe (Figure 5). Interestingly, PET imaging, performed 3 months after the completion of the treatment, suggested a scarce tendency to plaque reconstitution, because APP23 mice showed low B/$F_{40–60}$ ratios (0.10; 0.13; -0.04) similar to WT mice (-0.09; -0.01).

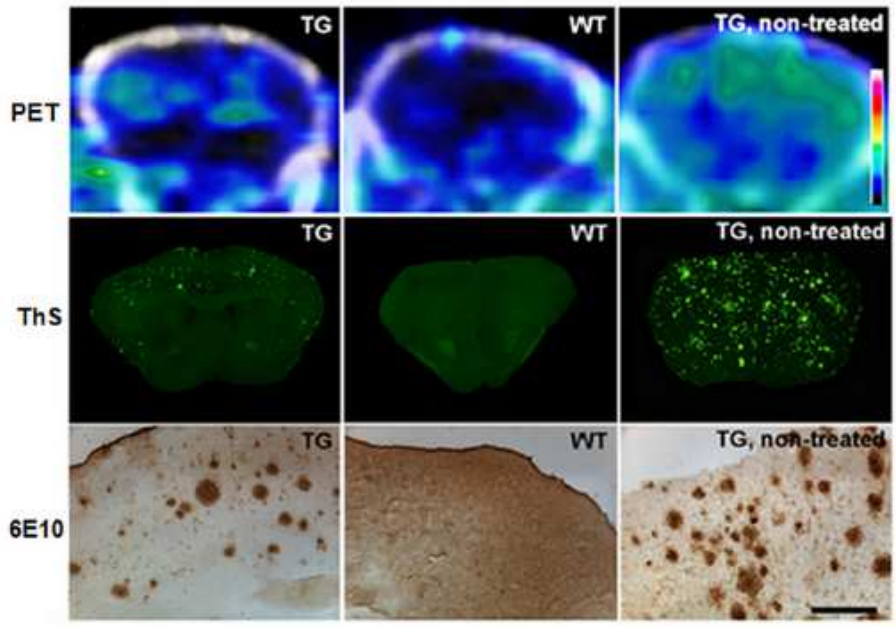

Figure 5. mApoE-PA-LIP treatment reduced Aβ plaque load, detected by [^{11}C]PIB PET, in the brain of APP23 Tg mice. APP23 Tg or WT mice were treated with mApoE-PA-LIP, and, at the end of treatment, animals were imaged repeatedly with 60 min dynamic [^{11}C]PIB PET scans. Three months after completion of the treatment, animals were imaged and subsequently killed. Brain Aβ deposition was evaluated on cortical cryosections. The figure displays summed (40–60 min after injection) PET

images (PET) or cortical sections stained with Thioflavin-S (ThS) or 6E10 anti-Aβ antibody (6E10) of Tg and WT mice 3 months after the completion of the treatment with mApoE–PA–LIP (n = 3 for each group). Additional images of untreated Tg mouse present the expected Aβ deposition in this model at 18 months of age. Scale bar, 200μm.

The effect of mApoE–PA–LIP-mediated plaque reduction in APP/PS1 mice was paralleled by a decrease in the total amount of brain Aβ levels, assayed by ELISA (Figure 6). After treatment, the amount of insoluble and soluble brain $A\beta_{1–40}$ (1249.7 ± 259.8 and 50.2 ± 12.1 pmol/g brain) was 33 and 32%, respectively, which is lower than in the brain of PBS-treated mice ($p = 0.0000053$, $p = 0.00022$ by Student's *t* test). The amount of insoluble and soluble brain $A\beta_{1–42}$ (1001.7 ± 221.0 and 60.2 ± 10.7 pmol/g) was 26 and 11% lower ($p = 0.007$, $p = 0.024$ by Student's *t* test), respectively.

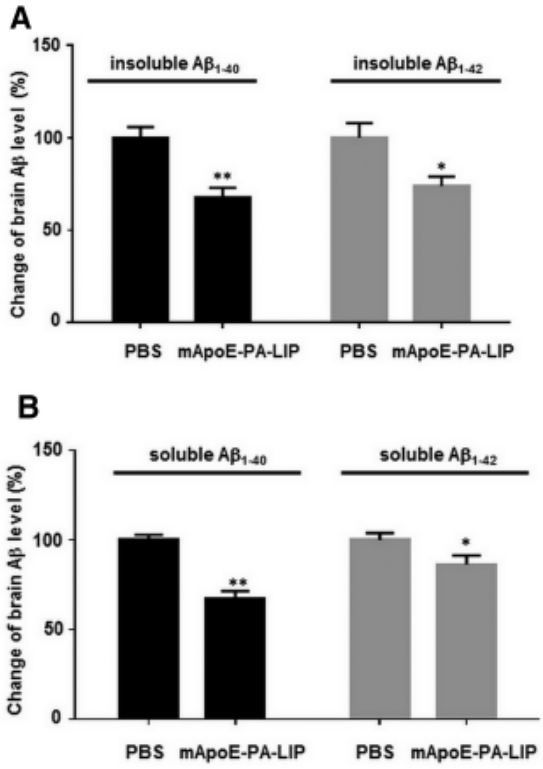

Figure 6. Aβ levels were significantly reduced in the brain of mApoE-PA-LIP-treated APP/PS1 Tg mice. APP/PS1 Tg or WT mice were treated with mApoE–PA–LIP or vehicle, and, at the end of treatment, brains were homogenized and soluble or insoluble $A\beta_{1-40}$ and $A\beta_{1-42}$ amounts were measured by ELISA. **A**, Percentage change of insoluble brain $A\beta_{1-40}$ and $A\beta_{1-42}$. **B**, Percentage change of soluble brain $A\beta_{1-40}$ and $A\beta_{1-42}$ levels. Data are expressed as mean ± SEM. Student's *t* test, $*p < 0.05$, $**p < 0.01$.

To assess whether the decrease of brain Aβ burden was also involving oligomers, recognized as the best correlate of synaptic dysfunction and disease severity (Lue et al., 1999; McLean et al., 1999), their content was analyzed on brain homogenates of treated mice. It is noteworthy that the treatment strongly reduced (-70.5%, $p < 0.001$) the levels of soluble Aβ species with MW up to 90 kDa (Figure 7). This also holds true for the band with an MW of ~100 kDa, likely corresponding to full-length APP (-33. 9%, $p = 0.055$).

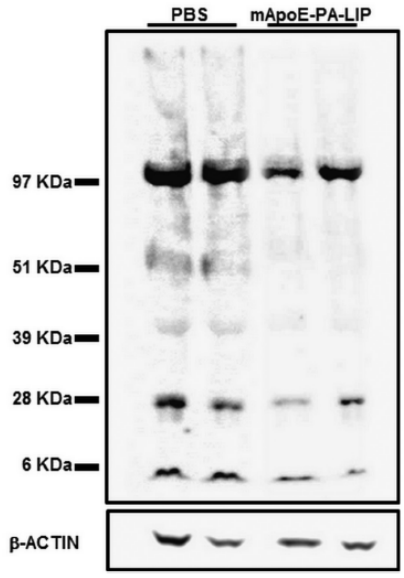

Figure 7. mApoE-PA-LIP significantly reduced Aβ oligomers in the brain of APP/PS1 Tg mice. APP/PS1 Tg or WT mice were treated with mApoE-PA-LIP or vehicle, and, at the end of treatment, brains were homogenized and soluble Aβ was submitted to SDS-PAGE or Western blot. Representative Western blot of brain-soluble Aβ probed with anti-Aβ 6E10 and visualized by ECL is shown.

Because of all this compelling evidence, highlighting the ability of the mApoE-PA-LIP to induce a significant brain Aβ decrease, we wondered what happened to the disappeared peptide. In an attempt to answer this question, we measured Aβ levels in organs and tissues of APP/PS1 mice treated with mApoE-PA-LIP. We found that the levels of Aβ in both the liver (Figure 8A) and the spleen (Figure 8B) had increased (liver, +18%, p = 0.038; spleen, +20%, p = 0.0057 by Student's *t* test), whereas Aβ levels in plasma, at the end of the treatment, did not significantly change with respect to PBS-treated mice (1.47 ± 0.69 versus 1.27 ± 0.79 pmol/ml Aβ).

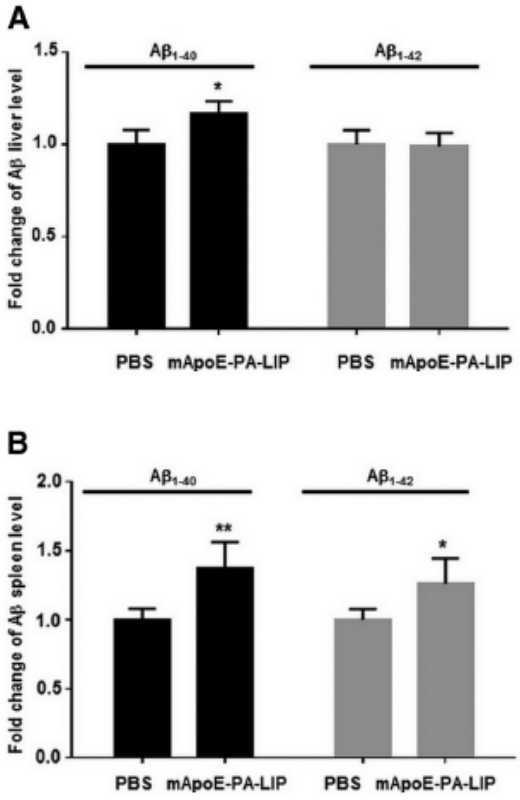

Figure 8. Aβ levels in the liver and spleen of APP/PS1 Tg mice are increased after treatment with mApoE-PA-LIP. APP/PS1 Tg or WT mice were treated with mApoE-PA-LIP or vehicle, and, at the end of treatment, liver and spleen were dissected and

homogenized and total Aβ was extracted. $A\beta_{1-40}$ and $A\beta_{1-42}$ amounts were measured by ELISA. Data are expressed as a fold change of Aβ levels. **A**, Histogram of liver $A\beta_{1-40}$ and $A\beta_{1-42}$ levels. **B**, Histogram of spleen $A\beta_{1-40}$ and $A\beta_{1-42}$ levels. Data are expressed as mean ± SEM. Student's *t* test, $*p < 0.05$.

The involvement of microglia and astrocytes in Aβ clearance (Agostinho et al., 2010) was ruled out through immunostaining experiments on APP/PS1 brains, which showed no increased activation in either the cortex or the hippocampus after mApoE-PA-LIP treatment (data not shown).

Finally, experiments with dually fluorescently labelled mApoE-PA-LIP were performed to assess their ability to cross the BBB in an intact form. After injection in APP/PS1 Tg mice, brain sections were imaged by confocal microscopy. Thanks to the incorporation of two different fluorophores into mApoE-PA-LIP, specific punctuated red and green signals with high level of co-localization were observed in the hippocampus (Figure 9).

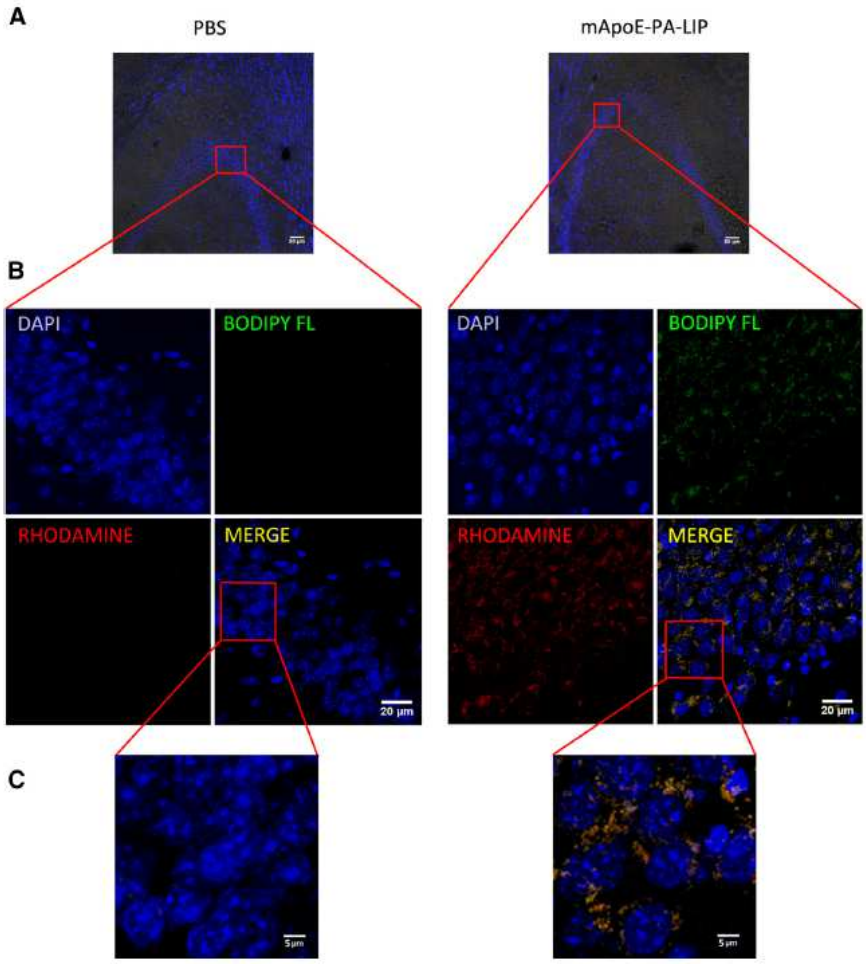

Figure 9. Dually fluorescently labeled mApoE-PA-LIP administered to APP/PS1 mice are detected intact in the hippocampal regions. **A**, Bright-field and DAPI fluorescence of brain sections from APP/PS1 mice treated with PBS or LIPs, acquired to focus the additional analysis on the hippocampal area. **B**, Representative images of brain hippocampal regions of mice treated with PBS or dually fluorescently labeled mApoE-PA-LIP. The images shown have been obtained as the sum of several focal planes with a thickness of 0.63µm each, giving information related to the entire volume of the analyzed sections. **C**, Magnification of the framed areas of **B**.

2.4 DISCUSSION

Considering the demographic increase and the global trend in population aging, the influence of AD will be even more pronounced in the future: it is estimated that the number of AD-afflicted individuals will triple by the year 2050. Unfortunately, there are currently no effective means to prevent or cure this disease. Biotechnological devices, such as nanoparticles, represent a possible tool to reach this goal, relying on the possibility of conferring on them multitask features. Despite the fact that several nanoparticles have been synthesized and proposed for therapy and diagnosis of AD, evidence of their efficacy *in vivo* has not yet been reached (Brambilla et al., 2011). Therefore, in the present investigation, we designed multitask LIPs and tested their therapeutic efficacy *in vivo* in AD mouse models. Based on our previous *in vitro* studies (Gobbi et al., 2010; Re et al., 2010, 2011; Bana et al., 2013), these tasks were assigned to LIPs bifunctionalized with PA, which binds Aβ in different aggregation forms, and with mApoE, obtained by modification of a decapeptide from ApoE, targets the BBB and facilitates its crossing. This peptide sequence contains only the receptor-binding domain of ApoE and not the Aβ-binding sequence. The combination of the two ligands on the LIP surface confers to them the unforeseen feature of disaggregating Aβ assemblies, *in vitro*, as we have reported recently (Bana et al., 2013) and herein confirmed. This ability, not displayed by monofunctionalized LIPs (with either PA or mApoE), could arise from the synergic interaction of both the negatively charged PA phosphate group and the positively charged mApoE amino acids with oppositely charged residues present on Aβ

peptide at physiological pH (Datta et al., 2000; Ahyayauch et al., 2012; Bana et al., 2013).

For the *in vivo* proof-of-principle, we used APP/PS1 as the AD mouse model. The APP/PS1 carry the human Swedish mutation and a deletion of the exon 9 on PS1 and show Aβ plaque deposition starting from 8–9 months of age (Lee et al., 1997; Jankowsky et al., 2001). Therefore, it represents a useful "early-onset" AD mouse model. We observed that the treatment with mApoE-PA-LIP induced an important reduction in the number of brain plaques. mApoE-PA-LIP-induced plaque reduction was also confirmed in some experiments on APP23 mice; APP23 mice were used also for PET imaging of plaques with [^{11}C]PIB, because it has been shown that this probe does not sufficiently bind to the plaques in the APP/PS1 mouse brain (Snellman et al., 2013). Noticeably, PET experiments showed that the plaque reduction was still present 3 months after treatment. The comparison with monofunctionalized LIPs indicates that bifunctionalization is crucial to either affect the Aβ plaque load or enhance the amount of radioactivity crossing the BBB after injection of radiolabeled LIPs. Finally, an approach based on the use of dually fluorescent LIPs coupled to confocal microscopy imaging (Tanifum et al., 2012) showed co-localization of the two fluorescent probes in the hippocampus of treated mice, suggesting that mApoE-PA-LIP reached the brain in an intact form. Considering the results obtained, it is reasonable to speculate that mApoE-PA-LIP exert their activity by crossing the BBB interacting with, and destabilizing, brain Aβ aggregates. Successively, the generated lower MW Aβ species may be facilitated to move from brain to blood and are peripherally cleared in the liver and spleen through the so-called sink effect (Matsuoka et

al., 2003; Biscaro et al., 2009; Sutcliffe et al., 2011), likely mediated by circulating mApoE-PA-LIP. To this regard, the peripheral increment of Aβ in the liver and spleen, detected at the end of the treatment, supports this hypothesis.

However, the increased Aβ recovery in peripheral organs is not sufficient to explain the total reduction of brain Aβ levels. Because we did not observe activation of microglia and astrocytes after treatment, we suggest that proteolytic degradation of brain Aβ might be integrated by the sink effect. The relevant role of proteolytic degradation in Aβ clearance, with respect to its elimination across the BBB, has been suggested recently (Ito et al., 2013).

In association with plaque reduction, the treatment with mApoE-PA-LIP also induced a significant recovery of Tg mouse impaired memory, at variance with monofunctionalized LIPs, which exerted a weaker effect that did not reach statistical significance.

However, these findings suggest that monofunctionalized LIPs might exert, when administered together, an effect comparable with that of bifunctionalized LIPs. A deeper investigation with a larger number of data will clarify this issue.

This observation, together with the fact that the mApoE-PA-LIP also induced a significant reduction of Aβ oligomers, makes the treatment even more compelling. Aβ oligomers are indeed recognized as the main species responsible of the neuropathological process underlying the onset and progression of AD and the best correlates of synaptic dysfunction and disease severity (Lue et al., 1999; McLean et al., 1999; Wilcox et al., 2011; Scopes et al., 2012). In experimental models, oligomers have been shown to specifically inhibit long-term

potentiation and mediate memory impairment, whereas Aβ monomer and fibrils were inactive (Walsh et al., 2002; Cleary et al., 2005; Balducci et al., 2010). Because it is more likely that different Aβ species, rather than a unique molecular assembly, affect neuronal functions at multiple levels, another relevant observation is that the Aβ oligomer reduction, mediated by the treatment, helps to reduce different MW species. It is also worth noting that full-length APP is seemingly reduced after treatment. This observation opens the possibility that additional mechanisms are underlying the effect of LIP. Of course, more focused studies are necessary to clarify these complex issues.

Together, our findings promote mApoE-PA-LIP as a well-tolerated valuable new nanotechnological means for AD therapy. It is important to point out that the treatment with mApoE-PA-LIP does not eliminate the cause of Aβ overproduction but could slow down the neurodegeneration process. Therefore, it is conceivable that possible therapeutic protocols could require chronic treatments to minimize the progression of the disease.

Acknowledgement

The research leading to these results has received funding from the European Community's Seventh Framework Program (FP7/2007-2013) under Grant 212043 (NAD, Nanoparticles for therapy and diagnosis of Alzheimer disease).

References

Agostinho P, Cunha RA, Oliveira C (2010) Neuroinflammation, oxidative stress and the pathogenesis of Alzheimer's disease. Curr Pharm Des 16:2766–2778.

Ahyayauch H, Raab M, Busto JV, Andraka N, Arrondo JL, Masserini M, Tvaroska I, Goni FM (2012) Binding of β-amyloid (1– 42) peptide to negatively charged phospholipid membranes in the liquid-ordered state: modeling and experimental studies. Biophys J 103:453– 463.

Antunes M, Biala G (2012) The novel object recognition memory: neurobiology, test procedure, and its modifications. Cogn Process 13:93–110.

Balducci C, Forloni G (2011) APP transgenic mice: their use and limitations. Neuromolecular Med 13:117–137.

Balducci C, Beeg M, Stravalaci M, Bastone A, Sclip A, Biasini E, Tapella L, Colombo L, Manzoni C, Borsello T, Chiesa R, Gobbi M, Salmona M, Forloni G (2010) Synthetic amyloid-beta oligomers impair long-term memory independently of cellular prion protein. Proc Natl Acad Sci U S A 107:2295–2300.

Bana L, Minniti S, Salvati E, Sesana S, Zambelli V, Cagnotto A, Orlando A, Cazzaniga E, Zwart R, Scheper W, Masserini M, Re F (2013) LIPosomes bifunctionalized with phosphatidic acid and an ApoE-derived peptide affect Aβ aggregation features and cross the blood-brain-barrier: implications for therapy of Alzheimer Disease. Nanomedicine. Advance online publication. Retrieved September 9, 2014. doi:10.1016/j.nano.2013.12.001.

Bertram L, Tanzi RE (2012) The genetics of Alzheimer's disease. Prog Mol Biol Transl Sci 107:79 –100.

Biscaro B, Lindvall O, Hock C, Ekdahl CT, Nitsch RM (2009) Abeta immunotherapy protects morphology and survival of adult-born neurons in doubly transgenic APP/PS1 mice. J Neurosci 29:14108 –14119.

Brambilla D, Le Droumaguet B, Nicolas J, Hashemi SH, Wu LP, Moghimi SM, Couvreur P, Andrieux K (2011) Nanotechnologies for Alzheimer's disease: diagnosis, therapy, and safety issues. Nanomedicine 7:521–540.

Bruggink KA, Mu¨ller M, Kuiperij HB, Verbeek MM (2012) Methods for analysis of amyloid-beta aggregates. J Alzheimers Dis 28:735–758.

Chang HI, Yeh MK (2012) Clinical development of liposome-based drugs: formulation, characterization, and therapeutic efficacy. Int J Nanomedicine 7:49–60.

Cleary JP, Walsh DM, Hofmeister JJ, Shankar GM, Kuskowski MA, Selkoe DJ, Ashe KH (2005) Natural oligomers of the amyloid-beta protein specifically disrupt cognitive function. Nat Neurosci 8:79–84.

Cramer PE, Cirrito JR, Wesson DW, Lee CY, Karlo JC, Zinn AE, Casali BT, Restivo JL, Goebel WD, James MJ, Brunden KR, Wilson DA, Landreth GE (2012) ApoE-directed therapeutics rapidly clear beta-amyloid and reverse deficits in AD mouse models. Science 335:1503–1506.

Datta G, Chaddha M, Garber DW, Chung BH, Tytler EM, Dashti N, Bradley WA, Gianturco SH, Anantharamaiah GM (2000) The

receptor binding domain of apolipoprotein E, linked to a model class A amphipathic helix, enhances internalization and degradation of LDL by fibroblasts. Biochemistry 39:213–220.

Gobbi M, Re F, Canovi M, Beeg M, Gregori M, Sesana S, Sonnino S, Brogioli D, Musicanti C, Gasco P, Salmona M, Masserini ME (2010) Lipid-based nanoparticles with high binding affinity for amyloid-beta1–42 peptide. Biomaterials 31:6519–6529.

Ito S, Matsumiya K, Ohtsuki S, Kamiie J, Terasaki T (2013) Contributions of degradation and brain-to-blood elimination across the blood-brain barrier to cerebral clearance of human amyloid-beta peptide(1– 40) in mouse brain. J Cereb Blood Flow Metab 33:1770 –1777.

Jankowsky JL, Slunt HH, Ratovitski T, Jenkins NA, Copeland NG, Borchelt DR (2001) Co-expression of multiple transgenes in mouse CNS: a comparison of strategies. Biomol Eng 17:157–165.

Lazarov O, Robinson J, Tang YP, Hairston IS, Korade-Mirnics Z, Lee VM, Hersh LB, Sapolsky RM, Mirnics K, Sisodia SS (2005) Environmental enrichment reduces Abeta levels and amyloid deposition in transgenic mice. Cell 120:701–713.

Lee MK, Borchelt DR, Kim G, Thinakaran G, Slunt HH, Ratovitski T, Martin LJ, Kittur A, Gandy S, Levey AI, Jenkins N, Copeland N, Price DL, Sisodia SS (1997) Hyperaccumulation of FAD-linked presenilin 1 variants in vivo. Nat Med 3:756 –760.

Lue LF, Kuo YM, Roher AE, Brachova L, Shen Y, Sue L, Beach T, Kurth JH, Rydel RE, Rogers J (1999) Soluble amyloid beta peptide concentration as a predictor of synaptic change in Alzheimer’s disease. Am J Pathol 155:853– 862.

Matsuoka Y, Saito M, LaFrancois J, Saito M, Gaynor K, Olm V, Wang L, Casey E, Lu Y, Shiratori C, Lemere C, DuffK (2003) Novel therapeutic approach for the treatment of Alzheimer's disease by peripheral administration of agents with an affinity to beta-amyloid. J Neurosci 23:29–33.

McLean CA, Cherny RA, Fraser FW, Fuller SJ, Smith MJ, Beyreuther K, Bush AI, Masters CL (1999) Soluble pool of Abeta amyloid as a determinant of severity of neurodegeneration in Alzheimer's disease. Ann Neurol 46:860–866.

Palop JJ, Mucke L (2010) Amyloid-beta-induced neuronal dysfunction in Alzheimer's disease: from synapses toward neural networks. Nat Neurosci 13:812– 818.

Re F, Cambianica I, Sesana S, Salvati E, Cagnotto A, Salmona M, Couraud PO, Moghimi SM, Masserini M, Sancini G (2010) Functionalization with ApoE-derived peptides enhances the interaction with brain capillary endothelial cells of nanoliposomes binding amyloid-beta peptide. J Biotechnol 156:341–346.

Re F, Cambianica I, Zona C, Sesana S, Gregori M, Rigolio R, La Ferla B, Nicotra F, Forloni G, Cagnotto A, Salmona M, Masserini M, Sancini G (2011) Functionalization of liposomes with ApoE-derived peptides at different density affects cellular uptake and drug transport across a blood-brain barrier model. Nanomedicine 7:551–559.

Re F, Gregori M, Masserini M (2012) Nanotechnology for neurodegenerative disorders. Maturitas 73:45–51.

Scopes DI, O'Hare E, Jeggo R, Whyment AD, Spanswick D, Kim EM, Gannon J, Amijee H, Treherne JM (2012) Abeta oligomer toxicity inhibitor protects memory in models of synaptic toxicity. Br J Pharmacol 167:383–392.

Selkoe D, Mandelkow E, Holtzman D (2012) Deciphering Alzheimer disease. Cold Spring Harb Perspect Med 2:a011460.

Snellman A, Lo´ pez-Pico´n FR, Rokka J, Salmona M, Forloni G, Scheinin M, Solin O, Rinne JO, Haaparanta-Solin M (2013) Longitudinal amyloid imaging in mouse brain with 11C-PIB: comparison of APP23, Tg2576, and APPswe-PS1dE9 mouse models of alzheimer disease. J Nucl Med 54:1434 –1441.

Steinerman JR, Irizarry M, Scarmeas N, Raju S, Brandt J, Albert M, Blacker D, Hyman B, Stern Y (2008) Distinct pools of beta-amyloid in Alzheimer disease-affected brain: a clinicopathologic study. Arch Neurol 65:906– 912.

Sutcliffe JG, Hedlund PB, Thomas EA, Bloom FE, Hilbush BS (2011) Peripheral reduction of beta-amyloid is sufficient to reduce brain beta-amyloid: implications for Alzheimer's disease. J Neurosci Res 89:808–814.

Tanifum EA, Dasgupta I, Srivastava M, Bhavane RC, Sun L, Berridge J, Pourgarzham H, Kamath R, Espinosa G, Cook SC, Eriksen JL, Annapragada A (2012) Intravenous delivery of targeted liposomes to amyloid-β pathology in APP/PSEN1 transgenic mice. PLoS One 7:e48515.

Valero J, Espan˜a J, Parra-Damas A, Martín E, Rodríguez-A´ lvarez J, Saura CA (2011) Short-term environmental enrichment rescues

adult neurogenesis and memory deficits in APP(Sw, Ind) transgenic mice. PLoS One 6:e16832.

Verbeek MM, Ruiter DJ, de Waal RM (1997) The role of amyloid in the pathogenesis of Alzheimer's disease. Biol Chem 378:937–950.

Walsh DM, Klyubin I, Fadeeva JV, Cullen WK, Anwyl R, Wolfe MS, Rowan MJ, Selkoe DJ (2002) Naturally secreted oligomers of amyloid beta protein potently inhibit hippocampal long-term potentiation in vivo. Nature 416:535–539.

Wan L, Pooyan S, Hu P, Leibowitz MJ, Stein S, Sinko PJ (2007) Peritoneal macrophage uptake, pharmacokinetics and biodistribution of macrophage-targeted PEG-fMLF (N-formyl-methionyl-leucyl-phenylalanine) nanocarriers for improving HIV drug delivery. Pharm Res 24:2110–2119.

Wilcox KC, Lacor PN, Pitt J, KleinWL (2011) Abeta oligomer-induced synapse degeneration in Alzheimer's disease. Cell Mol Neurobiol 31:939–948.

CHAPTER 3

The hunt for brain Aβ oligomers by peripherally circulating multifunctional nanoparticles: potential therapeutic approach for Alzheimer disease

Simona Mancini, Stefania Minniti, Maria Gregori, Giulio Sancini, Alfredo Cagnotto, Pierre-Olivier Couraud, Lara Ordóñez-Gutiérrez, Francisco Wandosell, Mario Salmona, Francesca Re

Nanomedicine: Nanotechnology, Biology, and Medicine, 2016; 12(1):43-52

Abstract

We previously showed the ability of liposomes bifunctionalized with phosphatidic acid and an ApoE-derived peptide (mApoE-PA-LIP) to reduce brain Aβ in transgenic Alzheimer mice. Herein we investigated the efficacy of mApoE-PA-LIP to withdraw Aβ peptide in different aggregation forms from the brain, using a transwell cellular model of the blood–brain barrier and APP/PS1 mice. The spontaneous efflux of Aβ oligomers (Aβo), but not of Aβ fibrils, from the 'brain' side of the transwell was strongly enhanced (5-fold) in presence of mApoE-PA-LIP in the 'blood' compartment. This effect is due to a withdrawal of Aβo exerted by peripheral mApoE-PA-LIP by sink effect, because, when present in the brain side, they did not act as Aβo carrier and limit the oligomer efflux. *In vivo* peripheral administration of mApoE-PA-LIP significantly increased the plasma Aβ level, suggesting that Aβ-binding particles exploiting the sink effect can be used as a therapeutic strategy for Alzheimer disease.

3.1 INTRODUCTION

Alzheimer disease (AD) is the most common form of dementia in the elderly, with no current therapy or definite diagnosis. Brain accumulation of amyloid-β (Aβ) peptides, eventually deposited as plaques, is one of the pathological hallmarks of AD (Hardy and Selkoe, 2002). Aβ accumulation has been hypothesized to result from an imbalance between Aβ production and clearance; indeed, Aβ clearance seems to be impaired in both early and late forms of AD and may contribute to the onset and progression of the disease (Bell and Zlokovic, 2009). Moreover, additional evidence suggests that about 80-90% of AD patients show cerebral amyloid angiopathy (CAA), characterized by Aβ accumulation in brain blood vessel walls (Rensink et al., 2003), altering the functionality of the BBB (Attems and Jellinger, 2014). Among the different aggregation forms of Aβ, a body of evidence indicates that soluble Aβ oligomers (Aβo), rather than insoluble deposits, such as Aβ fibrils (Aβf) and plaques, are primarily responsible for both neurodegeneration and synaptic impairment in AD. Therefore, in the last years, many efforts have focused at preventing Aβo formation or disassembling existing aggregates (Re et al., 2010a; Herrmann et al., 2011; Bana et al., 2014). Recently, a therapeutic strategy based on lowering the levels of soluble Aβ assemblies in the brain and in the cerebral blood vessel exploiting the peripheral-sink effect has been proposed (Matsuoka et al., 2003). To this purpose, it has been postulated that brain and plasma Aβ pools are in equilibrium through the BBB, and that the peripheral sequestration of Aβ may shift this equilibrium toward the peripheral blood circulation, eventually

drawing out the excess from the brain and/or from the brain vessels (Matsuoka et al., 2003).

DeMattos et al. reported that peripheral administration of a monoclonal anti-Aβ antibody to transgenic AD mice models resulted in an increase of Aβ in the plasma, despite minimal entry of the antibody into the brain, suggesting the equilibrium of Aβ between the brain and plasma (DeMattos et al., 2001, 2002). Because there are several problems associated with immunotherapy of AD (Boche et al., 2010), the use of molecules that are unrelated to antibodies, such as gelsolin, GM1 ganglioside (Matsuoka et al., 2003) or an extract from the root of *Withania somnifera*, has been proposed (Sehgal et al., 2012). The peripheral administration of these compounds in AD animal models was suggested to reduce the level of Aβ in the brain because of the sink effect. Therefore, it is conceivable that the design of compounds that bind Aβ with high affinity could reduce or prevent brain Aβ deposition in AD patients. In this context, nanoparticles are considered a promising tool due to the possibility of multifunctionalization of their surface with several copies of Aβ-specific ligands, increasing the affinity for Aβ by multivalent interactions (Gobbi et al., 2010). This feature makes them good candidates as sink effect promoters.

We have previously described liposomes (LIP) embedding acidic phospholipids (in particular phosphatidic acid, PA) and surface-decorated with a modified human ApoE-derived peptide (mApoE), i.e. mApoE-PA-LIP, which have very high binding affinity to Aβ (Bana et al., 2014). In the present study, we investigated the efficacy of mApoE-PA-LIP to withdraw Aβ peptide in different aggregation forms from the

brain, using a transwell cellular model of the blood-brain barrier and APP/PS1 mice.

3.2 MATERIALS AND METHODS

Materials

All chemical reagents were from Sigma–Aldrich, Milano, Italy. Bovine brain sphingomyelin (Sm), cholesterol (Chol) and 1,2-stearoyl-sn-glycero-3-phosphoethanolamine-N-[maleimide(-poly(ethylene glycol)-2000)] (mal-PEG-PE) were purchased from Avanti Polar Lipids (USA). Dimyristoyl phosphatidic acid (PA), $A\beta_{1-42}$ peptide and 1,1,3,3,3-hexafluoro-2-propanol (HFIP) were purchased from Sigma–Aldrich, Milano, Italy. [^{3}H]-propranolol and [^{3}H]-Sm were purchased from PerkinElmer. FITC-dextran and bovine serum albumin (BSA) were from Sigma Aldrich, Milano, Italy. Polycarbonate filters for extrusion procedure were purchased from Millipore Corp., Bedford, MA. Extruder was from Lipex Biomembranes, Vancouver, Canada. All the media and supplements for cell cultures were supplied by Invitrogen Srl, Milano, Italy. The hCMEC/D3 cell line was obtained under license from Institut National de la Sante et de la Recherche Medicale (INSERM, Paris, France). Rat type I collagen, 1/100 chemically defined lipid concentrated, and all the media and supplements for cell cultures were from Invitrogen Srl (Milano). For determination of $A\beta_{1-42}$, human β amyloid (1-42) ELISA kits (IBL) were used. Low-range rainbow molecular weight marker, horseradish peroxidase (HRP)-conjugated goat IgG anti-mouse antibody and ECL reagents were purchased from Amersham Biosciences (Castle Hill, NSW, Australia). Mouse monoclonal $A\beta_{1-42}$ antibody mAβ 6E10 was from Signet (Dedham, MA).

Preparation and characterization of liposomes

mApoE-PA-LIP composed of a Sm/Chol matrix (1:1, M:M) and bifunctionalized with PA (5 mol%) and with the peptide NH2-CWG-LRKLRKRLLR-CONH2 (MW 1698.18 g/mol, mApoE, 1.25 mol%) derived from the receptor-binding domain (a.a. residues 141-150) of human ApoE, modified by adding the tri-peptide CWG at the N-term, were prepared as previously described (Bana et al., 2014) by extrusion procedure using 100 nm diameter filter pores (Millipore). To prepare larger mApoE-PA-LIP, 400 nm diameter filter pores were used. Non-functionalized LIP (control LIP, composed by Sm/Chol 1:1), LIP mono-functionalized with PA (PA-LIP) or mono-functionalized with mApoE (mApoE-LIP), were used as a control. In some instance, [^{3}H]-sphingomyelin (less than 0.0001% of total lipids) was added as a tracer. Size and polydispersity index (PDI) of diluted LIP dispersions (at a final lipid concentration of 0.5 mg/ml in PBS pH 7.40) were measured by dynamic light scattering (DLS) technique (Brookhaven Instruments Corporation, Holtsville, NY, USA). ζ-Potential was measured for the same samples by using an interferometic Doppler velocimetry with the same instrument equipped with ZetaPALS device. Stability was measured in PBS by following size and PDI by DLS for 5 days (Bana et al., 2014).

Aβ peptide preparation and characterization

Aβ_{1-42} peptide was solubilized in HFIP at 1 mg/ml concentration. The peptide was allowed to air dry in a chemical fume hood overnight. The resulting clear film was stored at −20 °C. The peptide was resuspended before use in DMSO at a concentration of 5 mM and bath sonicated for

10 min to achieve a monomer-enriched preparation (Aβm). This preparation was diluted to 100 μM in cell culture medium and incubated 24 h at 4 °C to obtain an oligomer-enriched preparation (Aβo). Alternatively, the 5 mM Aβ preparation was diluted to 100 μM in 10 mM HCl and incubated at 37 °C for 24 h in order to obtain a fibril-enriched preparation (Aβf) (Dahlgren et al., 2002). The aggregation state of Aβm and Aβo (not Aβf because too large to be resolved) was assessed by SDS-PAGE gel electrophoresis on a 4-20% Tris-Glycine gel (Thermo Scientific, Milano), followed by immunoblotting analysis using 6E10 anti-$A\beta_{1-42}$ antibody (1:1000 dilution, Covance, Italy). Aβ assemblies were visualized with enhanced chemiluminescence (ECL) by ImageQuant LAS4000 (Bana et al., 2014). The morphology of Aβo and Aβf (not Aβm because below the AFM resolution limit) was assessed by Atomic Force Microscopy as previously described (Gregori et al., 2010).

Binding of mApoE-PA-LIP to Aβo or Aβf investigated by ultracentrifugation density gradient

The binding of mApoE-PA-LIP to Aβo or Aβf was investigated as previously described (Gobbi et al., 2010). Briefly, Aβ samples were incubated with radiolabeled mApoE-PA-LIP (1:2.5, peptide:lipids) in PBS pH 7.4 at 37 °C from 15 min. After incubation the peptide bound to LIP was separated from free peptide by flotation in a discontinuous sucrose density gradient performed as described (Gobbi et al., 2010). After ultracentrifugation in a Beckman MLS 50 rotor at 140.000 × g for 2 h in polycarbonate tubes, 10 fractions were collected from the top of the gradient and assayed for lipid and peptide content, by measuring the

lipid-associated radioactivity by liquid scintillation and by dot-blot procedure on a PVDF membrane, respectively. The proportion of Aβ bound to LIP was expressed as the % ratio between the amount of peptide in the fractions 1-5 over the total peptide amount, digitally semi-quantitatively estimating the chemiluminescent spots on PVDF membrane using ImageQuant LAS4000 software.

In vitro model of BBB

Human brain endothelial cells (hCMEC/D3) were obtained from Institut National de la Santé et de la Recherche Médicale (INSERM, Paris, France) and used as a representative human BBB model. hCMEC/D3 cells were cultured at 37 °C, 5% CO_2/saturated humidity in EBM-2 medium (Lonza, Basel, Switzerland) supplemented with 5% fetal bovine serum (FBS), 1% penicillin-streptomycin, 1.4 μM hydrocortisone, 5 μg/mL ascorbic acid, 1/100 chemically defined lipid concentrate (Invitrogen), 10 mM HEPES and 1 ng/mL basic FGF (bFGF) (Re et al., 2010b; Bana et al., 2014). To set up the BBB model, hCMEC/D3 cells, between passage 25 and 35, were seeded at a concentration of 60,000 cells/cm^2 onto collagen-coated (4 μg/cm^2 rat tail collagen type 1 Invitrogen) transwell filters (polycarbonate 12-well, pore size 0.4 μm, translucent membrane insert 1.12 cm^2; Euroclone) to establish a polarized monolayer (Tai et al., 2009; Vu et al., 2009; Bana et al., 2014). The layer of endothelial cells separates this system into an apical (‘blood’ side; 0.5 ml of volume) and basolateral (‘brain’ side; 1 ml of volume) compartment.

Impact of Aβ on cell monolayer properties

hCMEC/D3 cells were cultured on a transwell system as described above. Bioelectrical, morphological and functional properties of the cell monolayers were checked both in the presence or absence of 500 nM Aβ in the basolateral compartment. Bioelectrical properties of cell monolayer were checked by measuring the transendothelial electrical resistance (TEER) with STX2 electrode Epithelial Volt-Ohm meter (World Precision Instruments, Sarasota, Florida). Morphological and functional properties of cell monolayer were evaluated by examining cells under microscope, by measuring the paracellular permeability of 250 μM FITC-dextran (MW 4 kDa) and the transcellular permeability of 76 nM [^{3}H]-propranolol (0.5 μCi), as previously described (Bana et al., 2014). Cell viability was also assessed by MTT assay (Orlando et al., 2013).

Aβ cellular uptake and exchange across the BBB model in presence of liposomes

For Aβ exchange across the BBB model studies, hCMEC/D3 were cultured on a transwell system as described above. 500 nM Aβ was added to the basolateral compartment, exposed to the complete medium and different doses (0-200 nmol total lipids) of LIP (alone or in presence of different amounts of Aβo) were added to the apical compartment, exposed to PBS (Figure 1). In some instances, in order to mimic *in vivo*-like conditions, PBS-BSA 4% (w/v) solution was added to the apical compartment and PBS-BSA 0.015% (w/v) solution was added to the basolateral compartment. After different times of incubation (up to 4 h), aliquots were collected from the apical and

basolateral compartment and the Aβ content was measured by ELISA assay (IBL 96-well), following the manufacturer's instructions, and absorbance was read at 450 nm using a spectrophotometer Victor (Victor2 PerkinElmer). The concentration of Aβ was determined according to the standard curve prepared, as suggested by ELISA kit protocol. The Aβ endothelial permeability (EP) across the cell monolayer was calculated as described (Cecchelli et al., 1999):

$$EP = \frac{X}{Cd} * \frac{1}{\Delta t} * \frac{1}{Surface\ area}$$

where:

X = amount of drug (Aβ in our case) in the receptor chamber (upper compartment in our case) = nmol

Cd = Aβ concentration in the donor chamber (bottom compartment in our case) = nmol/cm^3

Δt = time = min

Surface area = area of transwell inset filter = cm^2

Cells were collected with 200 µl of lysis buffer 2% Triton X-100 with the addition of protease inhibitor cocktail (Sigma) and an aliquot was used to measure the Aβ content by ELISA assay to determine the Aβ cellular uptake.

Liposomes exchange across the BBB model

For LIP exchange across the BBB model, hCMEC/D3 were cultured on transwell system as described above. mApoE-PA-LIP (200 nmol total lipids), containing [^{3}H]-Sm (0.001 mol%) as a tracer, were added to the basolateral compartment in a medium containing 500 nM Aβ and

incubated at 37 °C for 2 h. The EP of LIP across the cell monolayers was estimated by measuring the radioactivity at different times (up to 2 h) of [^{3}H]-Sm in the apical and basolateral compartment by liquid scintillation counting, and calculated as described (Cecchelli et al., 1999).

Animal treatment

The double transgenic mice (APP/PS1) used in the present study incorporate a human APP construct bearing the Swedish double mutation and the exon-9-deleted PSEN1 mutation: B6.Cg-Tg (APPSwe, PSEN1dE9) 85Dbo/J (Jackson Laboratory, Bar Harbor: stock no. 005864). The genotype of the mice was confirmed by PCR of DNA isolated from tail biopsies (Ordóñez-Gutiérrez et al., 2015). All animal care and handling strictly followed the current Italian legislation and guidelines, and those of the European Commission (directive 2010/63/EU).

APP/PS1 mice (n = 7 mice/group) were intraperitoneally (I.P.) injected once every other day with mApoE-PA-LIP (100 μl, 73.5 mg of total lipids/kg) or with PBS as a control (100 μl), as already described (Balducci et al., 2014) with changes concerning the age of animals (16 months of age) and the duration of the treatment (two weeks). At the end of treatment, animals were sacrificed and blood was collected by cardiac puncture and processed for plasma separation. Brains were dissected, weighed and processed to extract Aβ (Balducci et al., 2014). Aβ levels in plasma and brain were quantified by ELISA assay, as described (Steinerman et al., 2008; Balducci et al., 2014).

Statistical analysis

Data were expressed as mean ± standard deviation and analyzed by Student's *t* test. A *P*-value < 0.05 was considered statistically significant.

3.3 RESULTS

Characterization of liposomes

In the present study, we utilized previously described mono-and bifunctionalized liposomes: PA-LIP, mApoE-LIP and mApoE-PA-LIP (Re et al., 2010b, 2011; Bana et al., 2014). Non-functionalized LIP have been used as a control. Size, polydisperisity and ζ-potential values are reported in Table 1.

Physicochemical features of liposomes.

Liposomes	Diameter (nm ± SD)	PDI	ζ-Potential (mV ± SD)
Control LIP	108.1 ± 2	0.099	−25.51 ± 0.82
PA-LIP	114.7 ± 5	0.109	−48.22 ± 2.34
mApoE-LIP	119.3 ± 7	0.123	−16.41 ± 1.36
mApoE-PA-LIP	139.4 ± 9	0.143	−18.32 ± 2.09

Table 1. Control LIP, control liposomes composed of Sm/Chol 1:1 M/M. PA-LIP, liposomes functionalized with 5 mol% of phosphatidic acid. mApoE-LIP, liposomes functionalized with 1.25 mol% of mApoE peptide. mApoE-PA-LIP, liposomes bifunctionalized with 5 mol% of phosphatidic acid and 1.25 mol% of mApoE peptide. PDI, polydispersity index. SD, standard deviation.

DLS analysis showed that LIP were monodispersed and their size remained constant, within the experimental error, for up to 5 days (data not shown). The yield of LIP surface functionalization with mApoE peptide ranged between 50% and 60%, according to data already published (Re et al., 2010b, 2011).

Characterization of Aβ samples

Aβ samples were prepared as described above and the aggregation state was assessed by SDS-PAGE/WB and atomic force microscopy (AFM). The results showed that Aβo samples were enriched in small assemblies

(MW < 20 kDa) (Figure 1, A, lane b; Figure 1, B) as compared to monomer-enriched ones (Figure 1, A, lane a) used as a control. AFM observations indicated that Aβo (Figure 1, B) had a spherical morphology and that no fibrils were present in the samples. Size distribution in AFM images appears to be coherent with SDS-PAGE/WB results. Aβf (Figure 1, C), as already reported in literature (Stine et al., 2003), appeared unbranched, bowed, and several micrometers long, with an apparent height of 6 nm.

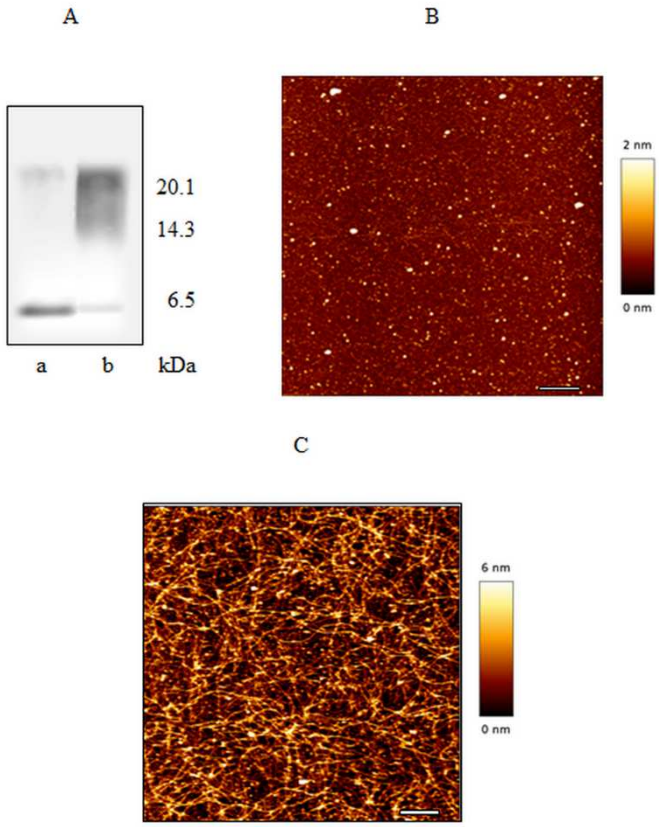

Figure 1. A, $A\beta_{1-42}$ samples were analyzed by SDS-PAGE electrophoresis gel and immunoblotted with anti-$A\beta_{1-42}$ 6E10, followed by ECL detection. Aβ preparation enriched in monomers (lane a) or in small aggregates (lane b) are shown. Molecular weights are indicated. **B**, AFM analysis of Aβ oligomers-enriched preparation. **C**, AFM analysis of Aβ fibrils-enriched preparation. Representative 4 × 4 μm AFM images of Aβ are shown. Bars: 500 nm.

Binding of mApoE-PA-LIP to Aβ

The ability of mApoE-PA-LIP to bind Aβo or Aβf was assessed by ultracentrifugation on a discontinuous sucrose density gradient allowing separating Aβ bound to LIP from the free peptide. Ten fractions were collected from the gradient and analyzed for lipid and peptide content by radiochemical technique and dot-blot assay, respectively. The results (Figure 2) showed that mApoE-PA-LIP were able to bind both Aβo (15.5% of Aβo bound to LIP) and Aβf (23.7% of Aβf bound to LIP), as compared to non-functionalized ones (control LIP). The binding to Aβ induced a change in liposomes density modifying the lipid distribution along the gradient fractions, as already reported (Re et al., 2008).

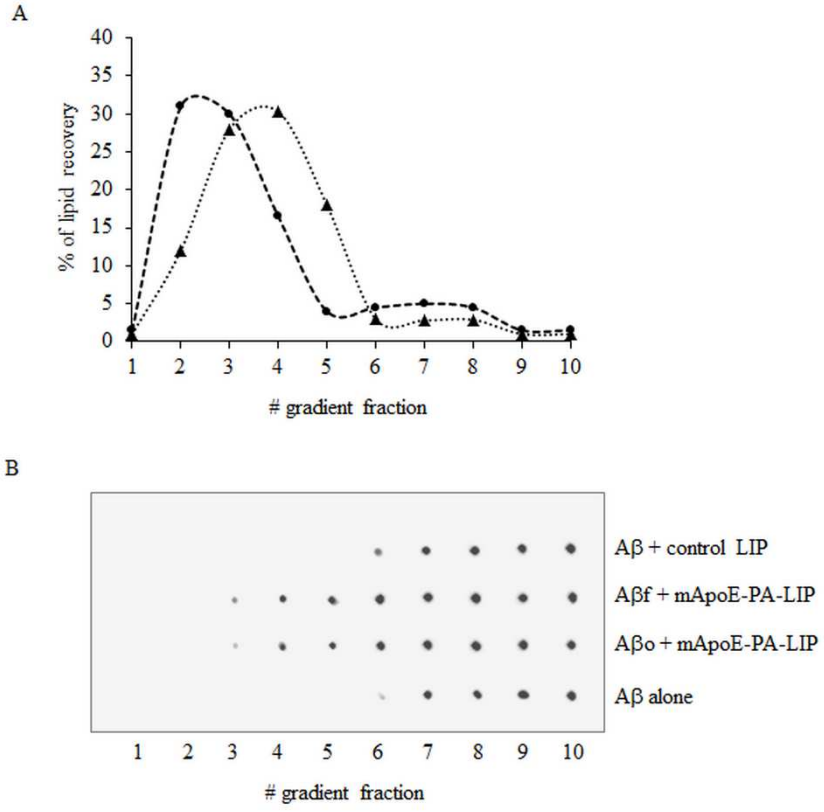

Figure 2. Binding of liposomes to Aβ by ultracentrifugation assay. Mixtures of $A\beta_{1-42}$ (oligomers- or fibrils-enriched samples) with liposomes (containing tritiated sphingomyelin as a tracer) were purified by ultracentrifugation on a discontinuous sucrose density gradient and 10 fractions were collected from the top of the gradient. **A**, Representative distribution of the liposome-associated radioactivity in the gradient fractions, before (dotted line) and after binding with Aβ (punctuated line). **B**, Representative distribution of Aβ in the different fractions of the gradient detected by dot-blot assay using anti-$A\beta_{1-42}$ 6E10, followed by ECL detection. The spot intensity associated with each fraction was determined using the LAS4000 software. 1-5 fractions represent the Aβ bound to liposomes; 6-10 fractions represent the free peptide.

In vitro BBB transwell model

To investigate mApoE-PA-LIP capacity to hunt Aβo by peripheral-sink effect, we set-up an *in vitro* BBB transwell model (Figure 3) composed by a monolayer of polarized endothelial cells seeded on a porous membrane, allowing an apical compartment ('blood' side) physically separated from a basolateral one ('brain' side).

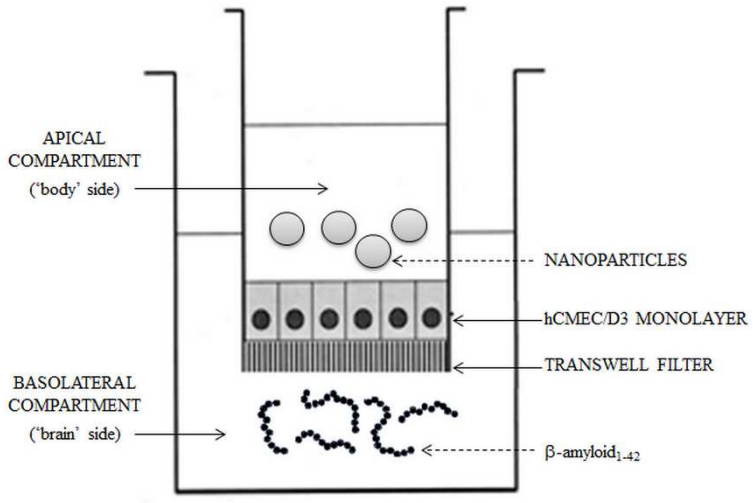

Figure 3. Graphical representation of the transwell system.

Immortalized human brain capillary endothelial cells (hCMEC/D3) were used as representative of human BBB model and the transwell system was characterized by measuring bioelectrical, morphological and functional properties. Trans-electrical endothelial resistance (TEER) was monitored during cell monolayer's formation and was found to gradually increase from 125.19 ± 5.6 $\Omega \cdot cm^2$ (at 12 days *in vitro*, DIV) to 149.90 ± 7.9 $\Omega \cdot cm^2$ (at 15 DIV). At 15 DIV, endothelial permeability (EP) values for [^{3}H]-propranolol and FITC-dextran (MW 4000 Da) were in the order of $2.3 \pm 0.06 \times 10^{-3}$ cm/min and $1.02 \pm 0.04 \times 10^{-6}$ cm/min, respectively, in agreement with the values reported in literature (Omidi et al., 2003). At 15 DIV, 500 nM Aβo were added to the basolateral compartment of the transwell system and the impact of Aβo on cell monolayer properties was checked. The results showed that the basolateral exposure of cell monolayer to Aβo did not significantly affect TEER values (145.72 ± 4.35 $\Omega \cdot cm^2$ after 2 h of incubation; 142.80 ± 1.93 $\Omega \cdot cm^2$ after 4 h of incubation) nor EP of trans- and para-cellular probes (EP [^{3}H]-propranolol = $2.1 \pm 0.05 \times 10^{-3}$ cm/min; EP FITC-dextran = $1.55 \pm 0.03 \times 10^{-6}$ cm/min). Moreover, the treatment did not affect cells viability (> 95% cells viability respect to untreated cells), as assessed by MTT assay. Similar results were also obtained with the addition of 500 nM Aβf in the basolateral compartment (data not shown).

Aβ clearance across the *in vitro* BBB model by mApoE-PA-LIP

Aβ passage across the BBB model (from the basolateral to the apical transwell compartment) was measured by ELISA assay in the presence or absence of LIP in the apical compartment.

The results showed that the amount of Aβo measured in the apical compartment increased over time (Figure 4), with an EP value of 2.62 ± 0.3 × 10^{-5} cm/min, in accordance with the literature (Bachmeier et al., 2010). On the contrary, Aβf efflux from the basolateral compartment was not detectable by ELISA assay.

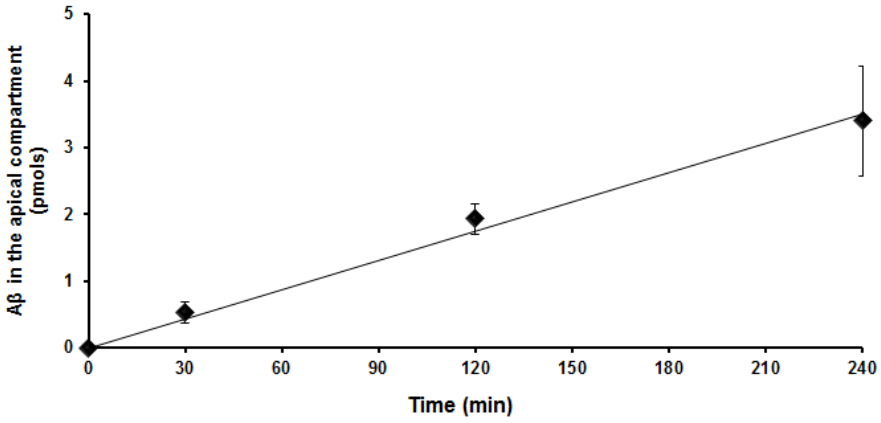

Figure 4. Aβ exchange across the BBB model. hCMEC/D3 cells were cultured on transwell system and 500 nM oligomers-enriched Aβ sample was added to the medium in the basolateral compartment and the amount of peptide in the apical compartment was measured by ELISA assay after different incubation times (0-240 min). The amount (pmol) of Aβ recovered in the apical compartment in the function of time is shown.

When different functionalized LIP (200 nmol total lipids) were present in the apical compartment, the basolateral-to-apical Aβo EP increased, with respect to the EP of Aβo alone (Figure 5, A). In particular, the highest EP value (5-fold increase respect to EP of Aβo alone) was registered when mApoE-PA-LIP were present in the apical compartment. Additionally, the basolateral-to-apical EP of Aβo was mApoE-PA-LIP dose-dependent, increasing with the amount of LIP in the apical compartment (Figure 5, B). On the contrary, when the experiments were carried out with Aβf, after 2 h of incubation with

mApoE-PA-LIP (200 nmol total lipids) in the apical compartment, no peptide was detectable by ELISA assay in the same compartment.

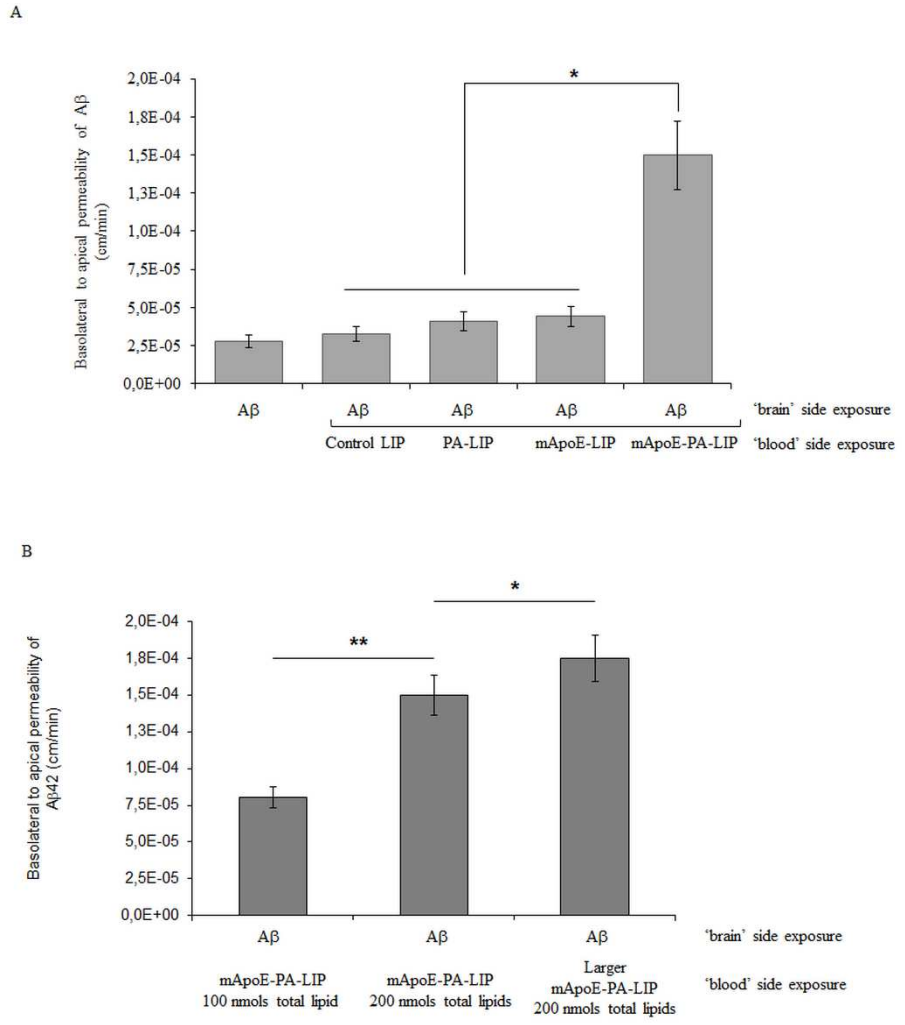

Figure 5. Aβ exchange across the BBB model in presence of liposomes. hCMEC/D3 cells were cultured on transwell system and 500 nM of oligomers-enriched Aβ sample was added to the medium in the basolateral compartment and differently functionalized liposomes were added to PBS in the apical compartment. The amount of Aβ in the apical compartment of the transwell system was measured by ELISA assay after different incubation times (0-240 min). **A**, Endothelial permeability values of Aβ alone or in presence of 200 nmol (total lipids) of different liposomes. **B**, Endothelial permeability values of Aβ in presence of different doses or size of mApoE-PA-LIP. *$p < 0.05$; **$p < 0.01$.

Additional experiments were carried to evaluate the Aβo efflux from the brain side out when different doses of Aβo were added, at the beginning of the experiment, to mApoE-PA-LIP (200 nmol total lipids) present in the apical compartment. The results show that, under these conditions, the EP of the peptide was strongly reduced (Figure 6).

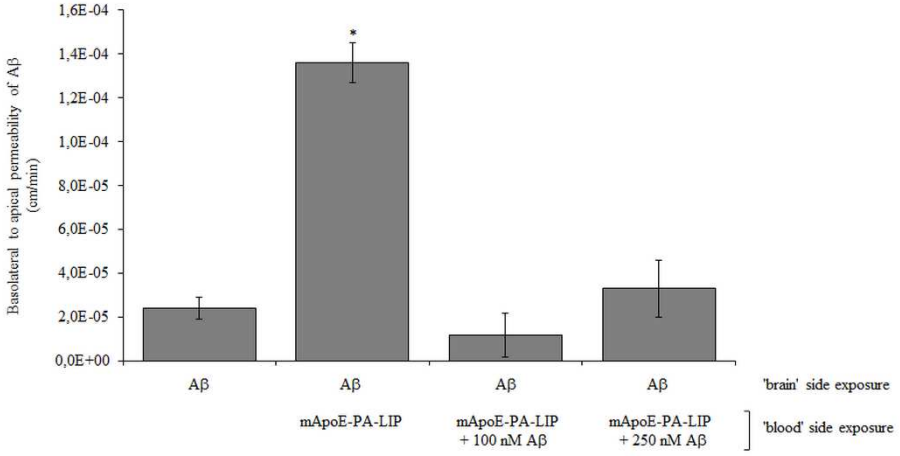

Figure 6. Aβ exchange across the BBB model in presence of liposomes/Aβo in the apical compartment. hCMEC/D3 cells were cultured on transwell system and 500 nM of oligomers-enriched Aβ sample was added to the medium in the basolateral compartment and mApoE-PA-liposomes (200 nmol total lipids) were added to PBS in the apical compartment alone or together with different doses of Aβo. The amount of Aβ in the apical compartment of the transwell system was measured by ELISA assay after different incubation times (0-240 min) and the endothelial permeability values were calculated as described in the Methods section. *$p < 0.05$.

Since the ability of mApoE-PA-LIP to cross the BBB, even if low, has been shown both *in vitro* and *in vivo* (Balducci et al., 2014; Bana et al., 2014), we took into account the possibility that Aβo efflux is affected by the presence of mApoE-PA-LIP in the basolateral compartment. At first, we evaluated the effect of mApoE-PA-LIP of larger size (diameter = 426.2 ± 10 nm; PDI = 0.176; ζ-potential = −16.33 ± 1.41 mV) with respect to the pores size (400 nm diameter) of the transwell filters on

the exchange of Aβo across the BBB. Larger sized radiolabeled [^{3}H]-sphingomyelin-mApoE-PA-LIP were added (200 nmol total lipids) to the apical compartment of the transwell and the radioactivity in the basolateral compartment was measured by liquid scintillation counting in order to verify their inability to reach the basolateral compartment. The results showed that after 2 h of incubation less than 0.1% of radioactivity present in the apical compartment was recovered in the basolateral one, confirming that these larger mApoE-PA-LIP were not able to cross the BBB. Successively, the efflux of Aβo from the basolateral compartment in the presence of these larger LIP in the apical compartment was measured by ELISA assay. The results showed that the Aβo EP was found to increase (+10%) in comparison with EP measured in the presence of smaller size mApoE-PA-LIP.

Secondly, we evaluated the effect of the presence of mApoE-PA-LIP in the basolateral compartment, together with Aβo, on peptide brain efflux. Radiolabeled [^{3}H]-sphingomyelin-mApoE-PA-LIP were added (200 nmol total lipids) to the basolateral compartment of the transwell and the radioactivity in the apical compartment was measured by liquid scintillation counting. The results showed that only 0.043% of the total lipids was recovered in the apical compartment after 2 h of incubation (EP = $3.23 \pm 0.4 \times 10^{-6}$ cm/min), ruling out the possibility that LIP act as conveyor of Aβ.

Aβo clearance across the *in vitro* BBB model by mApoE-PA-LIP in physiological conditions

The effect of mApoE-PA-LIP on Aβo brain efflux was also evaluated under conditions simulating the protein concentration in blood

(Mangas-Sanjuan et al., 2013) and CSF (Pisani et al., 2012), that are the presence of 4% BSA (w/v) in the apical compartment ('blood' side) and 0.015% BSA (w/v) in the basolateral one ('brain' side). The results (Figure 7) showed that also in these experimental conditions the basolateral-to-apical passage of Aβo was higher in the presence of mApoE-PA-LIP (EP = 4.30 ± 0.3 × 10^{-5} cm/min) in the apical compartment than in their absence (EP = 2.89 ± 0.2 × 10^{-5} cm/min).

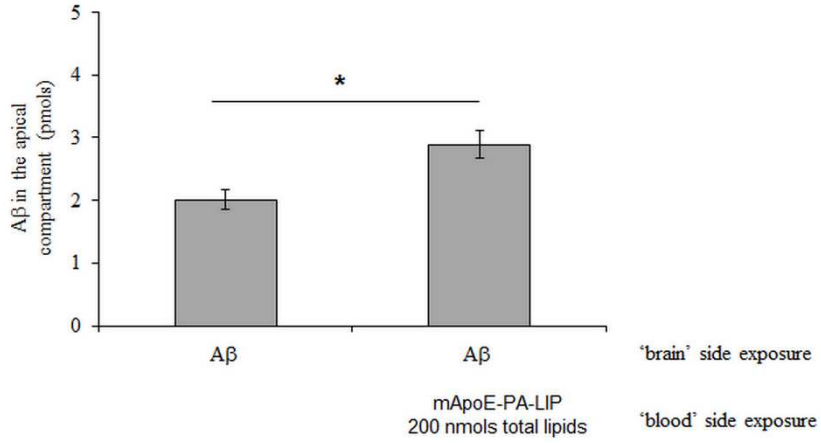

Figure 7. Aβ exchange across the BBB model in *in vivo*-like conditions. hCMEC/D3 cells were seeded on a transwell system and 500 nM oligomers-enriched Aβ sample was added to a solution of PBS/0.015% BSA in the basolateral compartment and 200 nmol (total lipids) of mApoE-PA-LIP were added to PBS/4% BSA in the apical compartment. After 2 h of incubation, the amount (pmol) of Aβ in the apical compartment of the transwell system was determined by ELISA assay. *$p < 0.05$.

Aβo clearance from the endothelial cells by mApoE-PA-LIP

We investigated the ability of mApoE-PA-LIP to draw out the peptide uptaken by hCMEC/D3 cells. For this purpose, the amount of Aβ uptaken by the cells from the basolateral compartment was measured by ELISA in the presence or absence of mApoE-PA-LIP (200 nmol total lipids) in the apical one. The results (Figure 8) showed that the amount of cell-associated Aβ decreased over time and, more

importantly, the decrease was more pronounced in the presence of mApoE-PA-LIP in the apical compartment (Aβ clearance = 0.93 pmol/h) with respect to the peptide alone (Aβ clearance = 0.27 pmol/h). The results were also confirmed in *in vivo*-like conditions (data not shown) using PBS/BSA as described.

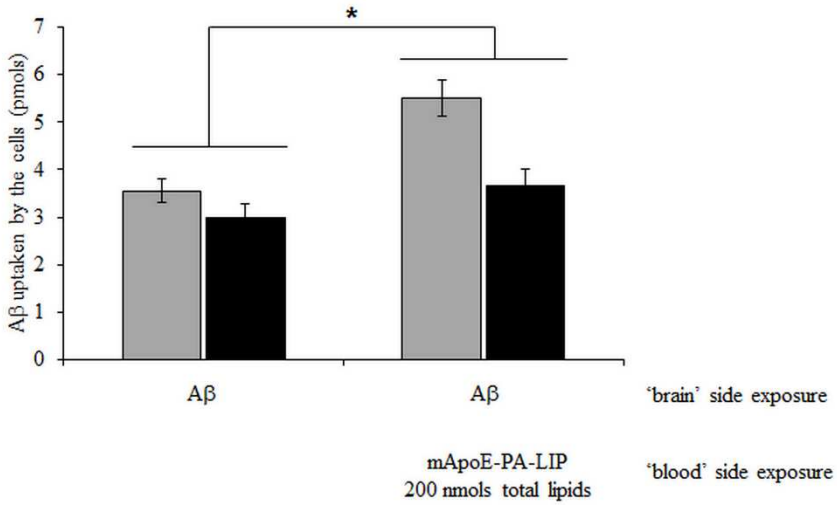

Figure 8. Aβ cellular uptake. hCMEC/D3 cells were cultured on transwell system and 500 nM of oligomers-enriched Aβ sample was added to the medium in the basolateral compartment and 200 nmol (total lipids) of mApoE-PA-LIP was added to the PBS in the apical compartment. After 2 h (gray bars) or after 4 h (black bars) of incubation, cells were collected in a lysis buffer added with protease inhibitors and the Aβ content was measured by ELISA assay to determine the Aβ cellular uptake. *$p < 0.01$.

In vivo proof-of-concept

In order to assess the *in vivo* proof-of-principle, APP/PS1 mice (n = 7 mice/group; 16 months of age) were I.P. treated with 100 μl, 40 mM total lipids of mApoE-PA-LIP or with 100 μl of PBS (3 injections/week for 2 weeks). After treatment, mice were sacrificed and blood and brain were collected. Aβ levels in plasma and brain samples were quantified by ELISA assay. The results showed that plasma Aβ levels (Figure 9, A) of mApoE-PA-LIP treated mice (1.62 ± 0.66 pmol/ml) were

significantly increased ($P < 0.05$, by Student's *t* test) as compared to PBS-treated mice (0.95 ± 0.48 pmol/ml). A decrease, not statistically significant, of brain Aβ levels (Figure 9, B) in mApoE-PA-LIP treated mice (3.53 ± 0.49 nmol/g brain) with respect to PBS-treated mice was detected (3.78 ± 0.54 nmol/g brain). The difference with respect to results previously reported (Bladucci et al., 2014) is probably due to the different treatment schedule used, as well as to the different age of animals.

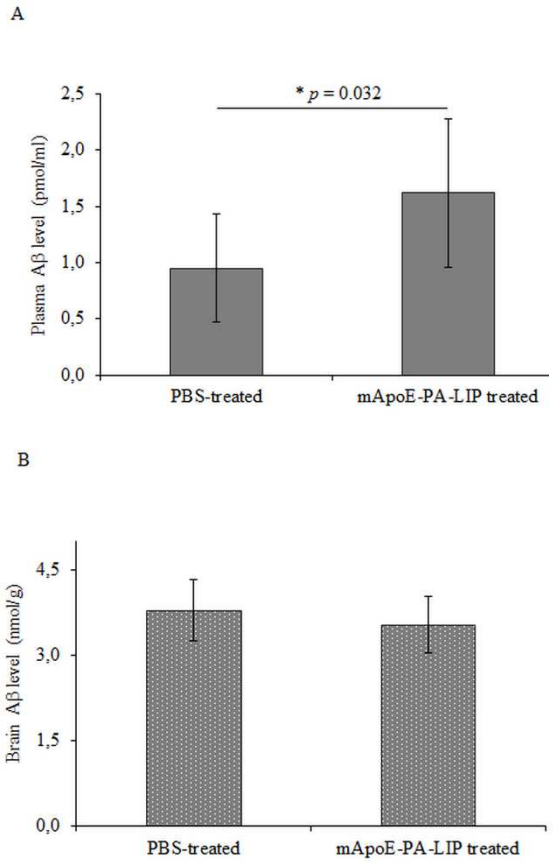

Figure 9. Aβ levels in APP/PS1 mice. APP/PS1 (16 months of age) mice were intraperitoneally (I.P.) injected with mApoE-PA-LIP or with PBS as a control once every other day for two weeks (n = 7 mice/group). At the end of treatment, animals were sacrificed and blood and brain were collected. Aβ levels were quantified by ELISA assays. **A**, Plasma Aβ levels. **B**, Brain Aβ levels. *$p < 0.05$.

3.4 DISCUSSION

The clearance of Aβo, the most culprit Aβ assembly, from the brain and/or from cerebral blood vessels is considered a primary therapeutic target to counteract the onset/progression of AD.

As already suggested by Matzuoka et al. (Matsuoka et al., 2003), a possible strategy to reduce Aβo is to exploit the peripheral-sink effect using Aβ-binding agents. In the present investigation we evaluated the possibility to utilize nanoparticles (Balducci et al., 2014; Bana et al., 2014) for this purpose, using an *in vitro* BBB transwell model and APP/PS1 as animal model of AD.

We chose mApoE-PA-LIP, that were previously showed to strongly reduce brain Aβ burden (Balducci et al., 2014) when administered to AD mice. The further functionalization with mApoE increases the binding affinity of PA-LIP to Aβo, likely due to the existence of a synergic action of PA and mApoE as already suggested (Bana et al., 2014) and, even though it increases PA-LIP ability to reach the brain *in vivo*, this remains anyway low (Balducci et al., 2014; Bana et al., 2014). Therefore, it is possible that mApoE-PA-LIP efficacy *in vivo* is due their ability to withdraw Aβ peptide from the brain to the blood via sink effect.

First of all, we demonstrated the ability of mApoE-PA-LIP to bind either Aβo or Aβf and confirmed their already reported (Bana et al., 2014) ability to bind Aβ.

Sink effect *in vitro* investigations were performed on a BBB model made by hCMEC/D3 monolayer that separates two compartments: the basolateral one, mimicking the brain, and the apical one, mimicking the blood. Aβ samples were added to the basolateral compartment to

resemble AD conditions. This model has been used herein not only as a prototype to study the effect of Aβ-binding particles on Aβ clearance from the brain across the BBB, as already proposed for Aβ-binding agents (Matsuoka et al., 2003), but also as a prototype to test the ability of Aβ-binding nanoparticles to remove Aβ from the endothelial cell monolayer. This makes the model useful as a tool to study potential therapeutic agents not only for AD, but also for CAA.

Initially, we verified the hypothesis by which Aβ is capable of moving across the BBB model establishing an equilibrium between 'brain' and 'blood' side (Zlokovic, 2004). Our results, showed that only small soluble Aβ assemblies, Aβo not Aβf, are spontaneously able to cross the endothelial monolayer. At the best of our knowledge, this is the first experimental demonstration of the assumption that large Aβ assemblies are not able to cross the endothelial cell layer used as a model of BBB.

In order to verify the hypothesized sink effect mechanism of action of mApoE-PA-LIP, Aβo efflux from the brain side was measured in presence of these liposomes in the apical compartment of the transwell system. The results here reported showed that in presence of mApoE-PA-LIP in the apical compartment, the permeability of Aβo from the basolateral compartment was strongly enhanced as compared to the presence of non- or mono-functionalized liposomes. The better performance of mApoE-PA-LIP with respect to other LIP is likely due to their higher binding affinity to Aβo (Bana et al., 2014).

The effect of mApoE-PA-LIP on Aβo brain efflux was also evaluated under conditions simulating the different protein concentration in blood (Mangas-Sanjuan et al., 2013) and CSF (Pisani et al., 2012). Also under these conditions, an increase of Aβ EP was detected, even in a lesser

extent, probably due to the formation of the so called ‘protein corona’, that might influence the mApoE-PA-LIP performance. This issue deserves further investigations.

Successively we took into account the possibility that Aβo efflux is affected by the presence of mApoE-PA-LIP in the basolateral compartment, since their ability to cross the BBB, even low, has been shown both *in vitro* and *in vivo* (Balducci et al., 2014; Bana et al., 2014). Actually, some experiment carried out using liposomes of large size unable to cross the *in vitro* BBB model showed an increased Aβo efflux. This suggests that the passage of mApoE-PA-LIP to the basolateral compartment could limit Aβ efflux, likely due to their binding avidity for Aβ. Further experiments, showing that mApoE-PA-LIP passed to the basolateral compartment were not able to turn back to the apical one, ruled out also the possibility that they may act as Aβo carrier from the brain to the blood.

In order to better clarify the mechanism underlying the increased Aβ efflux exerted by mApoE-PA-LIP in the apical compartment, experiments were carried out in the presence of peptide together with LIP. A strong reduction of peptide efflux from the brain side under these conditions was observed, likely due to the decreased ability of mApoE-PA-LIP, already engaged with Aβo added to the blood side, to withdraw new peptide arriving from the brain side.

All these results support the hypothesis that oligomers spontaneously cross the barrier model and, secondarily, they are caught by the LIP in the apical compartment. Then, the removal of Aβo by LIP is likely shifting the equilibrium of the peptide across the barrier toward the apical compartment, eliciting its efflux.

Taken together, these results suggest that mApoE-PA-LIP could exert the sink effect also *in vivo*. As a proof of this possibility, *in vivo* investigation showed that peripheral administration of mApoE-PA-LIP to transgenic APP/PS1 mice significantly increased plasma Aβ levels.

Finally, we took into account another aspect implicated in the development and/or progression of AD (Sagare et al., 2012): the deposition and aggregation of Aβ within the walls of the cerebral vasculature. Thus, we investigated the ability of mApoE-PA-LIP to draw out the peptide uptaken by hCMEC/D3 cells. The results showed that in the presence of mApoE-PA-LIP the amount of cell-associated Aβ decreased. This might open a parallel scenario concerning the possible use of mApoE-PA-LIP, not only for AD, but also as a potential treatment for CAA.

In conclusion, in the future outlook to design AD therapies, these results highlight the importance of designing multifunctional nanoparticles able to sequester peripheral blood Aβ (without the need to cross the BBB), taking into account the necessity to disaggregate brain Aβ aggregates to make Aβo available. It is also important to point out that also the alterations reported at charge of the BBB in AD (Zlokovic, 2011) should be considered.

Acknowledgement

The research leading to these results has received funding from the European Community's Seventh Framework Program (FP7/2007-2013) under grant agreement no. 212043 (NAD) and by Banca Intesa SanPaolo, grant 2014-2015 (to MS).

References

Attems J, Jellinger KA (2014) The overlap between vascular disease and Alzheimer disease-lessons from pathology. BMC Med 12:206.

Bachmeier C, Mullan M, Paris D (2010) Characterization and use of human brain microvascular endothelial cells to examine β-amyloid exchange in the blood-brain barrier. Cytotechnology 62:519-29.

Balducci C, Mancini S, Minniti S, La Vitola P, Zotti M, Sancini G, Mauri M, Cagnotto A, Colombo L, Fiordaliso F, Grigoli E, Salmona M, Snellman A, Haaparanta-Solin M, Forloni G, Masserini M, Re F (2014) Multifunctional liposomes reduce brain β-amyloid burden and ameliorate memory impairment in Alzheimer's disease mouse models. J Neurosci 34(42):14022-31.

Bana L, Minniti S, Salvati E, Sesana S, Zambelli V, Cagnotto A, Orlando A, Cazzaniga E, Zwart R, Scheper W, Masserini M, Re F (2014) Liposomes bifunctionalized with phosphatidic acid and an ApoE-derived peptide affect Aβ aggregation features and cross the blood-brain-barrier: implications for therapy of Alzheimer disease. Nanomedicine 10(7):1583-90.

Bell RD, Zlokovic BV (2009) Neurovascular mechanisms and blood-brain barrier disorder in Alzheimer disease. Acta Neuropathol 118:103-13.

Boche D, Denham N, Holmes C, Nicoll JA (2010) Neuropathology after active Abeta42 immunotherapy: implications for Alzheimer disease pathogenesis. Acta Neuropathol 120:369-84.

Cecchelli R, Dehouck B, Descamps L, Fenart L, Buée-Scherrer VV, Duhem C, Lundquist S, Rentfel M, Torpier G, Dehouck MP (1999) In vitro model for evaluating drug transport across the blood-brain barrier. Adv Drug Deliv Rev 36:165-78.

Dahlgren KN, Manelli AM, Stine Jr WB, Baker LK, Krafft GA, Ladu MJ (2002) Oligomeric and fibrillar species of amyloid-beta peptides differentially affect neuronal viability. J Biol Chem 277:32046-53.

DeMattos RB, Bales KR, Cummins DJ, Dodart JC, Paul SM, Holtzman DM (2001) Peripheral anti-Aβ antibody alters CNS and plasma Aβ clearance and decreases brain Aβ burden in amouse model of Alzheimer disease. Proc Natl Acad Sci U S A 98:8850-5.

DeMattos RB, Bales KR, Cummins DJ, Paul SM, Holtzman DM (2002) Brain to plasma amyloid-β efflux: a measure of brain amyloid burden in a mouse model of Alzheimer disease. Science 295:2264-7.

Gobbi M, Re F, Canovi M, Beeg M, Gregori M, Sesana S, Sonnino S, Brogioli D, Musicanti C, Gasco P, Salmona M, Masserini ME (2010) Lipid-based nanoparticles with high binding affinity for amyloid-beta1-42 peptide. Biomaterials 31:6519-29.

Gregori M, Cassina V, Brogioli D, Salerno D, De Kimpe L, Scheper W, Masserini M, Mantegazza F (2010) Stability of abeta (1-42) peptide fibrils as consequence of environmental modifications. Eur Biophys J 39:1613-23.

Hardy J, Selkoe DJ (2002) The amyloid hypothesis of Alzheimer disease: progress and problems on the road to therapeutics. Science 297:353-6.

Herrmann N, Chau SA, Kircanski I, Lanctôt KL (2011) Current and emerging drug treatment options for Alzheimer disease: a systematic review. Drugs 71:2031-65.

Mangas-Sanjuan V, González-Álvarez I, González-Álvarez M, Casabó VG, Bermejo M (2013) Innovative in vitro method to predict rate and extent of drug delivery to the brain across the blood-brain barrier. Mol Pharm 10:3822-31.

Matsuoka Y, Saito M, Lafrancois J, Saito M, Gaynor K, Olm V, Wang L, Casey E, Lu Y, Shiratori C, Lemere C, Duff K (2003) Novel therapeutic approach for the treatment of Alzheimer disease by peripheral administration of agents with an affinity to beta-amyloid. Neurosci 23(1):29-33.

Omidi Y, Campbell L, Barar J, Connel D, Akhtar S, Gumbleton M (2003) Evaluation of the immortalised mouse brain capillary endothelial cell line, b.End3, as an in vitro blood–brain barrier model for drug uptake and transport studies. Brain Res 990:95-112.

Ordóñez-Gutiérrez L, Re F, Bereczki E, Ioja E, Gregori M, Andersen AJ, Antón M, Moghimi SM, Pei JJ, Masserini M, Wandosell F (2015) Repeated intraperitoneal injections of liposomes containing phosphatidic acid and cardiolipin reduce amyloid-β levels in APP/PS1 transgenic mice. Nanomedicine 11(2):421-30.

Orlando A, Re F, Sesana S, Rivolta I, Panariti A, Brambilla D, Nicolas J, Couvreur P, Andrieux K, Masserini M, Cazzaniga E (2013) Effect of nanoparticles binding β-amyloid peptide on nitric oxide production by cultured endothelial cells and macrophages. Int J Nanomedicine 8:1335-47.

Pisani V, Stefani A, Pierantozzi M, Natoli S, Stanzione P, Franciotta D, Pisani A (2012) Increased blood-cerebrospinal fluid transfer of albumin in advanced Parkinson's disease. J Neuroinflammation 9:188.

Re F, Sesana S, Barbiroli A, Bonomi F, Cazzaniga E, Lonati E, Bulbarelli A, Masserini M (2008) Prion protein structure is affected by pH-dependent interaction with membranes: a study in a model system. FEBS Lett 582:215-20.

Re F, Airoldi C, Zona C, Masserini M, La Ferla B, Quattrocchi N, Nicotra F (2010a) Beta amyloid aggregation inhibitors: small molecules as candidate drugs for therapy of Alzheimer disease. Curr Med Chem 17:2990-3006.

Re F, Cambianica I, Sesana S, Salvati E, Cagnotto A, Salmona M, Couraud PO, Moghimi SM, Masserini M, Sancini G (2010b) Functionalization with ApoE-derived peptides enhances the interaction with brain capillary endothelial cells of nanoliposomes binding amyloid-beta peptide. J Biotechnol 156:341-6.

Re F, Cambianica I, Zona C, Sesana S, Gregori M, Rigolio R, La Ferla B, Nicotra F, Forloni G, Cagnotto A, Salmona M, Masserini M, Sancini G (2011) Functionalization of liposomes with ApoE-derived peptides at different density affects cellular uptake and drug transport across a blood-brain barrier model. Nanomedicine 7:551-9.

Rensink AA, De Waal RM, Kremer B, Verbeek MM (2003) Pathogenesis of cerebral amyloid angiopathy. Brain Res Rev 43:207-23.

Sagare AP, Bell RD, Zlokovic BV (2012) Neurovascular dysfunction and faulty amyloid β-peptide clearance in Alzheimer disease. Cold Spring Harb Perspect Med 2A011452.

Sehgal N, Gupta A, Valli RK, Joshi SD, Mills JT, Hamel E, Khanna P, Jain SC, Thakur SS, Ravindranath V (2012) Withania somnifera reverses Alzheimer disease pathology by enhancing low-density lipoprotein receptor-related protein in liver. Proc Natl Acad Sci U S A 109:3510-5.

Steinerman JR, Irizarry M, Scarmeas N, Raju S, Brandt J, Albert M, Blacker D, Hyman B, Stern Y (2008) Distinct pools of beta-amyloid in Alzheimer disease-affected brain: a clinicopathologic study. Arch Neurol 65:906-12.

Stine Jr WB, Dahlgren KN, Krafft GA, Ladu MJ (2003) In vitro characterization of conditions for amyloid-beta peptide oligomerization and fibrillogenesis. J Biol Chem 278:11612-22.

Tai LM, Reddy PS, Lopez-Ramirez MA, Davies HA, Male DK, Loughlin AJ, Romero IA (2009) Polarized P-glycoprotein expression by the immortalised human brain endothelial cell line, Hcmec/D3, restricts apical-to-basolateral permeability to rhodamine 123. Brain Res 1292:14-24.

Vu K, Weksler B, Romero I, Couraud PO, Gelli A (2009) Immortalized human brain endothelial cell line hCMEC/D3 as a model of the blood-brain barrier facilitates in vitro studies of central nervous system infection by Cryptococcus neoformans. Eukaryot Cell 8:1803-7.

Zlokovic BV (2004) Clearing amyloid through the blood-brain barrier. J Neurochem 89:807-11.

Zlokovic BV (2011) Neurovascular pathways to neurodegeneration in Alzheimer disease and other disorders. Nat Rev Neurosci 12:723-38.

CHAPTER 4

Hindering Alzheimer-like phenotype progression in APP/PS1 mice by multifunctional liposomes

Simona Mancini**,** Claudia Balducci, Edoardo Micotti, Daniele Tolomeo, Gianluigi Forloni, Massimo Masserini, Francesca Re

Submitted

Abstract

The contribution of Amyloid-β (Aβ) peptide to Alzheimer's disease (AD) pathogenesis is widely accepted, therefore Aβ-targeted treatment strategies can be theoretically possible, if they initiated before irreversible damage is present or after pathological cascades have been initiated. We previously developed liposomes multifunctionalized for crossing the blood-brain barrier and targeting Aβ that showed therapeutic efficacy on AD-like transgenic mice displaying pathology signatures. Herein, we further investigated on APP/PS1 mice the ability of a long-term treatment started at young, pre-symptomatic age, to prevent or slow down the onset of typical AD hallmarks.

Liposomes, administered weekly to 5-month-old APP/PS1 mice for 7 months, prevented the onset of the recognition memory impairment, slowed down the deposition of brain Aβ. At a structural brain level, both ventricle enlargement and entorhinal cortex thickness reduction were prevented.

Strikingly, all these multi-level impressive effects were maintained 3 months after treatment discontinuation, when an increase in the Aβ-degrading enzymes in brain was observed together with a reduction of the amyloid precursor protein level. Moreover, peripheral 'sink' effect also contributed to maintain low Aβ brain content, as suggested by the increase of Aβ levels in the liver. Worth of note, the 7-month treatment seems not to be toxic for all the organs analyzed, in particular for brain as suggested by the lower brain TNF-α level and higher level of SOD activity detected in treated mice.

Together, these findings promote multifunctional liposomes as a well-tolerated nanomedicine-based approach, potentially suitable for

delaying relevant features of AD seemingly fostering persistent neuroprotective effects.

4.1 INTRODUCTION

Alzheimer disease (AD) is the most common form of dementia, accounting for 60 to 80 percent of dementia cases (http://www.alz.org). Although the cause and progression of AD are still not well understood, the central role of Amyloid-β (Aβ) peptide in AD pathogenesis is widely accepted, even if a variety of additional factors, either dependent or independent from Aβ, appears to contribute to cognitive decline and progression of dementia (Palop and Mucke, 2010; Selkoe, 2012). In fact, Aβ is thought to directly damage the brain, disrupting the synaptic functionality, which strongly correlates with the cognitive deficits characteristic of the pathology. Given its pivotal role, many Aβ-centric strategies have been attempted and are still in progress. Aβ accumulation and deposition in the brain is a very early pathological process in AD and probably begins ~10–20 years prior to the onset of clinically detectable symptoms (Holtzman et al., 2011). This early stage is considered the most promising time frame to start with disease-modifying therapies (Sperling et al., 2013).

Nanomedicine has been suggested as a biotechnology potentially suitable for the treatment of Central Nervous System (CNS) diseases, exploiting the design of nanoparticles multifunctionalized toward specific targets (Re et al., 2012). Within this frame, we previously designed liposomes for AD treatment, dually functionalized with a synthetic peptide (mApoE) containing the receptor-binding domain of apolipoprotein-E, for blood-brain barrier targeting and crossing, and with phosphatidic acid (PA), for Aβ binding (Bana et al., 2014). Acute treatment with these liposomes (mApoE-PA-LIP) have already shown

the ability to decrease brain Aβ burden and ameliorate the memory deficit in symptomatic APP/PS1 AD mice (Balducci et al., 2014).
Herein, we further investigated on APP/PS1 mice the ability of a long-term treatment with liposomes, started at young, pre-symptomatic age, to prevent or slow down the onset of typical AD hallmarks, namely brain Aβ accumulation and memory impairment.

4.2 MATERIALS AND METHODS

Liposomes preparation and characterization

Liposomes composed of sphingomyelin and cholesterol (1:1 molar ratio), mixed with 2,5 mol% of mal-PEG-PE and with 5 mol% of phosphatidic acid (PA), for Aβ binding, were prepared by extrusion procedure using polycarbonate filters (100 nm pore size diameter) (Re et al., 2010; Bana et al., 2014). They were then functionalized with 1,25 mol% of a modified peptide (mApoE) derived from the receptor-binding domain of human apolipoprotein E, for blood-brain barrier targeting (Re et al., 2010; Re et al., 2011), through covalent coupling with mal-PEG-PE, resulting in mApoE-PA-LIP. mApoE-PA-LIP were freshly prepared on the same day of each injection.

Animals

Twenty APP/PS1 5-month-old Tg male mice (B6C3-Tg(APPswe, PSEN1dE9)85Dbo/Mmjax mice; The Jackson Laboratory), mean weight of 28-30g, and 20 non-Tg (WT) age-matched littermates were used. Mice were all drug and behavioral test naïve and no environmental enrichment was used because it notably improves AD pathology in mouse models of AD (Lazarov et al., 2005; Valero et al., 2011). All procedures involving animals and their care were conducted according to European Union (EEC Council Directive 86/609, OJ L 358,1; December 12, 1987) and Italian (D.L. n.116, G.U., Suppl. 40, February 18, 1992) laws and policies, and in accordance with the United States Department of Agriculture Animal Welfare Act and the National Institutes of Health (Bethesda, MA, USA) policy on Humane Care and Use of Laboratory Animals. They were reviewed and approved by the

Mario Negri Institute Animal Care and Use Committee that includes ad hoc members for ethical issues (1/04-D).

Animal treatment

All animals (Tg or WT) were intraperitoneally injected with mApoE–PA–LIP (100 μl, 73.5 mg of total lipids/kg) or with vehicle (100 μl PBS) once a week for 7 months. Therefore, two experimental groups were treated with mApoE–PA–LIP (Tg and WT mice, n = 10 for each) and two control groups were treated with PBS (Tg and WT, n = 10 for each). The weight of the animals was recorded before each treatment. To minimize the effect of subjective bias, the treatment was performed in blind. Mice were treated always at the same time of the day (9:00–10:00 A.M.) in a specific room inside the animal facility, following a randomized order based on the draw of the animal identification code. At the end of treatment, five animals per group were sacrificed to assess treatment effects. The rest of the animals was kept for other three months without any kind of treatment and then sacrificed to analyze the duration of the effects after treatment discontinuation.

Novel Object Recognition test (NORT)

NORT is a memory test that relies on spontaneous animal behavior without the need for stressful elements such as food or water deprivation or foot-shock (Antunes and Biala, 2012). In the NORT, mice are introduced into an arena containing two identical objects that they can explore freely. Twenty-four hours later, they are reintroduced into the arena, with two objects one of which had already been presented (familiar) and the other new and completely different (novel).

The day before the beginning of the treatment, after 4 months from its start and at the end of treatment, mice were tested in an open-square grey arena (40 × 40 cm), 30 cm high, with the floor divided into twenty-five squares by black lines, placed in a specific room dedicated to behavioral analysis and separate from the operator's room. The following objects were used: a black plastic cylinder (4 × 5 cm), a glass vial with a white cap (3 × 6 cm), and a metal cube (3 × 5 cm). The task started with a habituation trial during which the animals were placed in the empty arena for 5 min and their movements recorded as the number of line-crossings, which provide an indication of both the WT and Tg mouse motor activity. The next day, mice were again placed in the same arena containing two identical objects (familiarization phase). Exploration was recorded in a 10-min trial by an investigator blinded to genotype and treatment. Sniffing, touching, and stretching the head toward the object at a distance of not more than 2 cm were scored as object investigation. Twenty-four hours later (test phase), mice were again placed in the arena containing two objects: one of the objects presented during the familiarization phase (familiar object), and a new, different one (novel object), and the time spent exploring the two objects was recorded for 10 min. Mice were tested following a predefined scheme (five mice for each treatment group and the remaining mice by following the same scheme) so to precisely maintain the 24 h re-test for each mouse. Results were expressed as the percentage of time spent investigating objects in the 10 min or as a discrimination index (DI), i.e. (seconds spent on novel – seconds spent on familiar)/(total time spent on objects). Animals with no memory

impairment spent longer investigating the novel object, giving a higher DI.

MRI analysis

Animals were anesthetized with isoflurane in a mixture of O2 (30%) and N2O (70%). Body temperature was maintained at ~37°C by a warm water circulated heating cradle. Imaging was performed on a 7 T small bore animal Scanner (Bruker Biospec, Ettlingen, Germany). Two actively decoupled radio frequency coils were used: a volume coil of 7.2 cm diameter used as the transmitter and a surface coil as the receiver. A 3D RARE T2-weighted sequence was performed to assess anatomical changes. The morphological images were obtained with a voxel size of 117x147x147µm (matrix = 256x102x102 and Field of View = 3x1.5x1.5 cm); TR = 2500 ms, effective TE = 50 ms and a RARE factor of 16, for 1 average.

The volume measurements of structural MRI images were obtained using Java-based custom made software. ROIs were manually chosen by a trained expert following the Paxinos' atlas (Franklin and Paxinos, 1997). Total intracranial volume, whole brain, cortex, hippocampus, striatum and the ventricular system were measured. Data from each animal were obtained by the integration of averaged ROI area for slice thickness.

To measure thickness of the entorhinal cortex, nine coronal slices were selected at the level between Bregma -2.75 mm and Bregma -3.80 mm based on mouse brain atlases (Franklin and Paxinos, 1997), and the thickness was measured below the rhinal fissure (Yang et al., 2010). We visually inspected all the coronal acquisitions to choose a reference

image. We then registered all the other images to the reference one in order to avoid bias due to bad head positioning during the acquisition. For the image registration we used a 3D to 3D rigid body registration with 6 degrees of freedom (FLIRT) (Jenkinson and Smith, 2001; Jenkinson et al., 2002). The thickness of the entorhinal cortex was then measured six times (three for left and three for right) by a trained expert and the values were averaged to get the final values.

Blood and tissue collection

Animals were deeply anesthetized with an overdose of ketamine/medetomidine (1.5 and 1.0 mg/kg, respectively). The blood was collected from the heart for plasma separation and used for both Aβ level quantification and serum chemistry profile test. The latter test was performed using an automatic biochemistry analyzer (Cobas 8000, Roche Diagnostics GmbH, Mannheim, Germany). Afterward, liver, spleen, and brain were dissected, macroscopically analyzed and weighed. One brain hemisphere was fixed and processed for immunohistochemistry; the other hemisphere, liver, spleen and plasma were snap frozen in dry ice and stored at -80°C (Cramer et al., 2012) until Aβ, APP, proteolytic degrading enzyme activity and inflammatory and oxidative stress marker dosage.

Brain immunohistochemistry

APP/PS1 plaque deposition was examined using the 6E10 monoclonal anti-Aβ antibody (Covance). Brain coronal cryostat sections (30 μm; three slices per mouse) were incubated for 1 h at room temperature with blocking solution [6E10: 10% normal goat serum (NGS)] and then

overnight at 4°C with the primary antibody (6E10, 1:500). After incubation with the anti-mouse biotinylated secondary antibody (1:200; 1 h at room temperature; Vector Laboratories) immunostaining was developed using the avidin-biotin kit (Vector Laboratories) and diaminobenzidine (Sigma). Tissue analysis and image acquisition were done using an Olympus image analyzer and the Cell-R software. Plaques were quantified by an operator blind to genotype and treatment using Fiji software, through the application of a homemade macro.

Aβ quantification in animal organs

Mouse brains were treated as described previously (Steinerman et al., 2008) with some modifications. Mouse brain hemispheres were homogenized in a Tris buffer containing 50mM Tris-HCl, pH 7.4, 150mM NaCl, 50mM EDTA, 1% Triton X-100, and 2% protease inhibitor. After centrifugation (15.000 rpm, 21.000 × g, 4°C for 25 min), the supernatant was retained as the Triton-soluble fraction (soluble Aβ). The pellet was homogenized a second time in the presence of 70% formic acid (FA) (10% v/w) and ultracentrifuged (55.000 rpm, 100,000 × g, 4°C, 1 h), and the resulting FA-extracted supernatant was neutralized with 1 M Tris buffer, pH 11, representing the FA-extracted insoluble fraction (insoluble Aβ). Levels of $A\beta_{1–40}$ and $A\beta_{1–42}$ in each fraction were quantified by sandwich ELISA (ELISA kit; IBL). Liver and spleen were homogenized as the brain and their Aβ levels were quantified by ELISA in the Triton-soluble fraction.

Levels of plasma $A\beta_{1–40}$ and $A\beta_{1–42}$ were quantified by ELISA (Wako Chemicals). Each sample was assayed in triplicate.

Active proteolytic degrading enzyme, inflammatory and oxidative stress marker dosage in mouse organs

The Triton-soluble fraction, obtained from brain, liver and spleen as described in the previous section, was also used to quantify the amount of active Neprilysin (NEP) and Insuline Degrading Enzyme (IDE) (SensoLyte Activity Assay Kit; AnaSpec, Inc.), IL-1β and TNF-α level (Quantikine ELISA kit; R&D Systems), the amount of MDA adducts (OxiSelect Competitive ELISA kit; Cell Biolabs, Inc.) and SOD activity (OxiSelect Activity Assay; Cell Biolabs, Inc). For active NEP and IDE quantification, the non-interference of the analyzed samples with the activity of the enzymes was verify.

Brain APP, IDE, LRP-1 and RAGE levels analysis

Aliquots of the Triton-soluble factions obtained from brains were run on a precast NuPAGE 4-12% bis-Tris gel (Invitrogen corporation, Milano, Italy), transferred to a nitrocellulose membrane, probed with anti-APP antibody (1:1000 dilution, Chemicon), anti-IDE antibody (1:1000 dilution, Invitrogen), anti-LRP-1 antibody (1:1000 dilution, Thermo Fisher) or anti-RAGE antibody (1:1000 dilution, Thermo Fisher) and visualized with enhanced chemiluminescence (ECL) by ImageQuant LAS4000. The protein load was controlled by β-actin immunoblotting using β-actin loading control antibody (1:2000 dilution, Invitrogen). The content of APP, IDE, LRP-1 or RAGE were quantified by intensity of the chemiluminescent bands using ImageJ Software.

Statistical analysis

Data were expressed as mean ± SEM. For western blot, Aβ dosage and plaque quantification, data were analyzed by Student's *t* test. For NORT, MRI analysis, proteolytic degrading enzyme activity and inflammatory and oxidative stress marker dosage, data were analyzed by a two-way ANOVA. In the presence of a significant interaction between the factors Tg × treatment, the Tukey's *post hoc* test was applied. $p< 0.05$ was considered significant.

4.3 RESULTS

mApoE-PA-LIP treatment prevented memory impairment in APP/PS1 mice

5 month-old APP/PS1 Tg mice and age-matched WT littermates were intraperitoneally (IP) treated with mApoE-PA-LIP (treated mice; Tg n = 10, WT n = 10) or PBS (untreated mice; Tg n = 10, WT n = 10) once a week for 7 months and periodically submitted to the Novel Object Recognition memory test (NORT). The day before the first injection (Figure 1A and B), as assessed by NORT, 5 month-old WT were indistinguishable from Tg mice in their memory performance, as expected at this age (Lee et al., 1997). At 9 months, which is after 4 months treatment, untreated Tg mice displayed memory impairment with respect to WT mice (Figure 1A and C). On the contrary, Tg mice receiving mApoE-PA-LIP showed a significant memory preservation, since their performance was comparable to that of WT. The same pattern was observable at the end of treatment, after 7 months (Figure 1A and D). As a further control, the treatment of WT mice with mApoE-PA-LIP exerted no negative effect on their memory at any age.

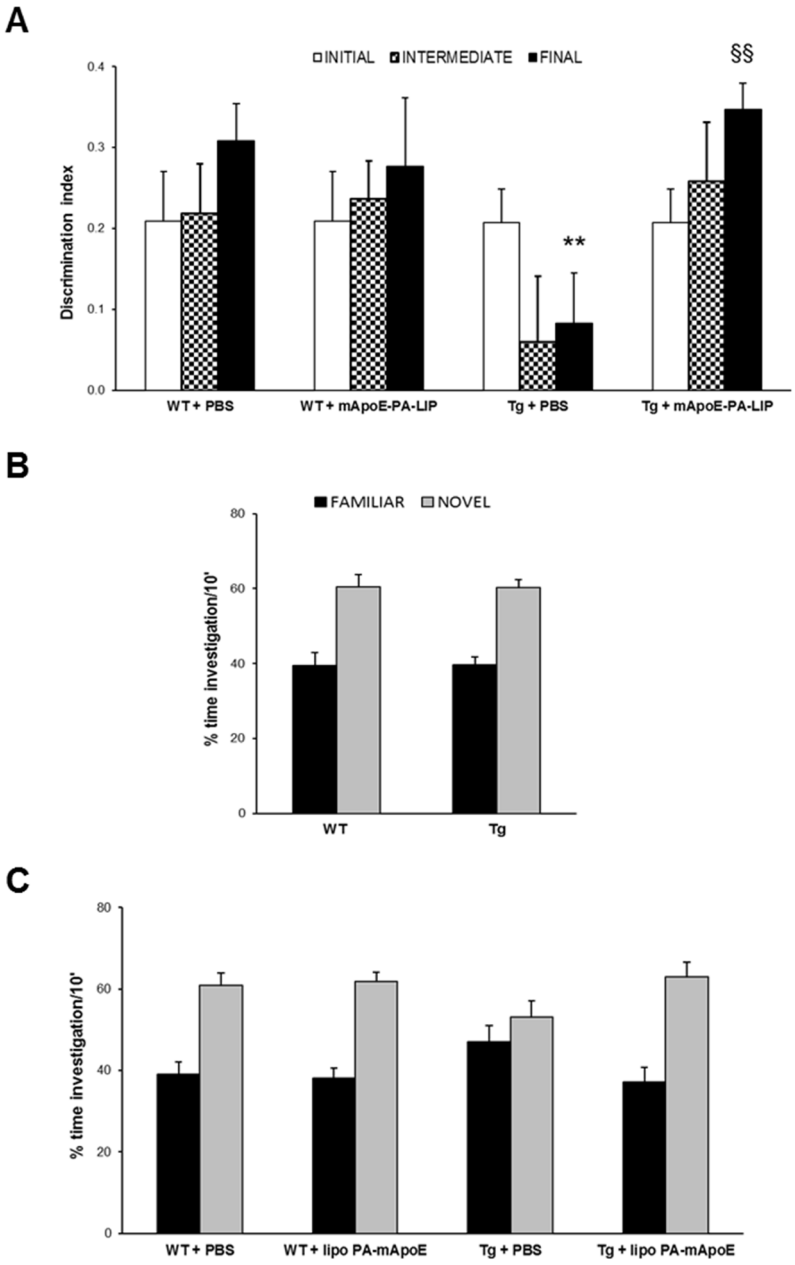
A
INITIAL
INTERMEDIATE
FINAL
§§
**
Discrimination index
0.4
0.3
0.2
0.1
0.0
WT + PBS
WT + mApoE-PA-LIP
Tg + PBS
Tg + mApoE-PA-LIP
B
FAMILIAR
NOVEL
% time investigation/10'
80
60
40
20
0
WT
Tg
C
% time investigation/10'
80
60
40
20
0
WT + PBS
WT + lipo PA-mApoE
Tg + PBS
Tg + lipo PA-mApoE

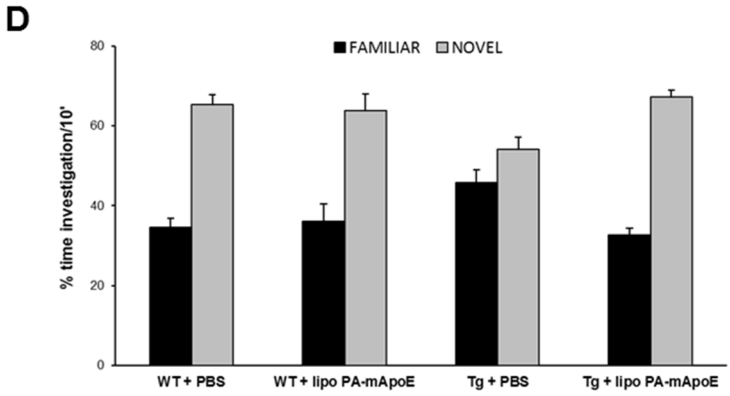

Figure 1. Effect of mApoE-PA-LIP treatment on long-term recognition memory. 5 month-old APP/PS1 Tg or WT mice were intraperitoneally treated with mApoE-PA-LIP (100 µl, 73.5 mg of total lipids/kg) or vehicle (100 µl PBS) once a week for 7 months and periodically submitted to NORT. **A**, Histograms show the discrimination index of the experimental groups the day before the first injection (white bars), after 4 months from beginning the treatment (checked bars) and at its end (black bars). **B**, Histograms show the time percentage of investigation of the familiar (black bars) and novel (grey bars) objects of the experimental groups tested the day before the first injection. **C**, Histograms show the time percentage of investigation of the familiar (black bars) and novel (grey bars) objects of the experimental groups tested after 4 months from the beginning of the treatment. **D**, Histograms show the time percentage of investigation of the familiar (black bars) and novel (grey bars) objects of the experimental groups tested at the end of treatment. Data are presented as mean ± SEM. One-way ANOVA, Tukey's *post hoc* test, $^{**}p < 0.01$ untreated Tg versus untreated WT mice; §§$p < 0.01$ treated versus untreated Tg mice; n = 10/group.

mApoE-PA-LIP treatment prevented the occurrence of AD cerebral anatomical abnormalities

At the end of treatment, a magnetic resonance imaging (MRI) analysis was carried out on treated and untreated mice to investigate eventual changes in volume or thickness of different brain areas. Representative MRI brain images of controls and treated and untreated Tg mice are reported in Figure 2.

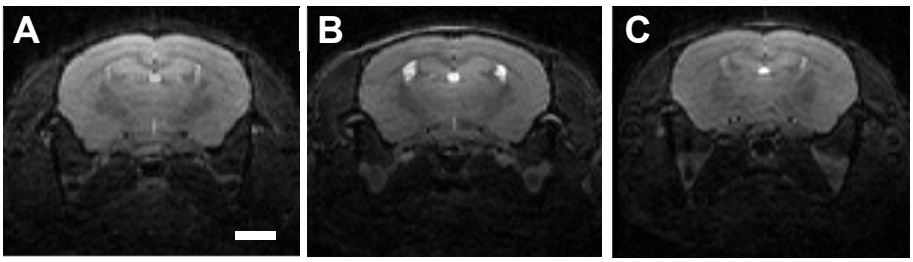

Figure 2. A, Representative MRI brain image of a control animal. **B**, Representative MRI brain image of an untreated Tg mice. **C**, Representative MRI brain image of a treated Tg mice. Scale bar, 2 mm.

The ventricle volume of treated Tg mice was smaller (-22%), while entorhinal cortex thickness was higher (+10%) than untreated Tg mice and were comparable to WT (Figure 3A and B).

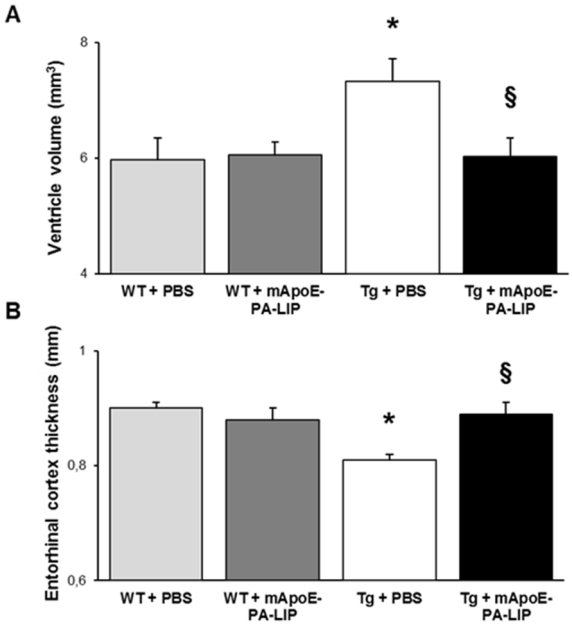

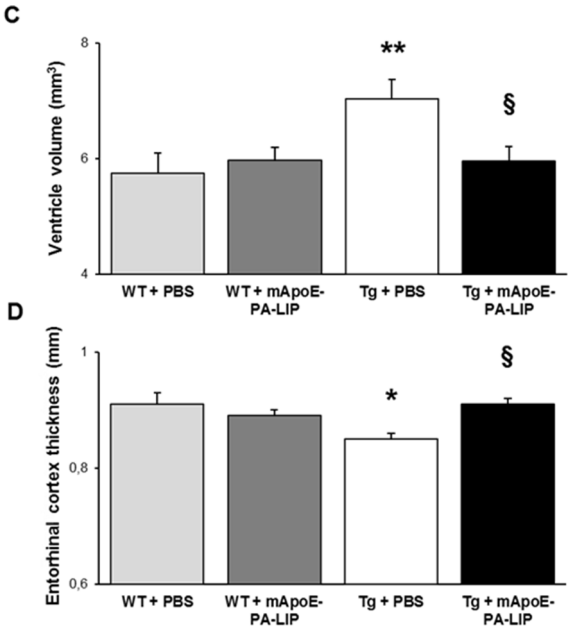

Figure 3. Effect of mApoE-PA-LIP treatment on brain structures. At the end of treatment, a MRI analysis was performed (**A**, **B**). After 3 months from treatment interruption, the MRI analysis was repeated on remaining animals and the same brain structures quantified in volume or thickness (**C**, **D**). **A** and **C**, Histograms show the change of ventricular volume in the brain of untreated or treated Tg mice with respect to untreated WT mice. **B** and **D**, Histograms show the change of entorhinal cortex thickness in untreated or treated Tg mice with respect to untreated WT mice. Data are presented as mean ± SEM. One-way ANOVA, Tukey's *post hoc* test, **p* < 0.05, ***p* < 0.01 untreated Tg *versus* untreated WT mice; § p < 0.05 treated *versus* untreated Tg mice; n = 10/group in **A** and **B**; n = 5/group in **C** and **D**.

The treatment did not exert any effect on whole brain, hippocampus, cortex or striatal volumes (data not shown).

mApoE-PA-LIP treatment slows down brain Aβ accumulation in APP/PS1 mice

At the end of treatment animals (n = 5 per group) were sacrificed and brains collected and analyzed to quantify plaque load and to measure Aβ levels. As shown in Figure 4A, untreated Tg mice exhibited

important plaque load, as expected at 12 months of age (Balducci and Forloni, 2011). Notably, the brains of mApoE-PA-LIP-treated Tg mice displayed a lower content of plaques, both in area (-29%) and in number (-31%) in both the cortex and the hippocampus (Figure 4B and C).

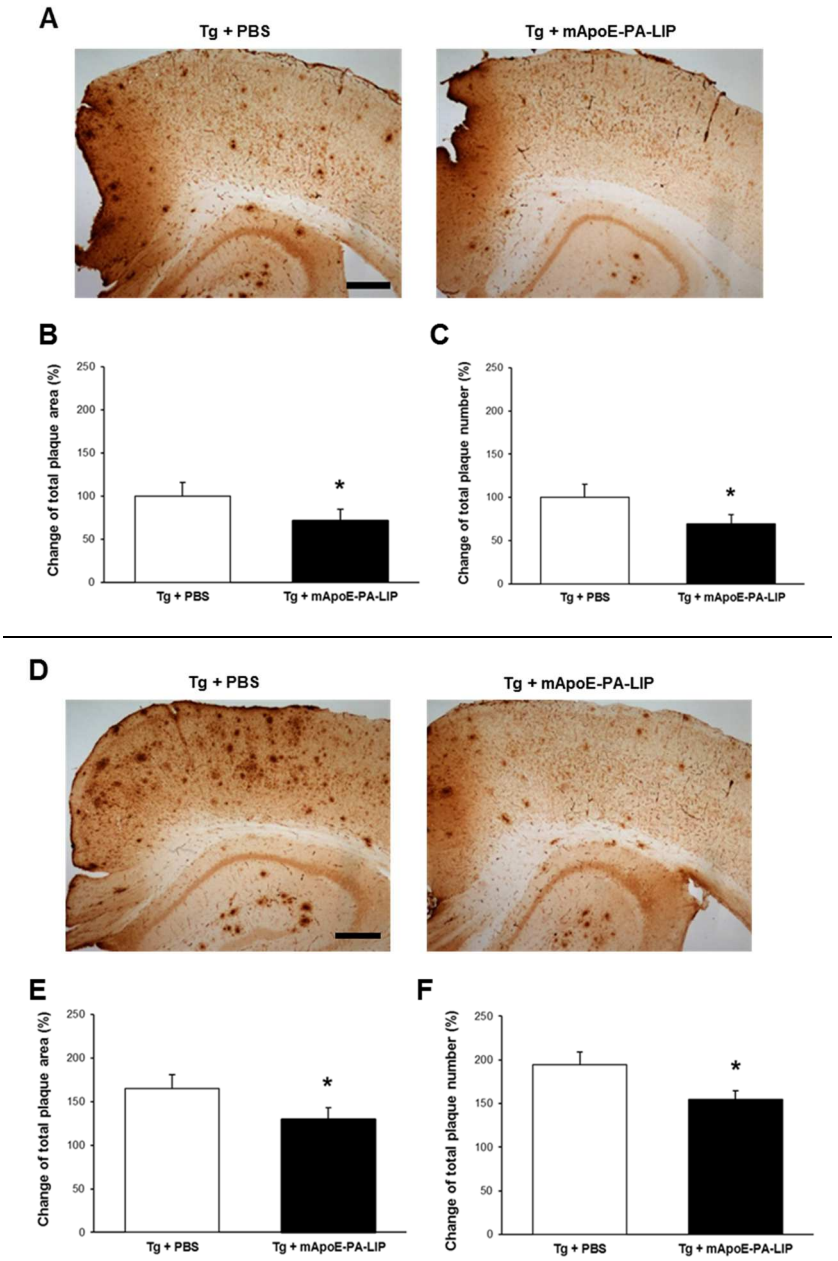

Figure 4. Effect of mApoE-PA-LIP treatment on Aβ plaque deposition. At the end of treatment, half of the animals was sacrificed and half brain was immunostained with the anti-Aβ 6E10 monoclonal antibody for plaque quantification (**A**, **B**, **C**). After three months from treatment interruption, the rest of the animals was sacrificed and their brain processed for plaque quantification (**D**, **E**, **F**). **A** and **D**, Representative brain sections of untreated and treated Tg mice, stained with the anti-Aβ 6E10 antibody, are shown. Scale bar = 250 μm. **B** and **E**, Histograms report the percentage difference in the total plaque area in treated and untreated Tg mice with respect to untreated Tg mice at the end of treatment. **C** and **F**, Histograms report the percentage difference in the number of plaques in treated and untreated Tg mice with respect to untreated Tg mice at the end of treatment. Data are presented as mean ± SEM. Student's *t* test, **p* < 0.05; n = 5/group.

In parallel, the content of insoluble Aβ species in the brain of treated mice was lower than in untreated ones (Figure 5A). In contrast, no difference was detected in soluble Aβ species (Figure 5B).

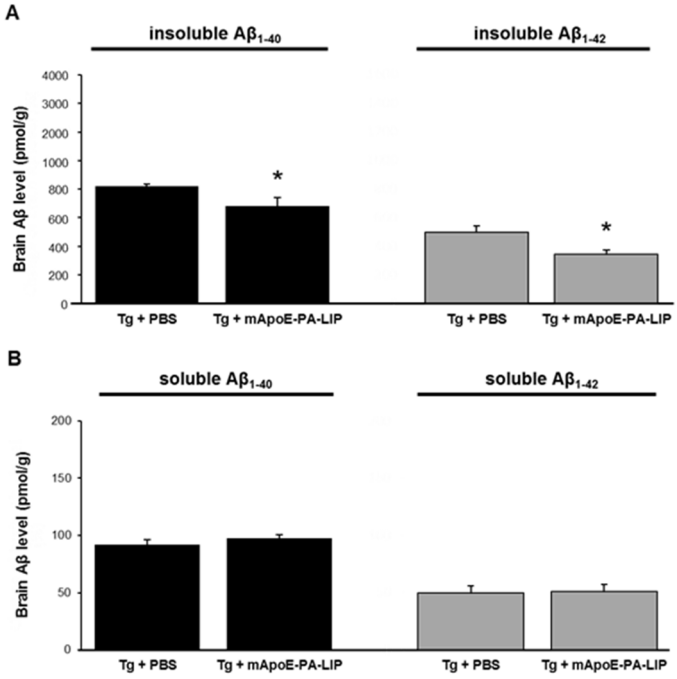

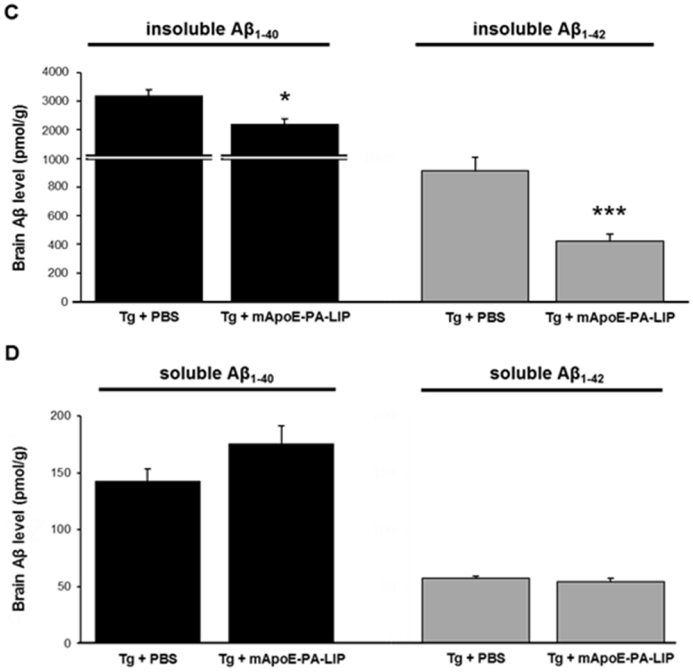

Figure 5. Effect of mApoE-PA-LIP treatment on brain Aβ burden. At the end of treatment, half of the animals was sacrificed, half brain was homogenized and insoluble and soluble $A\beta_{1\text{-}40}$ and $A\beta_{1\text{-}42}$ amounts were measured by ELISA (**A**, **B**). After three months from treatment interruption, the rest of the animals was sacrificed and their brain analyzed for Aβ content (**C**, **D**). **A** and **C**, Histograms display the level of insoluble Aβ1-40 and Aβ1-42 levels in the brain of treated and untreated Tg mice. **B** and **D**, Histograms display the level of soluble Aβ1-40 and Aβ1-42 levels in the brain of treated and untreated Tg mice. Data are presented as mean ± SEM. Student's *t* test, $*p < 0.05$, $***p < 0.001$; n = 5/group.

mApoE-PA-LIP treatment increased peripheral Aβ levels

At the end of treatment, we assessed the amount of brain Neprilysin (NEP) and Insulin degrading enzyme (IDE) (Nalivaeva et al., 2012). As shown in Figure 6A and B, the amount of active NEP and IDE in untreated Tg mice was lower (-60% and -35% respectively) than in WT, and was not affected by the treatment.

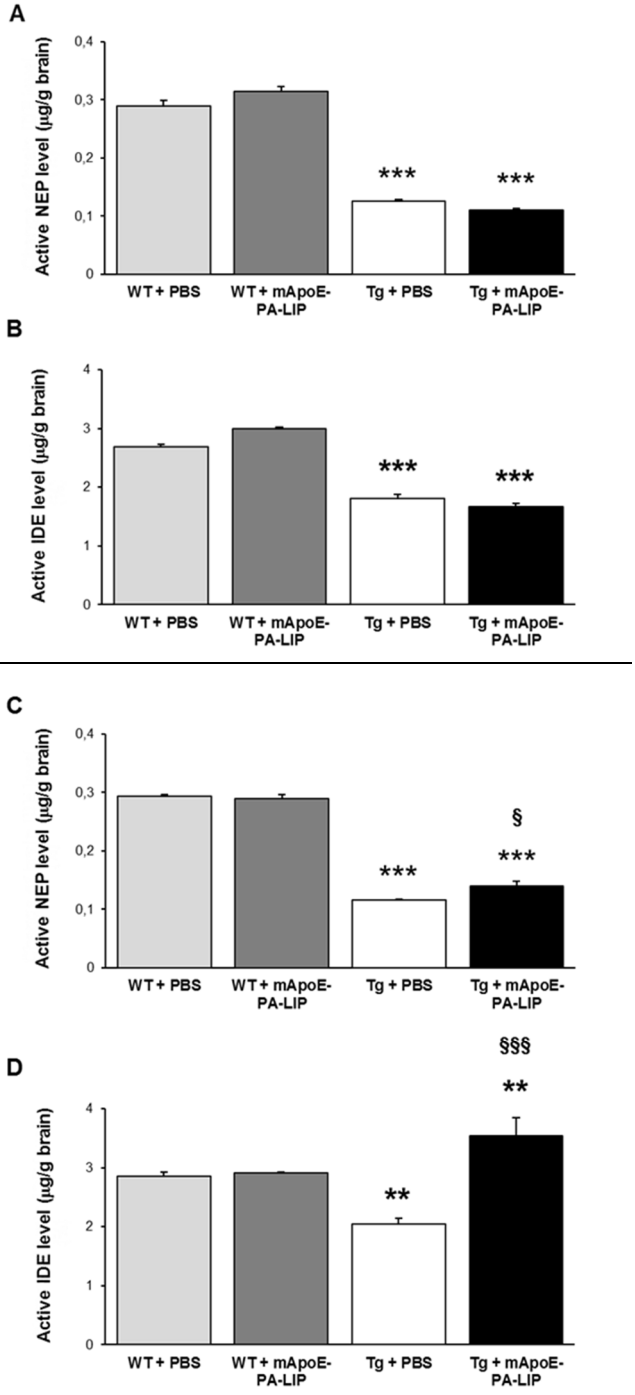

Figure 6. Effect of mApoE-PA-LIP treatment on the amount of active proteolytic degrading enzymes. At the end of treatment, half of the animals was sacrificed, half

brain was homogenized and the amount of active Neprilysin (NEP) and Insuline degrading enzyme (IDE) measured (**A**, **B**). After three months from treatment interruption, the rest of the animals was sacrificed and their brain analyzed for active NEP and IDE quantification (**C**, **D**). **A** and **C**, Histograms report the level of active NEP in the brain of treated and untreated WT or Tg mice. **B** and **D**, Histograms report the level of active IDE in the brain of treated and untreated WT or Tg mice. Data are presented as mean ± SEM. One-way ANOVA, Tukey's *post hoc* test, ***p* < 0.01, ****p* < 0.001 *versus* untreated WT mice; §*p* < 0.05, §§§*p* < 0.001 treated *versus* untreated Tg mice; n = 5/group).

As regards to brain APP, no difference between treated or untreated Tg mice was observed (Figure 7C dotted bars).

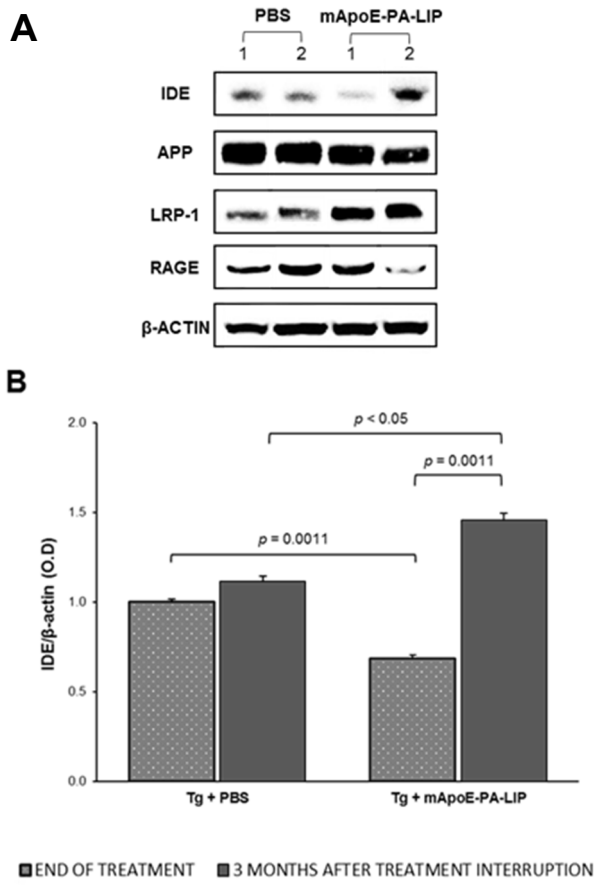

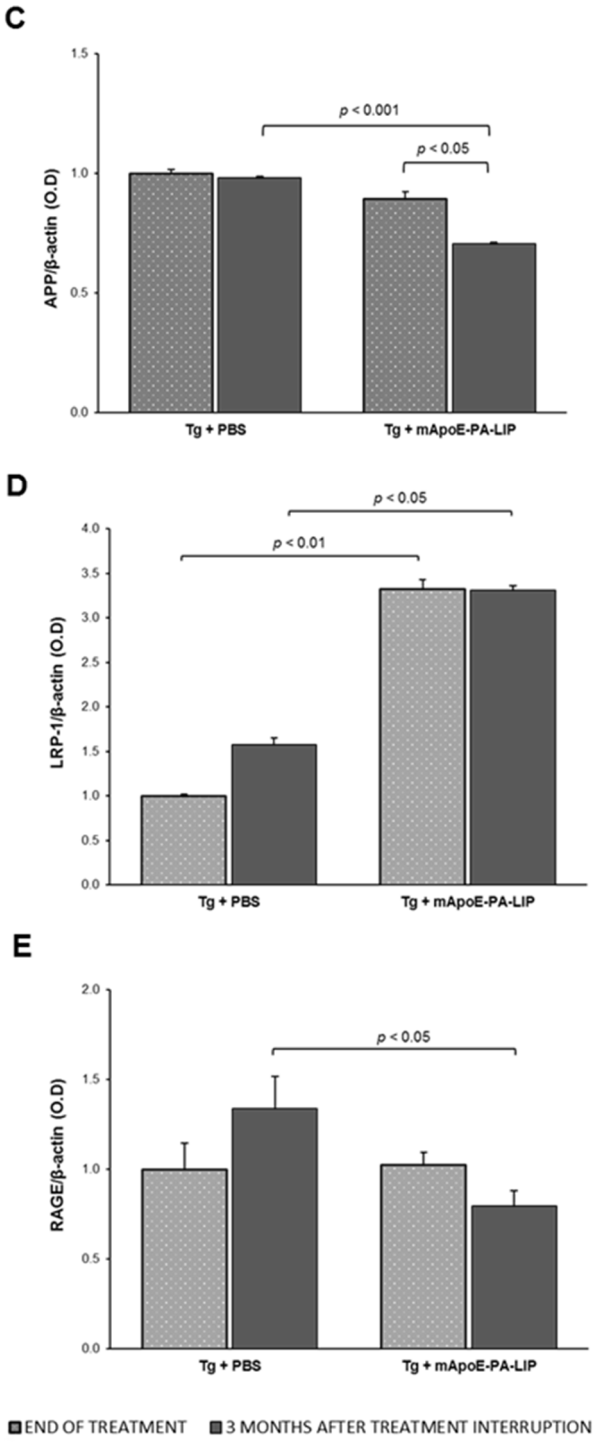
C
APP/β-actin (O.D)
1.5
1.0
0.5
0.0
p < 0.001
p < 0.05
Tg + PBS
Tg + mApoE-PA-LIP
D
LRP-1/β-actin (O.D)
4.0
3.5
3.0
2.5
2.0
1.5
1.0
0.5
0.0
p < 0.05
p < 0.01
Tg + PBS
Tg + mApoE-PA-LIP
E
RAGE/β-actin (O.D)
2.0
1.5
1.0
0.5
0.0
p < 0.05
Tg + PBS
Tg + mApoE-PA-LIP
END OF TREATMENT
3 MONTHS AFTER TREATMENT INTERRUPTION

Figure 7. Effect of mApoE-PA-LIP treatment on brain APP, IDE, LRP-1 and RAGE levels. At the end of treatment and three months after its interruption, animals were sacrificed and half brains homogenized and submitted to SDS-PAGE and Western blot (**A**, **B**, **C**, **D** and **E**). **A**, Immunoblots of brain homogenates from untreated (PBS) and treated (mApoE-PA-LIP) Tg mice. Lanes 1, at the end of the 7-month treatment; lanes 2, three months after treatment interruption. **B**, Relative quantification of the immunoblot bands of IDE on β-actin. **C**, Relative quantification of the immunoblot bands of APP on β-actin. **D**, Relative quantification of the immunoblot bands of LRP-1 on β-actin. **E**, Relative quantification of the immunoblot bands of RAGE on β-actin. Dotted bars, at the end of treatment; grey bars, 3 months after treatment interruption. Data are presented as mean ± SEM. Student's *t* test; n = 5/group.

Finally, after completion of the treatment, Aβ levels were found significantly increased (+36%) in the liver of treated Tg mice with respect to untreated Tg (data not shown).

mApoE-PA-LIP treatment effects persisted after its discontinuation

To investigate whether the effects exerted by the treatment would persist after its discontinuation, five animals per group were kept for 3 further months after the end of treatment. The memory test at the end of this period was not performed, due to the small number of animals, not suitable for a statistically significant evaluation. Brain MRI analysis showed that, after three months, both ventricle volume and entorhinal cortex thickness of treated Tg mice remained stable and comparable to WT, while untreated Tg mice still displayed enlarged ventricle volume (+23%) and thinner entorhinal cortex (-7%) (Figure 3C and D). No changes were detected on the other brain areas.

After MRI, animals were sacrificed and organs analyzed. Tg mice having received the mApo-PA-LIP treatment were compared with

untreated Tg mice and the results, 3 months after treatment discontinuation, can be summarized as follows:

i) the amount of plaques in both the cortex and the hippocampus as well as the total amount of brain insoluble and soluble Aβ species were still lower in treated Tg mice (Figure 4D, E and F and Figure 5C and D);

ii) Aβ levels in the liver remained significantly higher (+43%) (data not shown);

iii) The amount of NEP and IDE was higher (+21% and +73% respectively) (Figure 6C and D; Figure 7A and B);

iv) APP brain levels were significantly lower (-21%) (Figure 7A and C);

v) LRP-1 and RAGE brain levels were significantly different (+111% and -41%, respectively) (Figure 7A, D and E).

mApoE-PA-LIP treatment did not induce toxic effects either in the brain or in peripheral organs

The potential toxicity of mApoE-PA-LIP treatment was investigated both at the end of treatment and after its discontinuation. Body weight and motor activity of all mice were monitored throughout the 7 months of treatment and no significant changes among the groups was observed (data not shown). The serum values of total cholesterol, triglycerides, lipoproteins (high-density lipoproteins, HDL; low density lipoproteins, LDL) and transaminases (alanine transaminases, ALT; aspartate transaminases, AST) were not statistically different between experimental groups (data not shown), suggesting no effect of mApoE-PA-LIP treatment on hepatic function. In addition, macroscopic examination of livers, spleens and brains revealed a normal aspect,

without hyperplasia or necrosis, and the comparison of organ weights between treated and control groups did not show any significant difference (data not shown). At a molecular level, brains, livers and spleens also underwent a biochemical analysis for inflammation and reactive oxygen species (ROS) production.

As first, the effects on CNS were evaluated. Regarding inflammation, IL-1β and TNF-α were chosen as representative inflammatory markers (Wang et al., 2015). Brain TNF-α levels of treated Tg mice were lower than untreated Tg, and comparable with those of WT, both at the end of treatment (Figure 8B) and 3 months after its discontinuation (Figure 8D). The treatment of Tg mice, with respect to untreated, did not induce any change of brain IL-1β levels, which were higher than in WT, both at the end of treatment (Figure 8A) and 3 months after its discontinuation (Figure 8C).

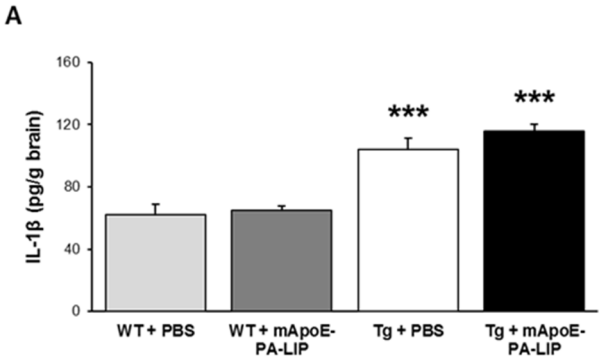

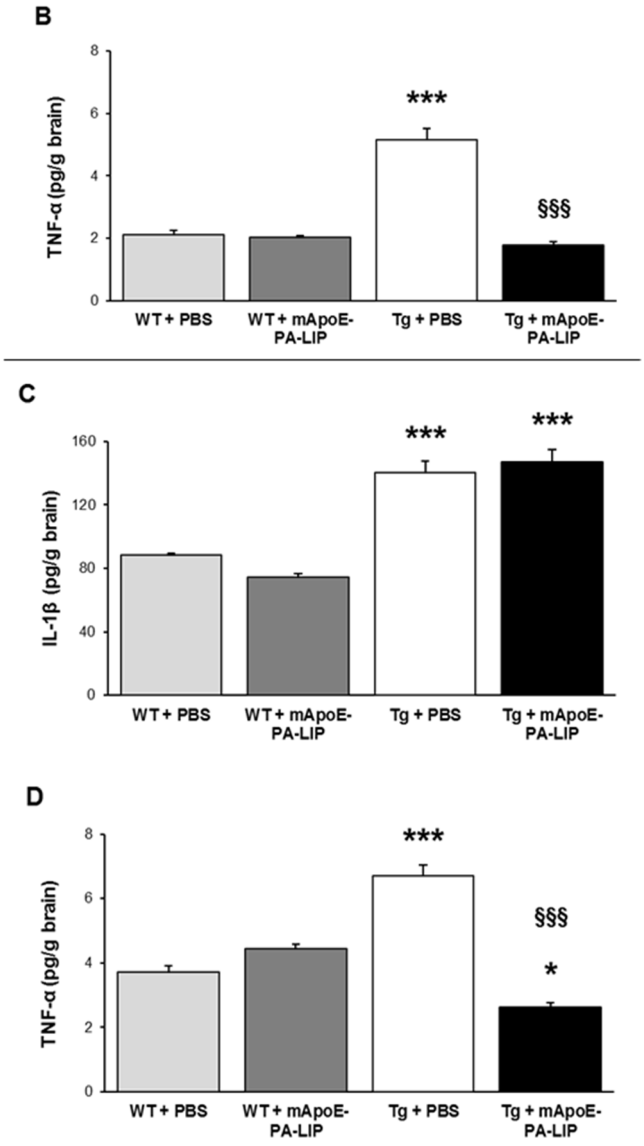

Figure 8. Effect of mApoE-PA-LIP treatment on brain inflammation. At the end of treatment, half of the animals was sacrificed, half brain was homogenized and inflammatory cytokine levels were measured (**A**, **B**). After three months from treatment interruption, the rest of the animals was sacrificed and their brain analyzed for inflammatory cytokine levels (**C**, **D**). **A** and **C**, Histograms indicate the level of IL-1β in the brain of treated and untreated WT or Tg mice. **B** and **D**, Histograms indicate the level of TNF-α in the brain of treated and untreated WT or Tg mice. Data are presented as mean ± SEM. One-way ANOVA, Tukey's *post hoc* test, **p* < 0.05, ****p* < 0.001 *versus* untreated WT mice; §§§*p* < 0.001 treated *versus* untreated Tg mice; n = 5/group).

Concerning oxidative stress, MDA and SOD activity were assumed as indicators (Chen and Zhong, 2014). Brain SOD of Tg mice increased after treatment with respect to untreated ones, reaching values comparable to WT, both at the end of treatment (Figure 9B) and after its discontinuation (Figure 9D).

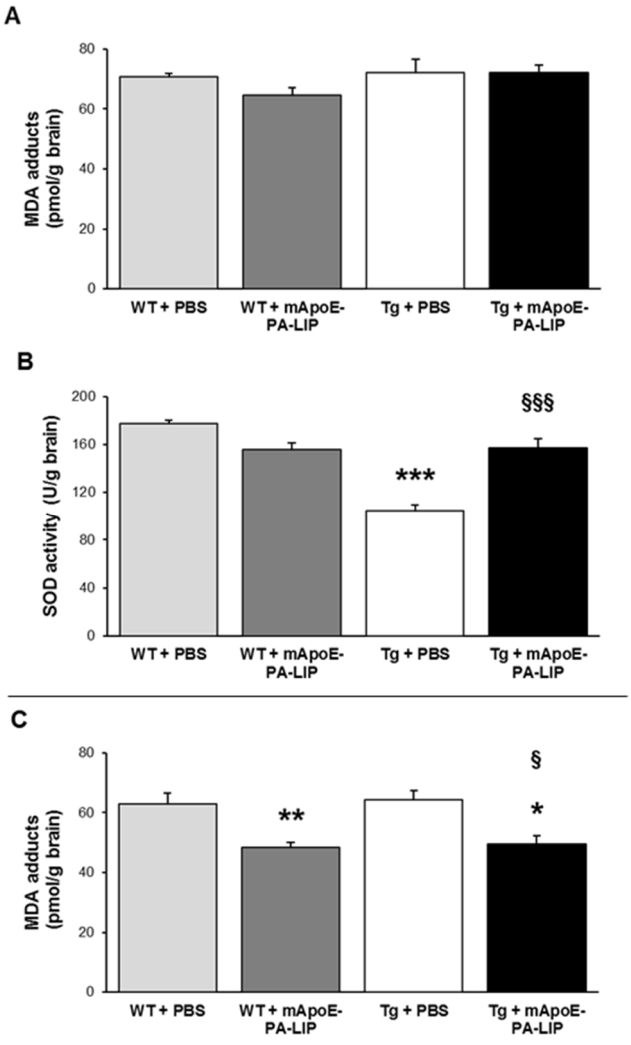

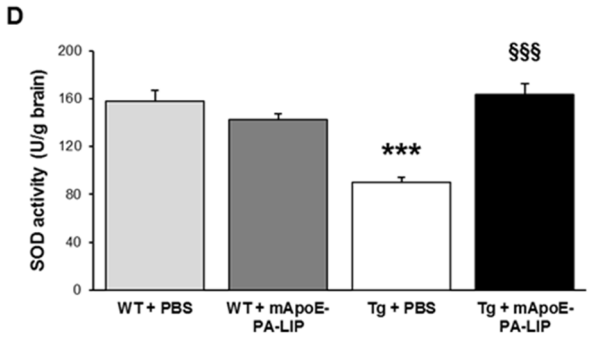

Figure 9. Effect of mApoE-PA-LIP treatment on brain oxidative stress. At the end of treatment, half of the animals was sacrificed, half brain was homogenized and oxidative stress indicator levels were measured (A, B). After three months from treatment interruption, the rest of the animals was sacrificed and their brain analyzed for oxidative stress indicator levels (C, D). A and C, Histograms show the level of MDA adducts in the brain of treated and untreated WT or Tg mice. B and D, Histograms show the level of SOD activity in the brain of treated and untreated WT or Tg mice. Data are presented as mean ± SEM. One-way ANOVA, Tukey's *post hoc* test, **p* < 0.05, ***p* < 0.01, ****p* < 0.001versus untreated WT mice; §*p* < 0.05, §§§*p* < 0.001 treated *versus* untreated Tg mice; n = 5/group.

Successively, peripheral organs were analyzed. TNF-α in the spleens was higher (+69%) in Tg mice at the end of the treatment with respect to untreated and WT, and decreased down to the values of other groups after treatment discontinuation (data not shown). On the contrary, MDA adducts were found decreased (-28%) in the livers both at the end of treatment and after its discontinuation (data not shown).

4.4 DISCUSSION

It is nowadays recognized that brain Aβ pathophysiological alterations leading to AD take place decades before the appearance of the first signs of dementia, providing a wide pre-symptomatic time window for intervention with Aβ-targeted therapies (Holtzman et al., 2011; Sperling et al., 2013; Tian et al., 2014). Within this frame, in the present investigation we evaluated the possibility to use mApoE-PA-LIP to hinder the progression of brain Aβ accumulation and memory impairment. We tested this possibility on APP/PS1 mice, starting a treatment at 5 months of age, when mice display initial brain Aβ deposition but no memory impairment, and ending at 12 months of age, when these features are clearly apparent (Lee et al., 1997; Yan et al., 2009; VanItallie, 2015).

A remarkable outcome of the treatment herein described with mApoE-PA-LIP is that the cognitive performance, in terms of memory evaluation, of Tg animals remained comparable to that of WT for the entire duration of the treatment, suggesting that liposomes could exert a preventive activity on memory loss. In fact, untreated Tg mice, although cognitively comparable with WT at the beginning of the treatment showed significant deficits at both 9 and12 months of age.

Another relevant result of this study is that brain Aβ deposition was strongly delayed in treated Tg mice, clearly showing a reduced number and area of plaques and a lower amount of brain insoluble Aβ levels.

Looking for a possible explanation of these striking results on brain Aβ reduction, it should be pointed out that no difference in NEP, IDE and APP brain levels were observed in treated Tg mice with respect to untreated, thus ruling out an effect on CNS Aβ metabolism exerted by

the treatment. Instead, the increase in liver Aβ levels of treated Tg mice suggests that the peptide is hauled from the brain to this organ. Thus, it is possible that mApoE-PA-LIP enter the brain and slow down Aβ aggregation, as previously demonstrated (Balducci et al., 2014; Bana et al., 2014), maintaining soluble Aβ species available for efflux to blood, triggered by circulating liposomes - the so called 'sink effect' (Matsuoka et al., 2003; Ordóñez-Gutiérrez et al., 2015; Mancini et al., 2016) - , and thus reducing the probability of brain deposition. This hypothesis is supported by the observation that no changes in soluble brain Aβ levels were measured, together with a reduced plaque deposition.

One of the most compelling outcomes of the present study is that the reduced brain Aβ burden detected in treated Tg mice was still detectable three months after the end of treatment. In fact, even if the amount of brain Aβ increased over time, the lower burden in treated ones was maintained, suggesting that the treatment could slow down the progression of the disease also for a given time after its discontinuation. The long-lasting effect of treatment on brain Aβ levels could be linked to a later involvement of NEP/IDE and APP, whose levels significantly increased or decreased, respectively, after the end of treatment.

Taking into account the short half-life of mApoE-PA-LIP in the blood (Bana et al., 2014), the fact that Aβ levels were still high in the liver of treated animals three months after discontinuation of the treatment suggests that the treatment could affect the Aβ transport pathways across the BBB. This possibility is partly supported by the observation that the brain levels of the two main transporters in either direction of

Aβ across the BBB, LRP-1 and RAGE (Deane et al., 2009), were found increased and decreased, respectively, in the brains of treated Tg mice. Concerning the positive effect induced by the treatment on cognitive impairment, this is reported to be strongly correlated with soluble Aβ levels (McLean et al., 1999); thus, it is questionable that our treatment induced memory recovery without changes in soluble brain Aβ levels. A possible explanation could be found in the lower TNF-α level or in the higher level of SOD activity detected in the brain of treated Tg mice with respect to untreated ones. These changes could prevent damage at synapses, which are considered as the primary Aβ target in AD pathogenesis (Selkoe, 2002). The hypothesis of neuronal protection is supported by the MRI analysis, showing that treated Tg mice displayed brain ventricle volume and entorhinal cortex thickness comparable to WT.

Regarding possible toxicity, the treatment proved to be apparently not toxic for all the organs analysed, despite its long duration, except for a possible toxicity on the spleen, indicated by the increase of TNF-α level observed at the end of treatment. On the other hand, the results indicate an anti-inflammatory action and a protective effect against ROS of liposomes in the brain, which persist after the end of treatment.

Taken together, all these findings indicate mApoE-PA-LIP as a new all-in-one multitask approach potentially suitable for early treatment of AD. To be pointed out that the long-term treatment with mApoE-PA-LIP could not cure AD, but could avoid the onset of cognitive deficits and brain structural changes and slow down the progression of Aβ accumulation.

Acknowledgement

The research leading to these results has received funding from the European Community's Seventh Framework Program (FP7/2007-2013) under grant agreement n° 212043 (NAD). We thank Dr. Alfredo Cagnotto from IRCCS-Mario Negri Institute (Milano, Italy) for providing mApoE peptide.

References

Alzheimer's Association national site – information on Alzheimer's disease and dementia symptoms, diagnosis, stages, treatment, care and support resources. http://www.alz.org. Updated June 30, 2016. Accessed June 30, 2016.

Antunes M, Biala G (2012) The novel object recognition memory: neurobiology, test procedure, and its modifications. Cogn Process 13:93-110.

Balducci C, Forloni G (2011) APP transgenic mice: their use and limitations. Neuromolecular Med 13(2):117-37.

Balducci C, Mancini S, Minniti S, La Vitola P, Zotti M, Sancini G, Mauri M, Cagnotto A, Colombo L, Fiordaliso F, Grigoli E, Salmona M, Snellman A, Haaparanta-Solin M, Forloni G, Masserini M, Re F (2014) Multifunctional liposomes reduce brain β-amyloid burden and ameliorate memory impairment in Alzheimer's disease mouse models. J Neurosci 34(42):14022-31.

Bana L, Minniti S, Salvati E, Sesana S, Zambelli V, Cagnotto A, Orlando A, Cazzaniga E, Zwart R, Scheper W, Masserini M, Re F (2014) Liposomes bifunctionalized with phosphatidic acid and an ApoE-derived peptide affect Aβ aggregation features and cross the blood-brain-barrier: implications for therapy of Alzheimer disease. Nanomedicine 10(7):1583-90.

Chen Z, Zhong C. Oxidative stress in Alzheimer's disease (2014) Neurosci Bull 30(2):271-81.

Cramer PE, Cirrito JR, Wesson DW, Lee CY, Karlo JC, Zinn AE, Casali BT, Restivo JL, Goebel WD, James MJ, Brunden KR, Wilson DA, Landreth GE (2012) ApoE-directed therapeutics

rapidly clear beta-amyloid and reverse deficits in AD mouse models. Science 335:1503-6.

Deane R, Bell RD, Sagare A, Zlokovic BV (2009) Clearance of amyloid-beta peptide across the blood-brain barrier: implication for therapies in Alzheimer's disease. CNS Neurol Disord Drug Targets 8(1):16-30.

Franklin KBJ, Paxinos G (1997) The Mouse Brain in Stereotaxic Coordinates. Press, A, London.

Holtzman DM, Morris JC, Goate AM (2011) Alzheimer's disease: the challenge of the second century. Sci Transl Med 3(77):77sr1.

Jenkinson M, Smith S (2001) A global optimisation method for robust affine registration of brain images. Med Image Anal 5(2):143-56.

Jenkinson M, Bannister P, Brady M, Smith S (2002) Improved optimization for the robust and accurate linear registration and motion correction of brain images. Neuroimage 17(2):825-41.

Lazarov O, Robinson J, Tang YP, Hairston IS, Korade-Mirnics Z, Lee VM, Hersh LB, Sapolsky RM, Mirnics K, Sisodia SS (2005) Environmental enrichment reduces Abeta levels and amyloid deposition in transgenic mice. Cell 120:701-13.

Lee MK, Borchelt DR, Kim G, Thinakaran G, Slunt HH, Ratovitski T, Martin LJ, Kittur A, Gandy S, Levey AI, Jenkins N, Copeland N, Price DL, Sisodia SS (1997) Hyperaccumulation of FAD-linked presenilin 1 variants in vivo. Nat Med 3(7):756 –60.

Mancini S, Minniti S, Gregori M, Sancini G, Cagnotto A, Couraud PO, Ordóñez-Gutiérrez L, Wandosell F, Salmona M, Re F (2016) The hunt for brain Aβ oligomers by peripherally circulating

multifunctional nanoparticles: potential therapeutic approach for Alzheimer disease. Nanomedicine 12(1):43-52.

Matsuoka Y, Saito M, LaFrancois J, Saito M, Gaynor K, Olm V, Wang L, Casey E, Lu Y, Shiratori C, Lemere C, Duff K (2003) Novel therapeutic approach for the treatment of Alzheimer's disease by peripheral administration of agents with an affinity to beta-amyloid. J Neurosci 23(1):29-33.

McLean CA, Cherny RA, Fraser FW, Fuller SJ, Smith MJ, Beyreuther K, Bush AI, Masters CL (1999) Soluble pool of Abeta amyloid as a determinant of severity of neurodegeneration in Alzheimer's disease. Ann Neurol 46(6):860-6.

Nalivaeva NN, Beckett C, Belyaev ND, Turner AJ (2012) Are amyloid-degrading enzymes viable therapeutic targets in Alzheimer's disease? J Neurochem 120 Suppl 1:167-85.

Ordóñez-Gutiérrez L, Re F, Bereczki E, Ioja E, Gregori M, Andersen AJ, Antón M, Moghimi SM, Pei JJ, Masserini M, Wandosell F (2015) Repeated intraperitoneal injections of liposomes containing phosphatidic acid and cardiolipin reduce amyloid-β levels in APP/PS1 transgenic mice. Nanomedicine 11(2):421-30.

Palop JJ, Mucke L (2010) Amyloid-beta-induced neuronal dysfunction in Alzheimer's disease: from synapses toward neural networks. Nat Neurosci 13(7):812-18.

Re F, Cambianica I, Sesana S, Salvati E, Cagnotto A, Salmona M, Couraud PO, Moghimi SM, Masserini M, Sancini G (2010) Functionalization with ApoE-derived peptides enhances the interaction with brain capillary endothelial cells of

nanoliposomes binding amyloid-beta peptide. J Biotechnol 156:341-6.

Re F, Cambianica I, Zona C, Sesana S, Gregori M, Rigolio R, La Ferla B, Nicotra F, Forloni G, Cagnotto A, Salmona M, Masserini M, Sancini G (2011) Functionalization of liposomes with ApoE-derived peptides at different density affects cellular uptake and drug transport across a blood-brain barrier model. Nanomedicine 7:551-9.

Re F, Gregori M, Masserini M (2012) Nanotechnology for neurodegenerative disorders. Nanomedicine 8 Suppl 1:S51-8.

Selkoe DJ (2002) Alzheimer's disease is a synaptic failure. Science 298(5594):789-91.

Selkoe DJ (2012) Preventing Alzheimer’s disease. Science 337(6101):1488-92.

Sperling RA, Karlawish J, Johnson KA (2013) Preclinical Alzheimer disease: the challenges ahead. Nat Rev Neurol 9(1):54-8.

Steinerman JR, Irizarry M, Scarmeas N, Raju S, Brandt J, Albert M, Blacker D, Hyman B, Stern Y (2008) Distinct pools of beta-amyloid in Alzheimer disease-affected brain: a clinicopathologic study. Arch Neurol 65:906-12.

Tian T, Zhang B, Jia Y, Li Z (2014) Promise and challenge: the lens model as a biomarker for early diagnosis of Alzheimer's disease. Dis Markers 2014:826503.

Valero J, España J, Parra-Damas A, Martín E, Rodríguez-Álvarez J, Saura CA (2011) Short-term environmental enrichment rescues adult neurogenesis and memory deficits in APP(Sw,Ind) transgenic mice. PLoS One 6(2):e16832.

VanItallie TB (2015) Biomarkers, ketone bodies, and the prevention of Alzheimer's disease. Metabolism 64(3 Suppl 1):S51-7.

Wang WY, Tan MS, Yu JT, Tan L (2015) Role of pro-inflammatory cytokines released from microglia in Alzheimer's disease. Ann Transl Med 3(10):136.

Yan P, Bero AW, Cirrito JR, Xiao Q, Hu X, Wang Y, Gonzales E, Holtzman DM, Lee JM (2009) Characterizing the appearance and growth of amyloid plaques in APP/PS1 mice. J Neurosci 29(34):10706-14.

Yang D, Xie Z, Stephenson D, Morton D, Hicks CD, Brown TM, Sriram R, O'Neill S, Raunig D, Bocan T (2010) Volumetric MRI and MRS provide sensitive measures of Alzheimer's disease neuropathology in inducible tau transgenic mice (rTg4510). Neuroimage 54(4):2652-8.

CHAPTER 5

Retro-inverso peptide inhibitor nanoparticles as potent inhibitors of aggregation of the Alzheimer's Aβ peptide

Maria Gregori, Mark Taylor, Elisa Salvati, Francesca Re, Simona Mancini, Claudia Balducci, Gianluigi Forloni, Vanessa Zambelli, Silvia Sesana, Maria Michael, Christos Michail, Claire Tinker-Mill, Oleg Kolosov, Michael Scherer, Stephen Harris, Nigel J. Fullwood, Massimo Masserini, David Allsop

Nanomedicine, 2017; 13(2):723-32

Abstract

Aggregation of amyloid-β peptide (Aβ) is a key event in the pathogenesis of Alzheimer's disease (AD). We investigated the effects of nanoliposomes decorated with the retro-inverso peptide RI-OR2-TAT (Ac-rGffvlkGrrrrqrrkkrGy-NH_2) on the aggregation and toxicity of Aβ. Remarkably low concentrations of these peptide inhibitor nanoparticles (PINPs) were required to inhibit the formation of Aβ oligomers and fibrils *in vitro*, with 50% inhibition occurring at a molar ratio of ~1:2000 of liposome-bound RI-OR2-TAT to Aβ. PINPs also bound to Aβ with high affinity (Kd = 13.2-50 nM), rescued SHSY-5Y cells from the toxic effect of pre-aggregated Aβ, crossed an *in vitro* blood–brain barrier model (hCMEC/D3 cell monolayer), entered the brains of C57/BL6 mice, and protected against memory loss in APP_{SWE} transgenic mice in a novel object recognition test. As the most potent aggregation inhibitor that we have tested so far, we propose to develop PINPs as a potential disease-modifying treatment for AD.

5.1 INTRODUCTION

There are currently ~36 million sufferers of Alzheimer's disease (AD) worldwide, costing the world economy US$604 billion in 2010, and these figures are set to rise dramatically in the future (Wimo and Prince, 2010). Current drug treatments only temporarily alleviate the symptoms of AD. Characteristic pathological changes of the disease are the presence of abundant senile plaques, containing amyloid-β peptide (Aβ) fibrils, and neurofibrillary tangles consisting of hyperphosphorylated Tau protein. However, Aβ oligomers are now thought to be the most toxic form of this peptide, with a potent ability to cause memory deficits and inhibition of oligomer formation is a potential strategy for disease modification therapy (Lambert et al., 1998; Walsh et al., 2002; Wang et al., 2002; Kim et al., 2003; Cleary et al., 2005; Haass and Selkoe, 2007; Walsh and Selkoe, 2007). It is also generally thought that Tau aggregation is a downstream consequence of Aβ aggregation (Ma et al., 2009). The most advanced clinical trials aimed at disease modification in AD are based on drugs targeting the production or clearance of Aβ (Howlett, 2011).

We have published data on a small peptide (OR2 = H_2N-RGKLVFFGR-NH_2) that inhibits the formation of Aβ oligomers and fibrils (Austen et al., 2008). RI-OR2 is a much more stable retro-inverted version of this peptide (Taylor et al., 2010). The addition of retro-inverted 'TAT' (HIV cell-penetrating peptide) to RI-OR2 allows it to enter cells and cross the blood–brain barrier (BBB) (Parthsarathy et al., 2013). Treatment of APPswe/PS1ΔE9 transgenic mice with RI-OR2-TAT caused reduction of brain Aβ burden (oligomers included), reduction of numbers of activated microglial cells, and an increase in

the number of young neurons in the dentate gyrus (Parthsarathy et al., 2013). However, RI-OR2-TAT only inhibits Aβ aggregation when present at relatively high concentrations (i.e. 1:5 molar ratio of inhibitor: Aβ at best) (Parthsarathy et al., 2013).

In recent years, there has been a growing interest in the use of liposomes as carriers for therapeutic agents, because of their attractive characteristics, such as biocompatibility, biodegradability, and chemical and physical stability (Torchilin, 2005). Moreover, liposomes can be multifunctionalized on their surface, and it has been shown that multi-ligand-decorated nanosystems can be more efficient (compared to single ligand systems) at recognizing their molecular targets (Stukel et al., 2010). In the present study, we have covalently attached RI-OR2-TAT to nanoliposomes (NLs) using 'click' chemistry. We show that very low concentrations of these peptide inhibitor nanoparticles (PINPs) were required to inhibit the aggregation of Aβ and to protect cultured SHSY-5Y cells from the toxic effect of pre-aggregated Aβ. Moreover, they were efficient at crossing an *in vitro* BBB model, entered the brains of healthy mice, and protected against memory loss in APP_{SWE} transgenic mice.

5.2 MATERIALS AND METHODS

Materials

Chemical reagents and Sepharose 4B-CL were from Sigma-Aldrich. Bovine brain sphingomyelin (Sm), cholesterol (Chol) and 1,2-distearoyl-sn-glycero-3-phosphoethanolamine-N-[maleimide (polyethylene glycol)-2000] (mal-PEG-PE) were from Avanti Polar Lipids Inc., USA. [^{3}H]-Sm, [^{3}H]-propranolol, [^{14}C]-sucrose, Ultima Gold scintillation cocktail and solvable tissue solubilizer were from PerkinElmer (Waltham, MA, USA). [^{14}C]-Chol was provided by Quotient Bioresearch Ltd. Polycarbonate filters for liposome extrusion were from Millipore Corp., Bedford, MA, USA and the extruder was from Lipex Biomembranes, Vancouver, Canada. Recombinant Aβ_{1-42}, Ultrapure, was from rPeptide, Bogart, Georgia, USA. All other chemicals were reagent grade.

Production of NL decorated with RI-OR2-TAT (PINPs) by click chemistry

NL were composed of Sm/Chol (1:1 molar ratio) mixed with 5 molar % of mal-PEG-PE. Lipids were resuspended in chloroform/methanol (2:1, v:v) and dried under a gentle stream of nitrogen. The resulting film was resuspended in PBS, pH 7.4, vortexed and extruded 10 times through a 100 nm pore polycarbonate filter under 20 bar nitrogen pressure, at room temperature, to create UD (undecorated) liposomes. In order to covalently attach the peptide to these liposomes, an additional cysteine residue was incorporated at the C-terminus. NL were incubated with this peptide for 2 h at 37 °C and then overnight at 4 °C to obtain PINPs. To remove unbound peptide, the liposome

suspension was passed through a Sepharose 4B-CL column (25 × 1 cm). The elution of PINPs was assessed by dynamic light scattering (DLS) and the amount of peptide bound to liposomes was quantified by Bradford assay (Bradford, 1976). Phospholipid recovery was determined by the method of Stewart (Stewart, 1980).

NL characterization

The size and polydispersity of NL were measured at 25 °C using a ZetaPlus particle sizer (Brookhaven Instruments Corporation, Holtsville, NY, USA). The particle size was assessed by DLS with a 652 nm laser, and polydispersity index was obtained from the intensity autocorrelation function of the light scattered at a fixed angle of 90°.
The NL were also analysed by use of a Nanosight machine (NanoSight Ltd., Minton Park, Amesbury, UK) with NL suspended in PBS, pH 7.4, and measured at 25 °C.

Aβ aggregation assays

These were performed using de-seeded $A\beta_{1-42}$ (Taylor et al., 2010).
ThT assays were conducted in 384-well, clear-bottomed microtitre plates, with 25 μM $A\beta_{1-42}$, 15 μM ThT, and a range of concentrations of PINPs, in 10 mM PBS, pH 7.4, with a total reaction volume of 60 μL. Aggregation was monitored using a BioTek Synergy plate reader (λex = 442 nm, λem = 483 nm) over 48 h at 30 °C, with the plate being shaken and read every 10 min. The results show average data from one of two experiments, each of which was performed in triplicate. Control assays involving incubation of pre-aggregated Aβ (incubated at 25 μM for 24 h) with ThT in the presence of each inhibitor ruled out the

possibility that the inhibitors interfere with binding of ThT to fibrils (Taylor et al., 2010).

For the sandwich immunoassay, Aβ oligomers were captured by monoclonal antibody 6E10 and detected by a biotinylated form of the same antibody (Taylor et al., 2010). Briefly, 96-well plates (Maxisorb) were coated with 6E10, diluted 1:1000 in assay buffer (Tris-buffered saline (TBS) (pH 7.4), containing 0.05% γ-globulins and 0.005% Tween 20). The incubated samples of peptide, with or without liposome (12.5 μM Aβ and a series of dilutions of PINPs in PBS, pH 7.4, at 25 °C), were diluted to 1 μM Aβ and incubated, in triplicate, in the 96-well plates for 1 h at 37 °C. The plates were washed with 10 mM PBS, containing 0.5% Tween 20 (PBS-T). Following this, 100 μL of TBS containing 1:1000 biotinylated 6E10 was added and the plates were incubated for 1 h at 37 °C and washed. Europium-linked streptavidin was added at 1:500 dilution in StrepE buffer (TBS containing 20 μM DTPA, 0.5% bovine serum albumin, and 0.05% γ-globulins), incubated for 1 h, and washed. Enhancer solution was added, and the plates were read on a Wallac Victor 2 plate reader. The results shown are average data from one of two experiments, each performed in triplicate. Pre-aggregated peptide controls ruled out the possibility that the inhibitors block binding of 6E10 to Aβ (Taylor et al., 2010).

Atomic force microscopy (AFM)

$A\beta_{1-42}$ was incubated at 25 μM in the presence or absence of 1.25 μM PINPs (total lipids) in PBS, pH 7.4, for 24 h. Samples were diluted 1:10 in PBS and a 2 μL aliquot was deposited onto a mica surface coated with poly-L-lysine (PLL) (Tinker-Mill et al., 2014) and allowed to dry.

Images were obtained in tapping mode using a Multimode™ SPM NanoScope IIIa microscope (Digital Instruments, NY, USA). The silicon cantilever tips were 125 μm long, 30 μm wide and had a radius <10 nm (Budget Sensors, Bulgaria). The resonance frequency was 300 kHz and force constants 40 N/m. All images were first order flattened and edited using WSxM 5.0 Develop 4.3 software, (Nanotech, Madrid, Spain) (Horcas et al., 2007).

Electron microscopy (EM) studies of PINPs incubated with Aβ

Negative stain EM was used to examine the structure of PINPs with and without incubation with Aβ. PINPS alone, or PINPs (25 μM total lipids) incubated with $A\beta_{1-42}$ (25 μM) at 37 °C for 48 h, were pipetted (4 μl) onto 300 mesh formvar and carbon coated copper grids (Agar Scientific, UK) and left for 1 min. The solvent was blotted away and the residue stained using 2% (w/v) phosphotungstic acid (PTA), pH 7.4. Immunogold labelling experiments were performed to identify any Aβ captured by PINPs. Here, the grids were blocked for 15 min in goat serum:PBS (1:10) and incubated at room temperature for 1 h with primary anti-Aβ antibody 6E10 (0.02 μl/ml). After washing, they were incubated with 10 nm colloidal gold-conjugated goat anti-mouse secondary antibody (G7777, Sigma-Aldrich) diluted 1/50 in PBS, for 2 h. After washing, any liquid remaining on the grids was blotted away, and the samples were stained with PTA. Grids were left to dry and examined by TEM.

Surface plasmon resonance (SPR) spectroscopy

SPR experiments were conducted using a Sensi Q semi-automatic SPR machine (ICx Nomadics). This apparatus has two parallel flow cells; one was used to immobilize $A\beta_{1-42}$ monomers, oligomers or fibrils, while the other was used as "reference" (empty surface). A COOH5 sensor chip (ICx Nomadics) was employed for this purpose and the peptide was immobilized by amine coupling chemistry. Briefly, after surface activation, the peptide was diluted to 10 μM in acetate buffer (pH 4.0) and injected for 5 min at a flow rate of 30 μL/min. Any remaining activated groups were blocked with ethanolamine (pH 8.0). The final immobilization level was ~5000 resonance units (1 RU = 1 pg of protein/mm^2). The empty "reference" surface was prepared in parallel using the same immobilization procedure, but without addition of peptide. Sensorgrams were obtained via injection of four different concentrations of PINPs (0.3 μM, 0.6 μM, 0.9 μM, 1.2 μM of exposed peptide) in solution (PBS with 0.005% Tween 20), over the immobilized ligand or control surface, in parallel, at the same time. These SPR data can be interpreted to provide an estimate for affinity of binding of liposomes to Aβ (Taylor et al., 2010; Parthsarathy et al., 2013).

MTS/LDH assay

Cultured SHSY-5Y human neuroblastoma cells were maintained in Dulbecco's modified eagle medium (DMEM, Gibco) containing 10% fetal calf serum, 100 U/mL penicillin, 50 μg/mL streptomycin, at 37 °C and 5% CO_2 in a humidified incubator. Cells were transferred to sterile 96-well growth plates at 20,000 cells per well and four wells per

condition. For the effect of PINPs alone on cells, the growth medium was DMEM. Cells were left to adhere for 24 h before the PINPs were added and cell viability was assessed using the CellTiter 96AqueousOne Solution Cell Proliferation (MTS) Assay kit (Promega) after further 24 h incubation. For the experiments looking at the protective effect of PINPs, the growth medium was changed to Optimem (Invitrogen) and $A\beta_{1\text{-}42}$ that had been pre-aggregated (for 24 h at 25 °C in PBS) was added to a concentration of 5 μM. The plates were returned to the incubator for 24 h and cell proliferation was assessed as above.

Uptake and transcytosis of NL by human brain endothelial cells

Immortalized hCMEC/D3 was cultured as described previously (Re et al., 2011a). 5×10^4 cells/cm^2 were seeded on 12-well transwell inserts coated with type I collagen and cultured with 0.5 mL and 1 mL of culture medium in the upper and lower chamber, respectively. Cells were treated with UD liposomes and PINPs when the transendothelial electrical resistance (TEER) value (measured by EVOMX meter, STX2 electrode; World Precision Instruments, Sarasota, FL, USA) was found to be the highest. The functional properties of cell monolayers were assessed by measuring the endothelial permeability (EP) of [^{14}C]-sucrose and [^{3}H]-propranolol (between 0 and 120 min) as described previously (Cecchelli et al., 1999). Radiolabeled NL (0.5 mL; 400 nmol/mL of total lipids) were added to the upper chamber and incubated for 120 min. After these periods of incubation, the radioactivity in the upper and lower chambers was measured by liquid scintillation counting to calculate the EP of NL across the cell monolayers, taking

account of their passage through the filter without cells (Cecchelli et al., 1999). After 2 h, hCMEC/D3 cells were washed with PBS and detached from the transwell inserts with trypsin/EDTA for 15 min at 37 °C. Cell-associated radioactivity was measured and the total lipid uptake calculated.

Assessment of LIP cytotoxicity on hCMEC/D3 cells

hCMEC/D3 cells were grown on 12-well plates until confluence. Medium was replaced and NL (400 nmol/mL of total lipids) suspended in cell culture medium were incubated at 37 °C with the cells for 24 h. After treatment, the cell viability was assessed by ([3-(4,5-dimethylthiazol-2-yl)-2,5-diphenyltetrazolium bromide]) (MTT) assay, as described previously (Re et al., 2011b). Each sample was analyzed at least in triplicate. Moreover, TEER and permeability of [^{14}C]-sucrose were also determined in the presence of NL to assess the effect of NL on monolayer integrity.

Biodistribution in healthy mice

Three C57/BL6 male mice were administered with 0.4 mM (total lipid) of ^{14}C-labelled cholesterol PINPs, at ~2.22×10^8 dpm/kg, into a tail vein. The amount of radioactivity that reached the brain was assessed by quantitative whole body analysis (QWBA), while the concentration in blood was measured by liquid scintillation counter from samples taken prior to sacrifice. This work was performed by Quotient Bioresearch (Rushden) Ltd., using mice supplied by Charles Rivers UK Ltd., Margate, Kent.

Novel object recognition test in Tg mice

Drug and behavioral test naïve 22-month-old Tg2576 (APP_{SWE}) and WT age-matched littermates were used. All experiments were conducted during the light cycle. Animals (Tg or WT) were injected intraperitoneally with PINPs (100 μl, 100 nmol of peptide/kg) or with PBS (100 μl) once a day for 21 days. The weight of the animals was monitored during treatment. Two experimental groups were treated with PINPs (Tg2576 and WT mice, n = 10 for each), two control groups were treated with PBS (Tg2576 and WT, n = 10 for each). In the NOR test, mice are introduced into an arena containing two identical objects that they can explore freely. Twenty-four hours later, mice are reintroduced into the arena containing the familiar object and a novel object. Exploration was recorded in a 10 min trial by an investigator blinded to the genotype and treatment and the time that each object was explored recorded. Results are expressed as percentage time of investigation on objects per 10 min, or as discrimination index (DI), i.e., (seconds spent on novel − seconds spent on familiar)/(total time spent on objects). Animals with no memory impairment spend a longer time investigating the novel object, giving a higher DI.

All procedures involving animals and their care were conducted according to EU laws and policies (EEC Council Directive 86/609, OJ L 358,1; 12 December 1987), the USDA Animal Welfare Act and NIH (Bethesda, MA, USA) policy on Humane Care and Use of Laboratory Animals. The procedures were reviewed and approved by the Mario Negri Institute Animal Care and Use Committee (1/04-D).

5.3 RESULTS

Preparation and characterization of peptide inhibitor nanoparticles (PINPs)

To attach RI-OR2-TAT (Figure 1A) covalently to the NL surface, we exploited a thiol-maleimide reaction employing an additional cysteine residue to provide the necessary thiol group (Nobs et al., 2004). This thiol function at the C-terminus of RI-OR2-TAT reacted with a maleimide-functionalized phospholipid present in the NL formulation (mal-PEG-PE) (Figure 1B). The yield of coupling was 80%-90% and, consequently, PINPs contained 2%-2.5 mol% of peptide. The total lipid recovery of NL, after the reaction with the peptide and the purification step, was about 65%. Final preparations of PINPs were monodispersed, with a mean size of 143 ± 10 nm as determined by DLS. Their stability was verified by DLS, which showed that the size and polydispersity index remained constant, in PBS, for up to 7 days. Analysis by a Nanosight instrument indicated an average size for PINPs of 131 ± 43 nm (Figure 1C). AFM images showed NL particles with a mean diameter of ~100 nm (Figure 1D), this slightly smaller size being most likely due to some dehydration of the sample.

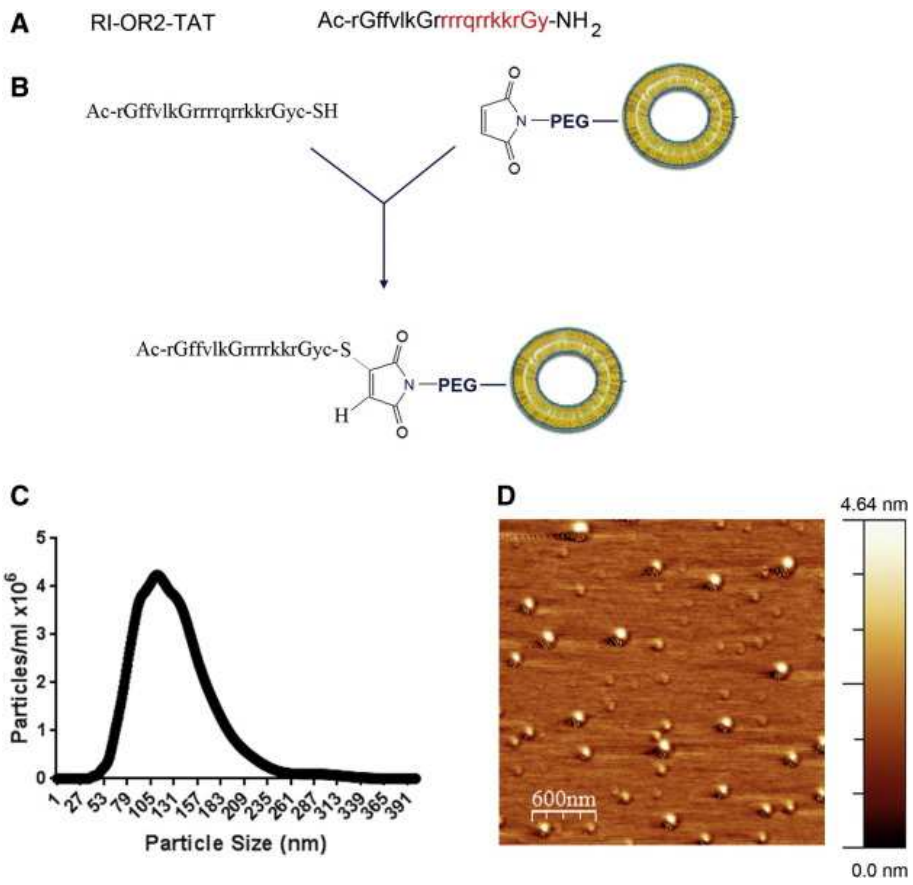

Figure 1. Preparation and characterization of PINPs. **A**, Amino acid sequence of RI-OR2-TAT. Black letters indicate the RI-OR2 peptide and red letters the TAT sequence, with D-amino acids in lower case. **B**, Construction of PINPs through 'click' chemistry involving a C-terminal cysteine residue. **C**, Size distribution of PINPs measured on a Nanosight instrument. **D**, AFM image of PINPs with no Aβ present.

Effects of PINPs on Aβ aggregation

RI-OR2-TAT alone was shown by ThT assay to inhibit $A\beta_{1-42}$ aggregation up to a molar ratio of 1:5 (inhibitor to $A\beta_{1-42}$), in agreement with previous data for RI-OR2 and RI-OR2-TAT (Taylor et al., 2010; Parthsarathy et al., 2013). When RI-OR2-TAT was attached to liposomes there was a dramatic improvement in ability to inhibit $A\beta_{1-42}$ fibril formation at low inhibitor concentrations (Figure 2A). This

finding is best illustrated in the dilution series shown in Figure 2B. Here, it can be seen that 50% inhibition occurs at around 1:50 molar ratio of lipid to $A\beta_{1-42}$ or, as the inhibitory peptide is only ~2.5% of total lipids, ~1:2000 of RI-OR2-TAT to $A\beta_{1-42}$. In contrast, when UD liposomes (1:1) were tested for their ability to inhibit $A\beta_{1-42}$ aggregation, we found a slight stimulatory effect at higher ratios of 1:1 and 1:2 (lipid:$A\beta_{1-42}$) but no effect below 1:10 (data not shown).

A sensitive immunoassay was used to detect Aβ oligomers present at the earlier $A\beta_{1-42}$ incubation time points (at around 4 h under our experimental conditions) (Taylor et al., 2010; Parthsarathy et al., 2013). PINPs inhibited the generation of an immunoassay signal at all time points examined, and at molar ratios down to as low as 1:100 lipid:$A\beta_{1-42}$ or 1:4000 inhibitory peptide:$A\beta_{1–42}$ (Figure 2C). The slight differences between ThT assay and ELISA results could reflect the fact that the former detects mainly fibrils, whereas the latter detects oligomers.

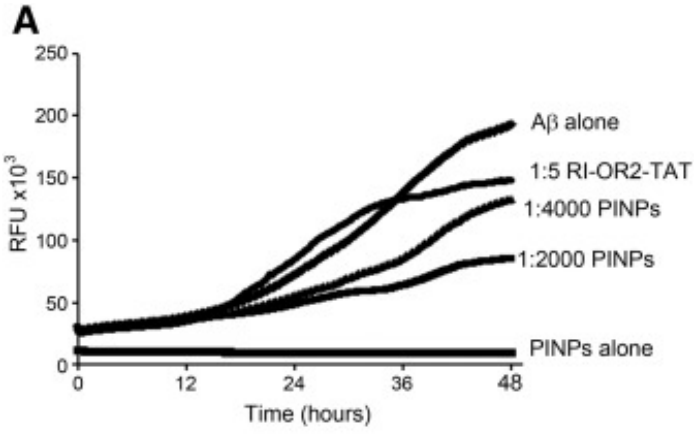

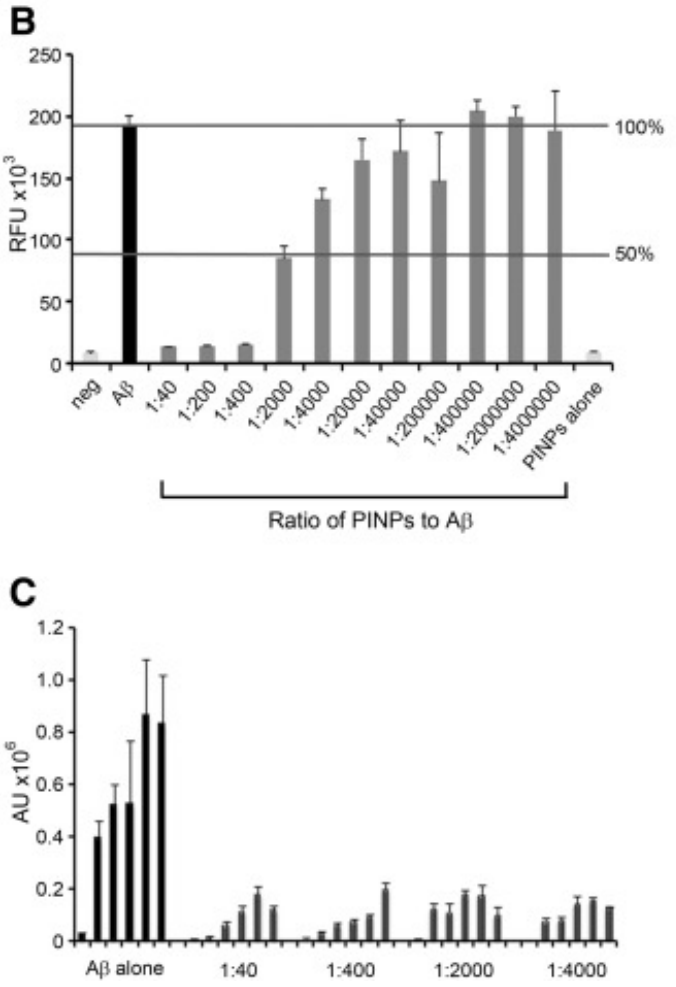

Figure 2. PINPs are potent inhibitors of $A\beta_{1-42}$ aggregation. All concentrations for PINPs refer to NL-linked inhibitory peptide, to allow comparison with free peptide. **A**, Time-course of $A\beta_{1-42}$ aggregation in the presence of non-linked RI-OR2-TAT (1:5 ratio of inhibitor to $A\beta_{1-42}$) or PINPs (1:400, 1:2000 ratio of NL-linked inhibitory peptide to $A\beta_{1-42}$), as determined by ThT assay. **B**, Dilution series of PINPs against the ThT signal after 48 h incubation. Note that a molar ratio of 1:2000 of NL-linked inhibitory peptide to $A\beta_{1-42}$ (or 1:50 total lipids to $A\beta_{1-42}$) gives ~50% inhibition. **C**, Data from an immunoassay for oligomeric Aβ. Samples were taken at 0, 2, 4, 8, 12 and 24 h (consecutive bars) from incubations of $A\beta_{1-42}$ alone, or $A\beta_{1-42}$ with 1:40, 1:400, 1:2000 and 1:4000 ratios of NL-linked inhibitory peptide to Aβ.

AFM images showed fibrils of $A\beta_{1-42}$ following 6 days of incubation in PBS (Figure 3A) and when incubated with UD liposomes (Figure 3B). Few or no fibrils were detected when PINPs were present at a molar ratio of 1:10 of total lipids:Aβ (Figure 3C), confirming that they inhibit aggregation. However, some structures possibly resembling small aggregates could be seen, suggesting that PINPs may not entirely inhibit aggregation. Negative stain EM revealed that the surface of the PINPs was smooth and their shape was generally spherical. However, when the PINPs were incubated with $A\beta_{1-42}$ they appeared to be covered with a 'furry' coat of what are possibly Aβ monomers or oligomers (Figure 3D). Intriguingly, some PINPs were found attached along the length of Aβ fibrils, and at their free ends, suggesting that the interaction of the PINPs had resulted in termination of fibril growth (Figure 3D). Further investigation with anti-Aβ immunogold labelling showed that the surface of the PINPs was decorated with gold particles, confirming capture of Aβ (Figure 3E).

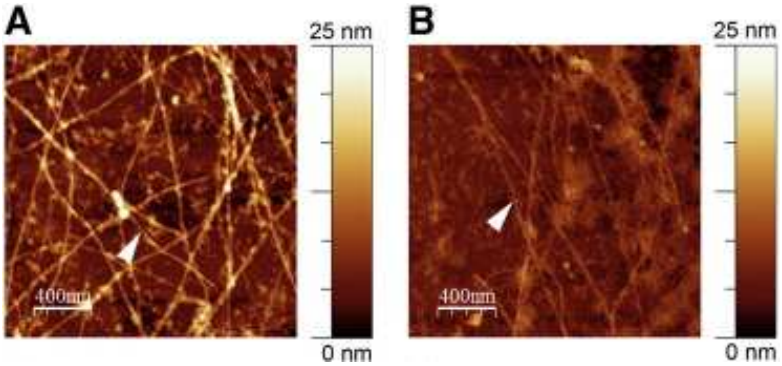

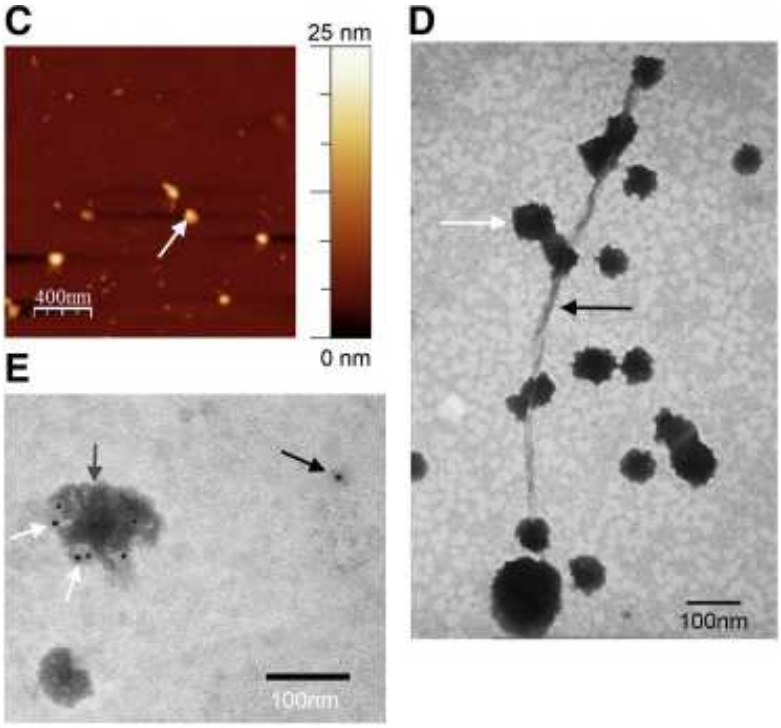

Figure 3. AFM and EM images confirm that PINPs interact with Aβ and inhibit its aggregation. **A**, $A\beta_{1-42}$ at 25 μM was incubated alone for 144 h and examined by AFM. **B**, Aβ with UD liposomes at a 1:20 ratio of lipids:Aβ. **C**, Aβ with PINPs at a 1:20 ratio of lipids:Aβ. The presence of fibres (white arrowheads) in **A** and **B** indicates that UD liposomes do not interfere with Aβ aggregation, whereas **C** shows the clear absence of fibrils. PINPs are indicated by the white arrow. **D**, $A\beta_{1-42}$ incubated with PINPs (4:1 ratio of lipids:Aβ) and stained with PTA. The PINPs (white arrow) are bound along the length of an amyloid fibril (black arrow) and to its termini. **E**, 6E10 immunogold labelling of a PINP (grey arrow) following incubation with $A\beta_{1-42}$. White arrows show regions where Aβ was detected. The black arrow shows an Aβ monomer (or small oligomer) labelled with immunogold.

Binding affinity between PINPs and Aβ

PINPs were injected over immobilized Aβ fibrils at different concentrations of RI-OR2-TAT (0.3, 0.6, 0.9, 1.2 μM) and were shown to bind in a concentration-dependent manner (Figure 4). Curves were fitted separately using the simplest Langmuir 1:1 interaction model, and the calculated apparent affinity (K_d) was 36-50 nM. In addition, K_d

values were 13.2 nM for Aβ oligomers (Figure 5A) and 22.5 nM for monomers (5B).

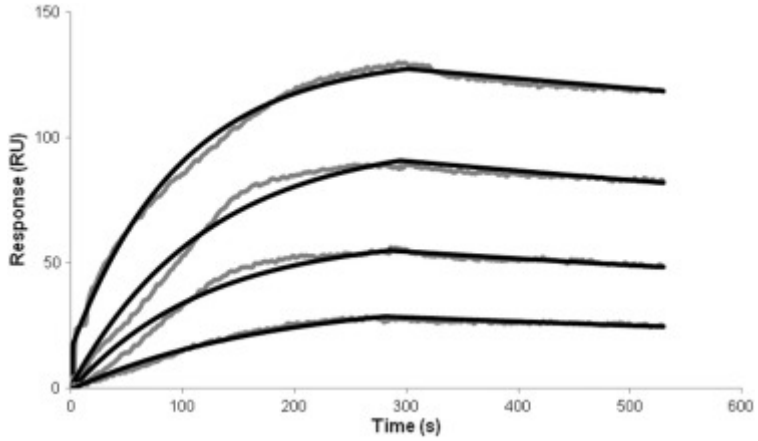

Figure 4. SPR data on binding of PINPs to Aβ fibrils. PINPs were injected at four different concentrations, for 5 min, at a flow rate of 30 µL/min (from bottom to top: 0.3 µM, 0.6 µM, 0.9 µM, 1.2 µM of exposed $A\beta_{1\text{-}42}$ peptide). The non-specific binding obtained from the reference surface has been subtracted from all data. Fitted curves are shown in black. The binding affinity (K_d) is calculated as 36-50 nM.

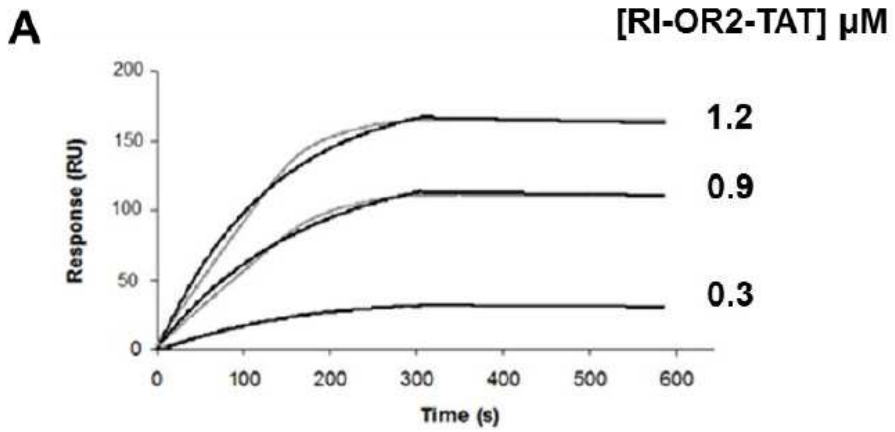

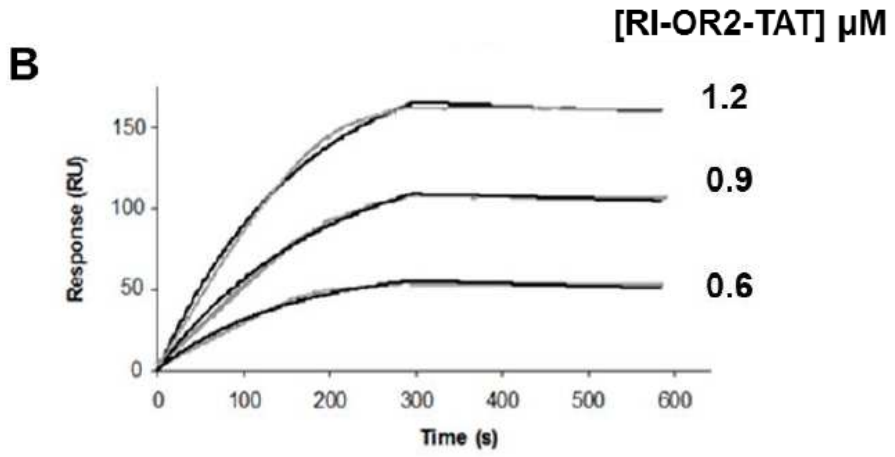

Figure 5. Representative SPR sensorgrams showing the binding of RI-OR2-TAT decorated liposomes (PINPs) to immobilized $A\beta_{1-42}$ oligomers (**A**) or monomers (**B**). Liposomes were injected at different concentrations (see figure), for 5 minutes at a flow rate of 30 µl/min. The non-specific binding obtained from the reference surface has been automatically subtracted from all data. Fitted curves are shown in black.

Effects of PINPs on the toxicity of Aβ

There was no loss in viability of SHSY-5Y cells, as measured by MTS assay, after 24 h incubation in the presence of PINPs at concentrations as high as 10 µM (total lipid) in normal (FCS supplemented DMEM) growth medium (Figure 6A). A similar result was also found using the LDH cell viability assay (data not shown). Treatment of SHSY-5Y cells with 5 µM Aβ for 24 h gave a 39% reduction in cell viability, and the presence of PINPs rescued the cells from Aβ toxicity at all doses tested (Figure 6B). UD liposomes were not toxic to neuroblastoma cells (Figure 6A), and they did not rescue cells from the toxic effect of pre-aggregated Aβ (Figure 6B).

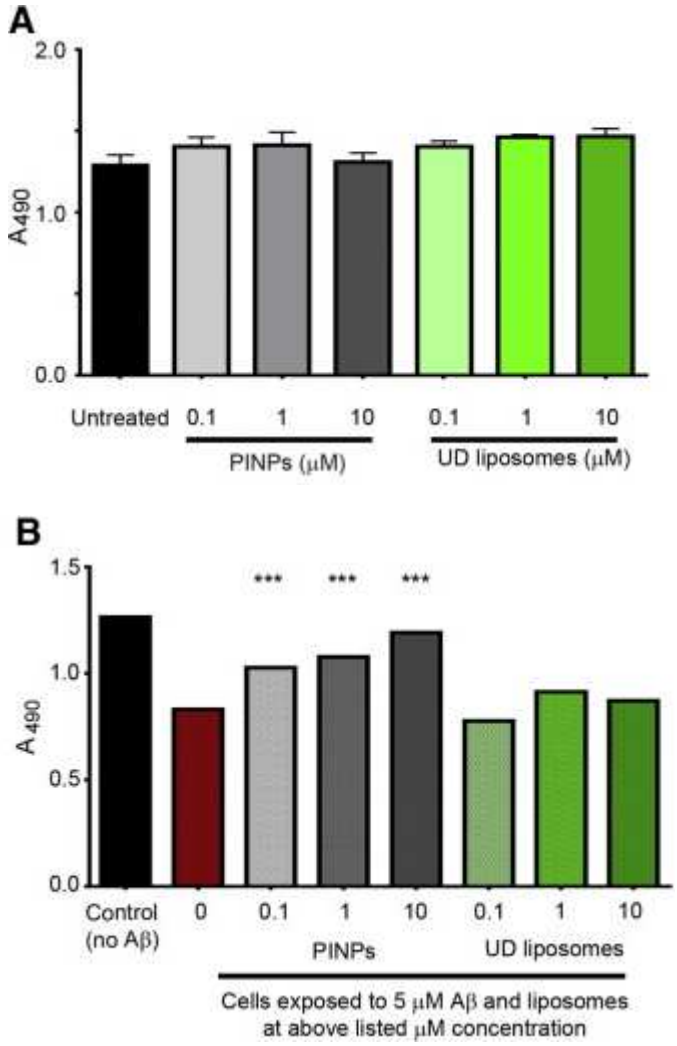

Figure 6. PINPs are not toxic and protect against the damaging effects of Aβ on cells. **A**, MTS assay data for SHSY-5Y cells grown in the presence of various concentrations (total lipids) of PINPs or UD liposomes. **B**, LDH assay data for cells exposed to pre-aggregated $A\beta_{1\text{-}42}$ (at 5 μM) in the presence or absence of varying concentrations (total lipids) of PINPs or UD liposomes. PINPs protected against the damaging effects of Aβ (* = $p < 0.001$). Error bars are too small to be seen.

Passage of PINPs across the blood–brain barrier

We measured the ability of PINPs to cross an artificial BBB model composed of a hCMEC/D3 cell monolayer (Poller et al., 2008).

hCMEC/D3 cells grown on transwell membrane inserts were incubated with UD liposomes or PINPs on day 12, when the maximal transendothelial electrical resistance (TEER) value was registered (123 ± 6 Ω · cm^2). Transport of [^{14}C]-sucrose and [^{3}H]-propranolol was measured, with paracellular EP values of 1.48×10^{-3} cm/min and 3.51×10^{-3} cm/min, respectively, in agreement with values reported in the literature (Summerfield et al., 2006). Radiolabelled UD liposomes or PINPs were added in the upper compartment and the cellular uptake and EP were measured up to 2 h of incubation. The radioactivity stably associated with cells was 1.19% ± 0.32% and 4.19% ± 0.24% of the administered dose ($p < 0.05$), respectively for UD liposomes and PINPs (Figure 7A). Also the EP across the cell monolayers was higher for PINPs ($1.08 \pm 0.13 \times 10^{-4}$ cm/min), compared to UD liposomes ($2.25 \pm 0.89 \times 10^{-5}$ cm/min) ($p < 0.05$) (Figure 7B). MTT assays showed that all of the preparations tested were nontoxic. Moreover, after hCMEC/D3 incubation with UD liposomes or PINPs, the TEER value and the permeability of [^{14}C]-sucrose (119 ± 8 Ω · cm^2 and 1.62×10^{-3} cm/min, respectively) did not change, within experimental error (<3%).

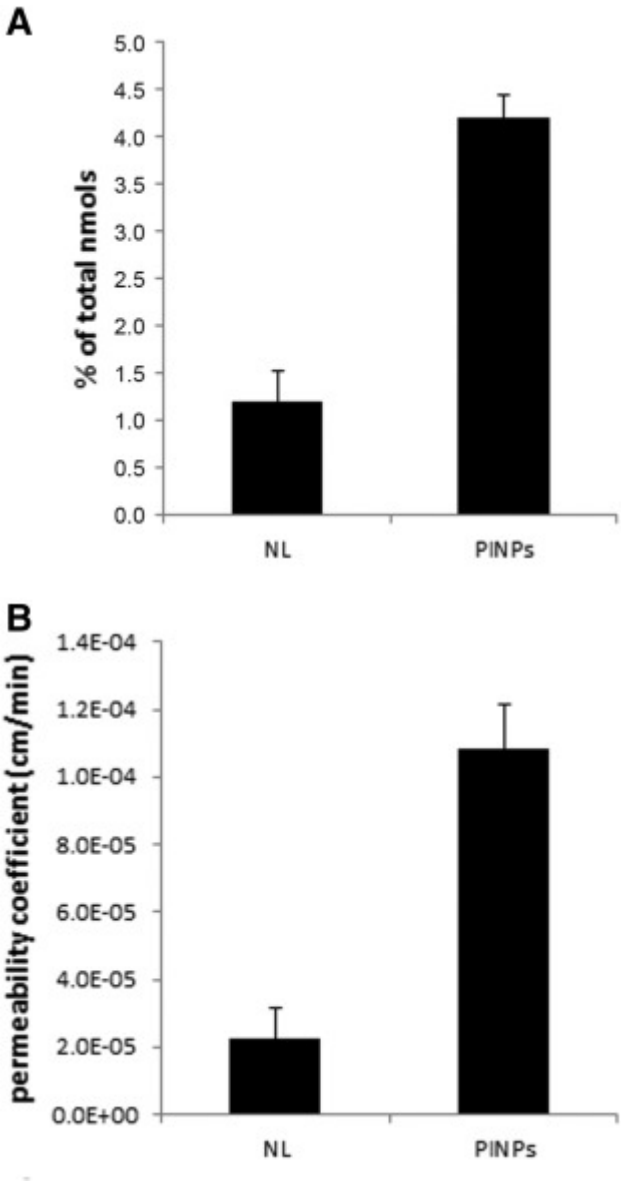

Figure 7. PINPs can flux across the hCMEC/D3 cell monolayer. 10^6 cells were incubated with UD liposomes (NL) or PINPs radiolabeled with ^{3}H-Sm, for 2 h at 37 °C, 5% CO_2. **A**, Cellular uptake of nanoparticles (NP). After incubation, the amount of ^{3}H-Sm incorporated into the cells was measured and the nmol of total NP taken up by the cells calculated. **B**, Transcytosis of NP through hCMEC/D3 cell monolayers. Radiolabeled UD liposomes (NLs) or PINPs were added to the upper chamber of the transwell monolayers and incubated for 2 h at 37 °C, 5% CO_2. The permeability across the cell monolayer was calculated. Each value is the mean (±SD) of at least three independent experiments. * = $p < 0.05$ by Student's *t* test.

Biodistribution of PINPs in healthy mice

QWBA measurements for biodistribution of PINPs are detailed in Table 1. Fifteen minutes after administration, 0.49%/g of the total dose was found in the brain and 0.952%/g in the blood, showing evidence for BBB penetration. However, the majority of the dose was found in lungs (~92%), and other tissues associated with phagocytosis by the mononuclear phagocyte system (i.e. adipose tissue, liver, bone marrow and spleen).

	µg equivalents of [^{14}C]-Cholesterol PEGylated nanoliposomes per gram of tissue (% of total dose/g)		
	Sample time after injection		
Tissue type	5 minutes	15 minutes	60 minutes
Brain	0.225 (0.415)	0.262 (0.490)	0.182 (0.362)
Liver	6.78 (12.5)	8.36 (15.6)	7.28 (14.5)
Kidney	1.52 (2.80)	1.19 (2.23)	0.889 (1.77)
Lung	32.1† (59.2)	49.4† (92.3)	22.8 (45.5)
Spleen	10.9 (20.0)	16 (29.8)	16 (31.8)
Blood	2.19 (4.04)	0.51 (0.952)	0.36 (0.718)

Table 1. Tissue distribution in CL57/Bl 6 mice using quantitative whole body analysis (QWBA).Mice were injected via a tail vein and sacrificed at 5, 15 and 60 minutes post injection. The amount of radioactivity was assessed using QWBA and converted to µg equivalents per gram of tissue (% of total dose/g in brackets).
† Above limit of accurate quantification (>23.5 µg equivalents/g) – extrapolated value reported.

NOR (memory) test

Figure 8 shows that, although PBS-treated Tg2576 mice were unable to discriminate between the familiar and the novel object (percentage time of investigation per 10 min: familiar, 53.5 ± 1.5; novel, 46.5 ± 1.5; DI, −0.07 ± 0.03; n = 19), after treatment mice receiving PINPs

significantly recovered their long-term recognition memory (percentage time of investigation per 10 min: familiar, 40.4 ± 1.6; novel, 59.6 ± 1.6; DI, 0.19 ± 0.03; n = 10), close to the values of PBS-treated WT mice (percentage time of investigation per 10 min: familiar, 39.6 ± 1.4; novel, 60.4 ± 1.4; DI, 0.23 ± 0.02; n = 10) (one-way ANOVA, Tukey's *post hoc* test. *$p < 0.05$).

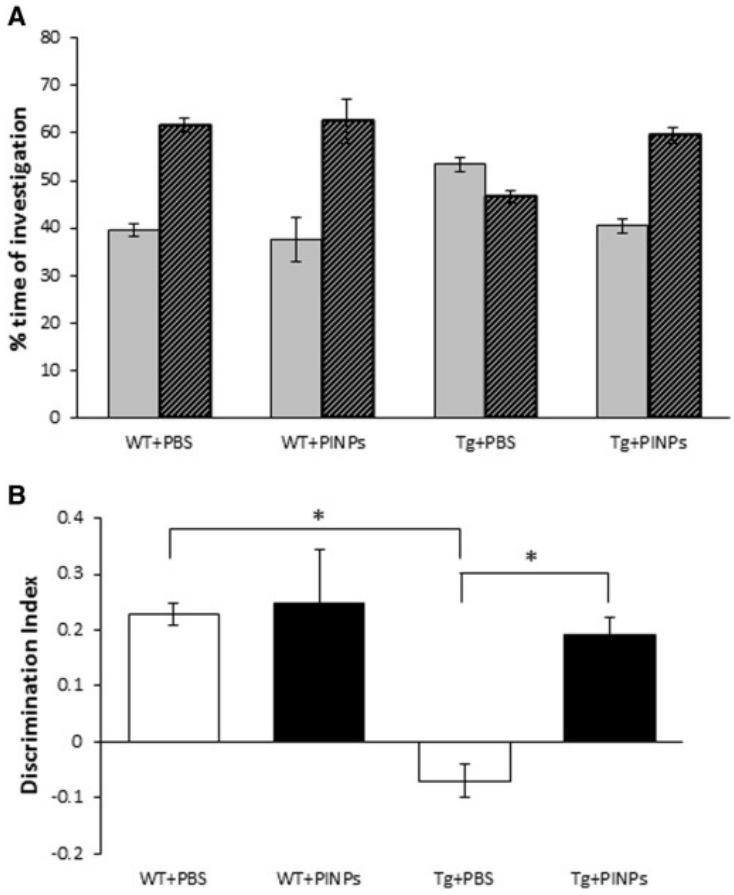

Figure 8. Treatment with PINPs significantly restores long-term recognition memory in Tg2576 mice. WT or Tg2576 mice were treated with PINPs or vehicle and, at the end of treatment, their memory was tested with the NOR test. **A**, Histograms indicate the time percentage (mean ± SEM) of investigation of the familiar (grey) and novel (black) objects of the experimental groups tested. **B**, Histograms report the corresponding DI (mean ± SEM). One-way ANOVA, Tukey's *post hoc* test. *$p < 0.05$.

In addition, we demonstrated that treatment with PINPs had no negative effect on the memory of WT mice (percentage time of investigation per 10 min: familiar, 37.5 ± 4.7; novel, 62.5 ± 3.4; DI, 0.25 ± 0.09; n = 10) and did not affect mouse weight and motor activity (data not shown).

5.4 DISCUSSION

Here, we linked RI-OR2-TAT covalently to the surface of NL composed of sphingomyelin and cholesterol. This lipid formulation has been widely utilized *in vivo* for therapeutic purposes and displays good blood circulation times, good biocompatibility, and high resistance to hydrolysis (Webb et al., 1995). In addition, the 130-140 nm diameter is optimal for moving at an appreciable rate through the brain extracellular space (Nance et al., 2012). We found that the presence of the carrier appears to increase the potency of RI-OR2-TAT as an aggregation inhibitor by 10-20 fold, where this is determined by the molar ratio of inhibitor:Aβ required to block the aggregation of $A\beta_{1-42}$ under standard experimental conditions. We did not observe this phenomenon with curcumin-NL (Taylor et al., 2011) and so it is not completely clear why there is this considerable jump in potency for PINPs compared to free peptide. However, creating multivalent peptide-dendrimers has been shown to increase the efficacy of a KLVFF peptide aggregation inhibitor (Chafekar et al., 2007) and this may be a factor in our study, due to several inhibitory peptides being able to interact simultaneously with oligomeric Aβ.

We reported previously a large increase in the affinity of RI-OR2-TAT for Aβ (K_d = 58-125 nM) compared to RI-OR2 alone (K_d = 9-12 μM), but this is not reflected in an equivalent jump in the ability of RI-OR2-TAT to inhibit Aβ aggregation at low concentrations of inhibitor (Taylor et al., 2010; Parthsarathy et al., 2013). We can conclude from this that an increase in binding affinity does not necessarily result in a more potent aggregation inhibitor. Here, we found that the affinity of PINPs for Aβ (K_d = 13.2-50 nM) is slightly higher than that obtained

previously for RI-OR2-TAT, but the ability of PINPs to inhibit Aβ aggregation at low concentrations of the inhibitory peptide was greatly improved. In addition to multivalent interactions between RI-OR2-TAT and Aβ, another possible explanation for the potency of PINPs is based on the fact that RI-OR2-TAT contains many positively charged amino acid residues and the presence of multiple copies of this peptide on the NL surface (each PINP has around 1600 molecules of RI-OR2-TAT attached) would give a highly positively charged external layer that could attract and capture Aβ monomers, or oligomers as they form (Wang et al., 2011). It is also feasible that Aβ is captured by the peptides exposed on the NL surface and is then incorporated into the lipid component of the NL, so effectively removing Aβ from solution. It is well known that Aβ oligomers insert into lipid membranes of cells and form pores or ion channels (Arispe et al., 1993a; Arispe et al., 1993b; Fraser et al., 1997).

The TAT portion of RI-OR-TAT, with its positively charged amino acid residues, also confers on the inhibitor an ability to cross the BBB and reach the brain (Parthsarathy et al., 2013). Here we show that this ability is maintained for PINPs. The PE of NL, using the *in vitro* BBB model, was much higher for PINPs than for UD liposomes, proving the effectiveness of the functionalized NL to flux across the cellular monolayer. Moreover, some PINPs are transported into the brain, through the BBB of healthy mice, and they show a protective effect on memory loss in Tg2576 mice. It is also possible that this is due to the 'sink' effect with the liposomes rapidly binding Aβ in blood before being removed, and this is driving export of Aβ from the brain.

Other NP-based treatments for AD are under investigation, including antibody-coated NP and secretase inhibitors as well as our previously published curcumin and lipid-ligand linked NL (Gobbi et al., 2010; Canovi et al., 2011; Richman et al., 2011; Taylor et al., 2011; Yoo et al., 2011; Bana et al., 2014). Despite promising preclinical data, no secretase inhibitor has succeeded in any advanced clinical trial (Anand et al., 2014) and, considering the serious side effects reported for immunisation with anti-Aβ antibodies (Delrieu et al., 2012), anti-Aβ-coated NP could be problematic. In contrast, PINPs have 'stealth' properties and so should not elicit any immune response. Moreover, the aggregation of Aβ seems to be a purely pathological phenomenon, and so inhibition of this process should not result in problematic side effects.

In addition to these therapeutic implications, PINPs also have potential as a molecular imaging agent (Re et al., 2012). The high affinity of RI-OR2-TAT for Aβ should allow specific labelling of amyloid plaques, and possibly Aβ oligomers, through addition of a relevant contrast agent (CT/MRI) or radiolabel (PET/SPECT) to form a multifunctional NP with 'theranostic' utility.

Acknowledgement

The research leading to these results has received funding from the European Community's Seventh Framework Programme (FP7/2007-2013) under grant agreement no. 212043, and from The Alzheimer's Society UK (grant number 210 (AS-PG-2013-032)). There were also contributions from Lancaster University's Defying Dementia campaign.

The authors thank Pierre-Olivier Couraud from Institut National de la Santé et de la Recherche Médicale (INSERM, Paris, France) for providing the hCMEC/D3 cells.

References

Anand R, Gill KD, Mahdi AA (2014) Therapeutics of Alzheimer's disease: Past, present and future. Neuropharmacology 76 Pt A:27-50.

Arispe N, Pollard HB, Rojas E (1993b) Giant multilevel cation channels formed by Alzheimer disease amyloid beta-protein [A beta P-(1-40)] in bilayer membranes. Proc. Natl. Acad. Sci. U S A. 90(22):10573-7.

Arispe N, Rojas E, Pollard HB (1993a) Alzheimer disease amyloid beta protein forms calcium channels in bilayer membranes: blockade by tromethamine and aluminum. Proc. Natl. Acad. Sci. U S A. 90(2):567-71.

Austen BM, Paleologou KE, Ali SA, Qureshi MM, Allsop D, El-Agnaf OM (2008) Designing peptide inhibitors for oligomerization and toxicity of Alzheimer's beta-amyloid peptide. Biochemistry 47(7):1984-92.

Bana L, Minniti S, Salvati E, Sesana S, Zambelli V, Cagnotto A, Orlando A, Cazzaniga E, Zwart R, Scheper W, Masserini M, Re F (2014) Liposomes bifunctionalized with phosphatidic acid and an ApoE-derived peptide affect Aβ aggregation features and cross the blood-brain-barrier: implications for therapy of Alzheimer disease. Nanomedicine 10(7):1583-90.

Bradford MM (1976) A rapid and sensitive method for the quantitation of microgram quantities of protein utilizing the principle of protein-dye binding. Anal. Biochem. 72:248-54.

Canovi M, Markoutsa E, Lazar AN, Pampalakis G, Clemente C, Re F, Sesana S, Masserini M, Salmona M, Duyckaerts C, Flores O,

Gobbi M, Antimisiaris SG (2011) The binding affinity of anti-Aβ1-42 MAb-decorated nanoliposomes to Aβ1-42 peptides in vitro and to amyloid deposits in post-mortem tissue. Biomaterials 32(23):5489-97.

Cecchelli R, Dehouck B, Descamps L, Fenart L, Buée-Scherrer V V, Duhem C, Lundquist S, Rentfel M, Torpier G, Dehouck MP (1999) In vitro model for evaluating drug transport across the blood-brain barrier. Adv. Drug. Deliv. Rev. 36(2-3):165-78.

Chafekar SM, Malda H, Merkx M, Meijer EW, Viertl D, Lashuel HA, Baas F, Scheper W (2007) Branched KLVFF tetramers strongly potentiate inhibition of beta-amyloid aggregation. Chembiochem. 8(15):1857-64.

Cleary JP, Walsh DM, Hofmeister JJ, Shankar GM, Kuskowski MA, Selkoe DJ, Ashe KH (2005) Natural oligomers of the amyloid-beta protein specifically disrupt cognitive function. Nat. Neurosci. 8(1):79-84.

Delrieu J, Ousset PJ, Caillaud C, Vellas B (2012) 'Clinical trials in Alzheimer's disease': immunotherapy approaches. J. Neurochem. 120 Suppl 1:186-93.

Fraser SP, Suh YH, Djamgoz MB (1997) Ionic effects of the Alzheimer's disease beta-amyloid precursor protein and its metabolic fragments. Trends Neurosci. 20(2):67-72.

Gobbi M, Re F, Canovi M, Beeg M, Gregori M, Sesana S, Sonnino S, Brogioli D, Musicanti C, Gasco P, Salmona M, Masserini ME (2010) Lipid-based nanoparticles with high binding affinity for amyloid-beta1-42 peptide. Biomaterials 31(25):6519-29.

Haass C, Selkoe DJ (2007) Soluble protein oligomers in neurodegeneration: lessons from the Alzheimer's amyloid β-peptide. Nat. Rev. Mol. Cell. Biol. 8:101-12.

Horcas I, Fernández R, Gómez-Rodríguez JM, Colchero J, Gómez-Herrero J, Baro AM (2007) WSXM: a software for scanning probe microscopy and a tool for nanotechnology. Rev. Sci. Instrum. 78(1):013705.

Howlett D (2011) APP transgenic mice and their application to drug discovery. Histol. Histopathol. 26:1611-32.

Kim HJ, Chae SC, Lee DK, Chromy B, Lee SC, Park YC, Klein WL, Krafft GA, Hong ST (2003) Selective neuronal degeneration induced by soluble oligomeric amyloid beta protein. FASEB J. 17(1):118-20.

Lambert MP, Barlow AK, Chromy BA, Edwards C, Freed R, Liosatos M, Morgan TE, Rozovsky I, Trommer B, Viola KL, Wals P, Zhang C, Finch CE, Krafft GA, Klein WL (1998) Diffusible, nonfibrillar ligands derived from Abeta1-42 are potent central nervous system neurotoxins. Proc. Natl. Acad. Sci. U S A. 95(11):6448-53.

Ma QL, Yang F, Rosario ER, Ubeda OJ, Beech W, Gant DJ, Chen PP, Hudspeth B, Chen C, Zhao Y, Vinters HV, Frautschy SA, Cole GM (2009) Beta-amyloid oligomers induce phosphorylation of tau and inactivation of insulin receptor substrate via c-Jun N-terminal kinase signaling: suppression by omega-3 fatty acids and curcumin. J. Neurosci. 29(28):9078-89.

Nance EA, Woodworth GF, Sailor KA, Shih TY, Xu Q, Swaminathan G, Xiang D, Eberhart C, Hanes J (2012) A dense poly(ethylene

glycol) coating improves penetration of large polymeric nanoparticles within brain tissue. Sci. Transl. Med. 4(149):149ra119.

Nobs L, Buchegger F, Gurny R, Allémann E (2004) Current methods for attaching targeting ligands to liposomes and nanoparticles. J. Pharm. Sci. 93(8):1980-92.

Parthsarathy V, McClean PL, Hölscher C, Taylor M, Tinker C, Jones G, Kolosov O, Salvati E, Gregori M, Masserini M, Allsop D (2013) A novel retro-inverso peptide inhibitor reduces amyloid deposition, oxidation and inflammation and stimulates neurogenesis in the APPswe/PS1ΔE9 mouse model of Alzheimer's disease. PLoS One 8(1):e54769.

Poller B, Gutmann H, Krähenbühl S, Weksler B, Romero I, Couraud PO, Tuffin G, Drewe J, Huwyler J (2008) The human brain endothelial cell line hCMEC/D3 as a human blood-brain barrier model for drug transport studies. J. Neurochem. 107(5):1358-68.

Re F, Cambianica I, Sesana S, Salvati E, Cagnotto A, Salmona M, Couraud PO, Moghimi SM, Masserini M, Sancini G (2011a) Functionalization with ApoE-derived peptides enhances the interaction with brain capillary endothelial cells of nanoliposomes binding amyloid-beta peptide. J. Biotechnol. 156(4):341-6.

Re F, Cambianica I, Zona C, Sesana S, Gregori M, Rigolio R, La Ferla B, Nicotra F, Forloni G, Cagnotto A, Salmona M, Masserini M, Sancini G (2011b) Functionalization of liposomes with ApoE-derived peptides at different density affects cellular uptake and

drug transport across a blood-brain barrier model. Nanomedicine 7(5):551-9.

Re F, Moresco R, Masserini M (2012) Nanoparticles for neuroimaging. J. Phys. D. Appl. Phys. 45:073001.

Richman M, Wilk S, Skirtenko N, Perelman A, Rahimipour S (2011) Surface-modified protein microspheres capture amyloid-β and inhibit its aggregation and toxicity. Chemistry 17(40):11171-7.

Stewart JCM (1980) Colorimetric determination of phospholipids with ammonium ferrothiocyanate. Anal. Biochem. 104:10-4.

Stukel JM, Li RC, Maynard HD, Caplan MR (2010) Two-step synthesis of multivalent cancer-targeting constructs. Biomacromolecules 11(1):160-7.

Summerfield SG, Stevens AJ, Cutler L, del Carmen Osuna M, Hammond B, Tang SP, Hersey A, Spalding DJ, Jeffrey P (2006) Improving the in vitro prediction of in vivo central nervous system penetration: integrating permeability, P-glycoprotein efflux, and free fractions in blood and brain. J. Pharmacol. Exp. Ther. 316(3):1282-90.

Taylor M, Moore S, Mayes J, Parkin E, Beeg M, Canovi M, Gobbi M, Mann DM, Allsop D (2010) Development of a proteolytically stable retro-inverso peptide inhibitor of beta-amyloid oligomerization as a potential novel treatment for Alzheimer's disease. Biochemistry 49(15):3261-72.

Taylor M, Moore S, Mourtas S, Niarakis A, Re F, Zona C, La Ferla B, Nicotra F, Masserini M, Antimisiaris SG, Gregori M, Allsop D (2011) Effect of curcumin-associated and lipid ligand-

functionalized nanoliposomes on aggregation of the Alzheimer's Aβ peptide. Nanomedicine 7(5):541-50.

Tinker-Mill C, Mayes J, Allsop D, Kolosov OV (2014) Ultrasonic force microscopy for nanomechanical characterization of early and late-stage amyloid-β peptide aggregation. Sci. Rep. 4:4004.

Torchilin VP (2005) Recent advances with liposomes as pharmaceutical carriers. Nat. Rev. Drug. Discov. 4:145-60.

Walsh DM, Klyubin I, Fadeeva JV, Cullen WK, Anwyl R, Wolfe MS, Rowan MJ, Selkoe DJ (2002) Naturally secreted oligomers of amyloid beta protein potently inhibit hippocampal long-term potentiation in vivo. Nature 416(6880):535-9.

Walsh DM, Selkoe DJ (2007) Aβ oligomers – a decade of discovery. Neurochem. 101:1172-84.

Wang HW, Pasternak JF, Kuo H, Ristic H, Lambert MP, Chromy B, Viola KL, Klein WL, Stine WB, Krafft GA, Trommer BL (2002) Soluble oligomers of beta amyloid (1-42) inhibit long-term potentiation but not long-term depression in rat dentate gyrus. Brain Res. 924(2):133-40.

Wang Q, Shah N, Zhao J, Wang C, Zhao C, Liu L, Li L, Zhou F, Zheng J (2011) Structural, morphological, and kinetic studies of β-amyloid peptide aggregation on self-assembled monolayers. Phys. Chem. Chem. Phys. 13(33):15200-10.

Webb MS, Harasym TO, Masin D, Bally MB, Mayer LD (1995) Sphingomyelin-cholesterol liposomes significantly enhance the pharmacokinetic and therapeutic properties of vincristine in murine and human tumour models. Br. J. Cancer 72(4):896-904.

Wimo A, Prince M (2010) Alzheimer's Disease International World Alzheimer Report 2010 The Global Economic Impact of Dementia. Alzheimer's Disease International (ADI); 2010.

Yoo SI, Yang M, Brender JR, Subramanian V, Sun K, Joo NE, Jeong SH, Ramamoorthy A, Kotov NA (2011) Mechanism of fibrillation inhibition of amyloid peptides by inorganic nanoparticles reveals functional similarities with proteins. Angew Chem. Int. Ed. 50:5110-5.

CHAPTER 6

Summary, conclusions and future perspectives

Accordingly to the amyloid cascade hypothesis, accumulation and aggregation of the beta-amyloid (Aβ) peptide in the brain are the primary toxic events in Alzheimer's disease (AD) pathogenesis. These occurrences cause a downstream series of pathological processes that finally lead to neuronal degeneration, cognitive dysfunction and memory loss, main clinical features of the disease. Alteration/prevention of brain Aβ aggregation, with consequent influence on downstream pathological pathways, could represent a possible way to halt the progression of the disease, for which a cure is still needed. The main obstacle in the development of therapeutic strategies is the presence of the blood-brain barrier (BBB), a highly complex structure that tightly regulates the movement of molecules from the blood to the brain, protecting it from injuries and diseases, but also limiting the passage of the majority of pharmaceuticals. Properly designed nanoparticles (NPs) represent a promising tool to enhance the CNS penetration of therapeutics, relying on the possibility of their multifunctionalization, allowing both BBB crossing and the targeting of molecules of interest, such as Aβ. Among the different NPs, liposomes are attractive tools for biomedical applications thanks to their biocompatibility, non-immunogenicity, non-toxicity, biodegradability, high physical stability and versatility in surface functionalization.

Focusing on brain Aβ as the target, the aim of the present work was the design and testing of liposomes functionalized to cross the BBB and to interact with Aβ. As herein reported, two different liposome preparations were developed: i) mApoE-PA-LIP, liposomes bifunctionalized with mApoE, a peptide derived from the apolipoprotein-E receptor-binding domain for BBB targeting, and with

PA, phosphatidic acid, for Aβ binding; ii) PINPs, liposomes functionalized with RI-OR2-TAT, a retro-inverted fusion peptide made by a combination of the Aβ aggregation inhibitor, RI-OR2, and the HIV 'TAT' cell penetrating peptide.

Considerations about NP design:

Both mApoE-PA-LIP and PINPs were composed of a matrix of sphingomyelin and cholesterol in equimolar ratio. This composition had already been utilized *in vivo* for therapeutic purposes showing good features in terms of circulation times, biocompatibility and resistance to degradation (Webb et al., 1995; Thomas et al., 2006). Moreover, with respect to the targeting purposes of the present work, Aβ was shown to bind Sm/Chol bilayers (Choucair et al., 2007) and the presence of cholesterol was proven to strengthen the Aβ-membrane interaction (Qiu et al., 2009). Finally, liposome-based nanodrugs made up with the same matrix had already been approved by FDA and extensively used in the clinic (i.e. Marqibo). This is important to speed up the regulatory process in view of a possible use in humans.

For surface functionalization, both mApoE and RI-OR2-TAT peptides were attached to PA-LIP or LIP, respectively, by covalent coupling between a maleimide-group on the NPs surface and a sulfhydryl group on the peptides. This type of coupling confers the best performance in terms of permeability across an *in vitro* model of the BBB with respect to other decoration strategies, such as biotin/streptavidin linkage (Salvati et al., 2013).

Considerations about NP targeting properties:

Regarding brain targeting, both liposome preparations were able to cross the BBB *in vivo*, as first shown by biodistribution studies in healthy mice. For both mApoE-PA-LIP and PINPs, the amount of NPs reaching the brain was higher (0.3% and 0.2% of injected dose/g brain, respectively) with respect to other brain targeting NPs (usually < 0.1% of injected dose/g brain) (Huang et al., 2011; Gaillard et al., 2014).

Considering Aβ targeting, both mApoE-PA-LIP and PINPs showed the ability to bind Aβ with high affinity and to interfere with its aggregation process *in vitro*. The binding affinity of PA and RI-OR2-TAT to Aβ was in the submicromolar range (Kd = 22-87 nM and Kd = 13.5-50 nM, respectively, depending on Aβ aggregation state), higher with respect to other Aβ ligands, such as curcumin analogs (Rubagotti et al., 2016), but far from those of anti-Aβ antibodies (Canovi et al., 2012). On the basis of the failure of clinical trials performed with anti-Aβ antibodies able to bind only Aβ in its monomeric form (Racke et al., 2005; Doody et al., 2014), it is important to notice that both liposome formulations herein considered are able to bind also oligomers and fibrils, similarly to those molecules still in clinical trials which seem to be partially effective (http://www.alzforum.org). Regarding the ability to interfere with Aβ aggregation/disaggregation process, our results showed that mApoE-PA-LIP and PINPs were best performing in hindering Aβ aggregation with respect to other NPs functionalized with anti-Aβ aggregating drugs (i.e. curcumin) (Mourtas et al., 2014). Moreover, mApoE-PA-LIP displayed the ability to disaggregate preformed aggregates, which is the most important feature for AD therapeutic purposes.

Considerations about NP efficacy for AD treatment:

Both mApoE-PA-LIP and PINPs showed to be effective against AD pathology when administered to AD Tg mice.

In the case of mApoE-PA-LIP, two type of *in vivo* treatment were evaluated: an acute treatment, on symptomatic APP/PS1 Tg mice (10 months of age), showing evident Aβ plaque deposition and cognitive impairment, taken as a model of severe AD, and a treatment to evaluate the possibility to delay the onset or the progression of the disease, on pre-symptomatic APP/PS1 Tg mice (5-month-old), showing an initial brain Aβ deposition in the absence of cognitive impairment and taken as a model of mild/moderately severe AD. The rationale for the performance of a preventive treatment is the evidence that brain Aβ pathophysiological alterations leading to AD take place decades before the appearance of the first signs of dementia, providing a wide pre-symptomatic time window for intervention with Aβ-targeted therapies (Holtzman et al., 2011; Sperling et al., 2013; Tian et al., 2014). Obviously, in humans this kind of treatment would be currently possible only in the presence of a genetic diagnosis of familiar AD, but with several concerns on MCI individuals. However, considering the recent advancement in AD diagnostic tools (Fraller, 2013), an early diagnosis of the pathology could be soon available, thus extending the disease-modifying potential of a preventive treatment to the most numerous cases of sporadic AD.

The acute therapeutic treatment (3 IP injections/week for 3 weeks, 73.5 mg of total lipids/kg) with mApoE-PA-LIP ameliorated mouse impaired memory and decreased total insoluble brain Aβ (-33%),

number and total area of brain Aβ plaques (-34%) and the most toxic Aβ oligomeric species (-70.5%). The comparison with monofunctionalized liposomes indicated that bifunctionalization is crucial either to affect the Aβ plaque load or to hinder the cognitive deficit. Plaque reduction was also confirmed in symptomatic APP23 Tg mice (15 months of age) by PET imaging with [^{11}C]Pittsburgh compound B (PIB). This animal model was necessary for PET since it has been shown that [^{11}C]PIB does not sufficiently bind to the plaques in the APP/PS1 mouse brain (Snellman et al., 2013).

On the other side, the long-term treatment on young mice with a weekly IP administration for 7 months of mApoE-PA-LIP (73.5 mg of total lipids/kg) slowed down brain Aβ deposition (-30%) and prevented the onset of memory impairment and the occurrence of typical AD cerebral anatomical abnormalities, i.e. ventricle enlargement and reduction of entorhinal cortex thickness. Notably, these effects were maintained up to three months after treatment discontinuation.

Both in the acute and in the long-term treatment, the reduction of brain Aβ was associated with its increase in peripheral organs, liver and spleen. On the basis of these results, a potential mechanism of action of mApoE-PA-LIP was speculated: a small proportion of liposomes would cross the BBB, subsequently destabilizing, or hindering, the deposition of brain Aβ aggregates. At this point, the generated lower MW Aβ species may be facilitated to move from brain to blood and would be peripherally cleared in the liver and spleen through the so-called sink effect (Matsuoka et al., 2003; Biscaro et al., 2009; Sutcliffe et al., 2011) mediated by the major proportion of mApoE-PA-LIP remained in the circulation. Besides the sink effect action, the long-term effects of

mApoE-PA-LIP were likely due to a deferred increase of brain Aβ-degrading enzymes levels, a decrease of amyloid precursor protein level and a change in Aβ-transporter (LRP1 and RAGE) levels on the BBB. The hypothesis of the mApoE-PA-LIP ability to draw out Aβ from the brain was further investigated *in vitro*, using a transwell cellular model of the BBB. The spontaneous efflux of Aβ oligomers, but not of Aβ fibrils, from the 'brain' side of the transwell was strongly enhanced (5-fold) in presence of mApoE-PA-LIP in the 'blood' compartment. Since mApoE-PA-LIP were not able to come back to 'blood' side once entered the 'brain' side, the effect was not due to a carrier action of liposomes, but likely to a withdrawal of Aβ exerted by sink effect. Of course, further investigations are needed in order to clarify mApoE-PA-LIP mechanism of action, particularly with regard to their influence on molecular pathways involving Aβ, and their ability to counteract memory loss. Apart from decreasing Aβ oligomers, the most neurotoxic species (Lue et al., 1999; McLean et al., 1999; Wilcox et al., 2011; Scopes et al., 2012), this latter ability could be linked to the anti-inflammatory and anti-oxidant activity, seen, respectively, as a decrease in TNF-α and an increase in SOD activity, exerted by mApoE-PA-LIP in the brain of treated Tg mice. These mApoE-PA-LIP-mediated actions could potentially prevent damage at synapses, primary Aβ targets in AD pathogenesis (Selkoe, 2002).

Regarding the *in vivo* testing of PINPs, their IP administration (once a day for 21 days, 100 nmol of peptide/kg) to symptomatic Tg2576 mice (22 months of age), showing evident Aβ plaque deposition and cognitive impairment, improved mouse impaired memory. In the case of PINPs, the effects on Aβ pathology have been less deepened and so

further investigations are needed in order to disclose what is the effect on Aβ oligomers and plaques. In addition, the mechanism of action of PINPs needs to be clarified.

Taken all together, these findings promote multi-functional liposomes as a valuable all-in-one multitask nanomedicine potentially suitable for the treatment of AD. Unlike Aβ-centered molecules recently tested, and resulted unsuccessful, in clinical trials on mild to moderate AD, such as anti-Aβ antibodies (i.e. Bapinezumab and Solanezumab) and BACE inhibitors (i.e. Verubecestat) (www.clinicaltrials.gov; www.alzforum.org; Doody et al., 2014; Salloway et al., 2014), the liposome formulations herein considered slowed down the progression of AD at all stages, displaying effectiveness also in advanced phases and thus fitting the current scenario of therapeutic need, where an accurate diagnosis, and consequently a specific therapy, is possible only in late stages. In comparison with antibodies and BACE inhibitors, for which often the positive effects on cognition were supposed from their ability to act on brain Aβ burden, but not directly tested (Bard et al., 2000; Kastanenka et al., 2016; Kennedy et al., 2016; Sevigny et al., 2016), should be noted that both mApoE-PA-LIP and PINPs showed a great ability to restore memory impairment in mouse models of AD. In addition, as an added value, the treatment with these nanoliposomes achieved amazing effects on cognition and brain Aβ in a short period of time (~ 3 weeks). Finally, both liposome formulations herein considered, especially mApoE-PA-LIP, for which the investigation was much more deepened, did not show any sign of cerebral or systemic toxicity, which is particularly important considering that the majority

of clinical trials with antibodies was halted due to brain imaging abnormalities caused by the treatments (Orgogozo et al., 2003; Salloway et al., 2009).

Talking about future perspectives and considering the recent reassessment of the amyloid cascade hypothesis in a wider and most complex way, an important step towards the possible successful clinical development of mApoE-PA-LIP and PINPs would be the investigation of their efficacy on other factors altered in AD, the most important of which is tau protein. The implementation of mApoE-PA-LIP and PINPs is another future possibility. Both liposome preparations could be loaded with both hydrophilic, entrapped in the aqueous core, or lipophilic compounds, dissolved in the lipid bilayer, resulting in multivalent therapeutic nanovectors. Moreover, exploiting the high affinity of mApoE-PA-LIP and PINPs for Aβ, the addition of an imaging tracer could combine therapy and specific labelling of amyloid plaques, forming multifunctional NPs with ‘theranostic’ utility.

References

Bard F, Cannon C, Barbour R, Burke RL, Games D, Grajeda H, Guido T, Hu K, Huang J, Johnson-Wood K, Khan K, Kholodenko D, Lee M, Lieberburg I, Motter R, Nguyen M, Soriano F, Vasquez N, Weiss K, Welch B, Seubert P, Schenk D, Yednock T (2000) Peripherally administered antibodies against amyloid beta-peptide enter the central nervous system and reduce pathology in a mouse model of Alzheimer disease. Nat. Med. 6(8):916-9.

Biscaro B, Lindvall O, Hock C, Ekdahl CT, Nitsch RM (2009) Abeta immunotherapy protects morphology and survival of adult-born neurons in doubly transgenic APP/PS1 mice. J. Neurosci. 29:14108 -19.

Canovi M, Lucchetti J, Stravalaci M, Re F, Moscatelli D, Bigini P, Salmona M, Gobbi M (2012) Applications of surface plasmon resonance (SPR) for the characterization of nanoparticles developed for biomedical purposes. Sensors (Basel) 12(12):16420-32.

Choucair A, Chakrapani M, Chakravarthy B, Katsaras J, Johnston LJ (2007) Preferential accumulation of Abeta(1-42) on gel phase domains of lipid bilayers: an AFM and fluorescence study. Biochim. Biophys. Acta 1768(1):146e54.

Doody RS, Thomas RG, Farlow M, Iwatsubo T, Vellas B, Joffe S, Kieburtz K, Raman R, Sun X, Aisen PS, Siemers E, Liu-Seifert H, Mohs R; Alzheimer's Disease Cooperative Study Steering Committee; Solanezumab Study Group (2014) Phase 3 trials of solanezumab for mild-to-moderate Alzheimer's disease. N. Engl. J. Med. 370(4):311-21.

Fraller DB (2013) State of the science: use of biomarkers and imaging in diagnosis and management of Alzheimer disease. J. Neurosci. Nurs. 45(2):63-70.

Gaillard PJ, Appeldoorn CC, Dorland R, van Kregten J, Manca F, Vugts DJ, Windhorst B, van Dongen GA, de Vries HE, Maussang D, van Tellingen O (2014) Pharmacokinetics, brain delivery, and efficacy in brain tumor-bearing mice of glutathione pegylated liposomal doxorubicin (2B3-101). PLoS One 9(1):e82331.

Holtzman DM, Morris JC, Goate AM (2011) Alzheimer's disease: the challenge of the second century. Sci. Transl. Med. 3(77):77sr1.

Huang FY, Lee TW, Kao CH, Chang CH, Zhang X, Lee WY, Chen WJ, Wang SC, Lo JM (2011) Imaging, autoradiography, and biodistribution of (188)Re-labeled PEGylated nanoliposome in orthotopic glioma bearing rat model. Cancer Biother. Radiopharm. 26(6):717-25.

Kastanenka KV, Bussiere T, Shakerdge N, Qian F, Weinreb PH, Rhodes K, Bacskai BJ (2016) Immunotherapy with Aducanumab Restores Calcium Homeostasis in Tg2576 Mice. J. Neurosci. 36(50):12549-58.

Kennedy ME, Stamford AW, Chen X, Cox K, Cumming JN, Dockendorf MF, Egan M, Ereshefsky L, Hodgson RA, Hyde LA, Jhee S, Kleijn HJ, Kuvelkar R, Li W, Mattson BA, Mei H, Palcza J, Scott JD, Tanen M, Troyer MD, Tseng JL, Stone JA, Parker EM, Forman MS (2016) The BACE1 inhibitor verubecestat (MK-8931) reduces CNS β-amyloid in animal models and in Alzheimer's disease patients. Sci. Transl. Med. 8(363):363ra150.

Lue LF, Kuo YM, Roher AE, Brachova L, Shen Y, Sue L, Beach T, Kurth JH, Rydel RE, Rogers J (1999) Soluble amyloid beta peptide concentration as a predictor of synaptic change in Alzheimer's disease. Am. J. Pathol. 155:853-62.

Matsuoka Y, Saito M, LaFrancois J, Saito M, Gaynor K, Olm V, Wang L, Casey E, Lu Y, Shiratori C, Lemere C, DuffK (2003) Novel therapeutic approach for the treatment of Alzheimer's disease by peripheral administration of agents with an affinity to beta-amyloid. J. Neurosci. 23:29–33.

McLean CA, Cherny RA, Fraser FW, Fuller SJ, Smith MJ, Beyreuther K, Bush AI, Masters CL (1999) Soluble pool of Abeta amyloid as a determinant of severity of neurodegeneration in Alzheimer's disease. Ann. Neurol. 46:860-6.

Mourtas S, Lazar AN, Markoutsa E, Duyckaerts C, Antimisiaris SG (2014) Multifunctional nanoliposomes with curcumin-lipid derivative and brain targeting functionality with potential applications for Alzheimer disease. Eur. J. Med. Chem. 80:175-83.

Orgogozo JM, Gilman S, Dartigues JF, Laurent B, Puel M, Kirby LC, Jouanny P, Dubois B, Eisner L, Flitman S, Michel BF, Boada M, Frank A, Hock C (2003) Subacute meningoencephalitis in a subset of patients with AD after Abeta42 immunization. Neurology 61(1):46-54.

Qiu L, Lewis A, Como J, Vaughn MW, Huang J, Somerharju P, Virtanen J, Cheng KH (2009) Cholesterol modulates the interaction of beta-amyloid peptide with lipid bilayers. Biophys. J. 96(10):4299-307.

Racke MM, Boone LI, Hepburn DL, Parsadainian M, Bryan MT, Ness DK, Piroozi KS, Jordan WH, Brown DD, Hoffman WP, Holtzman DM, Bales KR, Gitter BD, May PC, Paul SM, DeMattos RB (2005) Exacerbation of cerebral amyloid angiopathy-associated microhemorrhage in amyloid precursor protein transgenic mice by immunotherapy is dependent on antibody recognition of deposited forms of amyloid beta. J. Neurosci. 25(3):629-36.

Rubagotti, S., Croci, S., Ferrari, E., Iori, M., Capponi, P. C., Lorenzini, L., Asti, M. (2016) Affinity of nat/68Ga-Labelled Curcumin and Curcuminoid Complexes for β-Amyloid Plaques: Towards the Development of New Metal-Curcumin Based Radiotracers. Int. J. Mol. Sci. 17(9): 1480.

Salloway S, Sperling R, Gilman S, Fox NC, Blennow K, Raskind M, Sabbagh M, Honig LS, Doody R, van Dyck CH, Mulnard R, Barakos J, Gregg KM, Liu E, Lieberburg I, Schenk D, Black R, Grundman M; Bapineuzumab 201 Clinical Trial Investigators (2009) A phase 2 multiple ascending dose trial of bapineuzumab in mild to moderate Alzheimer disease. Neurology 73(24):2061-70.

Salloway S, Sperling R, Fox NC, Blennow K, Klunk W, Raskind M, Sabbagh M, Honig LS, Porsteinsson AP, Ferris S, Reichert M, Ketter N, Nejadnik B, Guenzler V, Miloslavsky M, Wang D, Lu Y, Lull J, Tudor IC, Liu E, Grundman M, Yuen E, Black R, Brashear HR; Bapineuzumab 301 and 302 Clinical Trial Investigators (2014) Two phase 3 trials of bapineuzumab in mild-to-moderate Alzheimer's disease. N. Engl. J. Med. 370(4):322-33.

Salvati E, Re F, Sesana S, Cambianica I, Sancini G, Masserini M, Gregori M (2013) Liposomes functionalized to overcome the blood-brain barrier and to target amyloid-β peptide: the chemical design affects the permeability across an in vitro model. Int. J. Nanomedicine 8:1749-58.

Scopes DI, O'Hare E, Jeggo R, Whyment AD, Spanswick D, Kim EM, Gannon J, Amijee H, Treherne JM (2012) Abeta oligomer toxicity inhibitor protects memory in models of synaptic toxicity. Br. J. Pharmacol. 167:383-92.

Selkoe DJ (2002) Alzheimer's disease is a synaptic failure. Science 298(5594):789-91.

Sevigny J, Chiao P, Bussière T, Weinreb PH, Williams L, Maier M, Dunstan R, Salloway S, Chen T, Ling Y, O'Gorman J, Qian F, Arastu M, Li M, Chollate S, Brennan MS, Quintero-Monzon O, Scannevin RH, Arnold HM, Engber T, Rhodes K, Ferrero J, Hang Y, Mikulskis A, Grimm J, Hock C, Nitsch RM, Sandrock A (2016) The antibody aducanumab reduces Aβ plaques in Alzheimer's disease. Nature 537(7618):50-6.

Snellman A, Lo´ pez-Pico´n FR, Rokka J, Salmona M, Forloni G, Scheinin M, Solin O, Rinne JO, Haaparanta-Solin M (2013) Longitudinal amyloid imaging in mouse brain with 11C-PIB: comparison of APP23, Tg2576, and APPswe-PS1dE9 mouse models of alzheimer disease. J. Nucl. Med. 54:1434 -41.

Sperling RA, Karlawish J, Johnson KA (2013) Preclinical Alzheimer disease: the challenges ahead. Nat. Rev. Neurol. 9(1):54-8.

Sutcliffe JG, Hedlund PB, Thomas EA, Bloom FE, Hilbush BS (2011) Peripheral reduction of beta-amyloid is sufficient to reduce brain

beta-amyloid: implications for Alzheimer’s disease. J. Neurosci. Res. 89:808-14.

Thomas DA, Sarris AH, Cortes J, Faderl S, O'Brien S, Giles FJ, Garcia-Manero G, Rodriguez MA, Cabanillas F, Kantarjian H (2006) Phase II study of sphingosomal vincristine in patients with recurrent or refractory adult acute lymphocytic leukemia. Cancer 106(7):1641.

Tian T, Zhang B, Jia Y, Li Z (2014) Promise and challenge: the lens model as a biomarker for early diagnosis of Alzheimer's disease. Dis. Markers 2014:826503.

Webb MS, Harasym TO, Masin D, Bally MB, Mayer LD (1995) Sphingomyelincholesterol liposomes significantly enhance the pharmacokinetic and therapeutic properties of vincristine in murine and human tumour models. Br. J. Cancer 72(4):896e904.

Wilcox KC, Lacor PN, Pitt J, KleinWL (2011) Abeta oligomer-induced synapse degeneration in Alzheimer’s disease. Cell. Mol. Neurobiol. 31:939-48.

Publications

Mancini S, Balducci C, Micotti E, Tolomeo D, Forloni G, Masserini M, Re F. *Hindering Alzheimer-like phenotype progression in APP/PS1 mice by multifunctional liposomes.* Submitted.

Gregori M, Taylor M, Salvati E, Re F, **Mancini S**, Balducci C, Forloni G, Zambelli V, Sesana S, Michael M, Michail C, Tinker-Mill C, Kolosov O, Scherer M, Harris S, Fullwood NJ, Masserini M, Allsop D. *Retro-inverso peptide inhibitor nanoparticles as potent inhibitors of aggregation of the Alzheimer's Aβ peptide.* Nanomedicine 2017;13(2):723-32.

Cimini S, Sclip A, **Mancini S**, Colombo L, Messa M, Cagnotto A, Di Fede G, Tagliavini F, Salmona M, Borsello T. *The cell-permeable Aβ1-6A2VTAT(D) peptide reverts synaptopathy induced by Aβ1-42wt.* Neurobiol Dis 2016;89:101-11.

Mancini S, Minniti S, Gregori M, Sancini G, Cagnotto A, Couraud PO, Ordóñez-Gutiérrez L, Wandosell F, Salmona M, Re F. *The hunt for brain Aβ oligomers by peripherally circulating multifunctional nanoparticles: Potential therapeutic approach for Alzheimer disease.* Nanomedicine 2016;12(1):43-52.

Gregori M, Masserini M, **Mancini S**. *Nanomedicine for the treatment of Alzheimer's disease.* Nanomedicine (Lond) 2015;10(7):1203-18.

Balducci C, **Mancini S**, Minniti S, La Vitola P, Zotti M, Sancini G, Mauri M, Cagnotto A, Colombo L, Salmona M, Snellman A, Haaparanta-Solin M, Forloni G, Masserini M, Re F. *Multifunctional liposomes reduce brain β-amyloid burden and ameliorate memory impairment in Alzheimer's disease mouse models.* J Neurosci 2014;34(42):14022-31.

Sclip A, Arnaboldi A, Colombo I, Veglianese P, Colombo L, Messa M, **Mancini S**, Cimini S, Morelli F, Antoniou X, Welker E, Salmona M, Borsello T. *Soluble Aβ oligomer-induced synaptopathy: c-Jun N-terminal kinase's role.* J Mol Cell Biol 2013;5(4):277-9.